ABSTRACT

THERMOCHEMISTRY REACTION PATHS AND OXIDATION KINETICS ON KETONYL AND ALDEHYDIC NITROGEN OXIDES, PROPENE AND ISOOCTANE: A THEORETICAL STUDY

by
Suarwee Snitsiriwat

Thermochemical properties for several atmospheric and combustion related species are determined using computational chemical methods coupled with fundamentals of thermodynamics and statistical mechanics. Enthalpies of formation ($\Delta H_\mathrm{f}{}^{\circ}{}_{298}$) are determined using isodesmic reaction analysis at the CBS-QB3 composite and the B3LYP density functional methods. Entropies ($S^{\circ}{}_{298}$) and heat capacities ($Cp^{\circ}(T)$) are determined using geometric parameters and vibration frequencies; internal rotor contributions are included in S and $Cp(T)$ values in place of torsion frequencies. Kinetic parameters are calculated versus pressure and temperature for the chemical activated formation and unimolecular dissociation. Multi-frequency quantum RRK (QRRK) analysis is used for $k(E)$ with Master Equation analysis for fall off.

Recommended values for enthalpies of formation of the most stable conformers of nitroacetone, acetonitrite, nitroacetate and acetyl nitrite are -51.6 kcal mol^{-1}, -51.3 kcal mol^{-1}, -45.4 kcal mol^{-1} and -58.2 kcal mol^{-1}, respectively. The calculated $\Delta_f H^o{}_{298}$ for nitroethylene is 7.6 kcal mol^{-1} and for vinyl nitrite is 7.2 kcal mol^{-1}. The chemically activated R• + NO$_2$ systems associations proceed to RCO• + NO via chemical activation reaction with a fraction to stabilized adducts and lower energy products at atmospheric pressure and temperature.

Thermochemical properties of isooctane (2,2,4-trimethyl pentane) and its four carbon radicals from loss of hydrogen atoms, and kinetics of the tertiary isooctane radical reaction with O_2 are determined. The computed standard enthalpy of formation of isooctane from this study is -54.40 kcal mol^{-1}. The major products from reaction of the *tert*-isooctane radical + O_2 to form a chemically activated *tert*-isooctane-peroxy radical are formation of isooctene plus HO_2. Next important products are cyclic ethers plus OH radical. This research is the first fundamentally based study of relevant pathways on the potential energy surfaces of *tert*-isooctane radicals + O_2 using high level composite calculation methods.

Kinetic modeling for OH addition to propene and subsequent O_2 association to the hydroxyl-propyl radical adduct shows that significant forward reaction goes to regenerate OH radicals over the range of temperature and pressure studied. Recycle of OH from the decomposition of the hydroxyl propyl-peroxy radical is up to 78%. Inclusion of activation energy resulting from OH addition to primary carbon (double activation) does not show increase in OH recycle. The introduction of the rate constants presented in this study into existing reaction mechanisms should lead to better kinetic models for olefin oxidation chemistry the atmospheric.

THERMOCHEMISTRY REACTION PATHS AND OXIDATION KINETICS ON KETONYL AND ALDEHYDIC NITROGEN OXIDES, PROPENE AND ISOOCTANE: A THEORETICAL STUDY

by
Suarwee Snitsiriwat

A Dissertation
Submitted to the Faculty of
New Jersey Institute of Technology
in Partial Fulfillment of the Requirements for the Degree of
Doctor of Philosophy in Environmental Science

Department of Chemistry and Environmental Science

May 2013

.

BIOGRAPHICAL SKETCH

Author: Suarwee Snitsiriwat

Degree: Doctor of Philosophy

Date: May 2013

Undergraduate and Graduate Education:

- Doctor of Philosophy in Environmental Science,
  New Jersey Institute of Technology, Newark, NJ, 2013

- Master of Science in Environmental Science,
  New Jersey Institute of Technology, Newark, NJ, 2009

- Bachelor of Science in Chemistry,
  Chulalongkorn University, Bangkok, Thailand, 2003

Major: Environmental Science

Publications:

Suarwee Snitsiriwat and Joseph W Bozzelli "Thermochemical Properties for Isooctane and Carbon Radicals: Computational Study" J. Phys. Chem. A. pp. 421-429, December 2012.

Suarwee Snitsiriwat, Rubik Asatryan and Joseph W Bozzelli "Structures, Internal Rotor Potentials, and Thermochemical Properties for a Series of Nitrocarbonyls, Nitroolefins, Corresponding Nitrites, and Their Carbon Centered Radicals" J. Phys. Chem. A., pp.13921-13930, October 2011.

Suarwee Snitsiriwat, Rubik Asatryan and Joseph W Bozzelli "Thermochemical properties for n-propyl, iso-propyl, and tert-butyl nitroalkanes, alkyl nitrites, and their carbon-centered radicals" Int. J. Chem. Kinet., pp. 181-199, March 2010.

Presentations (oral unless noted):

Suarwee Snitsiriwat "Thermochemistry, reaction paths and kinetics on the isooctane radical reactions with O_2" 7th US National Technical Meeting of the Combustion Institute, Atlanta, GA, March 2011.

Suarwee Snitsiriwat "Kinetics and thermochemistry of acetyl and formyl-methyl nitro and nitrites" 2010 AIChE Annual Meeting, Salt Lake City, UT, November 2010.

Suarwee Snitsiriwat "Double activation reaction of OH, O_2 addition, association to propene-regeneration of OH in atmospheric chemistry" 21st International Symposium on Gas Kinetics, Leuven, Belgium, July 2010 (poster).

Suarwee Snitsiriwat "Thermochemistry and kinetics of acetyl and carbonyl methyl radicals and their reactions with NO_2" 6th U.S. National Combustion Meeting; Eastern States Section of the Combustion Institute 2009, Fall Technical Meetings, College Park, MD, October 2009.

Suarwee Snitsiriwat "Kinetics and thermochemistry of acetyl and carbonyl-methyl nitro and nitrites" 36th Northeast Regional Meeting of the American Chemical Society, Hartford, CT, October 2009.

Suarwee Snitsiriwat "Thermochemistry and kinetics of acetyl and carbonyl methyl radicals and their reactions with NO_2" 6th U.S. National Combustion Meeting, Ann Arbor MI, May 2009.

Suarwee Snitsiriwat "Thermochemistry and kinetics on reaction of NO_2 with acetonyl, acetyl and formyl-methyl radicals: A theoretical study" The 27th Kinetics Meeting, Amherst, MA, January 2009.

Suarwee Snitsiriwat "Enthalpy, entropy, heat capacities, internal rotor potentials and bond energies of nitroalkanes and alkyl nitrites and their radicals" The 37th Northeast Regional Meeting of the American Chemical Society, Burlington, VA, June 2008.

Suarwee Snitsiriwat "Thermochemical properties for n-propyl, iso-propyl and tert-butyl nitroalkanes and alkyl nitrites and their carbon centered radicals" 37th Northeast Regional Meeting of the American Chemical Society, Burlington, VA, June 2008.

Mom, Dad and Sis…..

Thank you so much for giving me such a wonderful life.

I LOVE YOU

ACKNOWLEDGMENT

I would like to gratefully and sincerely thank Prof. Joseph W. Bozzelli, my adviser, for his guidance, patience, and most importantly, his friendliness during my graduate studies at NJIT.

I also thank Prof. Carol A. Venanzi, Prof. Tamara M. Gund, Prof. Nancy L. Jackson, Dr. Alexander D. Butherus and Dr. Wenjun Li for serving in my committee. Their comments are invaluable making a great input to my research.

Last, but not least, I would like to express profound gratitude to my parents, siblings, and friends here in the US and Thailand for uncomplaining patience, perennial support, and enormous encouragement during my stay in USA.

TABLE OF CONTENTS

LIST OF TABLES

LIST OF FIGURES

LIST OF FIGURES

(Continued)

LIST OF FIGURES

(Continued)

CHAPTER 1

INTRODUCTION

Detail kinetic models using reaction mechanisms comprised of many elementary chemical reaction steps, based upon fundamental thermochemical and kinetic principles, are presently used and being developed by researchers attempting to optimize or more fully understand a number of chemical complex systems. These systems include combustion, flame inhibition, ignition, atmospheric smog formation, stratospheric ozone depletion, municipal and hazardous wastes incineration, chemical vapor deposition, semiconductor etching, rocket propulsion and other related fields.

One important requirement for modeling and simulation of these systems is accurate thermochemical property data such as enthalpies of formation ($\Delta_f H^o_{298}$), entropy (S°_{298}), and heat capacities as functions of temperature ($Cp(T)$) for reactants, intermediates, final products, and reaction transition states. These data allow determination of equilibrium, and reverse rate constants from the forward rate constant and the equilibrium constant. *Ab initio* and density functional calculations provide an opportunity to accurately calculate these thermochemical properties data which are often difficult or impossible to obtain through experiment.

The objective of this dissertation is to apply well-known density functional theory and composite computational methods to calculate thermochemical properties and kinetics of hydrocarbons, oxygenates, and nitrocarbonyls. Calculating accurate and reliable thermochemical properties, including enthalpies of formation ($\Delta_f H^\circ_{298}$), entropies ($S(T)$), heat capacities ($Cp(T)$), and bond dissociation energies (BDEs), will aid in the

creation of chemical kinetic models while serving as representative species for larger related compounds. Calculated values are compared to experimental data, where available, or to high level calculations to gauge their accuracy and thus justifying their use.

In this study, thermochemical properties and transition state structures for the reactions of acetonyl radical and acetyl radical with NO_2 are analyzed to evaluate reaction paths and kinetics. The initial association reactions form nitro alkanes (RNO_2) or alkylnitrites (RONO) adducts. Enthalpies of formation ($\Delta_f H°_{298}$) are determined using isodesmic reaction analysis at the CBS-QB3 composite and density functional methods. Entropies ($S°_{298}$) and heat capacities ($Cp(T)$) are determined using geometric parameters and vibration frequencies obtained at the B3LYP/6-311G(2d,d,p) level of theory. Internal rotor contributions are included in $S°_{298}$ and $Cp(T)$ values in place of torsion frequencies. Detailed potential energy surfaces for the reactions are presented, with association rate constants from variational transition state analysis and intramolecular isomerization rate parameters from canonical transition state theory. The chemically activated R• + NO_2 systems are modeled using quantum Rice-Ramsperger-Kassel (QRRK) theory, with Master Equation analysis for falloff. Rate constants for abstraction of H from the above carbonyl species by NO to form acetylformaldehyde + HNO (or ketene + HONO in acetyl radical reaction) are also evaluated.

Isooctane is a highly branched molecule and its structure may have a significant affect on its thermochemistry and reaction barriers. A study on isooctane parent molecule and its radicals from loss of hydrogen atoms shows that carbon-hydrogen bond energies in isooctane were weaker than the conventional primary, secondary and tertiary C—H

bonds by ~1-2 kcal mol^{-1}. In this study, standard enthalpy ($\Delta_f H^o_{298}$) and dissociation bond enthalpies are reported for the species resulting from reactions in the *tert*-isooctane radicals + O_2 system. Transition state structures and intermediates that result from the isomerization and reactions of the radical are calculated using Density Functional and higher level composite *ab initio* based calculations. Kinetics parameters are reported for association reactions of *tert*-isooctane radicals with molecular oxygen to form R-O_2* chemically activated adducts from variational transition state theory.

Unsaturated hydrocarbon species are important reactive trace gases in the troposphere, originating from a number of natural and anthropogenic sources. The lighter alkenes, ethene and propene, are predominantly emitted from fossil fuel combustion, biomass burning, and the oceans. This study focuses on the reaction of the β - hydroxyalkyl radicals association with O_2 which includes unimolecular peroxy radical reactions leading to recycle of OH. This work includes reaction system modeled under conditions of atmospheric chemistry for varied NO_x. Thermochemical properties are estimated for reactants, intermediates, products, and transition states in the reaction paths using ab initio and density functional calculations. The thermochemical parameters are used to calculate high-pressure limit rate constants using canonical transition state theory (TST) and variational transition state theory (VTST). Rate constants as a function of temperature and pressure are estimated using a multifrequency quantum RRK analysis for $k(E)$ and master equation analysis for falloff. The data at relevant pressures and temperatures should be useful to both atmospheric and combustion models.

CHAPTER 2

THERMOCHEMICAL KINETICS

2.1 Computational Chemistry

Ab initio molecular orbital theory is concerned with predicting the properties of atomic and molecular systems. It is based upon the fundamental laws of quantum mechanics and uses a variety of mathematical transformation and approximation techniques to solve the fundamental equations, *i.e.,* Schrödinger partial differential quation,

$$\hat{H}\Psi = E\Psi \tag{2.1}$$

Here $\hat{H}$ is the *Hamiltonian,* a differential operator representing the total energy. E is the numerical value of the energy of the state, *i.e.,*, the energy relative to a state in which the constituent particles (nuclei and electrons) are infinitely separated and at rest. Ψ is a many-electron wavefunction, and it depends on the Cartesian coordinates of all particles and also on the spin coordinates. The square of the wavefunction, Ψ^2, is the probability distribution of the particles within the molecule.

The many-electron Schrodinger equation cannot be solved exactly, and approximations need to be introduced to provide practical methods. The approximation of separating electronic and nuclear motions is Born-Oppenheimer approximation that is basic to quantum chemistry. The Hartree-Fock (HF) approximation treats electron interactions between individual electrons by interactions between a particular electron and the average field created by all the other electrons. The HF model does not include a full treatment of the effects of instantaneous electron correction, *i.e.,* it does not include the energy contributions arising from electrons interacting with one another. This leads to

overestimation of the electron-electron repulsion energy and to too high a total energy.[1] Electron correction accounts for coupling or correction of electron motions, and leads to a lessening of the electron-repulsion energy and also leads to a lowering of the total energy.

The correction energy is defined as the difference between the Hartree-Fock energy and the experimental energy. A variety of theoretical methods, such as density functional, configuration interaction, and Moller-Plesset perturbation have been developed which include some effects of electron correction. Density functional models introduce an "approximate" correction term in an explicit manner, and they reduce computational cost than Hartree-Fork models. Configuration interaction models and Moller-Plesset models extend the flexibility of Hartree-Fock models by mixing ground-state and excited-state wavefunctions. They are significantly more costly than Hartree-Fock models. Traditionally, such methods are referred as post-SCF methods because they add this electron correlation correction to the basic Hartree-Fock model.

The density functional theory (DFT) is based on the fact that the sum of the exchange and correlation energies of a uniform electron gas can be calculated exactly knowing only its electron density. These DFT functionals partition the ground state electronic energy into several components: the kinetic energy, the electron-nuclear interaction, the Coulomb repulsion, and an exchange-correlation term, which accounts for the remainder of the electron-electron interactions.[2] A variety of functionals have been defined, generally distinguished by the way that they treat exchange and correlation components:

1. Local exchange and correlation functions based on the local spin density approximation.

2. Gradient-corrected functionals based on the generalized gradient approximation or Hartree-Fock exchange functional.[3]

Any exchange functional can be combined with any correlation functional. A commonly used gradient-corrected exchange functional is proposed by Becke,[4] and gradient-corrected correlation functional is the Lee, Yang and Parr (LYP) correlation functional. The combination of the two functionals forms the B-LYP method. The notation B3LYP denotes a DFT calculation with the Becke functional and the Lee-Yang-Parr correlation functional.

Configuration Interaction (CI) models calculate the correlation energy by mixing the ground-state (Hartree-Fock) wavefunction with "excited-state" wavefunctions. The configuration functions in a CI calculation are classified as singly excited, doubly excited, triply excited, ..., according to whether 1, 2, 3, ... electron are excited from occupied to unoccupied orbitals. It is reported that the first-order correction to the unperturbed (Hartree-Fock) wavefunction of a closed-shell state contains only double excited configuration functions, and the second-order correction to the Hartree-Fock function includes single, double, triple, and quadruple excitations.[1] The singly excited configuration functions are less important than double excitations in affecting the wave function, but single excitations have a significant effect on one-electron properties. Therefore single excitations are usually included in a CI calculation, and the most common type is CISD calculation which includes the singly and doubly excited configuration functions.[5] The CISD(T) method also includes the triple excited functions.

Another correction energy scheme is the second-order Moller-Plesset (MP2) model proposed by Moller-Plesset in 1934. The MP2 is a perturbation treatment of atoms and molecules in which the unperturbed wave function is the Hartree-Fock function. The perturbation is the difference between the true interelectronic repulsions and the Hartree-Fock interelectronic potential, and the molecular energy is taken as Hartree-Fock energy plus MP2 energy correction. The MP2 calculation are much fast than the CI calculations, but for species involving open-shell ground states, unrestricted SCF wave functions are not eigenfunction of the total spin operator $\hat{S}^2$ and this "spin contamination" can sometimes produce serious errors in UMP-calculated quantities.

Currently available functionals in DFT can not compute a thermodynamic energy such as heat of atomization and the enthalpy of formation with accuracy of 1 kcal mol^{-1}. High level configuration interaction methods with large basis sets can do this but too costly to be feasible except for small molecules. The composite CBS method[6] is reported to achieve 1 kcal mol^{-1} accuracy with a computational time that allows calculation on molecules containing several nonhydrogen atoms.[7] The CBS methods use special procedures designed to extrapolate calculated energies to the complete-basis-set limit. The CBS methods include several corrected calculations done at a geometry optimized at a lower level of theory. The highest-level calculation used is the QCISD(T)/6-31+G(d,p) in the CBS-Q method.

Model chemistry is characterized by the combination of theoretical procedure and a basis set. A basis set is a mathematical representation of the molecular orbitals within a molecule. The basis set can be interpreted as restricting each electron to a particular region of space. Large basis sets impose fewer constraints on electrons to particular

accurately approximate exact molecular orbitals. However, the computation of atomic or molecular properties with large basis sets requires correspondingly more and more computational resources.

Standard basis sets for electronic structure calculation use linear combinations of Gaussian functions to form the orbitals. Basis sets assign a group of basis functions to each atom within a molecule to approximate its orbitals. These basis functions themselves are composed of a linear combination of Gaussian functions. The linear combined basis functions are refereed to as contracted functions, and the component Gaussian functions are referred to as primitives. A basis function consisting of a single Gaussian function is termed uncontracted. Explanation of the nomenclature of 6-31 G basis set is:

- Six primitive Gaussians in the core function,

- Two sets of function in the valence region (one function consisting of three primitive Gaussian, one consisting of one primitive Gaussian).

The 6-31 G(d,p) indicates that it is the polarized 6-31G basis set with one d function added to the heavy atoms and one p function added to hydrogen atoms. The 6-311+G(3df,2p) is the basis set with diffuse functions added to heavy atoms, as well as three d functions and one f function added to heavy atoms, and 2 p functions added to the hydrogen atoms. If 6-311++G(3df,2p), then it also adds diffuse functions to hydrogen atoms.[2]

2.2 Thermochemical Properties

2.2.1 Enthalpy

Enthalpies of formation ($\Delta_f H^o{}_{298}$) are evaluated using calculated electronic energies, zero point vibration energy corrections (ZPVE) and thermal contributions (to 298 K) for each of species in the work reaction.[1, 8] Vibration frequencies are scaled by 0.9806 for B3LYP/6-31G(d,p) and CBS-QB3 level calculations as recommended by Scott and Radom.[9]

Calculated reaction enthalpies, $\Delta_{rxn} H^o{}_{298}$, are used to find $\Delta_f H^o{}_{298}$ of the target molecules:

$$\Delta_{rxn} H^o{}_{298} = \Sigma\, H_f\,(\text{products}) - \Sigma\, H_f\,(\text{reactants}) \tag{2.2}$$

where the two products and one reactant are the three reference molecules, the evaluated literature thermodynamic properties for the three reference species are used. As an example, the following equation is used to estimate $\Delta_f H^o{}_{298}$ for $CH_3CH_2CH_2NO_2$

$$CH_3CH_2CH_2NO_2 + C_2H_6 \rightarrow C_3H_8 + CH_3CH_2NO_2$$
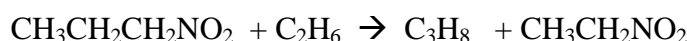
$\Delta_f H^o{}_{298}$ (kcal mol^{-1}):   Target   **-20.04**   **-25.02**   **-25.06**

Since enthalpies of formation of the three reference compounds (values above in bold) are well established in the literature. The heat of reaction, $\Delta_{rxn} H^o{}_{298}$, is calculated and the enthalpy of formation of the target molecule $CH_3CH_2CH_2NO_2$ is obtained as -30.64 kcal-mol^{-1} from Hess's law.

To evaluate the heats of formation of the molecule systems, a variety of homodesmic and isodesmic work reactions, where the bonding environments are similar in products and reagents are used. An isodesmic reaction is a hypothetical reaction where the number and type of bonds is conserved on each side of the work reaction; a homodesmic reaction conserves number and type of bonds, but also conserves

hybridization.[10] The method of isodesmic reactions utilizes a similarity in the bonding environments for reactant and product sets in a work reaction to effect a cancellation of systematic errors in the *ab initio* or density functional calculations.

2.2.2 Entropy and Heat Capacity

Entropy and heat capacity contributions as a function of temperature are determined from the calculated structures, moments of inertia, vibration frequencies, symmetry, electron degeneracy, number of optical isomers and the known mass of each molecule. The calculations use standard formulas from statistical mechanics for the contributions of translation, external rotation and vibrations using the "SMCPS" program.[11] This program utilizes the rigid-rotor-harmonic oscillator approximation from the frequencies along with moments of inertia from the optimized structures. Contributions from internal rotors using Rotator[12] and VIBIR are substituted for contributions from the corresponding internal rotor torsion frequencies. The rotator is a program for the calculation of thermodynamic functions from hindered rotations with arbitrary potentials based on the method developed by Krasnoperov, Lay and Shokhirev.[12] This technique employs expansion of the hindrance potential in the Fourier series, calculation of the Hamiltonian matrix in the basis of the wave functions of free internal rotation, and subsequent calculation of energy levels by direct diagonalization of the Hamiltonian matrix.

SMCPS

SMCPS[11] (<u>S</u>tatistical <u>M</u>echanics for Heat <u>C</u>apacity and Entropy Cp and S) is a program to determine H-H$_0$, Cp, S and zero point vibrational energy (ZPVE) of molecular species from computation chemistry results. The method of calculation is based on principles of

statistical mechanics and has no empirical factors or corrections, other than physical constants.

The basic foundation in statistical mechanics is the partition function; once the partition function is determined, all thermodynamic properties can be determined. The partition function describes the energy of the system over all the individual quantum levels. The canonical ensemble of the partition function is expressed as follows,

$$Q = \sum_i g_i e^{E_i/RT} \tag{2.3}$$

where Q is the partition function, g_i is the degeneracy, E_i is the energy of the ith quantum level, R is universal gas constant, and T is temperature. Thermodynamic properties, as related to partition function, are as follows,

Helmholtz free energy: $\qquad A = -RT \ln Q$ $\hfill (2.4)$

Gibbs free energy: $\qquad G = A + PV$ $\hfill (2.5)$

Internal Energy: $\qquad U = RT\left(\dfrac{\partial \ln Q}{\partial \ln T}\right)_V = -R\left(\dfrac{\partial \ln Q}{\partial(1/T)}\right)_V$ $\hfill (2.6)$

Enthalpy: $\qquad H \equiv U + PV$ $\hfill (2.7)$

Entropy: $\qquad S = \dfrac{U-A}{T} = R\ln Q + R\left(\dfrac{\partial \ln Q}{\partial \ln T}\right)_V$ $\hfill (2.8)$

Molar heat capacity at constant volume:

$$C_v = \left(\frac{\partial U}{\partial T}\right)_V = R\left(\frac{\partial \ln Q}{\partial \ln T}\right)_V + R\left(\frac{\partial^2 \ln Q}{\partial(\ln T)^2}\right)_V = \frac{R}{T^2}\left(\frac{\partial^2 \ln Q}{\partial(1/T)^2}\right)_V \tag{2.9}$$

The total energy of the system is the sum of all its parts that contribute to the energy, *i.e.,* translational, vibrational, external rotational, internal rotational, and electronic energies, $E_{tot,} = E_t + E_v + E_{ext.\ rot} + E_{int.\ rot} + E_e$. Substitution of the different constituents for energy, E_{tot}, and through some derivation, the partition function expression can be shown to be $Q_{tot} = Q_t\ Q_v\ Q_{ext.rot}\ Q_{int.rot}\ Q_e$. This will allow individual

considerations of thermodynamic properties to be determined, as well as the total contributions from these components. Once the partition functions are known, the thermodynamic properties from different contributions can be determined.

The translational partition function can be determined by solving the Schrodinger Equation for a system like "particle in a box." External rotation partition functions are difficult to derive, and as a result simplifications are made, *e.g.,* rigid rotator or linear rotator. Vibrational partition functions are determined from assumptions that the vibrations behave as harmonic oscillators. Electronic contributions, in general, are negligible compared to the other modes at room temperature. However, one can readily include the electronic contribution, providing energies in the low-lying electronic states are known.[13] Electronic contribution may be significant in radical species with strong spin-orbit coupling or having several low-lying electronic states. Ideal gas behavior is assumed in these cases.

Final terms for thermodynamic properties, after derivation from partition functions, for entropy are

$$S_{tot} = S_{trans} + S_{rot} + S_{vib} + S_e \tag{2.10}$$

$$S_{trans} = R\left[\frac{3}{2}\ln M_w + \frac{5}{2}\ln T - \ln P + \frac{5}{2} + \frac{3}{2}\ln\left(\frac{2\pi k_b}{h^2}\right) - \frac{5}{2}\ln N_A + \ln R\right] \tag{2.11}$$

$$S_{rot}^{linear} = R\left[1 + \ln\left(\frac{8\pi^2 k_b T}{h^2\sigma}I\right)\right] \tag{2.12}$$

$$S_{rot}^{non-linear} = \frac{3}{2}R + \frac{1}{2}R\ln\left[\frac{\pi}{\sigma^2}\left(\frac{8\pi^2 k_b T}{h^2}\right)^3 I_x I_y I_z\right] \tag{2.13}$$

$$S_{vib} = R\sum_i\left[\frac{x_i e^{-x_i}}{1 - e^{-x_i}} - \ln(1 - e^{-x_i})\right] \text{ where, } x_i = \frac{h\upsilon_i}{k_b T} \tag{2.14}$$

$$S_e = R\ln\omega_0 \tag{2.15}$$

Optical isomers are molecules that cannot be superimposed onto each other, but are a "mirror image" of each other and these also require an added consideration. Hydroperoxy species have one pair of optical isomers. The thermodynamic property that is affected by optical isomers, is entropy. The correction for a molecule with two optical isomers is:

$$S_{opt.iso} = R \ln \sigma_{opt.iso} \qquad (2.16)$$

And this correction entropy value is added to the above total entropy, S_{tot}, *i.e.,*

$$S_{corrected} = S_{tot} + S_{opt.iso} \qquad (2.17)$$

The molar heat capacity at constant volume and at constant pressure with assumption of ideal gas behavior, are expressed as follow:

$$C_{v,tot} = C_{V,trans} + C_{V,rot} + C_{V,vib} \text{ or } C_{P,tot} = C_{P,trans} + C_{P,rot} + C_{P,vib} \qquad (2.18)$$

$$C_{V,trans} = \frac{3}{2}R \text{ and with assumption of ideal gas behavior or } C_{P,trans} = \frac{5}{2}R \qquad (2.19)$$

$$C_{V,rot}^{linear} = C_{P,rot}^{linear} = \frac{2}{2}R \text{ and } C_{V,rot}^{non-linear} = C_{P,rot}^{non-linear} = \frac{3}{2}R \qquad (2.20)$$

$$C_{V,vib} = C_{P,vib} = R\sum_{i}\left[\frac{x_i^2 e^{-x_i}}{(1-e^{-x_i})^2}\right] \text{ where, } x_i = \frac{h\upsilon_i}{k_b T} \qquad (2.21)$$

Notation for above equation to find entropy and the molar heat capacity includes: universal gas constant (R), temperature (T), pressure (P), molecular weight (M_w), Boltzman's constant (k_b), Planck's constant (h), Avogadro's number (N_A), moment of inertia about the principle axis (I, I_x, I_y, I_z), i[th] vibrational frequency (υ_i), optical isomer ($\sigma_{opt.iso}$), and spin degeneracy (ω_0).

Hindered Rotor

It is well known that there are accuracy issues in determining the lower frequency torsions corresponding to internal rotations. Replacing these frequencies with methods to treat the internal rotations as hindered rotors increases the accuracy for *S(T)* and *Cp(T)*.

The initial research of Pitzer and Gwinn[15-17] addressed contributions from symmetrical and unsymmetrical rotating groups on a rigid frame. Later, work by Kilpatrick and Pitzer[18] was expanded to include balanced and unbalanced linked rotating groups. These studies still serve as a basis for current research and development for new methods for treating internal rotations.

VIBIR

Internal rotation contributions are calculated using the Pitzer and Gwinn[15-17] approximation method as calculated in the VIBIR[19] code. This method is best suited for rotations where the potential energy as a function of the angle, $V(\phi)$, can be expressed as

$$V(\phi) = \sum_m \frac{1}{2} V_m \, 1\text{-}\cos \sigma_m \phi_m \qquad (2.22)$$

where V_m is the height of the potential barriers and m is the foldness of the potential energy graphs for each bond rotation. Reduced moments of inertia are calculated based on the optimized geometries using the mass and radius of rotation for the rotational groups. There are no adjustments for coupling of internal rotor motion with vibration and VIBIR assumes that the rotational groups are symmetrical, which is accurate for primary and terminal methyl group rotation, for example. Other types of rotational barriers are also estimated using averages of the calculated barrier heights.

ROTATOR

Another method for calculation of internal rotation contribution is the ROTATOR[20] code. This technique employs expansion of the hindrance potential in Fourier series, calculation of the Hamiltonian matrix in the basis of free rotation wave functions and subsequent calculation of energy levels by direct diagonalization of the Hamiltonian matrix.

The following form of the Fourier series is often used for conventional representation of the dependence of hindered potential on torsional angle:[21 - 23] In ROTATOR the torsional potential calculated at a discreet torsional angle is fitted by a truncated Fourier series in the following:

$$V(\phi) = a_0 + a_1 \cos(\phi) + a_2 \cos(2\phi) + a_3 \cos(3\phi) + b_1 \sin(\phi) + b_2 \sin(2\phi) \qquad (2.23)$$

The matrix elements of individual sine and cosine terms in the basis of free rotor wave functions have a simple appearance. The terms $\sin(m\phi)$ and $\cos(m\phi)$ induce transitions with $\Delta K = \pm m$, where K is the rotational quantum number. Moreover, the matrix element does not depend on K, which leads to a simple form of the Hamiltonian matrix. The matrix has a band structure and consists of diagonal terms that are equal to those of the free rotor and subdiagonales of constant values that correspond to a different terms in the potential expansion.

The Hamiltonian matrix can therefore be truncated to the size of $2K_{max}+1$, where K_{max} is the maximum rotational quantum number. The truncated matrix (in reduced dimensionless form) is diagonalized, and calculated eigenvalues are used to calculate partition function, entropy, heat capacity, etc., using direct summation over the calculated energy levels. A detailed description with examples and comparisons can be found in a published by Krasnoperov, Lay and Shokhirev.[20]

2.3 Kinetic Analysis

2.3.1. Lindemann-Hinshelwood Mechanism for Unimolecular Reactions

In 1922, Lindemann[24] proposed a general theory for the thermal unimolecular reactions that forms the basis for the current theory of thermal unimolecular rates. He proposed that molecules become energized by bimolecular collisions, with a time lag between the moment of collisional energization and the time the molecule decomposes. Energized molecules could then undergo deactivating collisions before decomposition occurred. A major achievement of Lindemann's theory is its ability to explain the experimental finding that the reaction rate is pressure dependent, which is a failure in the Radiation Hypothesis. The mechanism in Lindemann theory is written as:

$$A + M \xrightarrow{k_1} A* + M$$

$$A* + M \xrightarrow{k_{-1}} A + M$$

$$A* \xrightarrow{k_2} Products$$
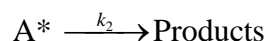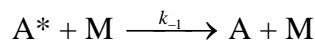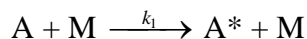
Rate k_{uni} and k_2 are defined as:

$$d[product]/dt = k_{uni} \times [A] = k_2 \times [A*] \tag{2.24}$$

The asterisk indicates that A contains sufficient internal vibration energy to decompose. This energy is denoted by E and must be greater than the unimolecular decomposition threshold energy E_0. The concept is that:

(a) A certain fraction of the molecules become energized by collision, *i.e.,* gain energy in excess of E_0.

(b) The rate of the energy transfer process depends upon the rate of bimolecular collisions. Energized molecules are de-energized by collision, which is a reverse reaction.

This de-energized rate is taken to be energy-independent and is equated with the collision number Z_1 by assuming that every collision of A* leads to a de-energized state. This is known as "strong collision assumption" for de-energizing collisions.

(c) There is a time-lag between the energy transfer and unimolecular dissociation and isomerization of the energized molecules. This unimolecular dissociation also occurs with a rate constant k_3 independent of the energy content of A*.

The overall concept can be expressed by the equations below, where M can represent a generic bath gas molecule, an added "inert" gas molecule; it may also represent a second molecule of reactant or product. In the simple Lindemann theory k_1, along with k_2 and k_3 are taken to be energy-independent and are calculated from the simple collision theory equation.

Application of the steady-state hypothesis to the concentration of A*, allows the unimolecular rate constant and the high pressure and low pressure limit rate and rate constants to be determined as follows:

$$\text{Rate} = k_{uni} [A] = k_2 [A^*] = k_1 k_2 [A] [M] / (k_{-1} [M] + k_2) \tag{2.25}$$

$$k_{uni} = k_1 k_2 [M] / (k_{-1} [M] + k_2) \tag{2.26}$$

$$\text{High-pressure limit rate, } [M] \rightarrow \infty, k_{uni} = k_\infty = k_1 k_2 / k_{-1} \tag{2.27}$$

$$\text{Low-pressure limit rate, } [M] \rightarrow 0, k_{uni} = k_0 = k_1 [M] \tag{2.28}$$

The unimolecular rate constant is then written as

$$k_{uni} = k_\infty / (1 + k_\infty / k_1 [M]) \tag{2.29}$$

One can expect the Lindemann theory to predict a linear change in the initial rate of a unimolecular reaction with respect to concentration of M at low pressure. The transition from high-pressure rate constant to low pressure is called "fall-off region".

The k_1 in the original Lindemann theory is taken from the collision theory

expression: $\quad\quad k_1 = Z_1 \exp(-E_0/k_b T)$ $\quad\quad\quad\quad\quad\quad\quad\quad$ (2.30)

$\quad\quad\quad$ with $Z_1 = (\sigma_d^2 N_A/R)(8\pi N_A k/\mu)^{1/2}(1/T)^{1/2}$ $\quad\quad\quad\quad\quad$ (2.31)

where Z_1 will be in Torr^{-1}-s^{-1} (consistent with [M] in Torr and k_2 in s^{-1}) when σ_d =

collision diameter in cm; μ = reduced molar mass in g-mol^{-1} = $(1/M_A + 1/M_B)^{-1}$; T =

temperature in Kelvin; N_A is Avogadro constant 6.022×10^{23} mol^{-1}; R is gas constant

6.2326×10^4 cm^3-Torr-K^{-1}-mol^{-1} or 0.082 atm-lit/mol-K; k_b (Bolzmann constant) =

1.3805×10^{-16} erg-K^{-1}.

The Lindemann theory, unfortunately, predicts the fall-off in k_{uni} to occur at much

higher pressure than what is observed experimentally.

Based on the Lindemann's suggestion that k_1 could be increased by assuming that

the required energy (energized molecules) could be drawn in part from the internal

degrees of freedom (mainly vibration) of the reactant molecule, Hinshelwood[25] increases

k_1 by using a much higher probability of a molecule possessing total energy $\geq E_0$ in s

classical degrees of freedom, $(E_0/k_b T)^{s-1}\exp(-E_0/k_b T)/(s-1)!$, than the simpler $\exp(-E_0/k_b T)$

Lindemann used. The result is

$\quad\quad\quad\quad\quad k_1 = [Z_1/(s-1)!](E_0/k_b T)^{s-1}\exp(-E_0/k_b T)$ $\quad\quad\quad\quad$ (2.32)

Since k_1 increases with s classical degrees of freedom in the Lindemann-

Hinshelwood theory, then $k_2 = k_\infty k_{-1}/k_1$ should decrease with s. Thus the lifetime of the

energized molecule t $\approx 1/k_2$ increases when the molecule can store energy among a

greater number of degrees of freedom. Then k_2 is expected to depend on the energy of

A*. Making k_2 energy-dependent, expressed as $k(E)$, the energy interval from E to $E+dE$

is considered:

$$A + M \xrightarrow{dk_1} A^* (E, E+dE) + M$$

$$A^*(E, E+dE) + M \xrightarrow{k_{-1}} A + M$$

$$A^*(E, E+dE) \xrightarrow{k(E)} Products$$
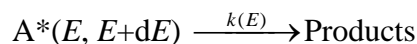
Then $dk_{uni} (E, E+dE) = k(E)(dk_1/k_{-1}) / (1 + k(E)/k_{-1} [M])$ $\hspace{2cm}$ (2.33)

It is assumed that for all pressure dk_1/k_{-1} represents the equilibrium probability and that the A* has energy between E and $E+dE$. This probability may be denoted $P(E)dE$. Also k_{-1} [M] is the collision frequency ω between A* and M, then

$$k_{uni} = \int_{E0}^{\infty} k(E)P(E)dE/(k(E)+\omega) \hspace{2cm} (2.34)$$

In order to make accurate quantitative predictions of the fall-off behavior of a unimolecular reaction, it is essential to take into account the energy dependence of the rate constant $k(E)$ (or k_2) for the conversion of energized molecules into activated complexes where products result from decomposition or reaction of the energized complex. Two quite different approaches may be taken to determine $k(E)$. One is to consider the explicit nature of the intramolecular motion of highly energized molecules, such as Slater theory. The other approach is based on statistical assumptions, such as RRK (Rice-Ramsperger-Kassel) theory and its extension, RRKM (Marcus) theory. Most modern theories of unimolecular reaction rates, including the Slater theory, the RRK theory and the RRKM theory, are based on the fundamental Lindemann mechanism involving collision energy transfer of the reactant molecules, and more specifically on Hinshelwood's development.

2.3.2 Slater Theory

Slater[26] in 1939 pictured a molecule as an assembly of harmonic oscillators. Decomposition is assumed to occur when a critical coordinate (*i.e.,* a bond length or bond angle) attains a critical displacement. The attainment of the reaction coordinate critical extension is not a statistical random process as in RRKM Theory, but depends on the energies and phases of the specific normal mode excited. Since energy does not flow freely within the molecule, the theory predicts intrinsic non-RRKM behavior. Overall the Slater Theory is unsuccessful in interpreting experiments.

2.3.3 RRK Theory of Unimolecular Reactions

The RRK theory was developed independently by Rice and Ramsperger[27] and Kassel.[28-30] Both Rice and Ramsperger theory and Kassel theory consider that for reaction to occur a critical energy E_0 must become concentrated in one part (specific vibration) of the molecule. They used the basic Lindemann-Hinshelwood mechanism of collision energy transfer and de-energization, but assumed more realistically that the rate constant for conversion of an energized molecule into products is proportional to a specific probability. This is a finite statistical probability that energy, E_0, is found in the relevant part of the energized molecule which contains total energy, E, is greater than E_0 since E of the molecule under consideration is assumed to be rapidly redistributed around the molecule. This probability will increase with E and make k_2 a function of its energy content; k_2 is not "energy" dependent.

      The difference between the two models (Rice and Ramsperger versus Kassel) is two-fold. First, Rice and Ramsperger used classical statistical mechanics throughout, while Kassel used classical methods and also developed a quantum treatment. The

quantum method turns out to be much more realistic and accurate. Second, different assumptions were made about the part of the molecule into which the critical energy E_0 has to be concentrated. The Kassel's model seems slightly more realistic by assuming the energy had to be concentrated into one oscillator. The quantum version of the Kassel theory serves as a theoretical basis for calculations performed in this thesis.

The classical RRK theory is based on the notion that the probability that a molecule of *s* classical oscillators with total energy *E* has energy greater than E_0 in one chosen oscillator, which is the critical mode leading to reaction. The assumptions used to derive the quantum RRK rate constant are similar to those for classical theory. In the quantum theory it is assumed there are s identical oscillators in the molecule, all having frequency, ν. The energized molecule has n quanta, so $E = nh\nu$. The critical oscillator must have m quanta for dissociation occurrence, m = $E_0/h\nu$.

The probability that one oscillator contains at least m quanta; probability (energy ≥ m quanta in one chosen oscillator) is then equal to:[31,32]

$$\text{Probability} = \frac{n!(n-m+s-1)!}{(n-m)!(n+s-1)!} \tag{2.35}$$

Hence,
$$k_a(nh\upsilon) = A\frac{n!(n-m+s-1)!}{(n-m)!(n+s-1)!} \tag{2.36}$$

Where A is a proportion constant and the same as the classical one.

The corresponding $k_1(E)$ of the Hinshelwood expression is now derived. It refers to energy transfer into a specific quantum state rather than into an energy range *E* to *E*+d*E*, as

$$k_1(nh\upsilon) = k_2\alpha^v(1-\alpha)^{s-1}\frac{(n+s-1)!}{n!(s-1)!} \tag{2.37}$$

Where $\alpha = \exp(-h\nu/k_bT)$
$$\tag{2.38}$$

Both classical and quantum versions RRK theory were developed, and in the limit of a large excitation energy E the two versions become identical.

In RRK theory, the assumption is made that the rate of conversion of energized molecules into products is related to the probability that the critical energy E_0 is concentrated in one part of the molecule, *e.g.,* in one oscillator (Kassel theory) or in one squared term (Rice-Ramsperger theory). This probability is a function of the total energy E of the energized molecule, and the total vibrations among which the vibration energy quanta can be distributed.

2.3.4 RRKM Theory of Unimolecular Reactions

The RRKM theory was developed using the RRK model and extending it to consider explicitly vibration and rotation energies and to include zero point energies. Several minor modifications of the theory have been made, primarily as a result of improved treatments of external degrees of freedom.

RRKM theory is a microcanonical transition state theory.

$$A^* \xrightarrow{\;k(E)\;} A^{\neq} \to \text{Products}$$
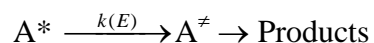
Where $A^{\neq}$ is the transition state.

Different experimental techniques, including static pyrolysis, carrier (flow) techniques, shock tube methods, and very-low-pressure-pyrolysis, have been used to measure k_{uni} as a function of temperature and pressure. One of the most significant achievements of RRKM theory is its ability to match measurements of k_{uni} with pressure.

2.3.5 Chemical Activation Reactions

The energization methods other than by molecular collision, such as photoactivation and chemical activation, may produce a non-equilibrium situation in which molecules acquire energies far in excess of the average thermal energy. This presence of excess energy in the energized adduct makes chemical activation reactions much more important in these systems. A treatment for the rate of conversion, which includes decomposition of energized adduct to product(s) (including back to reactant) and the competing rate of its collision stabilization, is needed.

The basic idea of the treatment of a chemical activation system is that a vibration excited molecule ABC^* formed by an association of reactants can reform reactants A + BC with a rate constant $k'(E)$, form decomposition products, AB + C, with a rate constant $k_a(E)$ or be de-energized to stable molecules ABC.

In the strong collision assumption the first order rate constant for de-energization is equal to the collision frequency, $\omega = Zp$ where p is the total pressure and Z is collision number. This assumes that stabilization occurs at energy collision.

Suppose that the fraction of molecules which are energized per unit time into the energy range between E and $E+dE$ is f(E)dE. To simplify, one can consider decomposition path (back to reactant, A + BC, as the decomposition path), then the fraction of ABC^* decomposing (path A + BC) compared with those stabilized (path ABC) is $k(E)/[k(E)+\omega]$. The fraction of molecules in the energy range between E and $E+dE$ decomposing to products is therefore $\{k(E)/[k(E)+\omega]\}f(E)dE$, and the total number of molecules decomposing per unit time (D), at all energies above the critical energy E_0, is:

$$D = \int_{E_0}^{\infty} \frac{k(E)}{k(E) + \omega} f(E) dE \tag{2.39}$$

Corresponding, the total rate of stabilization (S) is:

$$S = \int_{E_0}^{\infty} \frac{\omega}{k(E) + \omega} f(E) dE \tag{2.40}$$

Considering an average rate constant $<k>$ for all energies above E_0, one would have:

$$\frac{<k>}{\omega} = \frac{D}{S} = \frac{No.\,molecules\,decomposing\,per\,unit\,time}{No.\,of\,molecules\,being\,stabilized\,per\,unit\,time} \tag{2.41}$$

So,

$$<k> = \omega \frac{\int_{E_0}^{\infty} \{k(E)/[k(E) + \omega]\} f(E) dE}{\int_{E_0}^{\infty} \{\omega/[k(E) + \omega]\} f(E) dE} \tag{2.42}$$

The $f(E)$ is the distribution function of energized molecules in the energy range between E and $E+dE$. In the thermal energy transfer systems, this distribution function is simply the thermal quantum Boltzmann distribution $K(E)$ and the rate of energy transfer into the energy range between E and $E+dE$ is $K(E)dE = dk_1/k_2$. For the chemically activated system described here, the distribution function can be derived by applying the principle of detailed balancing to the reverse process to reactants. Consider a situation in which other processes can be ignored and equilibrium is established between A^* and reactants. Then the fraction of molecules with energy between E and $E+dE$ is Boltzmann distribution $K(E)dE$, so the rate of dissociation to reactants is then $K'(E)K(E)dE$, and by the principle of detailed balancing this also gives the rate of combination of reactants to give A^* in this energy range. The total rate of energy transfer to all levels above the minimum energy E_{min} (the minimum energy of A^*) is:

$$\text{Total rate of energization} = \int_{E_0}^{\infty} k'(E)K(E)dE \tag{2.43}$$

Therefore, the distribution function is given by:

$$f(E)\delta E = \frac{k'(E)K(E)dE}{\int_{E_0}^{\infty} k'(E)K(E)dE} \tag{2.44}$$

The f(E)dE can be incorporated into QRRK theory for $k(E)$ and $k_1(E)$ serves as a basis for the calculations for chemical activation reaction systems.

2.3.6 QRRK Analysis for Unimolecular and Chemical Activation Reactions

QRRK analysis, as initially presented by Dean[33-35] combined with the modified strong collision approach of Gilbert et al.[36-38], to compute rate constants for both chemical activation and unimolecular reactions, over a range of temperature and pressure. The computer program CHEMASTER, based on the QRRK theory outlined as above, and unimolecular dissociation and chemical activation formalism carries out all unimolecular and chemical activation reactions involved in this thesis. The input parameters for CHEMASTER are: (1) High-pressure limit rate constants (Arrhenius A factor and activation energy E_a) for each reaction included for analysis; (2) A reduced set of three vibration frequencies and their associated degeneracy; (3) Lennard-Jones transport parameters, (s (Angstroms) and e/k (Kelvin)), and (4) molecular weight of well species.

High pressure limit rate constants k_∞'s are fitted by three parameters A_∞, n, and Ea over temperature range from 298 to 2000 K, $k_\infty = A_\infty(T)^n \exp(-Ea/RT)$. Entropy differences between reactant and transition state are used to determine the pre-exponential factor, A, via canonical Transition State Theory (TST):

$$A = (k_b T/h)\exp(\Delta S^{\neq}/R), \qquad Ea = \Delta H^{\neq} \tag{2.45}$$

Where *h* is the Planck constant and k_B is the Boltzmann constant. $\Delta S^{\neq} = S(\text{TST}) - S(\text{reactants})$ and $\Delta H^{\neq} = H(\text{TST}) - H(\text{reactants})$. Treatment of the internal rotors for *S* and *Cp*(T) of reactants and the TST's is important here because these internal rotors are often lost in the cyclic transition state structures. Pre-exponential factors (A_{∞}), are calculated from structures determined by (Density Functional Theory) DFT or estimated from the literature and from trends in homologous series of reactions. Activation energies come from DFT plus evaluated endothermicity of reaction ΔU_{rxn}, from analysis of Evans-Polanyi relationships for abstractions plus evaluation of ring strain energy, and from analogy to similar reactions with known energies. Thermochemical properties are provided for each system.

Reduced sets of three vibration frequencies and their associated degeneracies are computed from fits to heat capacity data, as described by Ritter and Bozzelli et al. [39,40] These have been shown by Ritter to accurately reproduce molecular heat capacities, *Cp*(T), and by Bozzelli et al.[40] to yield accurate ratios of density of states to partition coefficient, $\rho(E)/Q$.

Lennard-Jones parameters, sigma (angstroms) and ε/k (Kelvin's), are obtained from tabulations[41] and from a calculation method based on molar volumes and compressibility.[42]

When necessary, estimation is done in a consistent and uniform manner via use of generic reaction rate constants with reference to literature, experiment or theoretical calculation in each case. The QRRK calculation input parameters and their references are listed in the table associated with the respective reaction system.

Quantum RRK /Master Equation Calculation.

The quantum RRK (QRRK) / master equation analysis is described by Chang et al.[33,43] The QRRK code utilizes a reduced set of three vibration frequencies which accurately reproduce the molecule's (adduct) heat capacity; the code includes contribution from one external rotation in calculation of the ratio of the density of states to the partition coefficient $\rho(E)/Q$.

Comparisons of ratios of these $\rho(E)/Q$ with direct count $\rho(E)/Q$'s are shown to be in good agreement.[37] Rate constant results from the quantum RRK - Master equation analysis are shown to accurately reproduce (model) experimental data on several complex systems. They also provide a reasonable method to estimate rate constants for numerical integration codes by which the effects of temperature and pressure can be evaluated in complex reaction systems.

CHAPTER 3

THERMOCHEMICAL PROPERTIES FOR A SERIES OF NITROCARBONYLS, NITROOLEFINS, CORRESPONDING NITRITES AND THEIR CARBON CENTERED RADICALS

3.1 Overview

Structures, enthalpy ($\Delta_f H^o{}_{298}$), entropy ($S^o(T)$), and heat capacity ($C_p(T)$) are determined for a series of nitrocarbonyls, nitroolefins, corresponding nitrites and their carbon centered radicals using the density functional B3LYP and composite CBS-QB3 calculations. Enthalpies of formation ($\Delta_f H^o{}_{298}$) are determined at the B3LYP/6-31G(d,p), B3LYP /6-31+G(2d,2p) and composite CBS-QB3 levels using several work reactions for each species. Entropy (S) and heat capacity ($C_p(T)$) values from vibration, translational, and external rotational contributions are calculated using the rigid-rotor-harmonic-oscillator approximation based on the vibration frequencies and structures obtained from the density functional studies. Contribution to $\Delta_f H^0(T)$, S, and $C_p(T)$ from analysis on the internal rotors is included. Recommended values for enthalpies of formation of the most stable conformers of nitroacetone *cc(=o)cno2*, acetonitrite *cc(=o)ono*, nitroacetate *cc(=o)no2* and acetyl nitrite *cc(=o)ono* are -51.6 kcal mol^{-1}, -51.3 kcal mol^{-1}, -45.4 kcal mol^{-1} and -58.2 kcal mol^{-1}, respectively. The calculated $\Delta_f H^o{}_{298}$ for nitroethylene *c=cno2* is 7.6 kcal mol^{-1} and for vinyl nitrite *c=cono* is 7.2 kcal mol^{-1}. An unusual phenomena is found, there is an isomerization with an unusual low barrier (3.6 kcal mol^{-1} in the acetyl-nitrite). Here the NO of the nitrite (R-ONO) in CH$_3$C(=O')ONO moves to the C=O' oxygen in a motion of a stretching frequency and then a shift to the carbonyl oxygen (marked as O' below).

$$\text{CH}_3\text{C(=O')ONO} \leftrightarrow \text{CH}_3\text{C(-O'NO)=O} \quad E_a = 3.6 \text{ kcal mol}^{-1}$$
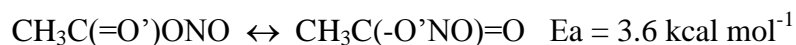
3.2 Previous Studies

Accurate formation enthalpies, $\Delta_f H^o_{298}$, for nitro and nitrite molecules are required to understand reaction paths and assist in the development of detailed chemical kinetic mechanisms which can be applied to model the formation and reactions of nitrogen species in a variety of environments, particularly for atmospheric and combustion chemistries. Since only a small fraction, about 0.02% of known organic species have had their heats of formation measured[44] the application of quantum chemistry methods for this data is of value, provided that reasonable accuracy can be obtained. The establishment of these values will also aid in the determination of the thermochemical properties of higher homologues *via* use of isodesmic reactions with group conservation (isogeitonic reactions). This study continues development and evaluation of thermochemical properties on simplest nitro- and nitrite compounds from previous analysis[45, 46]

Nitro (RNO_2) and nitrite (RONO) derivatives of hydrocarbons undergo thermal decomposition at relatively low temperatures and hence have potential as both propellants and energetic materials. The reaction barriers for bond cleavage of R-NO_2 (alkyl nitro compounds) and RO-NO (corresponding nitrites) are *ca.* 61 and 40 kcal mol^{-1}, respectively.[47-58] The nitro alkanes and alklyl nitrites can release NO and NO_2 and hence can serve as catalysts in oxidation of hydrocarbons.[59-61] In this regard, nitro compounds have been widely studied by both experimental and theoretical methods,[47-58, 62-85] nevertheless, the thermochemical data are surprisingly limited.

The structures, heats of formation, bond dissociation energy, etc. of nitro and nitrite molecules have been the subjects of many experimental and theoretical investigations. Shaw[86] used group additivity to predict $\Delta_f H^o{}_{298}$ in nitroethylene at 12.4 kcal mol^{-1} and Dewar[57] preformed MINDO/3 calculation with 17.8 kcal mol^{-1}. Gutowski [62] reported heat of formation by CCSD(T) calculation on energetic material with 9.5 kcal mol^{-1} for nitroethylene while Benson[87] also suggested 9 kcal mol^{-1}. Ashcraft[90] determined thermochemical properties and group values for nitrogen-containing molecule with CBS-QB3 based atomization method with spin-orbit and additivity corrections (BACs): $\Delta_f H^o{}_{298}$ of vinyl nitrite and nitroethylene are 8.5 kcal mol^{-1} and 8.9 kcal mol^{-1}, respectively.

In the present work, the formation enthalpies of several nitrocarbonyls, nitroolefins, corresponding nitrites and their carbon centered radicals are evaluated based on their most stable rotation conformers using multilevel and individual computational chemistry methods. Both complete basis set and Gaussian composite calculation methods are used. These methods employ a variety of different geometries, frequency determinations and higher order energy corrections. The accuracy of these methods has been demonstrated in previous studies on HONO isomers [45] and methyl and ethyl nitro and nitrite compounds.[46]

An interesting phenomona in an isomerization with an unusual low barrier (3.6 kcal mol^{-1} in the acetyl-nitrite is found. Here the NO of the nitrite (R-ONO) in $CH_3C(=O')ONO$ moves to the C=O' oxygen.

$$CH_3C(=O')ONO \leftrightarrow CH_3C(-O'NO)=O \quad Ea = 3.6 \text{ kcal mol}^{-1}$$
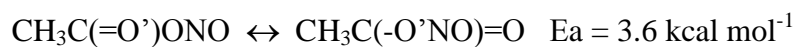
3.3 Computational Methods

The relative stability of RONO and RNO_2 isomers, homolytic bond dissociation energies and the heats of formation of radicals and molecules obtained from isodesmic reactions have been performed using B3LYP hybrid density functional theory method in conjunction with the 6-31G(d,p) and 6-31+G(2d,2p) basis sets, as well the complete basis set - QB3 composite method. CBS-QB3 is a multilevel model chemistry that combines the results of several *ab initio* and DFT individual methods and empirical terms to predict molecular energies with high accuracy and reasonable computational cost. The required electronic structure calculations are outlined as follows: (i) B3LYP/6-311G(2d,d,p) level geometry and frequencies; (ii) MP2/6-311G(3df,2df,2p) energy and CBS extrapolation; (iii) MP4-(SDQ)/6-31G(d(f),p) energy; (iv) CCSD(T)/6-31G energy corrections. All quantum chemical calculations have been performed within the Gaussian-03 suite of programs.[89]

The variety of homodesmic and isodesmic work reactions are used, where the bonding environments are similar in products and reagents. A homodesmic reaction is a hypothetical reaction where the number and type of bonds (according to the state of hybridization) are conserved on both sides of the reaction. An isodesmic reaction is one where the number of bonds of each type, are conserved on each side of the work reaction.
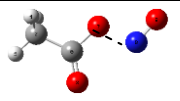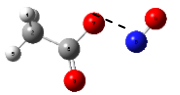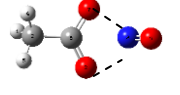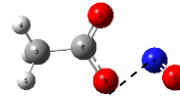
3.4 Results and Discussion

The optimized geometries at the CBS-QB3 composite level of theory (*viz.,* B3LYP/6-311(2d,d,p) calculations) for the target molecules and corresponding abbreviated nomenclatures are presented in Figure 3.1. The *trans* configurations of the nitrite group

(C-O-N-O dihedral angles) in acetonitrite, vinyl nitrite and acetyl nitrite are more stable than corresponding *cis* isomer by 0.12 kcal mol^{-1}, 1.72 kcal mol^{-1} and 3.94 kcal mol^{-1}, respectively. In nitroacetone and acetonitrite, nitro and nitrite group are also in *trans* configuration to carbonyl oxygen. One oxygen in nitroethylene and the nitrogen in vinyl nitrite are eclipsed with a hydrogen atom on the first carbon while one oxygen in nitroacetate and nitrogen in acetyl nitrite are eclipsed with carbonyl oxygen.

There is -N=O switching that occurs in the acetyl nitrite. The NO group in the nitrite moiety starts to leave in a stretching mode, then without any significant rotation of the $CH_3C(=O')O$--NO at about 2.02 angstroms separation the --NO moves (shifts without much rotation) to the carbonyl oxygen. This phenomena was observed in the scan of the $CH_3C(=O')$--NO bond cleavage which reverses the positions of the nitric-oxide group of the ONO, forming $CH_3C(O'NO)=O$ with a very low barrier of 3.6 kcal mol^{-1} Table 3.1 shows structures and the corresponding bond lengths of the cleaving and forming RO-- NO bonds in this nitric-oxide switching.

Table 3.1 Structures, Corresponding Bond Length and Relative Energy of the Oxygen Switching

Structure	Bond length (A°)		Relative energy (kcal mol^{-1})
	O_1 -- N	O_2 -- N	
	1.56	2.7	0
	1.76	2.76	3.6
	1.96	2.06	3.1
	2.36	1.7	2.9
	2.66	1.52	-0.1

CH₃C(=O)CH₂NO₂ (*cc(=o)cno2*) **CH₃C(=O)CH₂ONO** (*cc(=o)ono*) **CH₂=CHNO₂** (*c=cno2*)

Nitroacetone   Acetonitrite   Nitroethylene

CH₂=CHONO (*c=cono*)   **CH₃C(=O)NO₂** (*cc(=o)no2*)   **CH₃C(=O)NO₂** (*cc(=o)ono*)

Vinyl nitrite   Nitroacetate   Acetyl nitrite
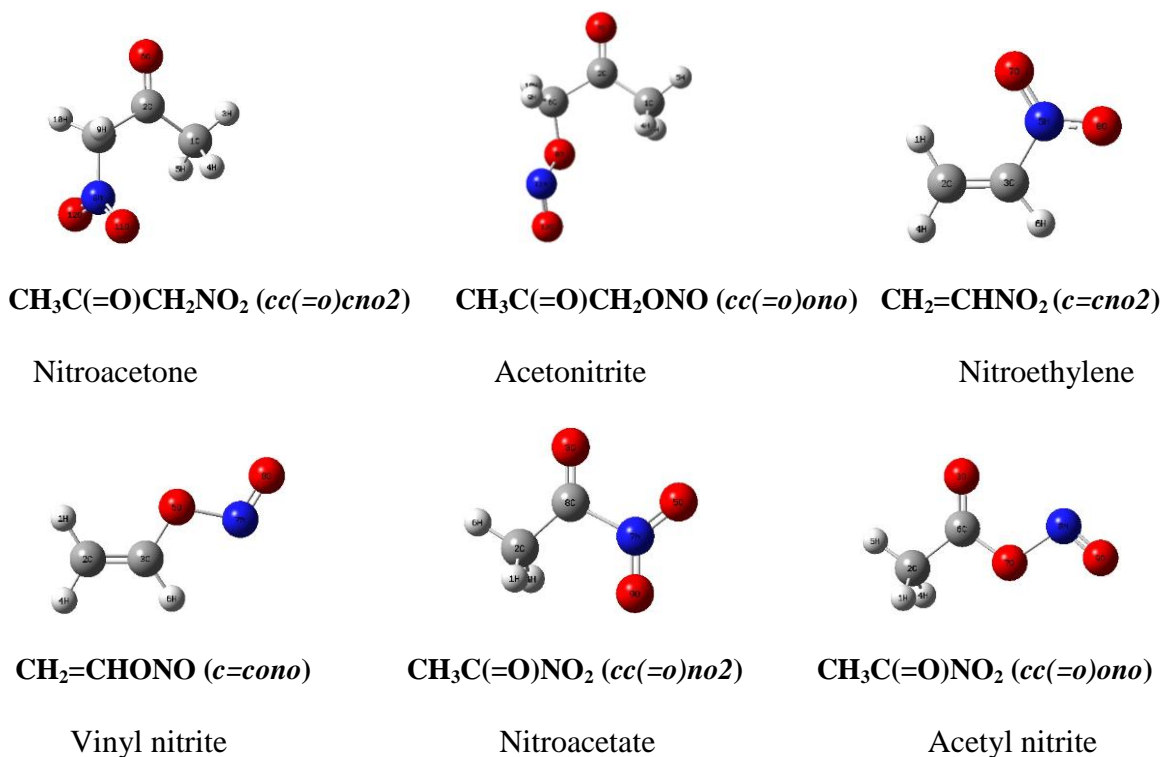
Figure 3.1 Geometry of the lowest energy conformer of the target molecules and abbreviated nomenclatures.

3.4.1 Enthalpies of Formation ($\Delta_f H^o_{298}$)

Energies of the lowest energy conformer from the CBS-QB3 composite level are used with a series of isodesmic reactions having bond conservation to estimate the enthalpy of formation ($\Delta_f H^o_{298}$) for target molecules (see internal rotor potential section below for further information on low energy structure) The total energies are corrected by zero-point vibration energies (ZPVE), which are scaled by 0.97 as recommended by Scott and Radom. Thermal correction, 0-298.15 K, is calculated to estimate $\Delta_f H^o_{298}$ at the 298.15 K. The calculated $\Delta_{rxn} H^{\circ}_{298}$ in the formula is used to find $\Delta_f H^o_{298}$ of the target reactant:

$$\Delta_{rxn} H^{\circ}_{298} = \Sigma\ H_f\ \text{products} -\ \Sigma\ H_f\ \text{reactants} \qquad (2.2)$$

where the two products and one reactant are the three reference molecules, the evaluated literature thermodynamic properties are used for the three reference species. The standard enthalpies of formation at 298.15 K of the reference species used in these reactions are summarized in Table 3.2

The method of isodesmic reactions utilizes a similarity in the bonding environments for reactant and product sets in a work reaction to effect a cancellation of systematic errors in the *ab initio* or density functional calculations. The basic requirement of an isodesmic reaction is that the number of each type of bond is conserved in the reaction. Calculations are performed on each species in three work reactions for each molecule. The enthalpies of formation of the target molecules obtained from the use of the reaction schemes are shown in Table 3.3. Lowest energy configuration structures of the radicals are illustrated in Figure 3.2. Summary of formation enthalpies for a series of nitrocarbonyls, nitroolefins compounds calculated at evaluated at different levels of theory are shown in Table 3.5. Values from CBS-QBS are recommended which is the highest level calculation method in this work. The accuracy of these methods has been demonstrated in previous studies[45, 46] on HONO isomers and methyl and ethyl nitro and nitrite compounds. Ashcraft and Green et al.[90] also reported thermochemical properties for several nitrogen-containing, stable molecules with the CBS-QB3 based atomization method which included spin-orbit and additivity corrections (BACs). Error limits are assigned as the sum of the following error bounds: Standard deviation of the three working reactions, reported errors for each of the standard species, and 0.11 estimate in thermal energy for each species in the work reaction (4 species, 0.44 total)

Table 3.2 Standard Enthalpies of Formation at 298.15 K of Reference Species

Species	$\Delta_f H^o_{298}$ (kcal mol^{-1})	Source (Ref. No.)
CH_4	-17.89	91
C_2H_4	12.54	91
C_2H_6	-20.04	91
C_3H_8	-25.02	91
C_3H_6	4.88	91
$CH_2=CHCH_2CH_3$	-0.15	91
$C{\bullet}H=CH_2$	71.00	91
$CH_3C{.}HCH_3$	22.00	91
$C{\bullet}H_2CH_2CH_3$	23.90	91
$CH_3C(=O)CH_3$	-51.90	91
$CH_2=CH{\bullet}CH_2$	39.13	92
$C{\bullet}H=CHCH3$	64.30	92
$CH_2=C{\bullet}CH_3$	58.89	92
CH_3NO_2	-17.67	45
CH_3ONO	-15.64	45
$CH_3CH_2NO_2$	-25.06	45
CH_3CH_2ONO	-23.58	45
$C{\bullet}H_2NO_2$	31.53	45
$C{\bullet}H_2C(=O)CH_3$	-8.34	93
$C{\bullet}H_2C(=O)H$	3.510	93
$CH_3C(=O)H$	-39.70	93

CH₂C(=O)CH₂NO₂

(cjc(=o)cno2)

CH₃C(=O)CHNO₂

(cc(=o)cjno2)

CH₂C(=O)CH₂ONO

(cjc(=o)cono)

CH=CHNO₂

(cj=cno2)

CH₂=CNO₂

(c=cjno2)

CH=CHONO

(cj=cono)

CH₂C(=O)NO₂

(cjc(=o)no2)

CH₂C(=O)ONO

(cjc(=o)ono)
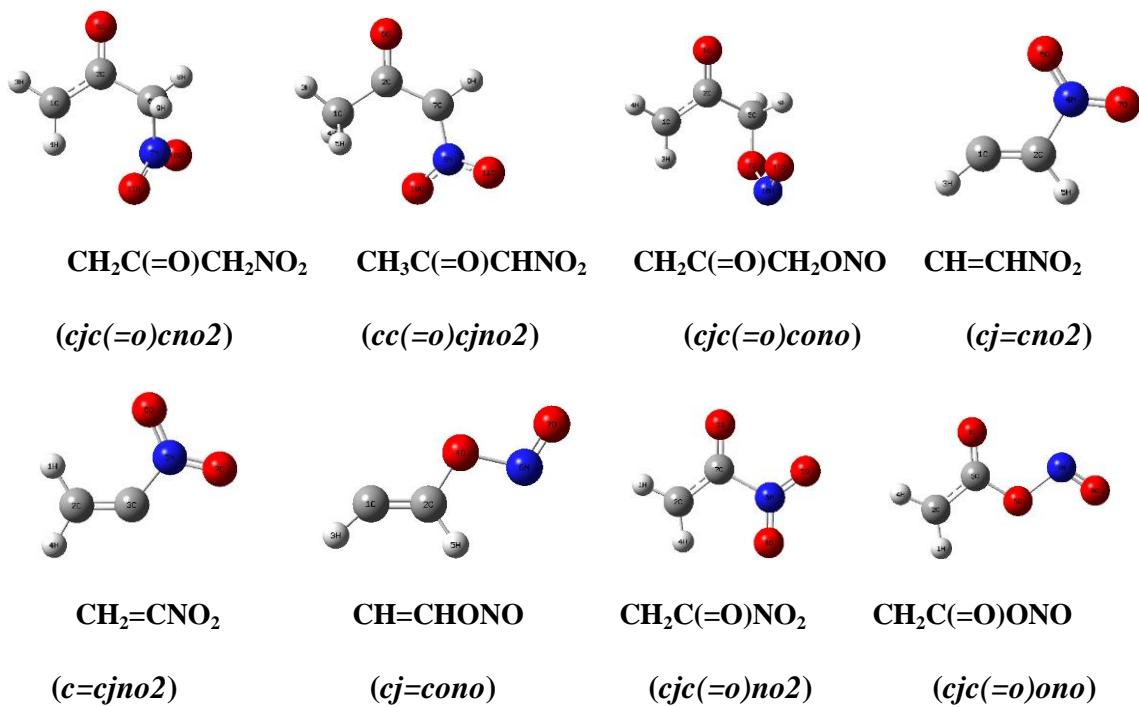
Figure 3.2 Structures and nomenclature for the lowest energy conformers of radicals corresponding to the loss of a hydrogen atom from parent molecules.

Table 3.3 Evaluated Enthalpies of Formation at 298 K of Target Molecules

Work Reactions							$\Delta_f H^o(298)$ kcal mol^{-1}		
							B3LYP		CBS-QB3
							6-31G(d,p)	6-31+G(2d,2p)	
CH$_3$C(=O)CH$_2$NO$_2$									
cc(=o)cno2	+	C$_2$H$_6$	--->	CH$_3$C(=O)CH$_3$	+	CH$_3$CH$_2$NO$_2$	-51.94	-51.13	-51.71
cc(=o)cno2	+	CH$_4$	--->	CH$_3$C(=O)CH$_3$	+	CH$_3$NO$_2$	-51.30	-50.95	-51.51
cc(=o)cno2	+	C$_3$H$_6$	--->	CH$_3$C(=O)CH$_3$	+	CH$_2$=CHCH$_2$NO$_2$	-50.29	-50.49	-51.52
				Average			**-51.18** ± 0.83	**-50.86** ± 0.33	**-51.58** ± 0.11
CH$_3$C(=O)CH$_2$ONO									
cc(=o)cono	+	C$_2$H$_6$	--->	CH$_3$C(=O)CH$_3$	+	CH$_3$CH$_2$ONO	-52.51	-51.74	-51.24
cc(=o)cono	+	CH$_4$	--->	CH$_3$C(=O)CH$_3$	+	CH$_3$ONO	-51.98	-51.84	-50.96
cc(=o)cono	+	C$_3$H$_6$	--->	CH$_3$C(=O)CH$_3$	+	CH$_2$=CHCH$_2$ONO	-51.18	-50.86	-51.57
				Average			**-51.89** ± 0.67	**-51.48** ± 0.54	**-51.26** ± 0.31
CH$_2$=CHNO$_2$									
c=cno2	+	C$_2$H$_6$	--->	CH$_2$=CHCH$_3$	+	CH$_3$NO$_2$	6.29	6.88	7.69
c=cno2	+	C$_3$H$_8$	--->	CH$_2$=CHCH$_2$CH$_3$	+	CH$_3$NO$_2$	5.89	7.48	7.42
c=cno2	+	C$_3$H$_8$	--->	CH$_2$=CHCH$_3$	+	CH$_3$CH$_2$NO$_2$	6.86	7.08	7.66
				Average			**6.34** ± 0.49	**7.17** ± 0.31	**7.59** ± 0.15

Table 3.3 Evaluated Enthalpies of Formation at 298 K of Target Molecules (Continued)

Work Reactions						$\Delta_f H^o(298)$ kcal mol^{-1}		
						B3LYP		CBS-QB3
						6-31G(d,p)	6-31+G(2d,2p)	
CH$_2$=CHONO								
c=cono	+ C$_2$H$_6$	--->	CH$_2$=CHCH$_3$	+	CH$_3$ONO	6.30	4.74	7.38
c=cono	+ C$_3$H$_8$	--->	CH$_2$=CHCH$_2$CH$_3$	+	CH$_3$ONO	5.90	5.34	7.1
c=cono	+ C$_3$H$_8$	--->	CH$_2$=CHCH$_3$	+	CH$_3$CH$_2$ONO	6.40	4.82	7.23
					Average	**6.2** ± 0.26	**4.97** ± 0.33	**7.23** ± 0.14
CH$_3$C(=O)NO$_2$								
cc(=o)no2	+ C$_2$H$_6$	--->	CH$_3$C(=O)CH$_3$	+	CH$_3$NO$_2$	-47.83	-45.26	-45.32
cc(=o)no2	+ C$_3$H$_6$	--->	CH$_3$C(=O)CH$_3$	+	CH$_2$=CHNO$_2$	-46.53	-44.55	-45.42
cc(=o)no2	+ C$_3$H$_8$	--->	CH$_3$C(=O)CH$_3$	+	CH$_3$CH$_2$NO$_2$	-47.26	-45.06	-45.35
					Average	**-47.21** ± 0.65	**-44.96** ± 0.37	**-45.36** ± 0.05
CH$_3$C(=O)ONO								
cc(=o)ono	+ C$_2$H$_6$	--->	CH$_3$C(=O)CH$_3$	+	CH$_3$ONO	-58.71	-58.15	-58.08
cc(=o)ono	+ C$_3$H$_6$	--->	CH$_3$C(=O)CH$_3$	+	CH$_2$=CHONO	-57.78	-55.66	-58.22
cc(=o)ono	+ C$_3$H$_8$	--->	CH$_3$C(=O)CH$_3$	+	CH$_3$CH$_2$ONO	-58.60	-58.07	-58.22
					Average	**-58.36** ± 0.51	**-57.29** ± 1.42	**-58.17** ± 0.08

3.4.2 Bond Dissociation Energies

Bond energies are reported from the calculated the $\Delta_{rxn}H^o{}_{298}$ of parent molecule and their radical corresponding to loss of hydrogen atoms, where the enthalpies of parent molecule and product species are calculated in this study in conjunction with the value of 52.10 kcal mol^{-1} for H[94], the data correspond to the standard temperature of 298.15 K. The individual bond dissociation enthalpy values computed from isodesmic enthalpies of formation are given in Table 3.4

Bond energies are compared against similar bond energies in ketone, and for purposes of comparison, RC--H bond energies in acetone as 95.8 kcal mol^{-1}are used. The bond dissociation energies for H--CH$_2$C(=O)CH$_2$NO$_2$ and H--CH$_2$C(=O)CH$_2$ONO are the same as in acetone. The C-H bond energies for *cc(=o)cjno2* radical site are 95.5 kcal mol^{-1}; ~5 kcal mol^{-1} increase from bond energies in secondary carbon in methyl ethyl ketone (MEK), this is due to loss of resonance (competition for the unpaired e$^-$ between the C=O and NO$_2$ groups) resonance of the radical between this alpha carbon and the carbonyl carbon. Kemnitz et al.[95] also find correlation between internal rotor barrier and resonance in C--N atom for Imides.

Nitro and nitrite group substitution for a hydrogen atom on carbonyl carbon in acetaldehyde increased bond energies ~ 1 kcal mol^{-1} in adjacent sp^3 methyl group H--CH$_2$C(=O)NO$_2$ (95.9 kcal mol^{-1}) and ~ 4 kcal mol^{-1} for H--CH$_2$C(=O)ONO (98.3 kcal mol^{-1}).

The RC--H bond energies in nitroethylene, H--CH=CHNO$_2$, is 115.0 kcal mol^{-1} and in vinyl nitrite, the H--CH=CHONO bond is 114.4 kcal mol^{-1} which is ~ 4.3 kcal mol^{-1} higher than that in ethylene. The RC--H bond energies in CH$_2$=C(--H)NO$_2$ (114.85

kcal mol^{-1}) increased ~ 6 kcal mol^{-1} compare to secondary bond energies in propylene. This results from the NO_2, ONO (electron withdrawing group) drawing an electron through the pi bond making the CH_2 carbon more electrophilic (carbon atom more positive) and subsequently the $O_2NCH=CH$--H bond stronger.

The *cc(=o)cjono* and *c=cjono* molecules do not exist because the RO--NO bond at 43 kcal mol^{-1} is much weaker than the carbonyl π bond (~ 80 kcal mol^{-1}) being formed in $CH_3C(=O)CH(=O)$ and ketene, $CH_2=C=O$, respectively. These molecules with the radical site adjacent to the --ONO group dissociate to form a carbonyl and NO radical immediately upon their formation.

Table 3.4 Calculated Enthalpies of Formation at 298 K and Bond Energy for Radicals

Work Reactions					$\Delta_f H°(298)$ kcal mol^{-1}		
					B3LYP		CBS-QB3
					6-31G(d,p)	6-31+G(2d,2p)	
CH$_3$C(=O)CH$_2$NO$_2$ system							
CH$_2$C(=O)CH$_2$NO$_2$ *(cjc(=o)cno2)*							
cjc(=o)cno2 +	CH$_3$C(=O)CH$_3$	--->	*cc(=o)cno2* +	C•H$_2$C(=O)CH$_3$	-7.97	-7.03	-8.16
cjc(=o)cno2 +	CH$_3$C(=O)H	--->	*cc(=o)cno2* +	C•H$_2$C(=O)H	-7.53	-6.8	-6.98
cjc(=o)cno2 +	C$_3$H$_8$	--->	*cc(=o)cno2* +	C•H$_2$CH$_2$CH$_3$	-9.67	-6.71	-8.41
			Average		**-8.39** ± 1.13	**-6.85** ± 0.17	**-7.85** ± 0.76
Bond Energy H--CH$_2$C(=O)CH$_2$NO$_2$					*94.89*	*96.01*	*95.83*
CH$_3$C(=O)CHNO$_2$ *(cc(=o)cjno2)*							
cc(=o)cjno2 +	CH$_3$C(=O)CH$_3$	--->	*cc(=o)cno2* +	C•H$_2$C(=O)CH$_3$	-10.35	-9.05	-9
cc(=o)cjno2 +	CH$_3$C(=O)H	--->	*cc(=o)cno2* +	C•H$_2$C(=O)H	-9.9	-8.82	-7.81
cc(=o)cjno2 +	CH$_3$NO$_2$	--->	*cc(=o)cno2* +	C•H$_2$NO$_2$	-9.65	-7.07	-7.86
			Average		**-9.97** ± 0.35	**-8.32** ± 1.08	**-8.22** ± 0.67
Bond Energy CH$_3$C(=O)CH(--H)NO$_2$					*93.31*	*94.55*	*95.46*
CH$_3$C(=O)CH$_2$ONO system							
CH$_2$C(=O)CH$_2$ONO *(cjc(=o)cono)*							
cjc(=o)cono +	CH$_3$C(=O)CH$_3$	--->	*cc(=o)cono* +	C•H$_2$C(=O)CH$_3$	-9.25	-7.43	-8.3
cjc(=o)cono +	CH$_3$C(=O)H	--->	*cc(=o)cono* +	C•H$_2$C(=O)H	-8.81	-7.19	-7.12
cjc(=o)cono +	C$_3$H$_8$	--->	*cc(=o)cono* +	C•H$_2$CH$_2$CH$_3$	-10.96	-7.1	-8.54
			Average		**-9.67** ± 1.14	**-7.24** ± 0.17	**-7.99** ± 0.76
Bond Energy H--CH$_2$C(=O)CH$_2$ONO					*94.32*	*96.34*	*95.37*

Table 3.4 Calculated Enthalpies of Formation at 298 K and Bond Energy for Radicals (Continued)

Work Reactions							$\Delta_fH^o(298)$ kcal mol^{-1}		
							B3LYP		**CBS-QB3**
							6-31G(d,p)	**6-31+G(2d,2p)**	
CH$_2$=CHNO$_2$ system									
CH=CHNO$_2$ *(cj=cno2)*									
cj=cno2	+	C$_2$H$_4$	--->	*c=cno2*	+	C•H=CH$_2$	70.32	70.66	70.73
cj=cno2	+	C$_3$H$_6$	--->	*c=cno2*	+	C•H=CHCH$_3$	70.38	71.73	70.97
cj=cno2	+	C$_3$H$_6$	--->	*c=cno2*	+	CH$_2$=CHC•H$_2$	70.34	71.46	69.9
				Average			**70.35** $\pm$ 0.03	**71.28** $\pm$ 0.56	**70.54** $\pm$ 0.56
			Bond Energy H--CH=CHNO$_2$				*114.85*	*115.79*	*115.04*
CH$_2$=CNO$_2$ *(c=cjno2)*									
c=cjno2	+	C$_2$H$_4$	--->	*c=cno2*	+	C•H=CH$_2$	70.32	70.66	70.73
c=cjno2	+	C$_3$H$_6$	--->	*c=cno2*	+	CH$_2$=C•CH$_3$	69.81	71.02	69.33
c=cjno2	+	C$_3$H$_8$	--->	*c=cno2*	+	CH$_3$C•HCH$_3$	71.92	73.3	70.97
				Average			**70.68** $\pm$ 1.10	**71.66** $\pm$ 1.43	**70.35** $\pm$ 0.89
			Bond Energy CH$_2$=C(--H)NO2				*115.19*	*116.17*	*114.85*
CH$_2$=CHONO system									
CH=CHONO *(cj=cono)*									
cj=cono	+	C$_2$H$_4$	--->	*c=cono*	+	C•H=CH$_2$	69.75	70.09	69.76
cj=cono	+	C$_3$H$_6$	--->	*c=cono*	+	C•H=CHCH$_3$	69.82	71.16	70
cj=cono	+	C$_3$H$_6$	--->	*c=cono*	+	CH$_2$=CHC•H$_2$	69.77	70.89	68.93
				Average			**69.78** $\pm$ 0.04	**70.71** $\pm$ 0.56	**69.56** $\pm$ 0.56
			Bond Energy H--CH=CHONO				*114.65*	*115.58*	*114.43*

Table 3.4 Calculated Enthalpies of Formation at 298 K and Bond Energy for Radicals (Continued)

Work Reactions					$\Delta_fH^o(298)$ kcal mol^{-1}		
					B3LYP		**CBS-QB3**
					6-31G(d,p)	**6-31+G(2d,2p)**	
CH₃C(=O)NO₂ system							
CH₂C(=O)NO₂ (*cjc(=o)no2*)							
cjc(=o)no2 + CH₃C(=O)CH₃ ---> *cc(=o)no2* + C•H₂C(=O)CH₃					-2.23	-1.86	-2.04
cjc(=o)no2 + CH₃C(=O)H ---> *cc(=o)no2* + C•H₂C(=O)H					-2.27	-0.14	0.23
cjc(=o)no2 + CH₂=CHCH₃ ---> *cc(=o)no2* + CH₂=CHC•H₂					-2.82	-0.72	-1.79
				Average	**-2.14** ± 0.33	**-1.28** ± 0.88	**-1.57** ± 1.24
			Bond Energy H--CH₂C(=O)NO₂		*95.34*	*96.19*	*95.9*
CH₃C(=O)ONO system							
CH₂C(=O)ONO (*cjc(=o)ono*)							
cjc(=o)ono + CH₃C(=O)CH₃ ---> *cc(=o)ono* + C•H₂C(=O)CH₃					-12.5	-12.7	-12.41
cjc(=o)ono + CH₃C(=O)H ---> *cc(=o)ono* + C•H₂C(=O)H					-10.55	-10.97	-10.14
cjc(=o)ono + CH₂=CHCH₃ ---> *cc(=o)ono* + CH₂=CHC•H₂					-13.1	-11.56	-12.16
				Average	**-12.42** ± 1.33	**-12.11** ± 0.88	**-11.93** ± 1.24
			Bond Energy H--CH₂C(=O)ONO		*97.86*	*98.17*	*98.34*

Table 3.5 Summary of Formation Enthalpies for a Series of Nitrocarbonyls, Nitroolefins Compounds Calculated at Evaluated at Different Levels of Theory (Recommended Values are in Bold)

[a] Standard deviation of the three working reactions + reported errors for each of the standard species (when available) + 0.11 estimate in thermal energy for each species in the work reaction (4 species, 0.44 total)

Species	$\Delta_f H^o(298)$ kcal mol^{-1}			[a]Error Limit (CBS-QB3)
	B3LYP		CBS-QB3	
	6-31G(d,p)	6-31+G(2d,2p)		
CH₃C(=O)CH₂NO₂	-51.18	-50.86	**-51.58**	± 0.81
cjc(=o)cno2	-8.39	-6.85	**-7.85**	± 1.88
Bond Energy H--CH₂C(=O)CH₂NO₂	*94.89*	*96.01*	*95.83*	
cc(=o)cjno2	-9.97	-8.32	**-8.22**	± 1.49
Bond Energy CH₃C(=O)CH(--H)NO₂	*93.31*	*94.55*	*95.46*	
CH₃C(=O)CH₂ONO	-51.89	-51.48	**-51.26**	± 1.05
cjc(=o)cono	-9.67	-7.24	**-7.99**	± 1.51
Bond Energy H--CH₂C(=O)CH₂ONO	*94.32*	*96.34*	*95.37*	
CH₂=CHNO₂	6.34	7.17	**7.59**	± 0.93
cj=cno2	70.35	71.28	**70.54**	± 1.28
Bond Energy H--CH=CHNO₂	*114.85*	*115.79*	*115.04*	
c=cjno2	70.68	71.66	**70.35**	± 1.60
Bond Energy CH₂=C(--H)NO₂	*115.19*	*116.17*	*114.85*	

Table 3.5 Summary of Formation Enthalpies for a Series of Nitrocarbonyls, Nitroolefins Compounds Calculated at Evaluated at Different Levels of Theory (Recommended Values are in Bold) (Continued)

Species	$\Delta_f H^o(298)$ kcal mol^{-1}			[a]Error Limit (CBS-QB3)
	B3LYP		CBS-QB3	
	6-31G(d,p)	6-31+G(2d,2p)		
CH$_2$=CHONO	6.2	4.97	**7.23**	± 0.82
cj=cono	69.78	70.71	**69.56**	± 1.27
Bond Energy H--CH=CHONO	*114.65*	*115.58*	*114.43*	
CH$_3$C(=O)NO$_2$	-47.21	-44.96	**-45.36**	± 0.80
cjc(=o)no2	-2.14	-1.28	**-1.57**	± 1.86
Bond Energy H--CH$_2$C(=O)NO$_2$	*95.34*	*96.19*	*95.9*	
CH$_3$C(=O)ONO	-58.36	-57.29	**-58.17**	± 0.81
cjc(=o)ono	-12.42	-12.11	**-11.93**	± 1.89
Bond Energy H--CH$_2$C(=O)ONO	*97.86*	*98.17*	*98.34*	

3.4.3 Internal Rotation Potentials

Rotation about the C-C, C-O, C-NO$_2$, C-ONO and O-NO bonds in the target molecules are needed to determine lowest energy conformer and energy contributions to entropy and heat capacity vs. temperature. Energy profiles for internal rotations were calculated to determine energies of the rotational conformers and interconversion barriers along with contributions to entropy and heat capacity for the low barrier (below 4.5 kcal mol^{-1}) rotors. Frequencies calculated by the Gaussian are examined by viewing the vibration mode movement; the contributions from frequencies corresponding to internal rotations are excluded from the entropy and heat capacity and replaced with a more accurate estimate of S and $C_p(T)$ from the internal rotor contributions. The total energies as a function of the dihedral angles were computed at the B3LYP/6-31G(d,p) level of theory by scanning the torsion angles between 0° and 360° in steps of 15°, while all remaining coordinates were fully optimized. All potentials were re-scanned when a lower energy conformer is found, relative to the initial low energy conformer. The total energy corresponding to the most stable molecular conformer was arbitrarily set to zero and used as a reference point to plot the potential barriers. The resulting potential energy barriers for internal rotations in the stable non-radical molecules are shown in Figure 3.3.A–3.3.F.

The calculated rotational barriers of methyl groups all show the symmetrical three-fold symmetry with the barrier between 1.0 and 1.5 kcal mol^{-1} which is lower compared to typical alkyl methyl rotations which range between 2.7 and 3.0 kcal mol^{-1}. The C-NO$_2$ rotors in nitroacetone and nitroacetate exhibited low, two-fold symmetric barriers of 1.4, and 2.0 kcal mol^{-1} heights, respectively while the potential for nitroethylene had two-fold symmetry with a barrier of 6.5 kcal mol^{-1}. RO--NO internal

rotors in acetonitrite and vinyl nitrite show symmetric two-fold high barriers of 13 kcal mol^{-1} heights while the potential in acetyl nitrite had two-fold barrier of 3.0 and 4.5 kcal mol^{-1}
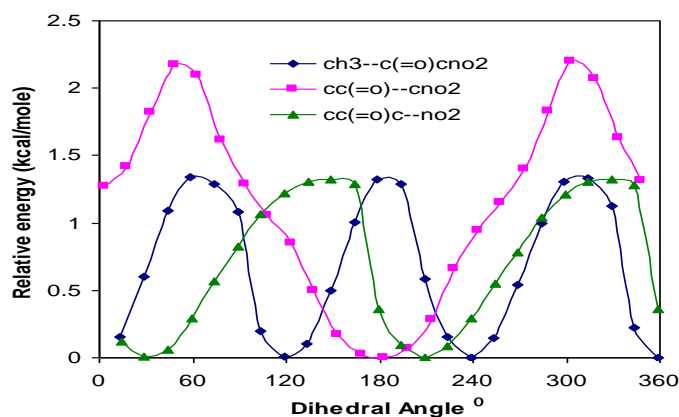
Figure 3.3.A Potential energy profiles for internal rotations in nitroacetone (*cc(=o)cno2*).
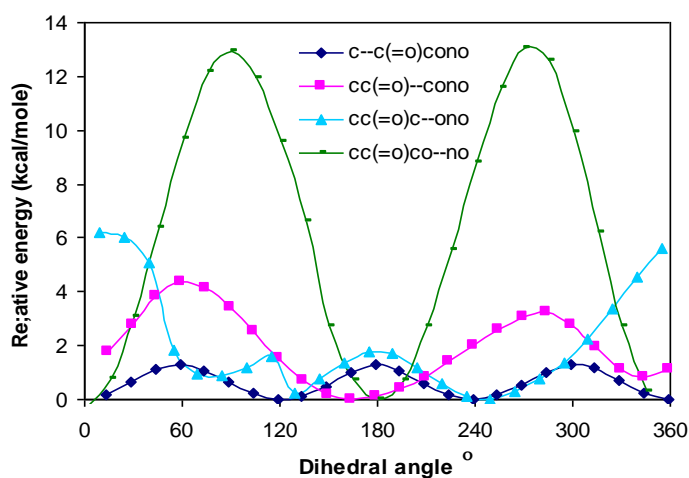
Figure 3.3.B Potential energy profiles for internal rotations in acetonitrite (*cc(=o)cono*).
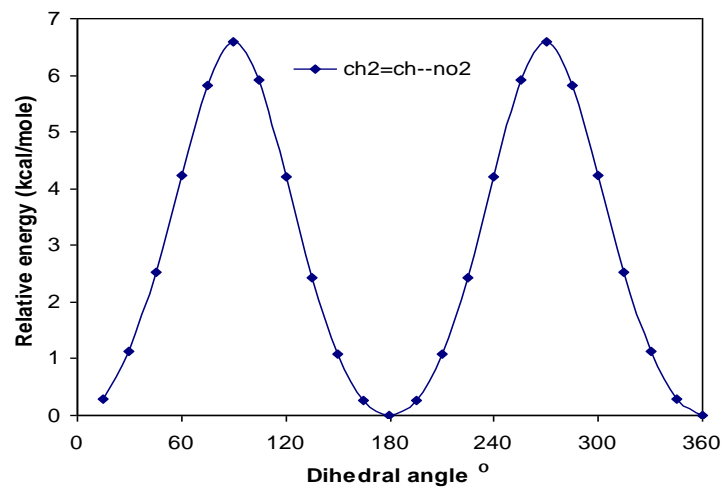
Figure 3.3.C Potential energy profiles for internal rotations in nitroethylene (*c=cno2*).
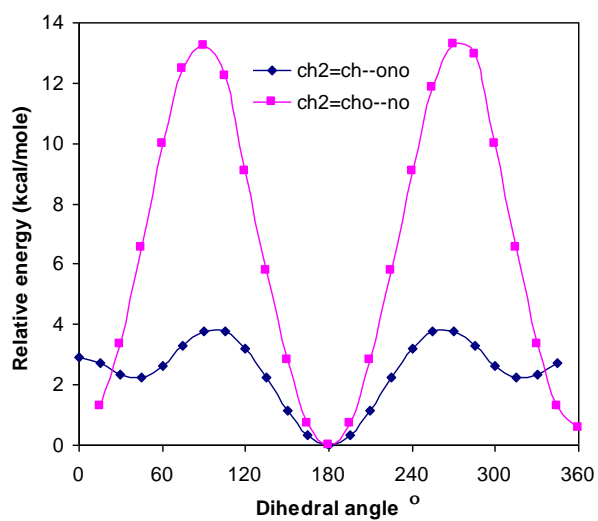
Figure 3.3.D Potential energy profiles for internal rotations in vinyl nitrite (*c=cono*).
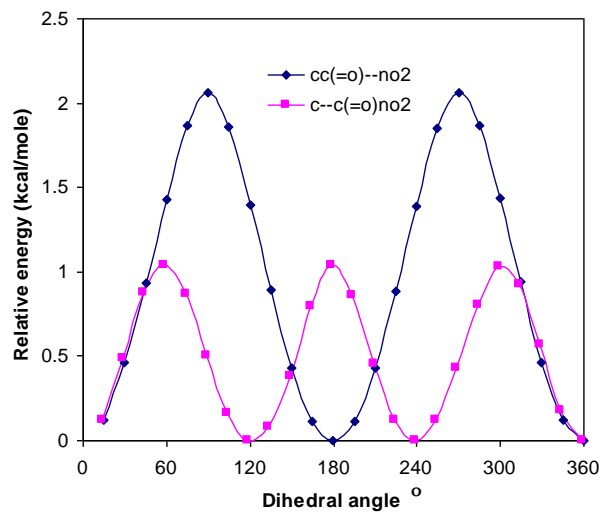
Figure 3.3.E Potential energy profiles for internal rotations in nitroacetate (*cc(=o)no2*).
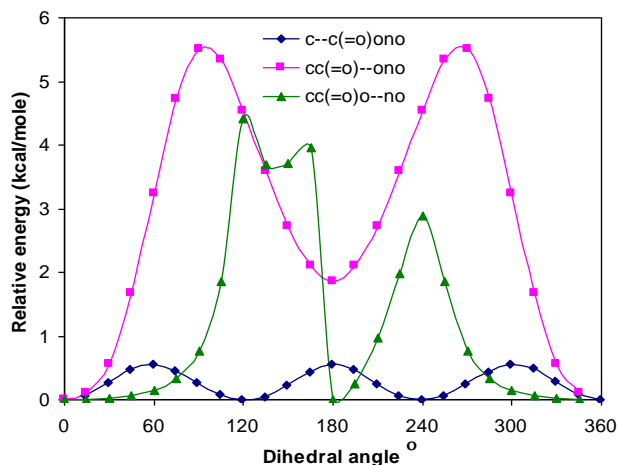
Figure 3.3.F Potential energy profiles for internal rotations in acetyl nitrite (*cc(=o)ono*).

cjc(=o)cno2 **and** *cc(=o)cjno2* **radical**

cjc(=o)--cno2 rotor and --NO$_2$ rotor barrier are similar to that in the parent *cc(=o)cno2*. The barrier for the *cj--c(=o)cno2* rotor (methyl radical site) is significantly increased (to 13 kcal mol^{-1}) and has a two-fold potential compared to three-fold for the parent. This barrier increase (11.6 kcal mol^{-1}) suggests a high degree of resonance between the carbon

radical and the carbonyl oxygen; this is interpreted as the difference between the barrier of the parent and was also observed by Kemnitz et al.[95]

The --NO$_2$ rotor in *cc(=o)cjno2* is increased from 2.1 kcal mol^{-1}in nitroacetone to 8 kcal mol^{-1} in this radical. This suggests 6 kcal mol^{-1} resonance. The *cc(=o)--cjno2* rotor has a two-fold potential with the barrier at 3.1 kcal mol^{-1} while the methyl rotor is similar to that in the parent.

cjc(=o)cono radical

There are significant differences in internal rotor potentials between *cjc(=o)cono* radical (*cis* configuration) and the parent (*trans* configuration). The *cjc(=o)c--ono* has a two-fold non symmetric with the barrier of 9 and 3 kcal mol^{-1} while the *cjc(=o)--cono* has a broad single barrier at 3.5 kcal mol^{-1}. The parent has a two-fold potential here. The *cjc(=o)co--no* rotor is similar to that in the parent with a two-fold potential and a high barrier (13 kcal mol^{-1}). The barrier for the *cj--c(=o)cono* rotor (methyl radical site) is increase from 1.5 kcal mol^{-1} in parent to 12 kcal mol^{-1} in this radical, this suggests 10.5 kcal mol^{-1} resonance.

cj=cno2 and *c=cjno2* radical

The --NO$_2$ rotor in *cj=cno2* has a two-fold potential with the barriers at 5 kcal mol^{-1} compare to the parent which is two-fold at 6.5 kcal mol^{-1}

The --NO$_2$ rotor in *c=cjno2* exhibits two-fold with some distortion of the symmetric two-fold potential of the parent and the barriers is decreased from 6.5 in parent to 2.5 kcal mol^{-1} in this radical.

cj=cono **radical**

All internal rotors in *cj=cono* are similar to those in the parent vinyl nitrite. *cj=co--no* rotor is similar to that in the parent with a two-fold potential and very high barrier (13.5 kcal mol^{-1}) while *cj=c--ono* has a three-fold potential with one at barrier at 2 kcal mol^{-1} and two barriers at 4 kcal mol$^{-1.}$

cjc(=o)no2 **radical**

The barrier for the *cj--c(=o)no2* rotor (methyl radical site) is significantly increased (to 12 kcal mol^{-1}) and symmetric dual potential compared to three-fold for the parent. This barrier increase (11 kcal mol^{-1}) suggests a high degree of resonance between the carbon radical and the carbonyl oxygen. *cjc(=o)—no2* rotor has 2 folds with the barrier of 4 kcal mol^{-1}

cjc(=o)ono **radical**

The barrier for the *cj--c(=o)ono* rotor (methyl radical site) is significantly increased (to 9 kcal mol^{-1}) and has a symmetric two fold potential compared to three-fold for the parent. This barrier increase, suggests 8.5 kcal mol^{-1} resonance. The cjc(=o)--ono and cjc(=o)o--no rotor barriers increase ~1 kcal mol^{-1} with two-fold compare to that in the parent.

3.4.4 Thermochemical Properties, Entropy and Heat Capacity Data

Entropy and heat capacity contributions as a function of temperature are determined from the calculated structures, moments of inertia, vibration frequencies, symmetry, electron degeneracy, number of optical isomers and the known mass of each molecule. The calculations use standard formulas from statistical mechanics for the contributions of translation, external rotation and vibrations using the "SMCPS" program. This program utilizes the rigid-rotor-harmonic oscillator approximation from the frequencies along with

moments of inertia from the optimized CBS-QB3 structures, *viz.* B3LYP/6-311G(2d,d,p) level. Contributions from internal rotors using Pitzer-Gwinn formalism are substituted for contributions from low frequencies internal rotor torsions where barriers were determined to be below 4.5 kcal mol^{-1}. These entropy and heat capacity data are needed to determine dependence of the enthalpy, entropy, Gibbs energy and equilibrium constants versus temperature. Entropy and heat capacity calculation were performed using complete basis set -QB3 determined geometries and harmonic frequencies summarized in appendix A

Table 3.6 presents a set of three representative frequencies and a degeneracy of each frequency that can be used to calculate the *Cp*(T) data at any temperature using the standard equation from statistical mechanics for the heat capacity contribution from a frequency as a function of temperature. The heat capacity at *Cp*(T-infinity) should be calculated from the contributions of translation, external rotation, the reported frequencies, plus contributions from internal rotors, where the number of internal rotors is [(3n-6) – Number of frequencies] for each molecule in Table 3.6.

Table 3.6 Harmonic Oscillator Fit for *Cp* (T)

Species	Mean Vibration: MODES	Frequency (cm⁻¹)	Species	Mean Vibration: MODES	Frequency (cm⁻¹)
	10.373	350.0		6.647	443.7
cc(=o)cno2	12.595	1302.5	*c=cjno2*	6.627	1410.7
	5.531	3030.2		1.726	3999.9
	9.946	376.1		8.834	488.8
cjc(=o)cno2	11.605	1234.2	*c=cono*	6.394	1483.4
	4.448	3086.9		2.772	3989.3
	10.322	373.2		7.850	428.9
cc(=o)cjno2	11.253	1223.2	*cj=cono*	5.327	1335.7
	4.425	3044.5		1.823	3999.1
	11.349	352.0		8.649	425.9
cc(=o)cono	12.011	1258.5	*cc(=o)no2*	9.963	1573.6
	5.640	2992.8		2.388	3999.3
	12.143	413.6		8.809	420.8
cjc(=o)cono	9.970	1236.4	*cjc(=o)no2*	7.638	1329.9
	4.387	3075.2		1.553	4000.0
	6.292	486.9		8.904	409.4
c=cno2	8.398	1269.8	*cc(=o)ono*	9.668	1491.0
	3.310	3130.2		2.429	3999.5
	6.128	450.4		9.062	364.8
cj=cno2	6.462	1192.1	*cjc(=o)ono*	7.377	1272.2
	2.410	3062.0		1.562	3999.7

3.4.5 Group Values for Use in the Group Additivity Method for Estimation of Thermochemical Properties.

Group additivity[96] is a straightforward and reasonably accurate calculation method to estimate thermodynamic properties of hydrocarbons and oxygenated hydrocarbons[97]; it is particularly useful for application to larger molecules and in codes or databases for the estimation of thermochemical properties in reaction mechanism generation. In this work, six nitrocarbonyls, nitroolefins, corresponding nitrites and eight carbon centered radicals groups, bond dissociation increment reflects to the loss of a hydrogen atom, are estimated by using the thermodynamic property data developed in this study, plus the alkyl-hydrocarbon groups in the literature. The fourteen groups are listed in the Table 3.7 along with standard hydrocarbon groups used.

Table 3.7 Group Thermochemical Values

Group	$\Delta_f H^o$(298) (kcal mol^{-1})	S°(298) (cal mol^{-1} K^{-1})	C°$_p$(T) (cal mol^{-1} K^{-1})					
			300K	400K	500K	600K	800K	1000K
Groups developed in this study								
C/CO/H2/NO2	-10.10	48.56	14.47	17.08	19.24	21.00	23.54	25.32
C/CO/H2/ONO	-9.66	45.56	16.14	18.98	21.16	22.84	25.19	26.81
CD/H/NO2	1.33	42.80	12.35	15.04	17.23	18.95	21.36	22.92
CD/H/ONO	0.97	48.42	14.66	16.95	18.68	19.98	21.77	22.93
CO/C/NO2	-35.28	52.97	15.49	17.34	18.85	20.07	21.89	23.03
CO/C/ONO	-48.09	56.96	16.49	18.53	20.11	21.29	22.89	23.82
BD Groups developed in this study								
CJCDOCNO2	96.20	-2.73	-0.91	-0.75	-0.91	-1.2	-1.88	-2.52
CCDOCJNO2	95.83	-3.97	-0.24	-0.11	-0.32	-0.68	-1.47	-2.18
CJCDOCONO	95.62	-2.22	-0.54	-0.39	-0.61	-0.97	-1.75	-2.42
CJDCNO2	115.64	2.04	0.31	-0.25	-0.9	-1.51	-2.48	-3.21
CDCJNO2	114.85	4.34	0.33	-0.58	-1.47	-2.21	-3.3	-4.07
CJDCONO	115.02	1.31	0.18	-0.41	-1.08	-1.7	-2.65	-3.34
CJCDONO2	96.85	-4.18	-0.08	0.24	0.09	-0.28	-1.18	-1.97
CJCDOONO	99.29	-1.62	0.55	0.42	-0.01	-0.52	-1.48	-2.25
Known groups								
C/CO/H3	-10.08	30.41	6.19	7.84	9.4	10.79	13.02	14.77
CO/C2	-31.40	15.01	5.59	6.32	7.09	7.76	8.89	9.61
CD/H2	6.26	27.61	5.10	6.36	7.51	8.50	10.07	11.27

3.5 Summary

Thermodynamic properties ($\Delta_f H^o_{298}$, S^o_{298}, and $C_p(T)$, ($5 \leq T \leq 5000$ K)) for nitrocarbonyls, nitroolefins, corresponding nitrites are reported. Standard enthalpies of formation, $\Delta_f H^o_{298}$, are calculated using density functional theory and isodesmic reactions. The enthalpies of formation of acetyl nitrite were found to be ~12 kcal mol^{-1} more stable (lower enthalpy) than the corresponding nitro while $\Delta_f H^o_{298}$ of nitroacetone is 0.3 kcal mol^{-1} more stable than the corresponding nitrite. The $\Delta_f H^o_{298}$ of Vinyl nitrite is 0.3 kcal mol^{-1} more stable than the corresponding nitro. The *trans* configuration respective to C-O-N-O dihedral angles in acetonitrite, vinyl nitrite and acetyl nitrite are more stable than corresponding *cis* isomer. Enthalpies of formation, entropy, $S^o(T)$ and heat capacity, $C^o_p(T)$, values are reported along with bond energies and corresponding thermochemical properties for radicals corresponding to loss of hydrogen atom from the carbons sites. The bond dissociation energies in all species were observed to increase from 0.5 to 6 kcal mol^{-1}. Rotational barrier potentials are reported for internal rotors and hindered internal rotor contributions for $\Delta_f H^o_{298}$, S^o_{298}, and $C_p(T)$ are calculated. Groups for use in group additivity are developed.

CHAPTER 4

THERMOCHEMISTRY AND KINETICS OF THE ACETONYL RADICAL AND ACETYL RADICAL + NO₂ REACTION SYSTEM: A THEORETICAL STUDY

4.1 Overview

Thermochemical properties and transition state structures for the reactions of acetonyl radical and acetyl radical with NO_2 are analyzed to evaluate reaction paths and kinetics. The initial association reactions form nitro alkane (RNO_2) or alkylnitrite (RONO) adducts. Enthalpies of formation ($\Delta H_f°_{298}$) are determined using isodesmic reaction analysis at the CBS-QB3 composite and density functional methods. Entropies ($S°_{298}$) and heat capacities ($Cp°(T)$) are determined using geometric parameters and vibration frequencies obtained at the B3LYP/6-311G(2d,d,p) level of theory. Internal rotor contributions are included in S and $Cp(T)$ values in place of torsion frequencies. Detailed potential energy surfaces for the reactions are presented, with association rate constants from variational transition state analysis and intramolecular isomerization rate parameters from canonical transition state theory. The chemically activated R• + NO_2 systems are modeled using quantum Rice-Ramsperger-Kassel (QRRK) theory for $k(E)$, with Master Equation analysis for falloff. At atmospheric pressure and temperature both association paths of the R• + NO_2 → reactions proceed almost primarily to RCO• + NO via chemical activation reaction with a fraction of stabilization adduct and lower energy products. Rate constants for abstraction of H from the above carbonyl species by NO to form acetylformaldehyde + HNO (or ketene + HONO in acetyl radical reaction) are also evaluated.

4.2 Previous Studies

Acetone, other ketones and aldehydes are important in atmospheric chemistry[98,99] because they are formed both biogenically and as intermediates in the atmospheric oxidation of hydrocarbons[100] through a series of reactions of secondary alkylradicals with oxygen and NO_x species. Specifically aldehydes and ketones are formed from the reactions of intermediate peroxy radicals with nitric oxide to form alkoxy radicals, and then the subsequent reactions of the alkoxy radicals with NO_2 and O_2. Acetone is considered the most abundant oxygenated organic[101] in the upper troposphere, impacting global ozone formation[102] and PAN formation.

These molecules are also important in combustion environments where they are formed from reactions of

$$R\bullet + O_2 \rightarrow ROO\bullet$$

Peroxy radical reaction with O_2

$$R\bullet + R'OO\bullet \rightarrow RO\bullet + R'O\bullet$$

$$RO\bullet \rightarrow \text{Aldehyde or ketone} + \text{radical}$$
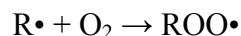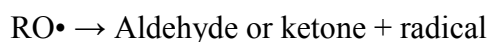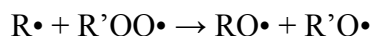
via beta scission, isomerization and reaction to carbonyl

$$CC(OO\bullet)CCC \rightarrow CC(OOH)CC\bullet C$$

$$CC(OOH)CC\bullet C + O_2 \rightarrow CC(OOH)CC(OO\bullet)C \rightarrow CC(=O)CC(OOH)C + OH$$
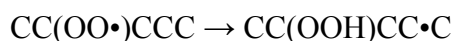
Thermochemical properties, such as enthalpies of formation and bond energies,[103] of radicals related to the aldehydes and ketones and their corresponding kinetic parameters for their reactions with active species and intermediates in combustion and the atmosphere are needed for assembly of elementary chemical kinetic models for both atmospheric and combustion chemistry.[104]

To this time, there is only one previous study of these reactions. Sehested et al[105] use pulse radiolysis experiments to study the kinetic of the reaction $CH_3C(=O)CH_2O_2$ with NO and NO_2 and report $1.6x10^{-11}$ cm^3 $molecule^{-1}$ s^{-1} ($9.63x10^{12}$ cm^3 $mole^{-1}$ s^{-1}) for $CH_3C(=O)C\bullet H_2$ + NO_2 → Product. This work reports $1.15x10^{12}$ cm^3 $mole^{-1}$ s^{-1} for $CH_3C(=O)C\bullet H_2$ + NO_2 → $CH_3C(=O)CH_2NO_2$ reaction at 298 K.

In this study, standard enthalpy ($\Delta_f H_{298}^0$) and dissociation bond energies are reported for the species resulting from the acetonyl and acetyl radical + NO_2 reactions. Transition state structures and intermediates that result from the isomerization and reactions of the radical are calculated using Density Functional (B3LYP/6-31g(d,p)) and *ab initio* (CBS-QB3) calculations. Thermochemical properties, reaction paths and kinetics parameters are reported for bimolecular abstraction of hydrogen atoms from the parent ketones by NO_2 and for association reactions of the acetonyl and acetyl radical to form R-NO_2* and RONO* chemically activated adducts.

4.3 Computational Methods

4.3.1 Computational Details

Geometries, vibration frequencies, moments of inertia, and internal rotor barriers for molecules and related radicals were initially optimized at the B3LYP/6-31G(d,p) level of theory. The B3LYP method combines the three parameter Becke exchange functional, B3, with Lee−Yang−Parr correlation functional, LYP. There is known to be a general consensus that B3LYP methods provide excellent low-cost performance for structure optimizations. The B3LYP/6-31G(d,p) level of theory is a reliable computational method for the determination of geometries of small polar compounds as well as being widely

used for the calculation of radical species. The higher level composite CBS-QB3 method was also used for calculations. CBS-QB3 is a multilevel model chemistry that combines the results of several ab initio and DFT individual methods and empirical correction terms to predict molecular energies with high accuracy and reasonable computational cost. It is based on B3LYP/CBSB7 calculations for the geometry optimization and frequencies, followed by a single point energy calculation at the CCSD(T)/6-31G +(d′) and MP4SDQ/CBSB4 level of theory. It includes a total energy extrapolation to the infinite basis-set limit using pair natural-orbital energies at the MP2/CBSB3 level, and an additive correction at the CCSD(T) level of theory. The B3LYP is thought to be one of the most reliable DFT methods available and has been shown by Curtiss et. al.[106-109] to have the smallest average absolute deviation, 3.11 kcal mol^{-1}, of the seven DFT methods studied using the G2 test set of molecules. Curtiss et al., and Ochterski co-workers reported mean absolute deviations of 1.1 kcal mol^{-1}for CBS-Q methods by comparing the energies of 125 computationally reactions to their corresponding experimental values. All calculations were performed using the Gaussian 03 program.

The CBS-QB3 reproduces the experimental results better than B3LYP/6-31G(d,p), are recommended where experimental values are not available. Further reference will reflect the values from CBS-QBS for standard enthalpies of formation of the lowest energy conformers, with the B3LYP/6-31G(d,p) being referred to when relevant.

4.3.2 Thermochemical Properties

To evaluate the heats of formation of the molecule systems, a homodesmic and isodesmic

reactions are used, where the bonding environments are similar in both products and

reagents. An isodesmic reaction is a hypothetical reaction where the number and type of

bonds is conserved on each side of the work reaction; a homodesmic reaction conserves

number and type of bonds, but also conserves hybridization. Previous studies show that

the computed enthalpies of formation via isodesmic work reactions for nitrogen species

are in very good agreement with the experimental data available.

Entropy and heat capacity contributions as a function of temperature are

determined from the calculated structures, moments of inertia, vibration frequencies,

symmetry, electron degeneracy, number of optical isomers and the known mass of each

molecule. The calculations use standard formulas from statistical mechanics for the

contributions of translation, external rotation and vibrations using the "SMCPS"

program.[11] This program utilizes the rigid-rotor-harmonic oscillator approximation from

the frequencies along with moments of inertia from the optimized CBS-QB3 structures,

viz. B3LYP/6-311G(2d,d,p) level. Contributions from internal rotors using Pitzer-Gwinn

formalism are substituted for contributions from internal rotor torsion frequencies. These

entropy and heat capacity data are needed to determine dependence of the enthalpy,

entropy, Gibbs Energy and equilibrium constants with temperature.

4.3.3 Kinetic Modeling

The thermochemical properties and potential energy surface are determined from the

calculation of structures, energies, internal rotor potentials and vibration frequencies of

stable parent molecules, products, intermediate radicals and transition state structures.

High pressure limit kinetic parameters are determined from use of statistical mechanics and canonical transition state theory for reactions with saddle points. Variational transition state or literature data are used for association and dissociation reactions that have no barrier other than enthalpy of reactions. Chemical activation and unimolecular dissociation reactions are analyzed using multifrequency quantum Rice Ramsperger-Kassel (QRRK) analysis is used for $k(E)$ with master equation analysis is used for falloff.

The QRRK Master equation analysis is described by Chang et al. It is shown to yield reasonable results and provides a framework by which the effects of temperature and pressure can be evaluated in complex reaction systems. The QRRK code utilizes a reduced set of three vibration frequencies which accurately reproduce the molecules'(adduct) heat capacity and include one external rotation in calculation of density of states $\rho(E)$/Q. Comparisons of ratios of these $\rho(E)$/Q (partition function Q) with direct count $\rho(E)$/Q are shown to be in good agreement. Nonlinear Arrhenius effects resulting from changes in the thermochemical properties of the respective transition state relative to the adduct with temperature are incorporated using a two parameter Arrhenius pre-exponential factor (A, n) in AT^n.

4.4 Results and Discussion

Optimized geometric structures for the reactants, transition states and adducts are calculated at the CBS-QB3 composite level of theory (B3LYP/6-311(2d,d,p) calculations) and corresponding abbreviated nomenclatures are listed in Figure 4.1. The *trans* and *cis* configurations of acetonitrite are near equal in energy, the *trans* conformer for the respective to C-O-N-O dihedral angle. Acetonitrite is calculated to be only 0.12 kcal mol⁻¹ more stable than corresponding *cis* isomer.
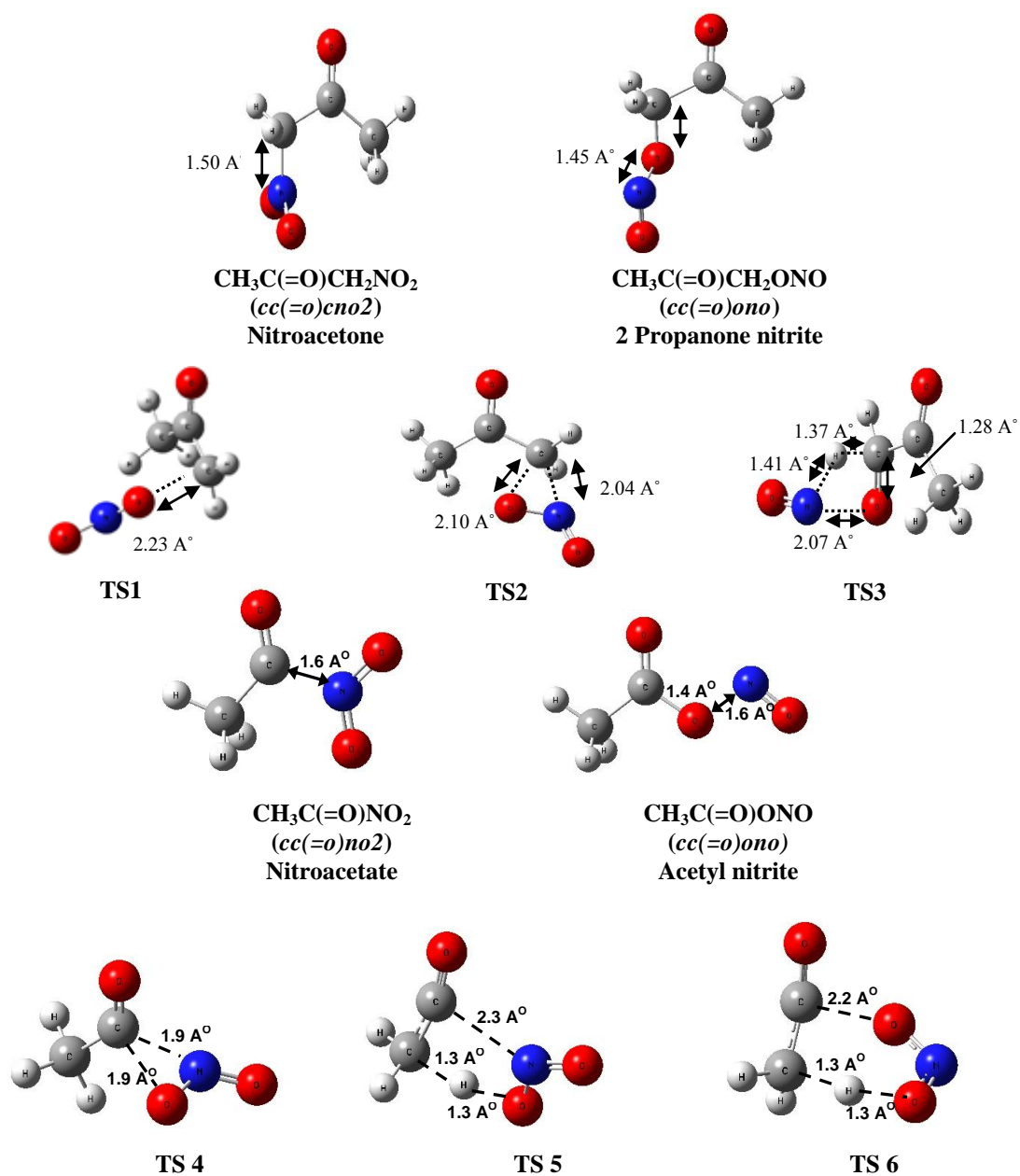
Figure 4.1 Geometry of the lowest energy conformer of the target molecules and abbreviated nomenclature.

The absence of imaginary frequencies verifies that structures are true minima at their respective levels of theory for stable molecule and radicals. Transition states (TS) are characterized as having only one negative eigenvalue of Hessian (force constant) matrices. Intrinsic reaction coordinate (IRC) calculations were performed at B3LYP/6-31G(d,p) level to ensure connectivity of stationary points. The final point geometries at both sides of TS were re-optimized to proper minima. The energy of each transition state structure is calculated from the corresponding reactant plus the energy difference between the TS structure and the reactant (adduct). If the TS is closer in structure to the product, then the enthalpies of formation of the transition state species is calculated from the corresponding product plus the energy difference between TS and product.

Enthalpies of formation ($\Delta_f H^0_{298}$) for species in the acetonyl radical and acetyl radical + NO_2 reaction mechanism are listed in Table 4.1. Entropy and heat capacity calculation as a function of temperature were performed using B3LYP/6-311G(2d,d,p) are summarized in Table 4.2. Frequencies calculation for the transition states are presented in appendix B.

Table 4.1 Enthalpies of Formation ($\Delta_f H^0_{298}$) for Species in the Acetonyl Radical and Acetyl Methyl Radical + NO$_2$ Reaction Mechanism

Species	$\Delta_f H^o_{298}$ (kcal mol^{-1})	Source (Ref. No.)
CH$_3$C(=O)CH$_2$NO$_2$	-51.6	This study
CH$_3$C(=O)CH$_2$ONO	-51.3	This study
CH$_3$C(=O)NO$_2$	-45.4	This study
CH$_3$C(=O)ONO	-58.2	This study
CH$_3$C•(=O)	-2.9	110
CH$_3$C(=O)O•	-45.3	THERM[111-113]
CH$_3$C(=O)C•H$_2$	-8.3	93
CH$_3$C(=O)CH$_2$O•	-33.9	THERM[111-113]
CH$_3$C(=O)CH(=O)	-64.8	114
NO$_2$	7.9	115
NO	21.6	115
HNO	25.6	116
HONO	-18.9	117
CH$_2$=C=O	-20.9	43
TS1	6.1	This study
TS2	14.0	This study
TS3	-15.2	This study
TS4	-18.5	This study
TS5	-9.6	This study
TS6	-12.7	This study

Table 4.2 Ideal Gas Phase Thermodynamic Properties, Cp(T) and S^O_{298} in cal mol^{-1} K^{-1}

Species	S^O_{298}	Cp 300K	Cp 400K	Cp 500K	Cp 600K	Cp 800K	Cp 1000K	Cp 1500K
CH$_3$C(=O)CH$_2$NO$_2$	90.42	26.25	31.24	35.73	39.55	45.45	49.70	56.05
CH$_3$C(=O)CH$_2$ONO	88.80	27.92	33.14	37.65	41.39	47.10	51.19	57.33
CH$_3$C(=O)NO$_2$	79.82	21.68	25.18	28.25	30.86	34.91	37.80	42.07
CH$_3$C(=O)ONO	85.19	22.68	26.37	29.51	32.08	35.91	38.59	42.52
TS1	84.20	26.13	31.56	36.25	40.10	45.93	50.06	56.22
TS2	93.24	27.57	32.78	37.32	41.11	46.87	50.99	57.17
TS3	87.73	27.17	32.30	36.88	40.76	46.71	50.89	56.90
TS4	75.69	21.47	25.08	28.22	30.85	34.90	37.78	42.06
TS5	78.63	22.34	26.25	29.52	32.20	36.20	38.95	42.85
TS6	75.06	22.13	26.19	29.57	32.31	36.35	39.08	42.93

4.4.1 Abstraction of Hydrogen Atoms from the Parent Ketones by NO$_2$

Kinetics parameters for the bimolecular abstraction of hydrogen atoms from the parent ketones by NO$_2$ are showed in Figure 4.2 and Table 4.3. There are three possible reaction paths, forming *cis* HONO, *trans* HONO and HNO$_2$. For the transition state of CH$_3$CH(=O) + NO$_2$ --> CH$_3$C•(=O) + HNO$_2$ reaction, the transition state energy is lower than product energy. This suggests transition state structure has significant interaction between N atom in nitro group and carbonyl group.
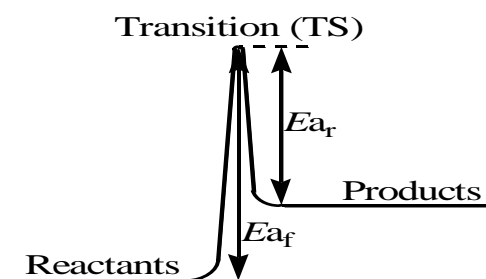
Figure 4.2 Energy for abstraction of hydrogen atoms from the parent aldehydes and ketones by NO$_2$ (see energy in Table 4.3).

Table 4.3 Enthalpies of Formation ($\Delta_f H^0_{298}$) for Reactants, Transition State, Products and Kinetic Parameter for Abstraction of Hydrogen atom from Aldehydes and Ketones by NO_2

Reaction	$\Delta_f H^0_{298}$ (kcal/mol)			Kinetic Parameters $k = A(T/K)^n \exp(-E_a/RT)$ ($300 \leq T/K \leq 2000$)		
	Reactant	TS	Product	A	n	E_a (kcal/mol)
$CH_3CH(=O) + NO_2 \rightarrow CH_3C\bullet(=O) +$ Cis HONO	-31.79	-17.2	-20.9	5.549×10^1	3.2	13.7
$CH_3CH(=O) + NO_2 \rightarrow CH_3C\bullet(=O) +$ Trans HONO	-31.79	-4.9	-21.4	6.024×10^1	3.3	26.1
$CH_3CH(=O) + NO_2 \rightarrow CH_3C\bullet(=O) + HNO_2$	-31.79	-14.3	-13.4	2.811×10^2	3.0	16.8
$CH_3C(=O)CH_3 + NO_2 \rightarrow CH_3C(=O)C\bullet H_2 +$ Cis HONO	-43.99	-17.6	-26.7	9.884×10^{-2}	4.3	24.8
$CH_3C(=O)CH_3 + NO_2 \rightarrow CH_3C(=O)C\bullet H_2 +$ Trans HONO	-43.99	-9.2	-27.2	7.619×10^{-1}	3.9	33.5
$CH_3C(=O)CH_3 + NO_2 \rightarrow CH_3C(=O)C\bullet H_2 + HNO_2$	-43.99	-16.7	-19.2	2.948×10^{-1}	3.9	25.9

4.4.2 Variational Transition State Analysis

The R• + NO$_2$ → R-NO$_2$ association reaction proceeds without any barrier, and determination of the kinetics of this reaction was analyzed by use of variational transition state theory (VTST). The elimination reaction of the R-ONO to RCO• + NO is also found to dissociate without a barrier, and this transition state is also treated variationally.

Potential energy scans were performed along the dissociating R–NO$_2$ and RCO–NO bonds and were calculated at the UB3LYP/6-31G(d,p) level, at 0.1A˚ intervals. The UB3LYP reaction energies between the points along the potential energy scans and the reactant were multiplied by a scaling factor, which is the ratio of the CBS-QB3 reaction enthalpy to the UB3LYP reaction energy. This procedure effectively uses the CBS-QB3 energy to provide the enthalpy of reaction and results on structure and vibration frequencies from the UB3LYP/6-31G(d,p) scan to the correct dissociation limit energy. Structure and frequency calculations were performed for transition-state structures along the minimum energy pathways start from R–NO$_2$ and RCO–NO bond length of 1.4 A˚ to 4.0 A˚ with 0.1 A˚ intervals for the total of 26 points.

Potential energy surfaces for R–NO$_2$ bond dissociations in nitroacetone and RO—NO dissociation in 2 propanone nitrite are shown in Figure 4.3 and Figure 4.4, respectively. Frequency calculations were performed at discrete points along the potential energy surface, for both reactions. Thermochemical properties and rate constants as a function of temperature were evaluated at each point along the potential energy surface. The minimum rate constant was located as a function of temperature and position for each reaction, providing the variational rate constant. Rate constants were fit to the three parameter form of the Arrhenius equation to yield the rate parameters A, n and E_a
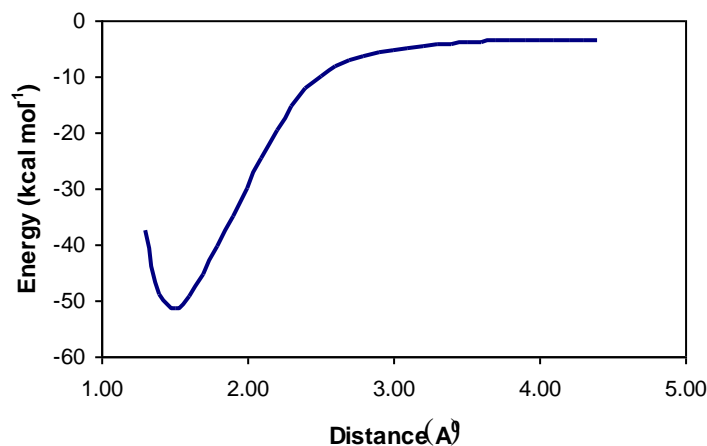
Figure 4.3 Potential energy surface for dissociation of the R–NO$_2$ in the nitroacetone (CH$_3$C(=O)CH$_2$NO$_2$).
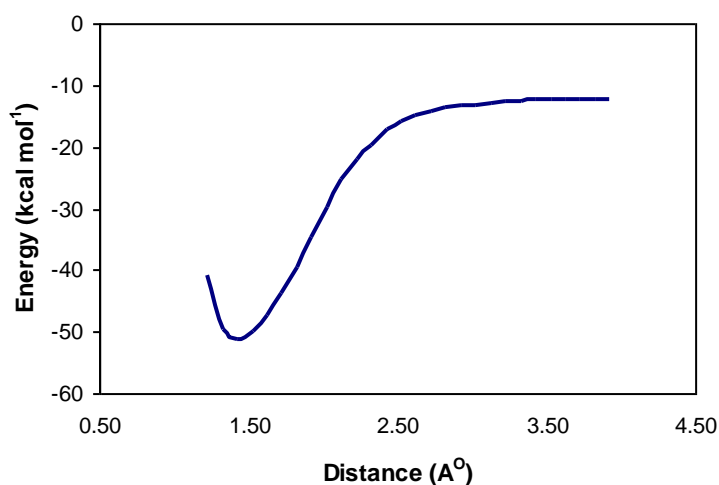
Figure 4.4 Potential energy surface for dissociation of the RO—NO in the 2 propanone nitrite (CH$_3$C(=O)CH$_2$ONO)**.**

For the acetonyl radical + NO$_2$ <--> CH$_3$C(=O)CH$_2$NO$_2$ association, the transition state occurs at a C—NO$_2$ bond length of 3.3 A˚ at 300 K, decreasing to 2.6 A˚ at 2000 K. Fitting the minimum rate constant as a function of temperature to the three parameter Arrhenius equation are calculated for the association reaction as $A = 1.81 \times 10^8$, $n = 1.5$, $E_a = -1.93 \times 10^2$ cal mol^{-1} and $A = 5.96 \times 10^{15}$, $n = -0.41$, $E_a = 5.15 \times 10^4$ cal mol^{-1} for dissociation reaction.

$$CH_3C(=O)C \cdot H_2 + NO_2 \; <--> \; CH_3C(=O)CH_2NO_2$$
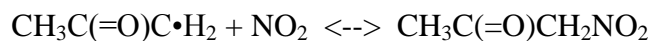
$$k_{association} \; = \; 1.81 \times 10^8 \, T^{1.5} \exp(97/T) \; cm^3 \, mol^{-1} \, s^{-1}$$

$$k_{dissociation} \; = \; 5.96 \times 10^{15} \, T^{-0.41} \exp(-25940/T) \; s^{-1}$$

Rate constants as a function of temperature for the $CH_3C(=O)CH_2NO_2 \; <-->$ $CH_3C(=O)CH_2 \cdot + NO_2$ dissociation are plotted in Figure 4.5 for the five contributing transition-state structures. A solid line indicate an empirical three-parameter Arrhenius fit of $k(T)$.
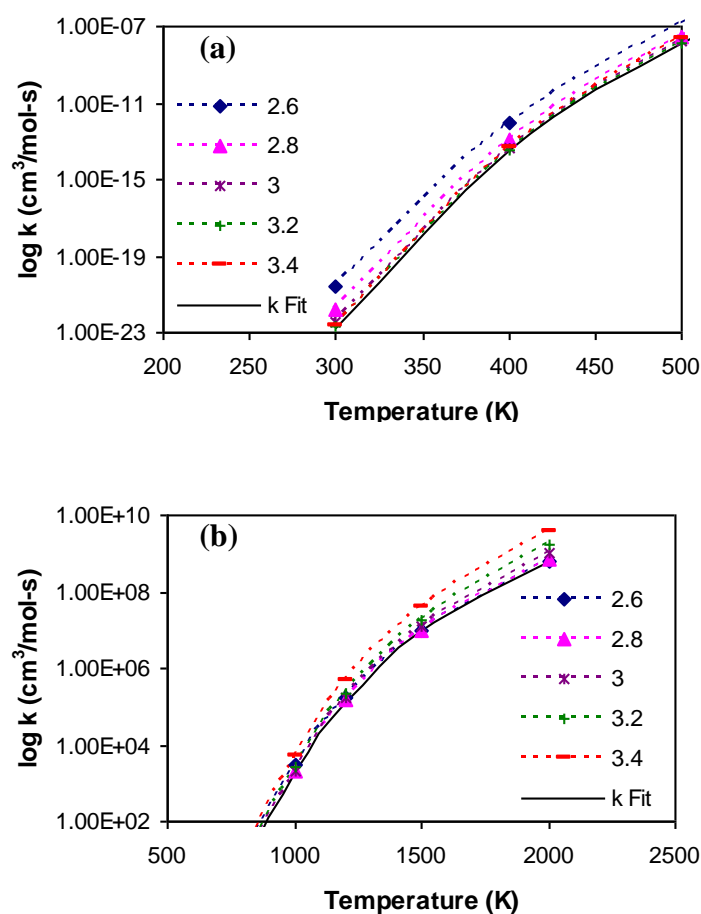
Figure 4.5 Rate constants as a function of temperature for contributing transition-state structures in the barrierless of the dissociation of $CH_3C(=O)CH_2NO_2$ → $CH_3C(=O)CH_2 \cdot$ + NO_2 reaction. Dashed line indicates a three-parameter Arrhenius fit of the variational rate constant. (a) Temperature range 200-500 K (b) Temperature range 500-2500 K

Similar analysis was performed for the RO-NO dissociation $CH_3C(=O)CH_2ONO$ <--> $CH_3C(=O)CH_2O\bullet$ + NO dissociation. The variational transition state is at a RO--NO bond length of 3.4 A° at 300 K, tightening to the 2.3 A° at 2000 K. Fitting the association variational rate constants to a three-parameter rate law, obtain $A = 5.7 \times 10^{11}$, $n = 0.2$, E_a = -8.78 x 10^2 cal mol^{-1} for association reaction and $A = 3.87 \times 10^{23}$, $n = -2.6$, $E_a = 4.22 \times 10^4$ cal mol^{-1} for dissociation reaction. Rate constants as a function of temperature for the $CH_3C(=O)CH_2ONO$ <--> $CH_3C(=O)CH_2O\bullet$ + NO dissociation are shown in appendix B.

$$CH_3C(=O)CH_2ONO \text{ <--> } CH_3C(=O)CH_2O\bullet \ + \ NO$$
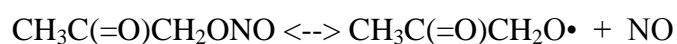
$$k_{\text{association}} \ = \ 5.7 \times 10^{11} \ T^{\,0.2} \ \exp(4421/T) \ \text{cm}^3 \ \text{mol}^{-1} \ \text{s}^{-1}$$

$$k_{\text{dissociation}} \ = \ 3.87 \times 10^{23} \ T^{\,-2.6} \ \exp(-20696/T) \ \text{s}^{-1}$$

For the acetyl reaction + NO_2 systems, the potential energy scans were performed using B3LYP/6-31G(d,) corrected by a scaling factor to use the CBS-QB3 energy for enthalpy of reaction. Frequency calculations were carry out by using B3LYP/6-31g(d,p) level DFT method. Figures describing the potential energy surfaces for R—NO_2 dissociation in nitroacetate are presented in appendix B. The association of acetyl radical with NO_2 to form nitro acetate ($CH_3C(=O)NO_2$), obtain $A = 3.11 \times 10^8$, $n = 1.5$, E_a = -1.54 x 10^3 cal mol^{-1}. The dissociation rate constant is $A = 4.25 \times 10^{21}$, $n = -1.65$, E_a = 5.17 x 10^4 cal mol^{-1}. The variational transition state is between 3.0 A° at 2000 K and 3.9 A° at 300 K.

$$CH_3C\bullet(=O) + NO_2 \text{ <--> } CH_3C(=O)NO_2$$
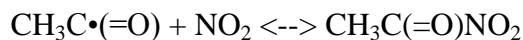
$$k_{\text{association}} \ = \ 3.11 \times 10^8 \ T^{\,1.5} \ \exp(773/T) \ \text{cm}^3 \ \text{mol}^{-1} \ \text{s}^{-1}$$

$$k_{\text{dissociation}} \ = \ 4.25 \times 10^{21} \ T^{\,-1.65} \ \exp(-26050/T) \ \text{s}^{-1}$$

4.4.3 Kinetics

Multifrequency quantum Rice Ramsperger- Kassel (QRRK) calculations for $k(E)$ with master equation analysis are performed on acetonyl + NO_2 chemical activation reaction system to estimate rate constants and to determine important reaction paths as a function of temperature and pressure. This kinetic analysis is for the chemical activation and the dissociation reaction systems. The master equation analysis uses an exponential-down model for the energy transfer function with (ΔE°_{down}) 900 cal/mol for N_2 as the third body. Rate constants, $k(E)$, were evaluated at 1.0 kcal mol^{-1} increments, to 70 kcal mol^{-1} above the highest barrier. Lennard-Jones parameters, σ (Å), and ε/κ (K) are obtained from tabulations and from an estimation method based on molar volumes and compressibility, σ = 6.2 Å and ε/k_b = 747 K. Table 4.4 presents high-pressure-limit elementary rate parameters used as input data and results versus pressure and temperature are in appendix B.

Table 4.4 High-Pressure-Limit Elementary Rate Parameter for reactions in the Acetonyl Radical + NO_2

Input Parameters for QRRK Calculations with Master Equation Analysis for Falloff
high-pressure-limit rate constants

Reaction			A	n	E_a (kcal/mol)
				k	
C•H$_2$C(=O)CH$_3$ + NO$_2$	=>	CH$_3$C(=O)CH$_2$ONO	2.93E+00	3.24	8.44
C•H$_2$C(=O)CH$_3$ + NO$_2$	=>	CH$_3$C(=O)CH$_2$NO$_2$	1.81E+08	1.48	-0.19
CH$_3$C(=O)CH$_2$ONO	=>	CH$_3$C(=O)CH$_2$O• + NO	3.87E+23	-2.56	42.20
CH$_3$C(=O)CH$_2$ONO	=>	CH$_3$C(=O)HC(=O)+HNO	2.47E+9	1.19	35.77
CH$_3$C(=O)CH$_2$ONO	=>	CH$_3$C(=O)CH$_2$NO$_2$	8.47E+10	1.10	65.12
CH$_3$C•(=O) + NO$_2$	=>	CH$_3$C(=O)ONO	6.02E+02	2.69	2.43
CH$_3$C•(=O) + NO$_2$	=>	CH$_3$C(=O)NO$_2$	3.11E+08	1.47	-1.54
CH$_3$C(=O)ONO	=>	CH$_3$C(=O)NO$_2$	4.64E+08	0.85	39.00
CH$_3$C(=O)ONO	=>	CH$_2$=C=O + HONO	2.22E+6	1.59	45.59
CH$_3$C(=O)NO$_2$	=>	CH$_2$=C=O + HONO	4.00E+8	1.50	35.50

4.4.4 Acetonyl Radical + NO$_2$ Reaction System

The potential energy diagrams for the chemical activation calculation of the acetonyl radical + NO$_2$ reactions are shown in Figure 4.6. The nitrite formation is calculated by B3LYP to be addition reaction, addition of R• to the O atom of the O=NO double bond. The barrier for nitrite association (R-ONO) is 9.10 kcal mol^{-1}.

No barrier is observed for the formation of nitro adduct (R-NO$_2$). The well depth (chemical activation) for nitro (CH$_3$C(=O)CH$_2$NO$_2$*) adduct is 51.4 kcal mol^{-1}. The nitro adduct has only a 0.3 kcal mol^{-1} lower energy than the nitrite adduct.

This data results in similar enthalpies for the two adducts, -51.6 kcal mol^{-1}for nitroacetone and -51.3 kcal mol^{-1} for 2 propanone nitrite, but they are separated by a high barrier for isomerisation.

The nitro (CH$_3$C(=O)CH$_2$NO$_2$*) energize adduct can undergo dissociation back to reactants, stabilization to CH$_3$C(=O)CH$_2$NO$_2$, or undergo a nitro to nitrite rearrangement to CH$_3$C(=O)CH$_2$ONO via three-member ring transition state. The barrier for isomerization from nitro to the nitrite isomer is 65.6 kcal mol^{-1} and this barrier, 14.3 kcal mol^{-1} above the entrance channel makes this isomerization reaction **un**-important in these reaction systems.

The nitrite (CH$_3$C(=O)CH$_2$ONO*) energize adduct can undergo dissociation back to reactants, isomerization to CH$_3$C(=O)CH$_2$NO$_2$ or undergo dissociation to CH$_3$C(=O)CH$_2$O• + NO (E_a = 38.9 kcal mol^{-1}) via simple RO-NO bond cleavage. The loose transition state and low energy of the simple NO dissociation reaction makes it the important product channel under all temperatures and pressures studied. The barrier for HNO elimination is 36.1 kcal mol^{-1} which is 14.9 kcal mol^{-1} below the entrance channel.

The molecular elimination of HNO with formation of acetylformaldehyde is also an important product.
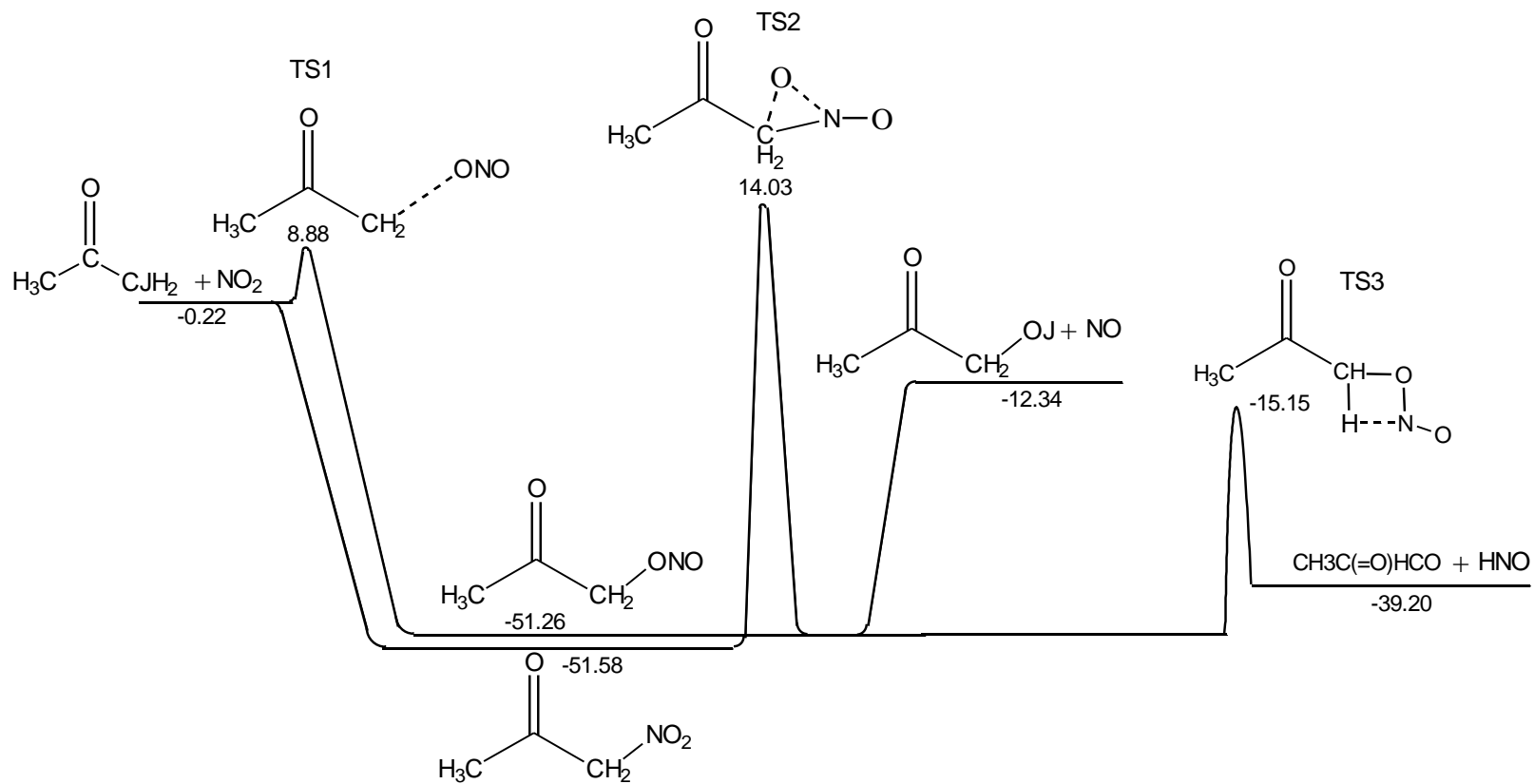
Figure 4.6 Potential energy diagrams for the acetonyl radical $(CH_3C(=O)CH_2\bullet)$ + NO_2 reaction system.

Chemical Activation Reaction, Acetonyl Radical + NO$_2$ → CH$_3$C(=O)CH$_2$ONO* → Products

Rate constants for acetonyl radical + NO$_2$ → CH$_3$C(=O)CH$_2$ONO* → products at 1 atm pressure versus 1000/T (K) are illustrated in Figure 4.7. All forward reaction goes to the low energy CH$_3$C(=O)CH$_2$O• + NO channel and this is the dominant reaction channel over all temperatures. CH$_3$C(=O)CH$_2$ONO stabilization is important below 700 K and falls off above 1000 K. The molecular dissociation (HNO elimination) channel is also important above 700 K.

Plots of calculated rate constants for acetonyl radical + NO$_2$ at 300 K versus log pressure (atm) are shown in Figure 4.8. At 300 K nitrite stabilization is the dominant path above 10 atm. The CH$_3$C(=O)CH$_2$O• radical + NO is an important reaction channel below 10 atm follow by the HNO elimination reaction which is four order of magnitude lower.

Rate constants at 1800 K versus pressure are shown in Figure 4.9. At high temperature, the CH$_3$C(=O)CH$_2$O• + NO channel dominates all of the pressure studied followed by molecular dissociation (HNO elimination) channel. Both reaction channels are independent to the pressure at this high temperature.

Figure 4.7 Plot of rate constants versus 1000/T (K) at 1 atm pressure for chemical activation of acetonyl radical + NO_2 → $CH_3C(=O)CH_2ONO^*$ → products.
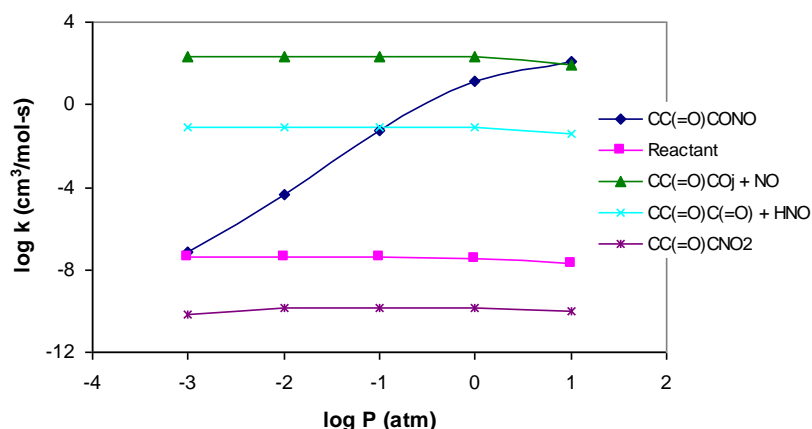
Figure 4.8 Plot of rate constants versus log pressure (atm) at 300 K for chemical activation of acetonyl radical + NO_2 → $CH_3C(=O)CH_2ONO^*$ → products.
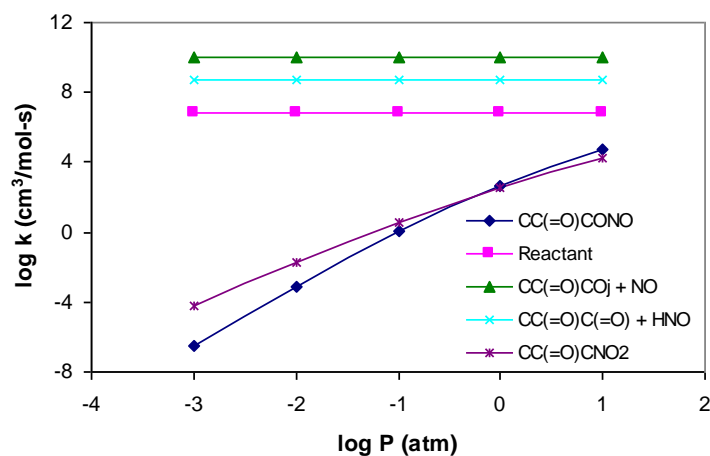
Figure 4.9 Plot of rate constants versus log pressure (atm) at 1800 K for chemical activation of acetonyl radical + NO_2 → $CH_3C(=O)CH_2ONO^*$ → products.

Chemical Activation Reaction, Acetonyl Radical + NO$_2$ → CH$_3$C(=O)CH$_2$NO$_2$* → Products

Chemical activation rate constants vs 1000/T at 1 atm for acetonyl radical + NO$_2$ → CH$_3$C(=O)CH$_2$NO$_2$* → products are presented in Figure 4.10. At atmospheric pressure, CH$_3$C(=O)CO• + NO is the dominant path at lower temperature and dissociation back to reactants reduces the forward paths at temperatures above 1000 K. Figure 4.11 and Figure 4.12 show plot of rate constants versus log P at 300 K and 1800 K, respectively. At 300 K, the CH$_3$C(=O)CH$_2$ONO adduct and the dissociation to CH$_3$C(=O)CH$_2$O• + NO are the dominant channels. At 1800 K, forward reactions go to CH$_3$C(=O)CH$_2$O• + NO follow by HNO molecular elimination are dominant channel and both reaction paths are independent to the pressure at this high temperature.
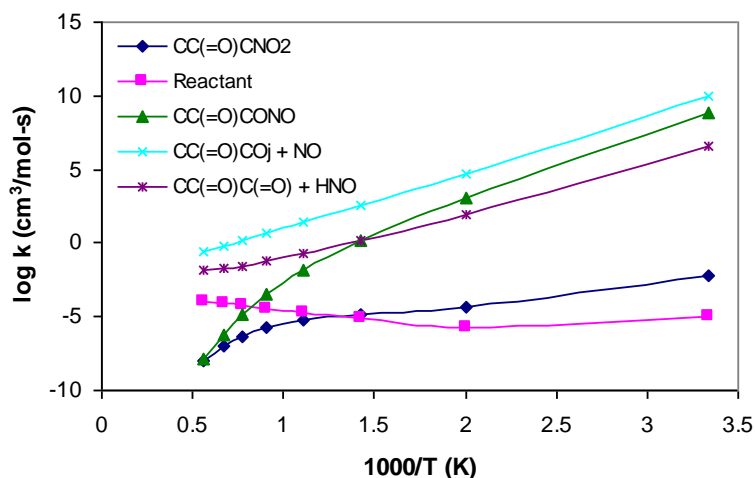
Figure 4.10 Plot of rate constants versus 1000/T (K) at 1 atm pressure for chemical activation of acetonyl radical + NO$_2$ → CH$_3$C(=O)CH$_2$NO$_2$* → products.
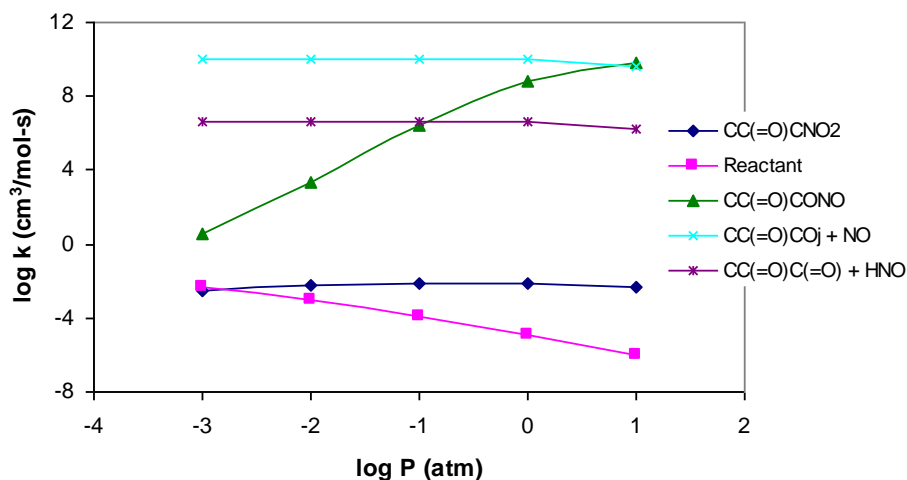
Figure 4.11 Plot of rate constants versus log P (atm) at 300 K for chemical activation of acetonyl radical + NO_2 → $CH_3C(=O)CH_2NO_2*$ → products.
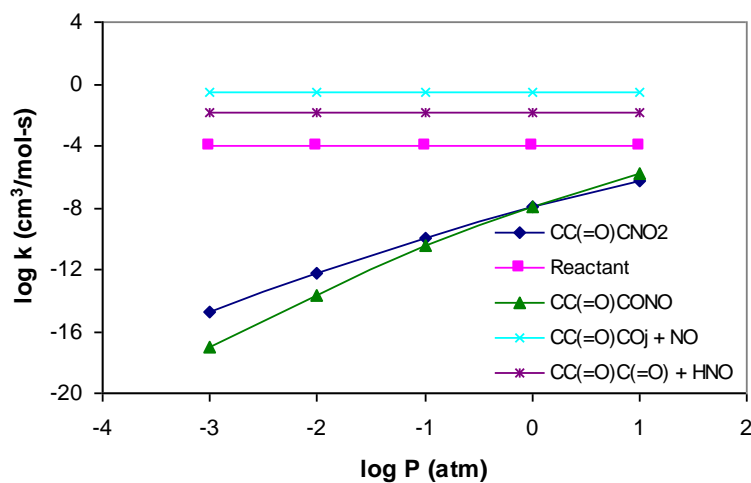
Figure 4.12 Plot of rate constants versus log P (atm) at 1800 K for chemical activation of acetonyl radical + NO_2 → $CH_3C(=O)CH_2NO_2*$ → products.

Unimolecular Dissociation of 2 Propanone nitrite and Nitro acetone

Rate constants for $CH_3C(=O)CH_2ONO$ dissociation at 1 atm pressure versus 1000/T are illustrated in Figure 4.13. $CH_3C(=O)CH_2O\bullet$ + NO and $CH_3C(=O)HC(=O)$ + HNO product channels are important at all range temperature and pressure studied. The high barrier for isomerization to $CH_3C(=O)CH_2NO_2$ results in it being the least favour channel.

There are two channels for dissociation of nitro acetone adduct, isomerisation to CH$_3$C(=O)CH$_2$ONO and dissociation back to reactants. The C•H$_2$COCH$_3$ + NO$_2$ (reactant) channel is the dominant channel because of the lower barrier 51.2 kcal mol^{-1} compare to 65.6 kcal mol^{-1} for isomerization.
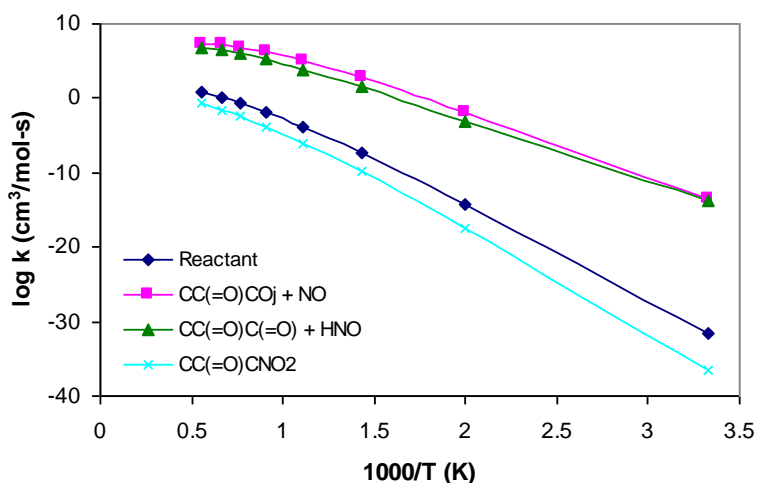
Figure 4.13 Plot of rate constants versus 1000/T (K) at 1 atm pressure for CH$_3$C(=O)CH$_2$ONO dissociation.

4.4.5 Acetyl Radical + NO$_2$ Reaction System

Figure 4.14 illustrates the potential energy diagram for the acetyl radical reaction with NO$_2$ to form chemically activated 1 nitro ethanal (CH$_3$C(=O)NO$_2$*) and ethanal 1 nitrite (CH$_3$C(=O)ONO*). The association barrier for nitrite formation of CH$_3$C(=O)ONO is 2.8 kcal mol^{-1} while formation of the nitro-acetyl adduct is observed to have no barrier, with a well depth of 51.0 kcal mol^{-1}. This (CH$_3$C•(=O)--NO$_2$) bond is similar to the acetonyl systems above. The nitrite bond formed in the (CH$_3$C(=O)--ONO) group is significantly stronger (13 kcal mol^{-1}), due to the oxygen bonding to the carbonyl group in this acetyl system.

The ($CH_3C(=O)NO_2$) nitro compound undergoes molecular elimination to form ketene plus HONO through 5-member ring transition state over a barrier that is 15.2 kcal mol^{-1} below the entrance channel and 36 kcal mol^{-1} above the stabilized nitro adduct. This channel, has a tight transition state structure, which limits formation of this product set; it is the second path in importance for the nitro adduct. Isomerization of this nitroacetate to form an acetyl nitrite isomer has a lower barrier at 26.8 kcal mol^{-1} above the nitro adduct. This reaction path is a more important channel for the dissociation of nitroacetate adduct over all pressures and temperatures studied.

The nitrite isomer is formed with 63.6 kcal mol^{-1} activation energy and has a low energy exit channel to form acetyloxyl (acetic acid) radical plus NO; this simple dissociation reaction is 29.3 kcal mol^{-1} below the entrance channel. The loose transition state and low energy of this simple dissociation results in $CH_3C(=O)O\bullet$ + NO reaction path as the major product channel under all temperatures and pressures studied. There is also a HONO molecular elimination, which is 18.4 kcal mol^{-1}, below the entrance channel.
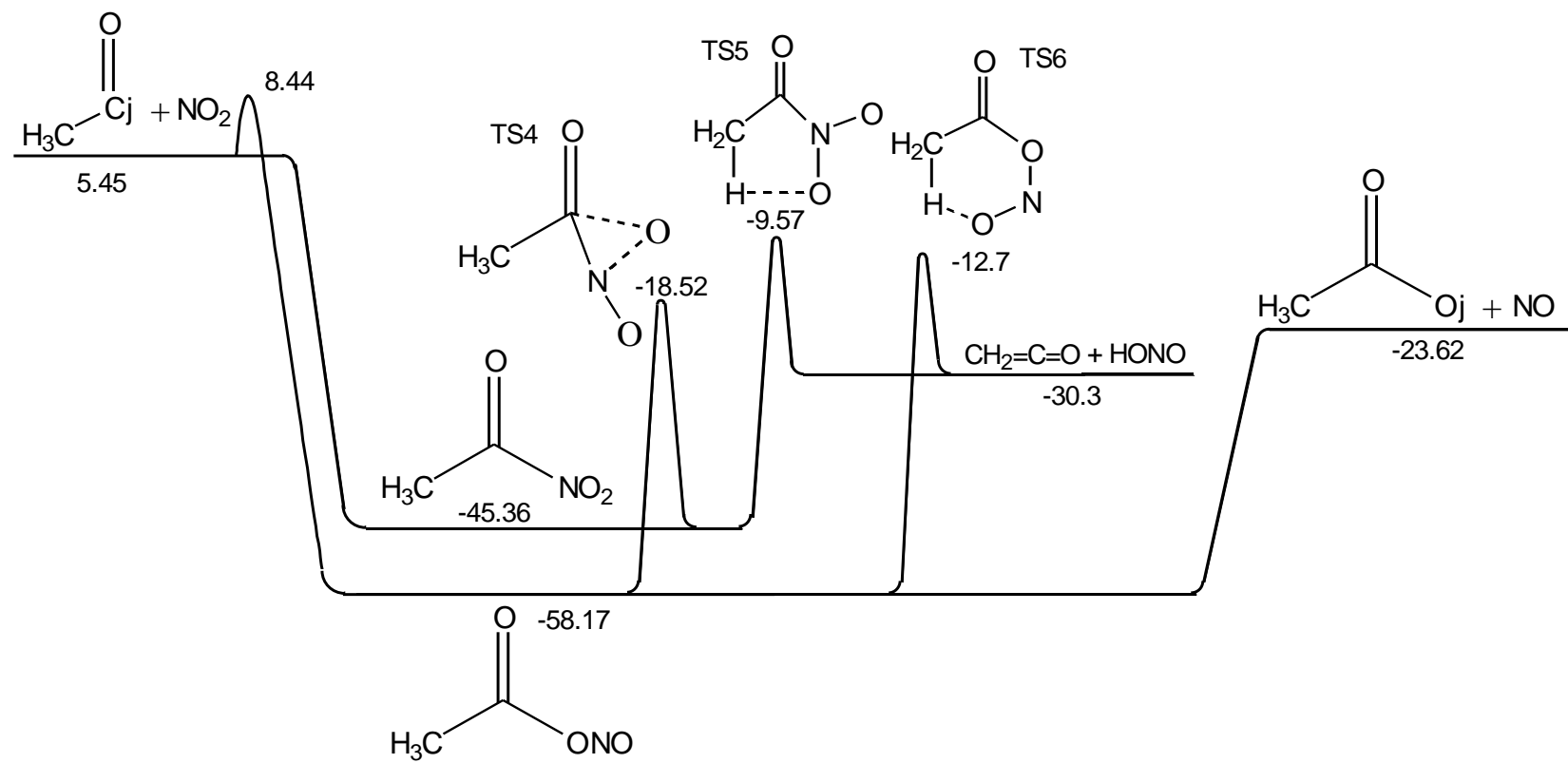
Figure 4.14 Potential energy diagram for the acetyl radical ($CH_3C\bullet(=O)$) + NO_2 reaction system.

Chemical Activation Reaction, Acetyl Radical + NO₂ → CH₃C(=O)NO₂* → Products

The chemical activation kinetics for the acetyl radical + NO₂ reaction are shown in Figure 4.15 one atmosphere pressure versus inverse temperature. The stabilized 1-nitro ethanal channel is dominant at low temperatures and it falls off rapidly above 500 K. At higher temperatures, 500-900 K, chemically activated 1 nitro ethanal (CH₃C(=O)NO₂*) dissociation to CH₃C(=O)O• + NO is important channel. Reverse dissociation of the energized adduct back to NO₂ + CH₃C•(=O) increases at higher temperature and reduces the importance of the acetyloxyl radical plus NO formation above 900 K.

Figure 4.16 shows the chemical activation rate constants for formation of the nitro adduct versus pressure at 300 K where stabilization dominates at high pressures and the acetyloxyl radical + NO reaction channel dominates below 0.1 atm. Rate constants versus pressure at 1800 K are shown in Figure 4.17. At high temperature, all forward reactions go to the CH₃C(=O)O• + NO reaction path and to HONO molecular elimination reaction.
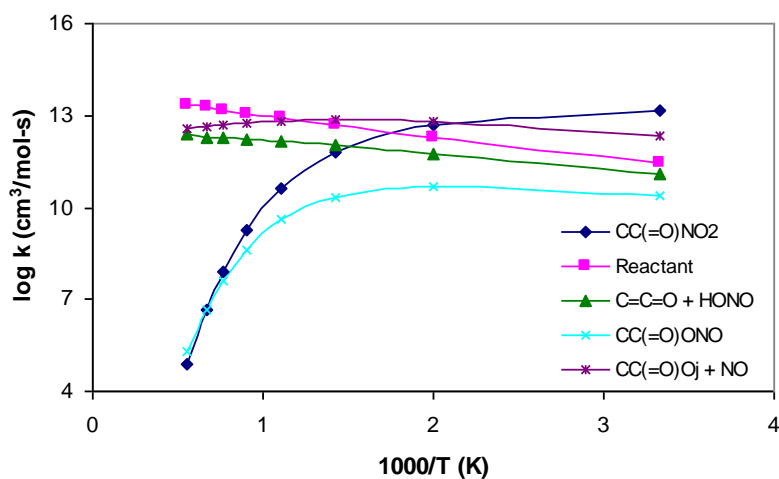
Figure 4.15 Chemical activation rate constants vs 1000/T at 1 atm for acetyl radical + NO₂ → CH₃C(=O)NO₂* → products.
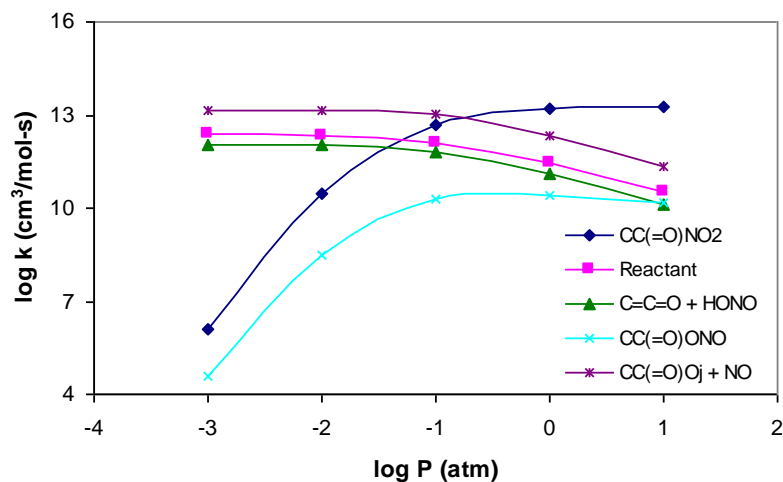
Figure 4.16 Chemical activation rate constants vs log P at 300 K for acetyl radical + NO_2 $\rightarrow$ $CH_3C(=O)NO_2^*$ $\rightarrow$ products.
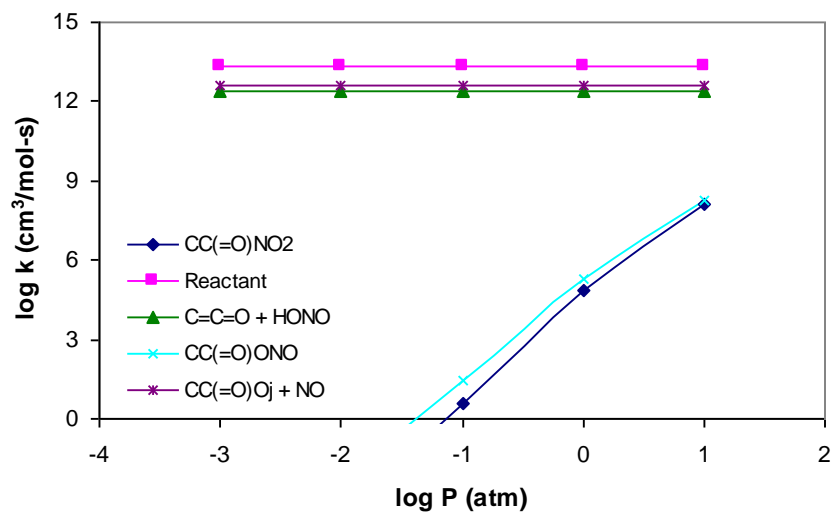
Figure 4.17 Chemical activation rate constants vs log P at 1500 K for acetyl radical + NO_2 $\rightarrow$ $CH_3C(=O)NO_2^*$ $\rightarrow$ products.

Chemical Activation Reaction, Acetyl Radical + NO_2 $\rightarrow$ $CH_3C(=O)ONO^*$ $\rightarrow$ Products

Chemical activation of acetyl nitrite mainly proceeds to the acetyloxyl radical+ NO reaction path which is a dominant reaction channel in all temperature and pressures due to the loose transition state and the lowest barrier in this reaction system at 35 kcal mol^{-1} above the nitrite adduct.
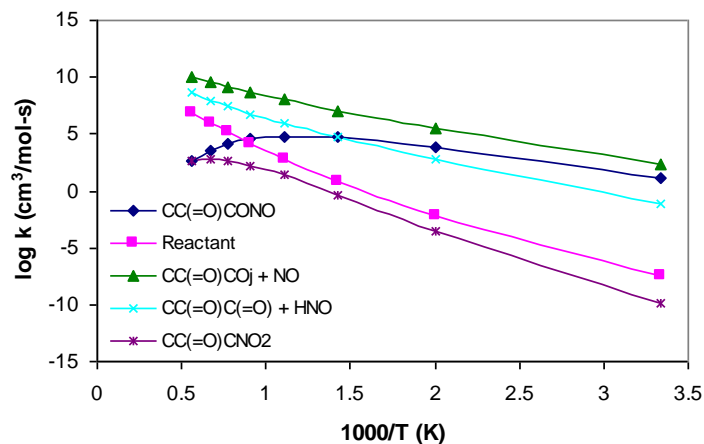
Plot of rate constants versus 1000/T (K) at 1 atm pressure for chemical activation of acetyl radical + NO_2 → $CH_3C(=O)ONO^*$ → products are presented in Figure 4.18. Figure 4.19 and Figure 4.20 show plot of rate constants versus log P at 300 K and 1500 K, respectively. The $CH_3C(=O)O\bullet$ + NO product are dominant in all dissociations.
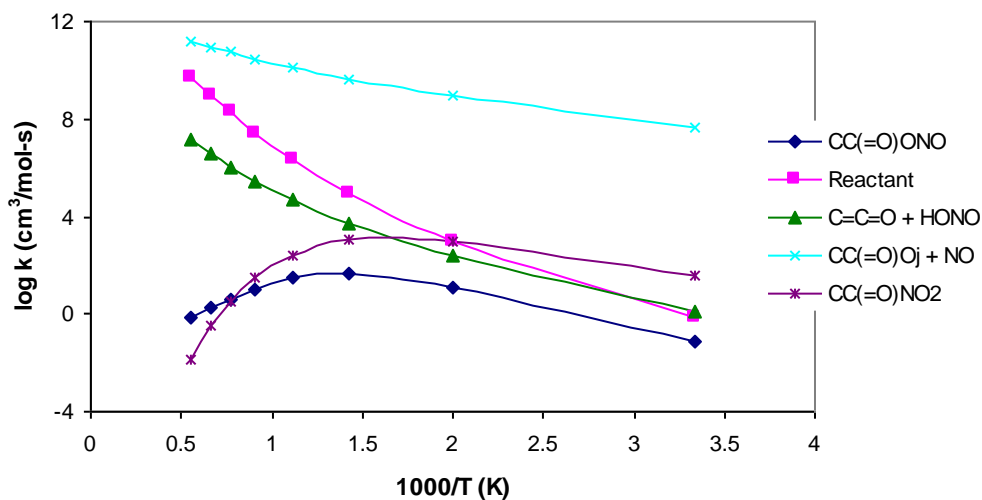
Figure 4.18 Chemical activation rate constants vs 1000/T at 1 atm for acetyl radical + NO_2 → $CH_3C(=O)ONO^*$ → products.
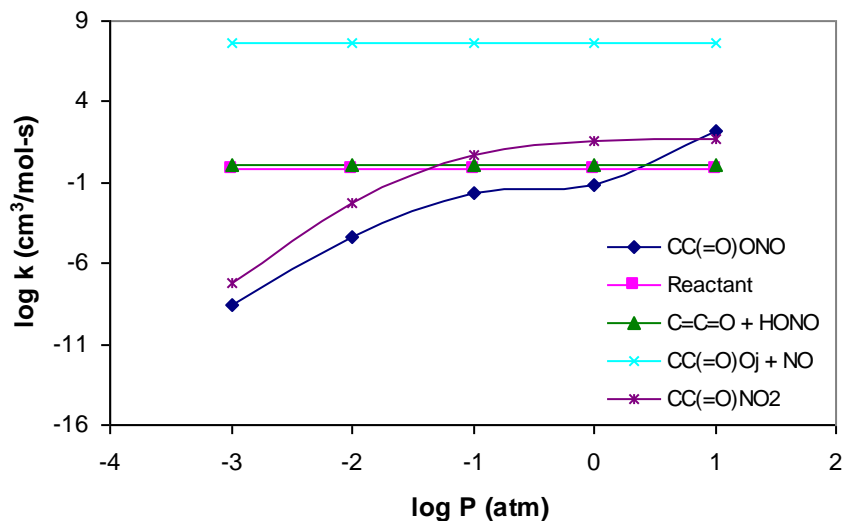
Figure 4.19 Chemical activation rate constants vs log P at 300 K for acetyl radical + NO_2 → $CH_3C(=O)ONO^*$ → products.
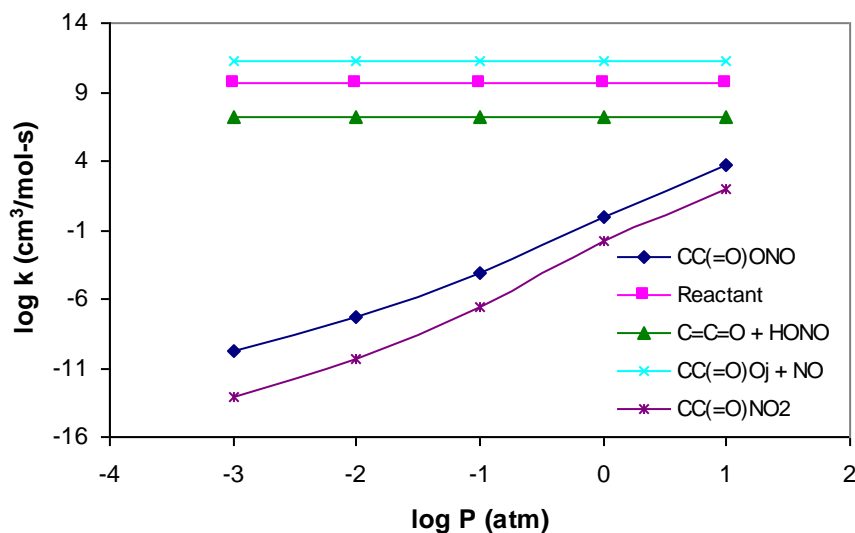
Figure 4.20 Chemical activation rate constants vs log P at 1500 K for acetyl radical + NO_2 → $CH_3C(=O)ONO^*$ → products.

Unimolecular Dissociation of Nitroacetate and Acetyl Nitrite

Figure 4.21 shows the QRRK calculated rate constants for the dissociation of nitro acetate. The low isomerisation barrier to to $CH_3C(=O)ONO$ of 27 kcal mol^{-1} makes the nitro-nitrite isomerisation an important reaction channel at all pressures and temperatures studied; this is followed by the ketene + HONO reaction channel which is a second lowest barrier, 36 kcal mol^{-1}. The nitrite isomer will dissociate to

The calculated rate constants for chemical dissociation of acetyl nitrite are illustrated in Figure 4.22. The dominant unimolecular dissociation channel for acetyl nitrite is to the acetyloxyl radical+ NO product set which has a loose transition state at a barrier of 34.6 kcal mol^{-1}. The second most important channel for acetyl nitrite dissociation is the isomerization from nitrite to nitro isomer through three-member ring transition state at E_a = 39.7 kcal mol^{-1}. Another important reaction path is ketene + HONO reaction channel.
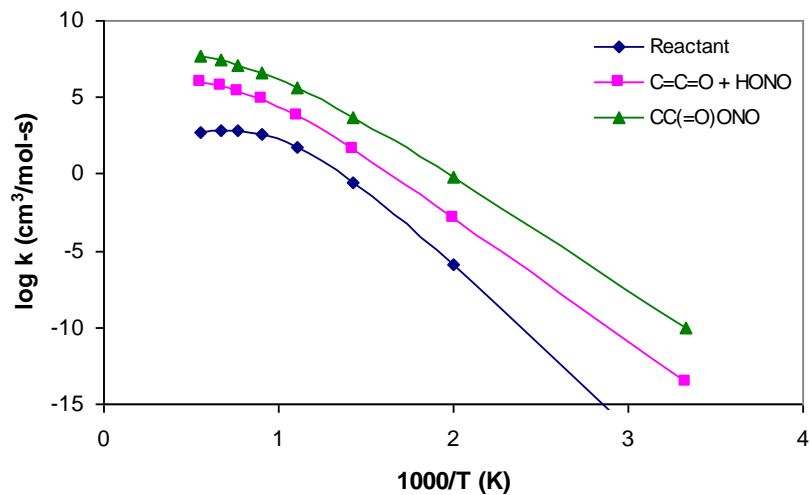
Figure 4.21 Plot of rate constants versus 1000/T (K) at 1 atm for $CH_3C(=O)NO_2$ dissociation.
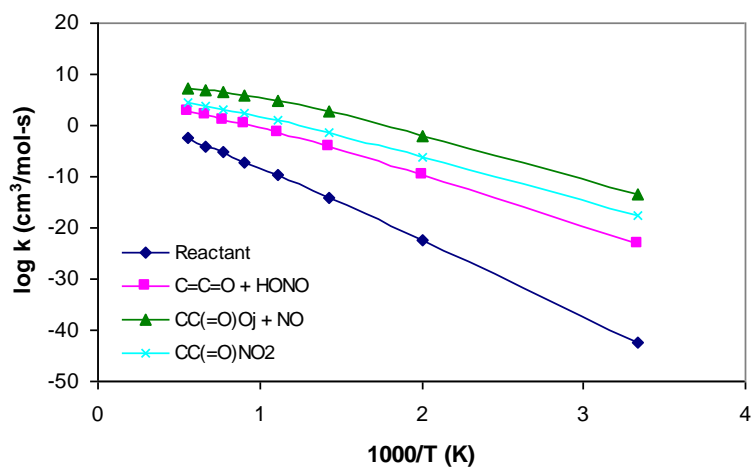
Figure 4.22 Plot of rate constants versus 1000/T (K) at 1 atm for $CH_3C(=O)ONO$ dissociation.

4.5 Summary

Thermochemical properties of intermediate radicals and transition state structures for the acetonyl radical and acetyl radical with NO_2 reaction systems are calculated using density functional and ab initio methods with enthalpies of formation ($\Delta H°f_{298}$) at the CBS-QB3 level. Entropies ($S°_{298}$) and heat capacities ($Cp(T)$) are also determined, which include internal rotor contributions. In this association of NO_2 to a carbonyl radical, the nitrite has a 7.3 kcal mol^{-1} deeper well than the nitro adduct, 58.4 versus 51.2, respectively. There is a 6.4 kcal mol^{-1} barrier for nitrite formation and no barrier is found for the formation of nitro adduct. The dissociation of 2 propanone nitrite and nitroacetate to form RCO• + NO have similar barriers at 39.1 kcal mol^{-1} for 2 propanone and 34.6 kcal mol^{-1} for nitroacetate. At atmospheric pressure and temperature both of the association paths for the R• + NO_2 → reactions proceed almost primarily to RCO• + NO reaction channel with a fraction of stabilization adduct and lower energy products. At combustion temperatures, the R• + NO_2 → R-ONO* adduct primarily dissociates to RCO• + NO via chemical activation reaction. The loose transition state and low energy of the simple dissociation results in the RO• + NO reaction path as the major dissociation reaction for 2 propanone nitrite and acetyl nitrite. The major dissociation reaction path for $CH_3C(=O)NO_2$ and $CH_3C(=O)CH_2NO_2$ adduct is the isomerization to the corresponding nitrite and dissociation of the nitrite to RC• (=O) + NO.

CHAPTER 5

THERMOCHEMICAL PROPERTIES FOR ISOOCTANE AND CARBON RADICALS: A COMPUTATIONAL STUDY

5.1 Overview

Thermochemical properties for isooctane, its internal rotation conformers and radicals with corresponding bond energies are determined by use of computational chemistry. Enthalpies of formation are determined using isodesmic reactions with B3LYP density function theory and composite CBS-QB3 methods. Application of group additivity with comparison to calculated values is illustrated. Entropy and heat capacities are determined using geometric parameters, internal rotor potentials and frequencies from B3LYP/6-31G(d,p) calculations for the lowest energy conformer. Internal rotor potentials are determined for the isooctane parent, the primary, secondary and tertiary radicals in order to identify isomer energies. Intramolecular interactions are shown to have a significant effect on the enthalpy of formation of the isooctane parent and its radicals. The computed standard enthalpy of formation for the lowest energy conformers of isooctane from this study is -54.40 ± 1.60 kcal mol^{-1}, which is 0.8 kcal mol^{-1} lower than the evaluated experimental value -53.54 ± 0.36 kcal mol^{-1}. The standard enthalpy of formation for the primary radical for a methyl on the quaternary carbon is -5.00 ± 1.69 kcal mol^{-1}, primary radical on the tertiary carbon is -5.18 ± 1.69 kcal mol^{-1}, the secondary isooctane radical is -9.03 ± 1.84 kcal mol^{-1}, and the tertiary isooctane radical is -12.30 ± 2.02 kcal mol^{-1}. Bond energy values for the isooctane radicals are 100.64 ± 1.73, 100.46 ± 1.73, 96.41 ± 1.88 and 93.14 ± 2.05 kcal mol^{-1} for C3•CCCC2, C3CCCC2•, C3CC•CC2 and

C3CCC•C2, respectively. Entropy and heat capacity values are reported for the lowest energy homologues.

5.2 Previous Studies

Isooctane, 2,2,4-trimethylpentane, holds an octane rating of 100 and is a major component in spark ignition engine fuels; it is widely used as a model (surrogate) compound in detailed reaction mechanisms that are applied to model ignition in spark and HCCI internal combustion engines. The ignition kinetics and oxidation product profiles of isooctane have been studied extensively using varied shock and flow experimental techniques and modeling has been performed with a number of detailed kinetic models.[118-125] The thermochemistry for species used in the kinetic models has routinely invoked group additivity or similar estimation techniques for thermochemical properties with bond energies from smaller molecule systems. Kinetic parameters involving reaction paths and rate constants have also been based on theoy or experimental data from smaller molecule reaction systems. Isooctane is however a highly branched molecule and its structure may have a significant affect on its thermochemistry and reaction pre exponentials and barriers.

In this study, the thermochemical properties, enthalpy of formation, entropy and heat capacities of isooctane and carbon centered radicals corresponding to loss of a hydrogen atom at primary, secondary and tertiary sites are evaluated. The calculated $\Delta_f H^o(T)$, $Cp(T)$ and $S^0(T)$ values for the parent isooctane are in good agreement with evaluated literature data,[126,127-129,]; enthalpy data on the radicals is different from that of smaller hydrocarbons used as models.

5.3 Computational Methods

The structures of isooctane, radicals corresponding to loss of H atom, one-dimensional internal rotor potentials, bond dissociation energies, and standard enthalpies of formation for the radicals and parent have been calculated using B3LYP hybrid density functional theory in conjunction with the 6-31G(d,p) basis set, as well the complete basis set-QB3 composite method. CBS-QB3 is a multilevel model chemistry that combines the results of several *ab initio* and DFT individual methods and empirical correction terms to predict molecular energies with high accuracy and reasonable low computational cost. The required electronic structure calculations are outlined as follows: (i) B3LYP/6-311G(2d,d,p) level geometry and frequencies; (ii) MP2/6-311G(3df,2df,2p) energy and CBS extrapolation; (iii) MP4-(SDQ)/6-31G(d(f),p) energy; (iv) CCSD(T)/6-31+G(d') energy corrections. All quantum chemical calculations have been performed within the Gaussian-03 suite of programs.

To more accurately evaluate the heats of formation ($\Delta_f H^o_{298}$) of the parent molecule and radicals a variety of homodesmic and isodesmic work reactions are used, where the bonding environments are similar in products and reagents. An isodesmic reaction is a hypothetical reaction where the number and type of bonds is conserved on each side of the work reaction; a homodesmic reaction conserves number and type of bonds, but also conserves hybridization. $\Delta_{rxn} H^o_{298}$ is calculated and known $\Delta_f H^o_{298}$ values of the reference molecules are used with the calculated $\Delta_{rxn} H^o_{298}$ to determine the standard enthalpies of formation. The similar structure components on both sides of the work reaction provide a cancellation of error in the calculated $\Delta_{rxn} H^o_{298}$ and a thus increase in accuracy.

5.3.1 Methods to Determine Thermodynamic Properties of Isooctane and Its Radicals

Curtiss et al. and Ochterski and co-workers reported mean absolute deviations of 1.1 kcal mol^{-1}for CBS-Q methods by comparing the energies of 125 computationally reactions to their corresponding experimental values.[106-109] These values, however, include molecules and reactions that are dissimilar to the systems studied here. In order to assess the accuracy of the calculation method for the standard enthalpies of formation of isooctane and its radicals, eleven reactions were used to calculate and compare results with literature values. Table 5.1 lists the 15 reference reactions and shows a root mean square (RMS) deviation of 0.73 kcal mol^{-1}for CBS-QB3 and 1.33 kcal mol^{-1} for B3LYP/6-31G(d,p). The 95% confidence limit values are 1.56 kcal mol^{-1}for CBS-QB3 and 2.84 kcal mol^{-1} for B3LYP/6-31G(d,p). The calculation error for these small size molecules may be lower than for the eight carbon isooctanes; however there is less cancellation of error from the small molecule reference reactions, than there is in this research work reactions, because of the similar bonding environments on each side. The error for these work reactions with larger species should be similar or less than the error limits from Table 5.1.

The CBS-QB3 reproduces the experimental results better than B3LYP/6-31G(d,p), are recommended where experimental values are not available. Further reference will reflect the values from CBS-QBS for standard enthalpies of formation of the lowest energy conformers of isooctane and its radicals, with the B3LYP/6-31G(d,p) being referred to when relevant.

Table 5.1 Comparison of Experimental $\Delta_{rxn}H^o{}_{298}$ with Values Determined Using CBS-QB3 and B3LYP/6-31G(d,p) in this Study (kcal mol^{-1})

[a] For standard enthalpies of formation at 298 K of reference species please see Table 5.3.

Reactions [a]	Experimental	CBS-QB3	B3LYP/6-31G(d,p)
$\bullet C_2H_5 + \bullet CH_3 \rightarrow C_3H_8$	-88.47	-89.70	-85.48
$\bullet CH_3 + CH_2=C\bullet H \rightarrow CH_2=CHCH_3$	-101.27	-101.32	-98.51
$n\text{-}\bullet C_3H_7 + CH_4 \rightarrow C_3H_8 + \bullet CH_3$	3.91	2.99	4.08
$i\text{-}\bullet C_3H_7 + \bullet H \rightarrow \bullet C_2H_5 + \bullet CH_3$	-10.65	-9.22	-11.39
$i\text{-}\bullet C_4H_9 \rightarrow t\text{-}\bullet C_4H_9$	-6.38	-5.47	-7.84
$\bullet CH_3 + CH_2=CHCH_3 \rightarrow i\text{-}\bullet C_4H_9$	-22.45	-21.87	-21.10
$C_2H_6 + H_2 \rightarrow 2\ CH_4$	-15.53	-14.72	-16.27
$\bullet CH_3 + \bullet H \rightarrow CH_4$	-104.93	-105.39	-105.54
$\bullet C_2H_5 + \bullet H \rightarrow C_2H_6$	-100.53	-101.70	-100.78
$n\text{-}\bullet C_4H_9 \rightarrow s\text{-}\bullet C_4H_9$	-3.34	-2.77	-3.87
$\bullet C_2H_5 + CH_4 \rightarrow \bullet CH_3 + C_2H_6$	4.40	3.69	4.76
$\bullet C_2H_5 + C_3H_8 \rightarrow n\text{-}\bullet C_3H_7 + C_2H_6$	0.49	0.70	0.68
$t\text{-}\bullet C_4H_9 + n\text{-}C_4H_{10} \rightarrow s\text{-}\bullet C_4H_9 + t\text{-}C_4H_{10}$	2.95	1.96	3.34
$i\text{-}\bullet C_4H_9 + CH_4 \rightarrow \bullet CH_3 + t\text{-}C_4H_{10}$	3.38	2.73	3.94
$s\text{-}\bullet C_4H_9 + C_3H_8 = i\text{-}\bullet C_3H_7 + n\text{-}C_4H_{10}$	-0.30	-0.23	-0.23
RMS		**0.73**	**1.33**
95% confidence limits		**1.56**	**2.84**

5.3.2 Calculation of Hindered Rotation Contribution to Thermodynamic Parameters (Rotator)[12]

A technique for the calculation of thermodynamic functions from hindered rotations with arbitrary potentials has been developed by Krasnoperov, Lay and Shokhirev[12].This technique employs expansion of the hindrance potential in the Fourier series, calculation of the Hamiltonian matrix in the basis of the wave functions of free internal rotation, and subsequent calculation of energy levels by direct diagonalization of the Hamiltonian matrix.

The torsional potential calculated at discrete torsional angles is represented by a truncated Fourier series:

$$V(\phi) = a_0 + a_1 \cos(\phi) + a_2 \cos(2\phi) + a_3 \cos(3\phi) + b_1 \sin(\phi) + b_2 \sin(2\phi) \qquad (2.23)$$

where values of the coefficients a_i were calculated to provide the minima and maxima of the torsional potentials.

Evaluation of the matrix elements of individual sine and cosine terms is on the basis of the free rotor wave functions. Eigenvalues are used to calculate the partition function, entropy, heat capacity, *etc.* using direct summation over the calculated energy levels according to standard expressions of statistical thermodynamics.

5.4 Result and Discussion

5.4.1 Structure of Isooctane and Its Radicals, Internal Rotation Potentials

The optimized geometries at the CBS-QB3 composite level of theory, *viz.,* B3LYP/6-311(2d,d,p) calculations, for the target molecules and corresponding abbreviated nomenclatures are presented in Figure 5.1. Vibration frequencies, and moments of inertia for all structures are available in the appendix C.
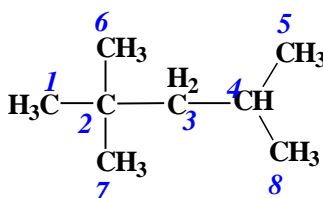
Scheme 5.1 Definition of Skeletal Atom in Isooctane Molecule and Carbon Atom Numbering
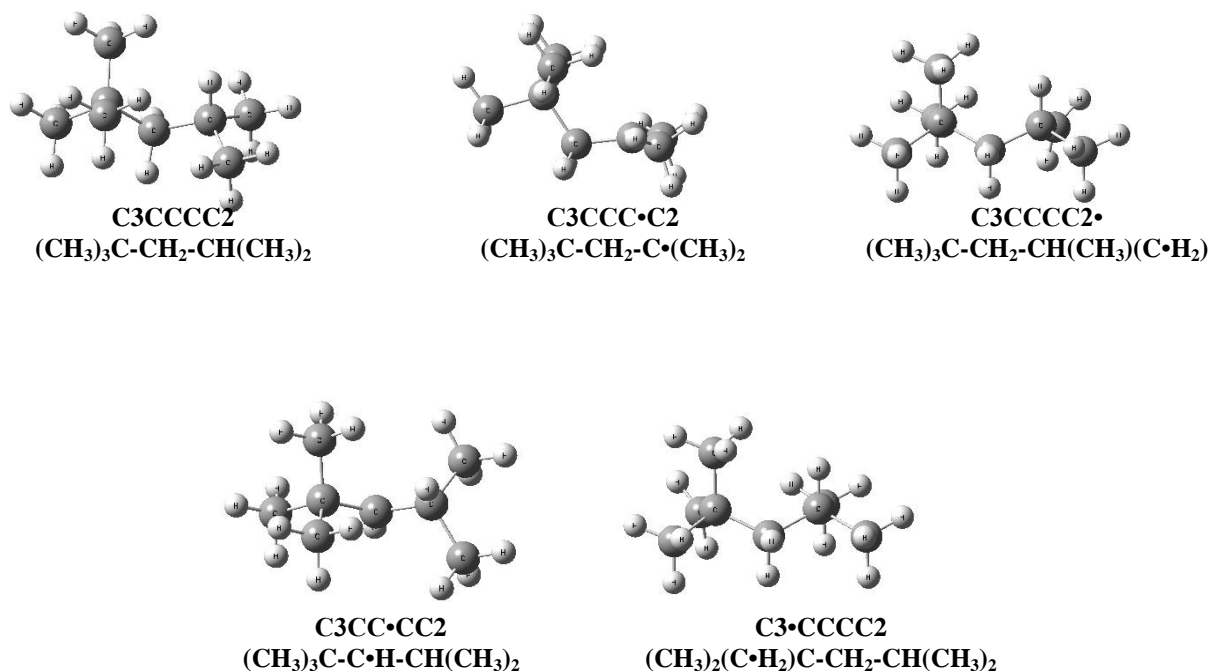
Figure 5.1 Geometry of lowest energy conformer of isooctane and its carbon radicals.

Energy profiles for internal rotation about the C-C bonds in the isooctane were calculated to determine lowest energy configurations, relative energies of the rotational conformers and for use in determination of entropy and heat capacity values versus temperature. The total energies as a function of the corresponding dihedral angles were computed at the B3LYP/6-31G(d,p) level of theory by scanning the torsion angles between 0° and 360° in steps of 15°, while all remaining coordinates were fully optimized. All potentials were re-scanned when a lower energy conformer was found (relative to the initial low energy structure) in order to verify identification of the lowest energy conformer. The total energy of the corresponding low energy conformer was arbitrarily set to zero and used as a reference point to plot the potential barriers. The resulting potential energy barriers for internal rotations about the C3—C4, the C2—C3 and methyl rotors in isooctane (2,2,4-trimethylpentane) are shown in Figure 5.2. The

calculation shows the energy of the barriers and isomers relative to the most stable form; zero point energies are not included in the potential curves.

Isooctane (C3CCCC2)

The lowest configuration of isooctane has the two methyls (C5 and C8) on the tertiary carbon anti to two methyls on the quaternary carbon (C2) The higher energy conformer in the internal rotor potential (3.5 kcal mol^{-1} higher than the minimum) has two methyls on the tertiary carbon near eclipsed to two methyls on the quaternary carbon. Each maximum on this potential curve corresponds to one methyl on the tertiary carbon gauche (between) two methyls on the quaternary carbon.

The calculated rotational barriers of methyl groups in isooctane show three-fold symmetry with barriers of 3.5-3.7 kcal mol^{-1} for all five methyl rotors; these are slightly higher ~ 0.5 kcal mol^{-1} than methyl rotor potentials in *n*-hydrocarbons. Rotational barriers of the *tert*-butyl group (C3C—R) exhibit three-fold symmetry with barriers of 4.1 kcal mol^{-1}. The secondary-tertiary carbon rotor (C3—C4) has two-fold symmetry and a barrier of 7.2 kcal mol^{-1}. The methyl rotor shown in Figure 5.2 is the C1 – C2 rotor.
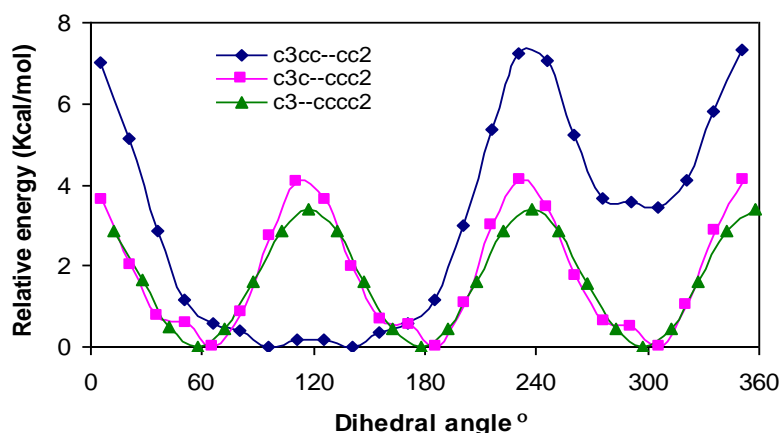
Figure 5.2 Potential energy profiles for internal rotations in isooctane.

Isooctane Tertiary Radical (C3CCC•C2)

The lowest energy configuration of the isooctane tertiary carbon radical (C3CCC•C2), forms a near planar isopropyl radical group with one methyl on the isopropyl gauche to two methyls on the quaternary carbon. The radical has two quasi planes separated by the tertiary carbon − secondary carbon bond. One can consider the top plane as that of the three methyl groups on the quaternary carbon at a 30° slope up. From the quaternary carbon to the secondary carbon is a step down to the near planar (horizontal) *tert*-radical radical system see Figure 5.1. There is ~ 5 degree bend of the *tert*-radical system out of plane, away from the quaternary carbon system and the potential is near 20 kcal mol^{-1} at ± 20° from equilibrium. The frequency describing the symmetric bending (motion that would correspond to inversion in ammonia but here the minimum is near planar) is calculated as 305 cm^{-1}.The potential appears harmonic and is illustrated in the appendix C. Internal rotation of the isopropyl group has two maxima each having an isopropyl methyl eclipsed to the secondary carbon (C3) and one methyl gauche to two methyls on the quaternary carbon.

Potential Energy Curves for Internal Rotation in C3CCC•C2. The quaternary carbon (*tert* butyl) rotor in this tertiary radical, C3C—CC•C2, is similar to C2—C3 rotor in the parent isooctane. The C3—C4 rotor, C3CC—C•C2, exhibits two-fold symmetry with a barrier of 4.5 kcal mol^{-1} this is reduced from the parent by 2.7 kcal mol^{-1} (7.2 kcal mol^{-1} in parent isooctane).

Secondary Radical (C3CC•CC2) in Isooctane

The lowest energy configuration of secondary radical (C3CC•CC2) has C2-C3-C4 a structure similar to that described above in the parent isooctane. The C3—C4 rotor has

one broad 4.5 kcal mol^{-1} barrier. The quaternary—secondary carbon rotor (C2—C3) has low (0.5 kcal mol^{-1}) three-fold, symmetric barrier that results from rotation of the symmetric *tert*-butyl group.

Potential Energy Profiles for Internal Rotations in C3CC•CC2. The rotation barrier of the *tert*-butyl rotor in secondary radical, C3C—C•CC2, is reduced to 0.5 kcal mol^{-1}, approaching a free rotor, with a three-fold symmetry. The C3CC•—CC2 rotor exhibits one broad barrier at 4.5 kcal mol^{-1}.

Isooctane Primary (Methyl) Radical on *tert*-Butyl Site (C3•CCCC2)

The lowest energy configuration of a methyl radical on a quaternary carbon (C1, C6, C7), C3•CCCC2, occurs when the tertiary carbon is near eclipsed to the methyl radical on the quaternary carbon. Three maxima correspond to the tertiary carbon (C4) eclipsing one of the methyls from quaternary carbon.

Potential Energy Profiles for Internal Rotations in C3•CCCC2. The *tert*-butyl rotor with a primary carbon radical on *tert*-butyl site, C3•C—CCC2, has a distorted three-fold potential at 5.8 kcal mol^{-1}; this is higher than that in the parent (4.1 kcal mol^{-1}). The C3•CC—CC2 rotor potential is similar to C3—C4 rotor in the parent. The methyl radical rotor, C3•—CCCC2, has a broad two-fold potential at 1.6 kcal mol^{-1} compared to three-fold symmetry for the parent.

Isooctane Primary Radical on Isopropyl Site (C3CCCC2•)

The lowest configuration for a methyl radical (C5, C8) on isopropyl site C3CCCC2•, is similar to that described above for a methyl radical on a *tert*-butyl site. Two maxima occur when a methyl on the tertiary carbon is eclipsed with the quaternary carbon (C2).

Potential Energy Profiles for Internal Rotations in C3CCCC2•. The *tert*-butyl rotor in this intermediate with a primary carbon radical on the isopropyl site, C3C—CCCC2•, is similar to C2—C3 rotor in the parent; it has three-fold symmetry with 4.1 kcal mol^{-1} barrier. The methyl radical rotor, C3CCC—C2•, is similar to the one in primary radical on *tert*-butyl site with a broad two-fold potential at 1.4 kcal mol^{-1}. The C3—C4 (C3CC—CC2•) rotation barrier increases to 9.0 kcal mol^{-1} relative to that in the parent (7.2 kcal mol^{-1}), probably due to the change of structure by the formed sp2 radical of the isopropyl group.

5.4.2 Enthalpies of Formation and Bond Dissociation Energies

The enthalpies of formation for isooctane and each of the four radicals, two primary sites, one secondary and one tertiary site, are calculated from five work reactions. The standard enthalpies of formation for two additional tertiary radicals, 2-methylbut-2-yl and 2-methylpent-2-yl, and one secondary radical, 2-methylbut-3-yl are calculated. The additional two tertiary radicals and one secondary radical were calculated for use as comparisons of bond energies and as reference species.

Contributions to the entropy and heat capacity from the symmetric bending of the *tert*-butyl radical C3CCC•C2 were determined using the corresponding frequency. The potential vs. bend angle for this motion is illustrated in Figure C1 in the appendix C

The standard enthalpies of formation at 298 K for reference species used in the work reactions are summarized in Table 5.3. The zero point energies are scaled by 0.9806 for B3LYP/6-31G(d,p) calculations as recommended by Scott et al.

Enthalpies of formation of the isooctane molecule and the four radicals along with a listing of the work reactions are in Table 5.4 which also lists the uncertainty for each work reaction. The uncertainty is determined from the square root of the sum of squares of the uncertainty in the reference species and the uncertainty of each calculation method, $\pm$ 1.56 kcal mol^{-1} for CBS-QB3 and $\pm$ 2.84 kcal mol^{-1} for B3 B3LYP/6-31g(d,p) as shown in Table 5.1.

Enthalpy of formation for the parent isooctane is calculated at -54.40 $\pm$ 1.60 kcal mol^{-1}, which is 0.8 kcal mol^{-1} lower than the value reported by Rossini[1] at -53.57 $\pm$ 0.32 kcal mol^{-1} and -53.54 $\pm$ 0.36 [36] kcal mol^{-1} There are two recent, calculated enthalpy values reported for isooctane, an empirical estimation method developed by Mavrovouniotis[27] based on contributions of atoms and bonds lists an enthalpy of formation for isooctane as -53.61 kcal mol^{-1}. A higher level theoretical study by Karton et al[28] using the Quasi-W4 computational method for a series of hydrocarbons reports -53.29 kcal mol^{-1}for the standard enthalpy of formation of isooctane.

Bond dissociation energies are determined using the derived $\Delta_r H^o_{298}$ of parent molecules and of the radicals corresponding to the loss of a hydrogen atom. 52.10 $\pm$ 0.00 kcal mol^{-1} is used for the standard enthalpy of formation of hydrogen atom at 298 K and the literature value for isooctane -53.54 is used in bond energy determinations. The bond dissociation enthalpies computed from isodesmic enthalpies of formation are in Table 5.4.

Work reactions, enthalpies of formation and bond dissociation energies for tertiary radicals, 2-methylbut-2-yl, 2-methylpent-2-yl and the secondary radical, 2-methylbut-3-yl are listed in the appendix C. The CBS-QB3 calculated bond enthalpies for

the tertiary C—H bond dissociation energies on 2-methylbut-2-yl radical ($(CH_3)_2C \cdot CH_2CH_3$) and 2-methylpent-2-yl radical ($(CH_3)_2C \cdot CH_2CH_2CH_3$) are 95.95 ± 1.69 and 95.68 ± 1.69 kcal mol^{-1}, respectively. These are in good agreement with accepted tertiary C—H bond energy of isobutane at 95.17 ± 0.72 kcal mol^{-1}.

The secondary bond dissociation energy in 2-methylbut-3-yl radical ($(CH_3)_2CHC \cdot HCH_3$) is 97.86 ± 1.69 kcal mol^{-1} in agreement with the secondary C—H bond dissociation energies, 97.82 ± 0.49 from C—H bond energy of the secondary carbon in propane, as presented in Table 5.2.

Table 5.2 C-H Bond Dissociation Energies for Primary, Secondary and Tertiary Carbon in Propane and Isobutene Compared to C-H Bond Energy in Isooctane

System	C—H bond dissociation energy (kcal mol^{-1})
Primary C-H bond energy	
$CH_3CH_2CH_3 \longrightarrow CH_3CH_2C \cdot H_2 + H$	101.02 ± 0.51
$(CH_3)_2(H\text{----}CH_2)C\text{-}CH_2\text{-}CH(CH_3)_2$	100.64 ± 1.73
$(CH_3)_3C\text{-}CH_2\text{-}CH(CH_3)(H\text{----}CH_2)$	100.46 ± 1.73
Secondary C-H bond energy	
$CH_3CH_2CH_3 \longrightarrow CH_3C \cdot HCH_3 + H$	97.82 ± 0.49
$(CH_3)_3C\text{-}(H\text{----}CH)\text{-}CH(CH_3)_2$	96.41 ± 1.88
Tertiary C-H bond energy	
$(CH_3)_3CH \longrightarrow (CH_3)_3C \cdot + H$	95.17 ± 0.72
$(CH_3)_3C\text{-}CH_2\text{-}(C\text{----}H)(CH_3)_2$	93.14 ± 2.05
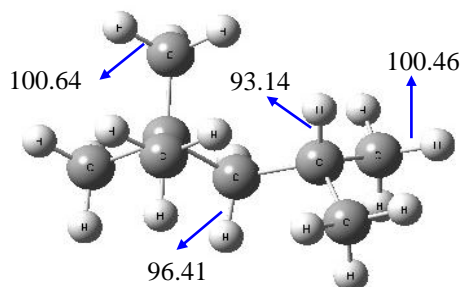
Scheme 5.2 C—H Bond Dissociation Energy in Isooctane (kcal mol^{-1})

Isooctane bond dissociation energies (BDE) for primary radicals at C1,C6 and C7 positions (see scheme 5.2) are 100.64 ± 1.73. The BDE for the secondary radical (C3) is 96.41 ± 1.88 and the BDE for the tertiary radical (C4), level is 93.14 ± 2.05 kcal mol^{-1}. Bond enthalpies for primary carbons of the isopropyl group at C5 and C8 positions are 100.46 ± 1.73 kcal mol^{-1}.

The tertiary C—H bond energies of isooctane at 93.14 ± 2.05 kcal mol^{-1} is 2.03 kcal mol^{-1} lower than that of a tertiary butyl carbon (95.17 kcal mol^{-1}) and is expected to be more easily cleaved by radicals at low to mid cylinder temperatures preceding ignition in internal combustion engines. Under these conditions the reaction of *tert*-isooctane alkyl radical association with O_2 to generate an activated *tert*-isooctane peroxy adduct [30] will be important.

The C—H bond energies on the secondary carbon of isooctane (C3) at 96.41 ± 1.88 kcal mol^{-1} is about 1.41 kcal mol^{-1} lower than secondary bond energies on a normal alkane (97.82 kcal mol^{-1}), and the primary C—H bond energies of isooctane at 100.64 ± 1.73 and 100.46 ± 1.73, are about 0.5 kcal mol^{-1} lower than primary C—H bonds energies on normal alkanes, 101.02 kcal mol^{-1}.

Table 5.3 Standard Enthalpies of Formation at 298 K for Reference Species

[a] From this study, work reactions are provided in the Appendix C

Species	$\Delta_fH^o_{298}$ (kcal mol^{-1})	Species	$\Delta_fH^o_{298}$ (kcal mol^{-1})
H	52.10 ± 0.00 [94]	$(CH_3)_3CHCH_2CH_2(CH_3)_2$	-53.54 ± 0.36 [130]
CH_4	-17.78 ± 0.10 [130]	$(CH_3)_2CHCH_2CH_2CH_3$	-41.78 ± 0.24 [130]
C_2H_6	-20.03 ± 0.10 [130]	$(CH_3)_3CCH_2CH_3$	-44.48 ± 0.24 [130]
C_2H_5	28.40 ± 0.50 [130]	$(CH_3)_3CCH_2CH_2CH_3$	-49.21 ± 0.36 [130]
C_3H_8	-25.02 ± 0.12 [130]	$(CH_3)_3CH$	-32.07 ± 0.17 [130]
CH_3	35.05 ± 0.07 [131]	$(CH_3)_2(C•H_2)CH$	17.38 ± 0.53 [132]
$CH_3C•HCH_3$	20.70 ± 0.50 [132]	Neopentane	-40.32 ± 0.19 [130]
$CH_3CH_2CH_2CH_3$	-30.02 ± 0.17 [130]	$(CH_3)_2C•CH_2CH_3$	7.37 ± 1.26 [a]
$CH_3CH_2C•HCH_3$	16.00 ± 0.50 [110]	$(CH_3)_2CHC•HCH_3$	9.28 ± 1.26 [a]
$(CH_3)_2CHCH_2CH_3$	-36.74 ± 0.24 [130]	$(CH_3)_2C•CH_2CH_2CH_3$	2.06 ± 1.26 [a]
$CH_3CH_2C•H_2$	23.90 ± 0.50 [110]	$(CH_3)_3C•$	11.00 ± 0.70 [110]
$(CH_3)_2C=CH_2$	-4.04 ± 0.22 [130]	$CH_3CH_2CH_2C•H_2$	19.34 ± 0.53 [132]
$CH_2=C•H$	71.00 ± 1.00 [110]	$CH_2=CHCH_3$	4.78 ± 0.19 [130]

Table 5.4 Evaluated Enthalpies of Formation and Bond Energies at 298 K for Isooctane and Radicals

[a] Uncertainty is square root of the sum of squares the uncertainty in the reference species (Table 5.3) and the species uncertainties; 95% confidence limit, of each methods, $\pm$ 1.56 kcal mol^{-1} for CBS-QB3 and $\pm$ 2.84 kcal mol^{-1} for B3 B3LYP/6-31g(d,p) as shown in Table 5.1

Work Reactions						$\Delta_f H^o(298)$ kcal mol^{-1}	
						B3LYP/6-31g(d,p)	CBS-QB3
c3cccc2							
C3CCCC2	+	C_2H_6	-->	$(CH_3)_2CHCH_2CH_3$	+	$(CH_3)_4C$	-52.57 $\pm$ 2.86	-54.21 $\pm$ 1.59
C3CCCC2	+	C_3H_8	-->	$(CH_3)_2CHCH_2CH_3$	+	$(CH_3)_3CCH_2CH_3$	-53.89 $\pm$ 2.86	-54.55 $\pm$ 1.60
C3CCCC2	+	$CH_3CH_2CH_2CH_3$	-->	$(CH_3)_2CHCH_2CH_3$	+	$(CH_3)_3CCH_2CH_2CH_3$	-53.78 $\pm$ 2.88	-54.23 $\pm$ 1.63
C3CCCC2	+	$CH_3CH_2CH_2CH_3$	-->	$(CH_3)_3CCH_2CH_3$	+	$(CH_3)_3CCH_2CH_3$	-57.00 $\pm$ 2.87	-54.73 $\pm$ 1.61
C3CCCC2	+	C_3H_8	-->	$(CH_3)_4C$	+	$(CH_3)_3CCH_2CH_3$	-55.74 $\pm$ 2.86	-55.27 $\pm$ 1.59
						Average	-54.60 $\pm$ 2.86	**-54.40 $\pm$ 1.60**
c3jcccc2							
C3•CCCC2	+	C_2H_6	-->	C3CCCC2	+	C_2H_5	-5.87 $\pm$ 2.91	-5.14 $\pm$ 1.68
C3•CCCC2	+	C_3H_8	-->	C3CCCC2	+	$CH_3CH_2C•H_2$	-6.06 $\pm$ 2.91	-5.35 $\pm$ 1.68
C3•CCCC2	+	$(CH_3)_3CH$	-->	C3CCCC2	+	$(CH_3)_2(C•H_2)CH$	-5.68 $\pm$ 2.92	-5.08 $\pm$ 1.69
C3•CCCC2	+	$CH_3CH_2CH_2CH_3$	-->	C3CCCC2	+	$CH_3CH_2C•HCH_3$	-4.60 $\pm$ 2.91	-5.00 $\pm$ 1.69
C3•CCCC2	+	$CH_3CH_2CH_2CH_3$	-->	C3CCCC2	+	$CH_3CH_2CH_2C•H_2$	-5.13 $\pm$ 2.92	-4.43 $\pm$ 1.69
						Average	-5.47 $\pm$ 2.91	**-5.00 $\pm$ 1.69**
Bond dissociation energy		$(CH_3)_2(H\text{----}CH_2)C\text{-}CH_2\text{-}CH(CH_3)_2$					**100.64 $\pm$ 1.73**	

Table 5.4 Evaluated Enthalpies of Formation and Bond Energies at 298 K for Isooctane and Radicals (Continued)

Work Reactions						$\Delta_f H°(298)$ kcal mol^{-1}	
						B3LYP/6-31g(d,p)	CBS-QB3
c3cccc2j							
C3CCCC2•	+	C$_2$H$_6$	-->	C3CCCC2 +	C$_2$H$_5$	-6.00 ± 2.91	-5.33 ± 1.68
C3CCCC2•	+	C$_3$H$_8$	-->	C3CCCC2 +	CH$_3$CH$_2$C•H$_2$	-6.19 ± 2.91	-5.53 ± 1.68
C3CCCC2•	+	(CH$_3$)$_3$CH	-->	C3CCCC2 +	(CH$_3$)$_2$(C•H$_2$)CH	-5.81 ± 2.92	-5.26 ± 1.69
C3CCCC2•	+	CH$_3$CH$_2$CH$_2$CH$_3$	-->	C3CCCC2 +	CH$_3$CH$_2$C•HCH$_3$	-4.72 ± 2.91	-5.18 ± 1.69
C3CCCC2•	+	CH$_3$CH$_2$CH$_2$CH$_3$	-->	C3CCCC2 +	CH$_3$CH$_2$CH$_2$C•H$_2$	-5.25 ± 2.92	-4.61 ± 1.69
				Average		-5.59 ± 2.91	**-5.18 ± 1.69**
	Bond dissociation energy		**(CH$_3$)$_3$C-CH$_2$-CH(CH$_3$)(H----CH$_2$)**			**100.46 ± 1.73**	
c3ccjcc2							
C3CC•CC2	+	C$_3$H$_8$	-->	C3CCCC2 +	CH$_3$C•HCH$_3$	-9.61 ± 2.91	-8.93 ± 1.68
C3CC•CC2	+	CH$_3$CH$_2$CH$_2$CH$_3$	-->	C3CCCC2 +	CH$_3$CH$_2$C•HCH$_3$	-9.53 ± 2.91	-8.86 ± 1.69
C3CC•CC2	+	(CH$_3$)$_2$CHCH$_2$CH$_3$	-->	C3CCCC2 +	(CH$_3$)$_2$CHC•HCH$_3$	-9.65 ± 3.44	-9.17± 2.50
C3CC•CC2	+	C$_2$H$_6$	-->	C3CCCC2 +	C$_2$H$_5$	-10.81 ± 2.91	-9.00 ± 1.68
C3CC•CC2	+	C$_3$H$_8$	-->	C3CCCC2 +	CH$_3$CH$_2$C•H$_2$	-10.99 ± 2.91	-9.21± 1.68
				Average		-10.12 ± 3.02	**-9.03 ± 1.84**
	Bond dissociation energy		**(CH$_3$)$_3$C-(H----CH)-CH(CH$_3$)$_2$**			**96.41 ± 1.88**	
c3cccjc2							
C3CCC•C2	+	(CH$_3$)$_3$CH	-->	C3CCCC2 +	(CH$_3$)$_3$C•	-12.98 ± 2.95	-12.95 ± 1.76
C3CCC•C2	+	(CH$_3$)$_2$CHCH$_2$CH$_3$	-->	C3CCCC2 +	(CH$_3$)$_2$C•CH$_2$CH$_3$	-12.31 ± 3.44	-12.27 ± 2.50
C3CCC•C2	+	(CH$_3$)$_2$CHCH$_2$CH$_2$CH$_3$	-->	C3CCCC2 +	(CH$_3$)$_2$C•CH$_2$CH$_2$CH$_3$	-12.32 ± 3.44	-12.27 ± 2.50
C3CCC•C2	+	CH$_3$CH$_2$CH$_2$CH$_3$	-->	C3CCCC2 +	CH$_3$CH$_2$C•HCH$_3$	-13.36 ± 2.91	-11.96 ± 1.69
C3CCC•C2	+	C$_3$H$_8$	-->	C3CCCC2 +	CH$_3$C•HCH$_3$	-13.43 ± 2.91	-12.03 ± 1.68
				Average		-12.88 ± 3.13	**-12.30 ± 2.02**
	Bond dissociation energy		**(CH$_3$)$_3$C-CH$_2$-(C----H)(CH$_3$)$_2$**			**93.14 ± 2.05**	

Figure 5.3 shows enthalpies of formation for isooctane as a function of temperature comparing data from this study with literature data, Stull[127], Rossini[128] and Scott[129], where the Scott enthalpy data is calculated from his reported heat capacity data. The curves from this study are labeled ViBir[19] and Rotator and the calculation methods are described below. The plots of enthalpies of formation vs. temperature from this study are calculated from this research heat capacity data and start with the enthalpy of formation at 298 K from the experimental value, -53.57 kcal mol^{-1}. The Pitzer-Gwinn method (ViBir) data is close to that of Rossini. The Rotator data in Figure 5.3 is considered more accurate and falls in between the data of Scott and Stull.
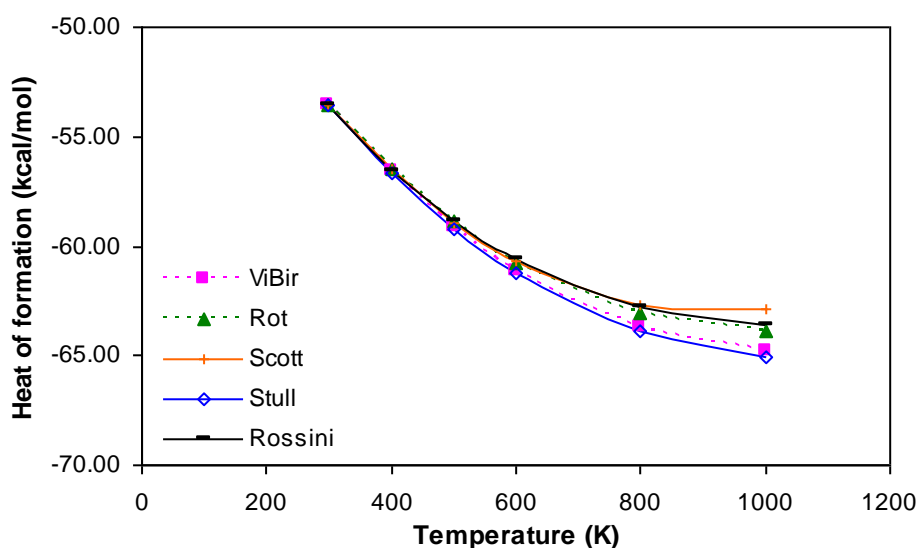
Figure 5.3 Enthalpies of formation for isooctane as a function of temperature comparing this work and literature data. ,Stull[127], Rossini[128] and Scott[129], where Scott data is calculated from his reported heat capacity values.(b) The dotted lines take the heat capacity data of this study; but starting at the experimental data of Rossini (-53.57 kcal mol^{-1}). (c) VibIR determines contribution from internal rotors using Pitzer-Gwinn formalism. (d) Rot - Rotator - program for entropy and heat capacity for internal rotors.

5.4.3 Group Additivity Method for Estimation of Thermochemical Properties

Group additivity [13,113] is a straightforward and reasonably accurate calculation method used to estimate thermodynamic properties of hydrocarbons and oxygenated hydrocarbons and corresponding radicals. It is particularly useful for application to larger molecules, for use in codes or databases, and for the estimation of thermochemical properties in reaction mechanism generation. Heat of formation at 298 K for isooctane and the radicals estimated by group additivity after including appropriate gauche and 1,5 interaction groups result in good agreement with both the DFT and ab initio calculated values. Group additivity contributions for isooctane include three of the gauche interactions and one of 1,5 interaction. All isooctane radicals have three gauche interactions.

Table 5.5. Summary of Formation Enthalpies ($\Delta_fH^o_{298}$)

Species	$\Delta_fH^o(298)$ kcal mol^{-1}				
	B3LYP/ 6-31g(d,p)	CBS-QB3	by THERM (Group additivity)^a		
			No interaction	Includes interaction Terms	
C3CCCC2	-54.60 ± 2.86	-54.40 ± 1.60	-57.33	-53.43	3 Gauche and 1 of 1,5 Interaction
C3•CCCC2	-5.47 ± 2.91	-5.00 ± 1.69	-8.33	-5.93	3 Gauche
C3CCCC2•	-5.59 ± 2.91	-5.18 ± 1.69	-8.33	-5.93	3 Gauche
C3CC•CC2	-10.12 ± 3.02	-9.03 ± 1.84	-10.98	-8.58	3 Gauche
C3CCC•C2	-12.88 ± 3.13	-12.30 ± 2.02	-12.93	-10.53	3 Gauche

5.4.4. Entropy and Heat Capacity

Entropy and heat capacity contributions as a function of temperature are determined from the calculated structures, moments of inertia, vibration frequencies, symmetry, electron degeneracy, number of optical isomers and the known mass of each molecule. The

calculations use standard formulas from statistical mechanics for the contributions of translation, external rotation and vibrations using the "SMCPS" program. This program utilizes the rigid-rotor-harmonic oscillator approximation from the frequencies along with moments of inertia from the optimized CBS-QB3 structures, *viz.* B3LYP/6-311G(2d,d,p) level. Contributions from internal rotors using Pitzer-Gwinn formalism (ViBir)[19] and Rotator are substituted for contributions from internal rotor torsion frequencies. The Pitzer-Gwinn contributions are developed for internal rotors of given foldness and assume equal barrier.

A relaxed scan and a non relaxed (fixed structure) scan were performed on each rotor. The C3C--isopropyl rotor shows a barrier of over 30 kcal mol^{-1} in the fixed structure scan and is the one internal rotor are treated with a torsion frequency, as opposed to internal rotor contribution. The relaxed scans are needed to find the lowest energy conformers.

Entropy and heat capacity calculations were performed using CBS-QB3 determined geometries and harmonic frequencies are summarized in Table 5.6. The comparison of heat capacity and entropy as a function of temperature from this work with the experimental data[127-129] for isooctane is listed in Tables 5.7.A and 5.7.B.

Table 5.6 Ideal Gas-phase Thermochemical Properties *vs.* Temperature for Isooctane and Radicals. $S°(T)$ and $C_p^o(T)$ in cal mol^{-1} K^{-1}

T(K)	C3CCCC2		C3•CCCC2		C3CC•CC2		C3CCC•C2		C3CCCC2•	
	Cp(T)	S^o(T)	Cp(T)	S^o(T)	Cp(T)	S^o(T)	Cp(T)	S^o(T)	Cp(T)	S^o(T)
50	13.24	54.42	11.74	56.58	14.22	59.71	17.00	56.59	11.48	54.05
100	19.94	65.41	19.70	67.08	20.65	71.28	22.82	70.16	20.51	64.66
150	27.52	74.96	27.04	76.49	27.89	81.05	28.11	80.43	28.84	74.61
200	33.94	83.76	33.33	85.13	34.01	89.92	32.91	89.16	35.49	83.83
250	39.98	91.97	39.46	93.21	39.85	98.12	38.00	97.03	41.59	92.39
298	45.89	99.48	45.48	100.64	45.57	105.59	43.36	104.14	47.39	100.18
350	52.39	107.36	51.99	108.45	51.80	113.39	49.48	111.58	53.59	108.27
400	58.52	114.74	57.99	115.78	57.59	120.68	55.33	118.55	59.28	115.79
500	69.73	129.00	68.71	129.87	68.01	134.65	66.12	132.06	69.42	130.11
600	79.24	142.56	77.59	143.19	76.72	147.82	75.27	144.93	77.86	143.51
700	87.23	155.37	84.97	155.70	84.01	160.19	82.92	157.10	84.92	156.04
800	94.00	167.45	91.24	167.45	90.23	171.81	89.38	168.59	90.96	167.77
1000	104.81	189.61	101.32	188.91	100.28	193.04	99.61	189.66	100.78	189.14
1500	121.56	235.62	117.23	233.32	116.20	237.02	115.31	233.34	116.42	233.26
2000	130.17	271.87	125.55	268.28	124.53	271.69	123.31	267.71	124.65	267.98
2500	134.91	301.46	130.19	296.83	129.15	300.01	127.69	295.73	129.22	296.31
3000	137.71	326.32	132.97	320.82	131.89	323.81	130.27	319.25	131.94	320.13
3500	139.46	347.68	134.74	341.46	133.62	344.28	131.88	339.46	133.65	340.60
4000	140.62	366.38	135.94	359.53	134.76	362.19	132.94	357.14	134.77	358.52
4500	141.41	382.99	136.78	375.59	135.54	378.11	133.66	372.84	135.54	374.44
5000	141.97	397.92	137.39	390.03	136.09	392.42	134.17	386.95	136.09	388.75

Table 5.7.A Comparison of Calculated *Cp*(T) with the Experimental Data for Isooctane (C3CCCC2)

Temperature (K)	Cp (cal mol^{-1} K^{-1})				
	Scott[129]	Stull[127]	Group Additvity	ViBir	Rotator
298	45.03	45.14	-	44.06	45.89
300	45.28	45.35	45.36	-	-
400	58.46	57.36	58.28	57.29	58.52
500	70.13	68.32	69.78	69.03	69.73
600	80.20	77.67	79.47	78.94	79.24
700	88.90	85.66	-	87.23	87.23
800	96.40	92.50	94.25	94.23	94.00
900	102.90	98.43	-	-	-
1000	108.70	103.60	105.00	105.31	104.81

Table 5.7.B Comparison of Calculated S^0(T) with the Experimental Data for Isooctane (C3CCCC2)

Temperature (K)	S (cal mol^{-1}K^{-1})			
	Stull[127]	Rossini[128]	ViBir	Rotator
298	101.15	101.15	97.62	99.48
300	101.43	101.41	-	-
400	116.15	116.8	110.61	114.74
500	130.16	131.3	123.29	129.00
600	143.46	144.9	135.69	142.56
700	156.05	157.8	147.59	155.37
800	167.94	169.9	158.93	167.45
900	179.19	181.4	-	-
1000	189.13	192.3	179.92	189.61

5.5 Summary

The computed enthalpies of formation via isodesmic work reactions for isooctane, -54.40 ± 1.60 kcal mol^{-1}, is in agreement with the experimental data available, -53.57± 0.32 [128] kcal mol^{-1} and -53.54 ± 0.36 [130] kcal mol^{-1}. Bond energy values for the isooctane radicals are 100.64 ± 1.73, 100.46 ± 1.73, 96.41 ± 1.88 and 93.14 ± 2.05 kcal mol^{-1} for C3•CCCC2, C3CCCC2•, C3CC•CC2 and C3CCC•C2, respectively. These are ~1-2 kcal mol^{-1}lower than commonly accepted values for primary, secondary and tertiary radicals of 101.02 ± 0.51, 97.82 ± 0.49 and 95.17 ± 0.72 kcal mol^{-1}, respectively. Entropy and heat capacity values versus temperature were also determined. For group additivity, isooctane has three gauche interactions and one 1,5 interaction. All isooctane radicals have three gauche interactions.

CHAPTER 6

THERMOCHEMISTRY, REACTION PATHS AND KINETICS ON THE *tert*-ISOOCTANE PEROXIDE, REACTION WITH O$_2$

6.1 Overview

Thermochemical properties of *tert*-isooctane hydroperoxide and its radicals are determined by computational chemistry. Enthalpies are determined using isodesmic reactions with B3LYP density function and CBS QB3 methods. Application of group additivity with comparison to calculated values is illustrated. Entropy and heat capacities are determined using geometric parameters and frequencies from the B3LYP/6-31G(d,p) calculations for the lowest energy conformer. Internal rotor potentials are determined for the *tert*-isooctane hydroperoxide and its radicals in order to identify isomer energies. Recommended values derived from the most stable conformers of *tert*-isooctane hydroperoxide of are -77.8 ± 0.44 kcal mol^{-1}. Intramolecular interactions are shown to have a significant effect on the enthalpy of isooctane parent and its radicals on peroxy / peroxide systems, the R• + O$_2$ well depths and unimolecular reaction barriers. Transition states and kinetic parameters for intramolecular hydrogen atom transfer and molecular elimination channels are characterized to evaluate reaction paths and kinetics. Kinetic parameters are determined versus pressure and temperature for the chemical activated formation and unimolecular dissociation of the peroxide adducts. Multi-frequency quantum RRK (QRRK) analysis is used for k(E) with Master Equation analysis for fall off. The major reaction paths at 1000 K, are formation of isooctane plus HO$_2$ followed by cyclic ether plus OH. Stabilization *tert*-isooctane hydroperoxy radical becomes important at lower temperature.

6.2 Previous Studies

Isooctane (2,2,4-trimethylpentane, neopentylpropane) is a component of Primary Reference Fuel[133-135] and elementary mechanisms for its oxidation have been studied extensively[118, 120-125, 136], although a detailed analysis of its thermochemistry and oxidation kinetics by high-level quantum chemical methods has been limited by its complex structure and large size. Reduced reactivity of isooctane at low-temperature and its resistance to ignition, as opposed to linear alkanes, are generally attributed to its high degree of branching. Current kinetic models are mainly based on empirical rules, bond enthalpies and generic rate parameters, yet branched semi-rigid structural features of isooctane introduce specific reaction channels that are either irrelevant or non-feasible in smaller model systems.

Isooctane is a highly branched molecule and its structure may have a significant affect on its thermochemistry and reaction barriers. A study[137] on isooctane parent molecule and its radicals from loss of hydrogen atoms shows that carbon-hydrogen bond energies in isooctane were weaker than the conventional primary, secondary and tertiary C—H bonds by ~1-2 kcal mol^{-1}. In this study, standard enthalpy ($\Delta_f H^o_{298}$) and dissociation bond enthalpies are reported for the species resulting from reactions in the *tert*-isooctane radicals + O_2 system. Transition state structures and intermediates that result from the isomerization and reactions of the radical are calculated using Density Functional and higher level composite *ab initio* based calculations. Kinetics parameters are reported for association reactions of *tert*-isooctane radicals with molecular oxygen to form R-O_2* chemically activated adducts from variational transition state theory.

6.3 Computational Methods

The relative stabilities of *tert*-isooctane hydroperoxide, bond dissociation energies and the heats of formation of its radicals and molecules have been calculated using B3LYP hybrid density functional theory in conjunction with the 6-31G(d,p) basis set, as well the complete basis set-QB3 composite method

Higher level ab initio and DFT-based composite methods G3MP2B3[138, 139] and CBS-QB3[140] are utilized in work reaction calculations which are more reliable in predicting accurate energies as shown in previous studies[137, 141-143] G3MP2B3 is a modified version of the G3MP2[144] method where the geometries and zero-point vibration energies are from B3LYP/6-31G(d) calculations. CBS-QB3 uses the B3LYP/6-311G(2d,d,p) level to calculate geometries and frequencies followed by several single point energy calculations at the MP2, MP4SDQ, and CCSD(T) levels. The final energies are determined with a CBS extrapolation. CBS-QB3 is considered a complete basis set method that is practical for the molecules and radicals in this study with an addition of G3MP2B3 method for transition states. All calculations were performed using the Gaussian 03 program suite. Standard enthalpy values are determined with both the B3LYP density functional theory and CBS-QB3 method where the B3 method has lower computational costs and plausible application to larger molecules when using isodesmic work reactions. The B3LYP is thought to be one of the most reliable DFT methods available and has been shown by Curtiss et al.[85] to have the smallest average absolute deviation, 3.11 kcal mol^{-1}, of the seven DFT methods studied using the G2 test set of molecules. Curtiss et al., and Ochterski co-workers reported mean absolute deviations of

1.1 kcal mol^{-1}for CBS-Q methods by comparing the energies of 125 computationally reactions to their corresponding experimental values.[106-109]

To more accurately evaluate the heats of formation ($\Delta_f H^o_{298}$) of the molecule systems used a variety of homodesmic and isodesmic work reactions, where the bonding environments are similar in products and reagents. An isodesmic reaction is a hypothetical reaction where the number and type of bonds is conserved on each side of the work reaction, a homodesmic reaction conserves number and type of bonds, but also conserves hybridization $\Delta_{rxn}H^o_{298}$ is calculated and known $\Delta_f H^o_{298}$ values of the reference molecules are used with the calculated $\Delta_{rxn}H^o_{298}$ to determine the standard enthalpy. The similar structure components on both sides of the work reaction provides a cancellation of systematic errors in $\Delta_f H^o_{298}$ values by using the calculated $\Delta_{rxn}H^o_{298}$ and a thus provides increased accuracy. This cancellation can be observed in the good relative accuracy of the B3 method calculation relative to the higher level CBS-QB3 data provided below.

6.4 Results and Discussion

The optimized geometries at the CBS-QB3 composite level of theory, *viz.,* B3LYP/6-311(2d,d,p) calculations, for the target molecules and corresponding abbreviated nomenclatures are presented in Figure 6.1. Vibration frequencies, and moments of inertia for all structures are available in the appendix D.
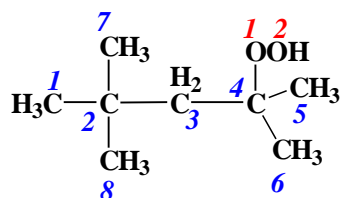
Scheme 6.1 Definition of Skeletal Atom in *tert*-Isooctane Hydroperoxide and Its Radicals

The lowest configuration of *tert*-isooctane hydroperoxide, 2,4,4-trimethylpentan-2-yl hydroperoxide (C3CCCQC2) has two methyls on the tertiary carbon (C_4) near eclipsed to two methyl on the quarternary (C_2) and hydro peroxide group eclipsed to the third methyl. The position of the hydroperoxide group for the lowest energy conformer is when the oxygen (O_1) bonded to the hydrogen on the hydroperoxide (O_2) is gauche between secondary carbon (C_3) and one methyl on the tertiary carbon (C_5 or C_6).

C3CCCQC2
$(CH_3)_3C-CH_2-C(OOH)(CH_3)_2$

C3CCCQ•C2
$(CH_3)_3C-CH_2-C(OO•)(CH_3)_2$

C3•CCCQC2
$(CH_3)_2(C•H_2)C-CH_2-C(OOH)(CH_3)_2$

C3CCCQC2•
$(CH_3)_3C-CH_2-C(OOH)(CH_3)(C•H_2)$

C3CC•CQC2
$(CH_3)_3C-C•H-C(OOH)(CH_3)_2$
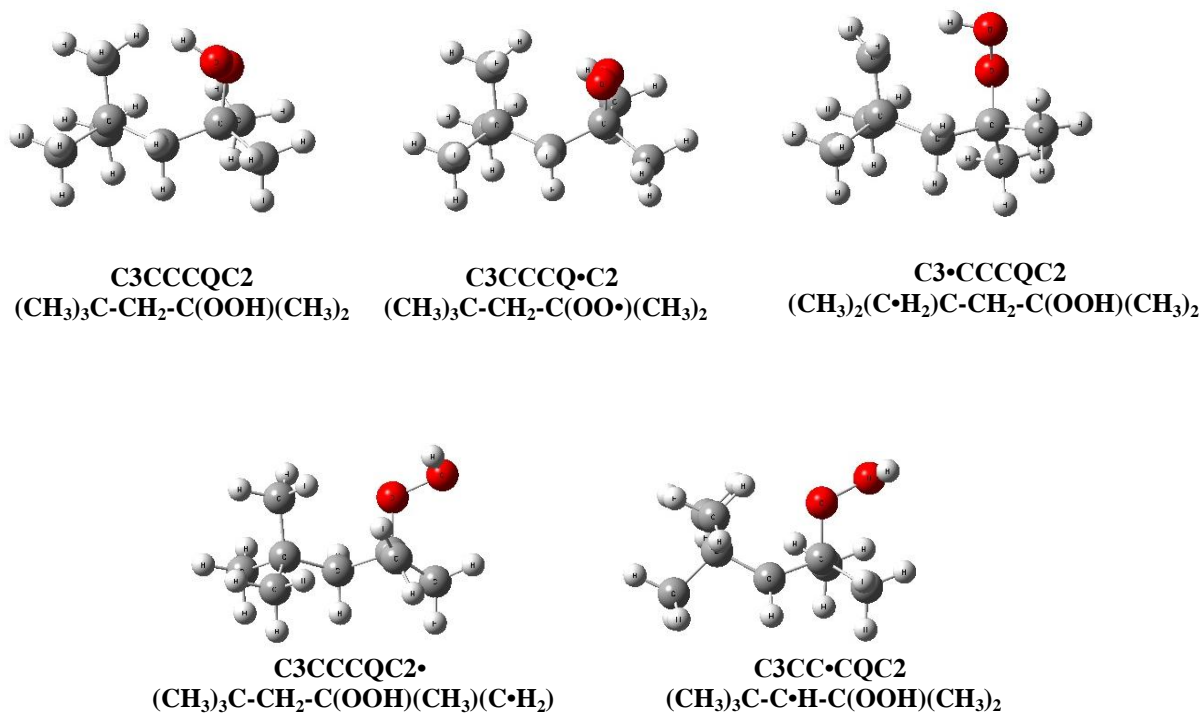
Figure 6.1 Geometry of lowest energy conformer of *tert*-isooctane hydroperoxide and its radicals.

6.4.1 Internal Rotation Potentials

Energy profiles for internal rotations about the C-C, C-OO and CO-OH bonds in *tert*-isooctane hydroperoxide and its radicals were calculated to determine lowest energy configuration and energies of the rotational conformers. The total energies as a function of the corresponding dihedral angles were computed at the B3LYP/6-31G(d) level of theory by scanning the torsion angles between 0° and 360° in steps of 15°, while all remaining coordinates were fully optimized. All potentials were re-scanned when a lower energy conformer, relative to the initial low energy conformer was found. The total energy of the corresponding most stable molecular conformer was arbitrarily set to zero and used as a reference point to plot the potential barriers. The resulting potential energy barriers for internal rotations in the *tert*-isooctane hydroperoxide is shown in Figure 6.2.

The calculated rotational barriers of methyl groups in *tert*-isooctane hydroperoxide show three-fold symmetry with barriers of 3.0 kcal mol^{-1}; these are similar to the methyl rotor potentials in *n*-hydrocarbons. Rotational barriers of butyl group (C3C--CCQC2) exhibit three-fold symmetry with barriers of 4.1 kcal mol^{-1}. The C3CC--CQC2 rotor has asymmetry three-fold potential barriers at 5.8 kcal mol^{-1}. The maximum of the RO—OH rotor potential, 7.0 kcal mol^{-1} barrier, is when the hydrogen atom on the hydroperoxide eclipse with tertiary carbon (C_4)
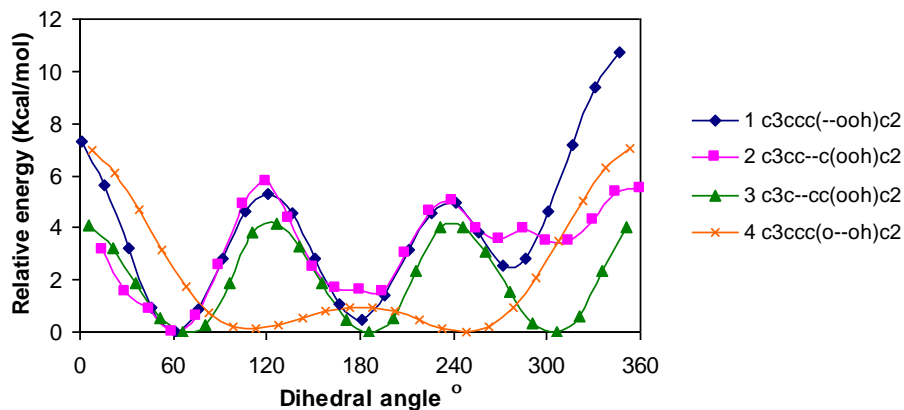
Figure 6.2 Potential energy profiles for internal rotations in *tert*-isooctane hydroperoxide.

6.4.2 Enthalpies of Formation and Bond Dissociation Energies

The methods of isodesmic or homodesmic work reactions rely on the similarity of bonding environment in the reactants and products, which leads to the cancellation of systematic errors in calculation of reaction enthalpy($\Delta_{rxn}H^o_{298}$) in the ab initio and density functional theory calculations. The zero point energies are scaled by 0.9806 for B3LYP/6-31G(d,p) calculations as recommended by Scott et al. The standard enthalpies of formation at 298.15 K for reference species used in these reactions are summarized in Table 6.1. The enthalpies of formation of the target molecules obtained from the use of the reaction schemes are shown in Table 6.2.

Bond enthalpies are derived from $\Delta_rH^o_{298}$ of parent molecules and its radicals corresponding to the loss of hydrogen atoms. For the standard enthalpy of formation of hydrogen atom at 298.15 K, the values 52.10 ± 0.003 kcal mol^{-1} were used. The resulted bond dissociation enthalpies computed from isodesmic enthalpies of formation are in Table 6.2. The resulting bond energies were compared against primary, secondary and tertiary bonds in normal alkanes.

C—H bond dissociation enthalpy (BDE) for secondary carbon (C_3) at 98.1 kcal mol^{-1} is similar to that in secondary carbon on a normal alkane (98.5 kcal mol^{-1}), and the primary C—H bonds energies for primary methyl radicals on the *tert*-butyl group (C_1, C_7 and C_8) are at 100.2 kcal mol^{-1} are ~ 1 kcal mol^{-1} lower than that in primary C—H bonds on normal alkanes (101.1 kcal mol^{-1}). The C—H BDE of the primary methyl carbons on the isopropyl group adjacent to the peroxide (C_5 and C_6 positions) is 101.4 kcal mol^{-1}, similar to primary C—H bonds energies on normal alkanes.

Bond energy for ROO—H in *tert*-isooctane hydroperoxide is 83.1 kcal mol^{-1} as computed at the CBS-QB3 level, 3.2 kcal mol^{-1} lower than ROO—H bond on normal alkanes (86.3 kcal mol^{-1})[103]. The peroxy radical center being located in the middle of molecule has access to all other H-atoms to undergo Intramolecular H atom transfer (5 – 7 member rings) to form hydroperoxide-alkyl radicals.

Table 6.1 Standard Enthalpies of Formation at 298 K for Reference Species

$\Delta_f H^o{}_{298}$ for reference molecule			
Species	kcal mol^{-1}	Species	kcal mol^{-1}
C_2H_6	-20.04 ± 0.07 [145]	$(CH_3)_2(C{\bullet}H_2)CH$	17.00 ± 0.50 [110]
C_2H_5	28.40 ± 0.50 [110]	$(CH_3)_3COOH$	-57.24 ± 0.22 [147]
C_3H_8	-24.82 ± 0.14 [126]	$(CH_3)_3COO{\bullet}$	-24.67 ± 0.19 [147]
$CH_3CH_2C{\bullet}H_2$	23.90 ± 0.50 [110]	$CH_3CH_2OO{\bullet}$	-6.00 [148]
$CH_3C{\bullet}HCH_3$	21.50 ± 0.40 [146]	CH_3CH_2OOH	-39.50 ± 0.70 [149]
$CH_3CH_2CH_2CH_3$	-30.03 ± 0.16 [145]	$(CH_3)_2CHOOH$	-47.86 ± 0.22 [147]
$CH_3CH_2C{\bullet}HCH_3$	16.00 ± 0.50 [110]	$(CH_3)_2CHOO{\bullet}$	-14.80 ± 0.22 [147]
$(CH_3)_3CCH_2CH_3$	-44.35 ± 0.23 [126]	$(CH_3)_3CCH_2CH_2CH_3$	-49.29 ± 0.32 [126]
$(CH_3)_3CH$	-32.07 ± 0.15 [145]	$(CH_3)_3CCH_2CH(CH_3)_2$	-53.57 ± 0.32 [126]

Table 6.2 Evaluated Enthalpies of Formation and Bond Energies at 298 K for *tert*-Isooctane Hydroperoxide and Its Radicals

Work Reactions						$\Delta_f H^o 298$ kcal mol^{-1}	
						B3LYP/6-31g(d,p)	CBS-QB3
C3CCCQC2							
C3CCCQC2	+	C_2H_6	-->	$(CH_3)_3COOH$ +	$(CH_3)_3CCH_2CH_3$	-76.5	-78.07
C3CCCQC2	+	C_3H_8	-->	$(CH_3)_3COOH$ +	$(CH_3)_3CCH_2CH_2CH_3$	-76.87	-78.05
C3CCCQC2	+	$(CH_3)_3CH$	-->	$(CH_3)_3COOH$ +	$(CH_3)_3CCH_2CH(CH_3)_2$	-77	-77.31
					Average	-76.79 ± 0.26	**-77.81** ± 0.44
C3CCCQ•C2							
C3CCCQ•C2	+	CH_3CH_2OOH	-->	C3CCCQC2 +	$CH_3CH_2OO•$	-45.41	-45.73
C3CCCQ•C2	+	$(CH_3)_2CHOOH$	-->	C3CCCQC2 +	$(CH_3)_2CHOO•$	-45.68	-45.84
C3CCCQ•C2	+	$(CH_3)_3COOH$	-->	C3CCCQC2 +	$(CH_3)_3COO•$	-45.37	-45.76
					Average	-45.49 ± 0.17	**-45.78** ± 0.05
		$(CH_3)_3CCH_2C(OO\text{---}H)(CH_3)_2$		Bond dissociation energy		84.1	

Table 6.2 Evaluated Enthalpies of Formation and Bond Energies at 298 K for *tert*-Isooctane Hydroperoxide and Its Radicals (Continued)

Work Reactions						$\Delta_f H°298$ kcal mol^{-1}	
						B3LYP/6-31g(d,p)	CBS-QB3
C3•CCCQC2							
C3•CCCQC2	+	C_2H_6	-->	C3CCCQC2	+	C_2H_5	-30.71	-29.45
C3•CCCQC2	+	C_3H_8	-->	C3CCCQC2	+	$CH_3CH_2C•H_2$	-30.71	-29.87
C3•CCCQC2	+	$(CH_3)_3CH$	-->	C3CCCQC2	+	$(CH_3)_2(C•H_2)CH$	-30.66	-29.78
					Average	-30.69 ± 0.03	**-29.70** ± 0.22
$(CH_3)_2(H\text{---}CH_2)CCH_2C(OOH)(CH_3)_2$			Bond dissociation energy			100.2	
C3CC•CQC2							
C3CC•CQC2	+	C_2H_6	-->	C3CCCQC2	+	C_2H_5	-34.41	-32.1
C3CC•CQC2	+	C_3H_8	-->	C3CCCQC2	+	$CH_3C•HCH_3$	-32.62	-31.44
C3CC•CQC2	+	$CH_3CH_2CH_2CH_3$	-->	C3CCCQC2	+	$CH_3CH_2C•HCH_3$	-33.14	-31.96
					Average	-33.39 ± 0.92	**-31.83** ± 0.35
$(CH_3)_3C(HC\text{---}H)C(OOH)(CH_3)_2$			Bond dissociation energy			98.1	
C3CCCQC2•							
C3CCCQC2•	+	C_2H_6	-->	C3CCCQC2	+	C_2H_5	-29.17	-28.26
C3CCCQC2•	+	C_3H_8	-->	C3CCCQC2	+	$CH_3CH_2C•H_2$	-29.17	-28.67
C3CCCQC2•	+	$(CH_3)_3CH$	-->	C3CCCQC2	+	$(CH_3)_2(C•H_2)CH$	-29.12	-28.58
					Average	-29.15 ± 0.03	**-28.50** ± 0.22
$(CH_3)_3CCH_2C(OOH)(H\text{---}CH_2)(CH_3)$			Bond dissociation energy			101.4	

6.4.3 Group Additivity Method for Estimation of Thermochemical Properties

Group additivity is a straightforward and reasonably accurate calculation method used to estimate thermodynamic properties of hydrocarbons and oxygenated hydrocarbons; it is particularly useful for application to larger molecules, for use in codes or databases, and for the estimation of thermochemical properties in reaction mechanism generation. Heat of formation at 298 of *tert*-isooctane hydroperoxide and its radicals estimated by group additivity after adding interaction groups result in good agreement to DFT and ab initio calculated values. Group additivity contributions for *tert*-isooctane hydroperoxide include three gauche interaction and two 1,5 interaction All *tert*-isooctane hydroperoxide radicals have three for gauche interaction and one of 1,5 interaction in their low energy form.

Table 6.3 Summary of Formation Enthalpies ($\Delta_f H^o{}_{298}$)

Species	$\Delta_f H^o{}_{298}$ kcal mol^{-1}				
	B3LYP/ 6-31g(d,p)	CBS-QB3	By Therm (Group additivity)		
			No interaction	After adding interaction	
C3CCCQC2	-76.79	-77.81	-83.83	-78.43	3 Gauche and 2 of 1,5 Interaction
C3CCCQ•C2	-45.49	-45.78	-49.63	-45.73	3 Gauche and 1 of 1,5 Interaction
C3•CCCQC2	-30.69	-29.70	-34.83	-30.93	3 Gauche and 1 of 1,5 Interaction
C3CC•CQC2	-33.39	-31.83	-37.48	-33.58	3 Gauche and 1 of 1,5 Interaction
C3CCCQC2•	-29.15	-28.50	-32.83	-28.93	3 Gauche and 1 of 1,5 Interaction

6.4.4 Entropy and Heat Capacity Data

Entropy and heat capacity contributions as a function of temperature are determined from the calculated structures, moments of inertia, vibration frequencies, symmetry, electron degeneracy, number of optical isomers and the known mass of each molecule. The calculations use standard formulas from statistical mechanics for the contributions of

translation, external rotation and vibrations using the "SMCPS" program This program utilizes the rigid-rotor-harmonic oscillator approximation from the frequencies along with moments of inertia from the optimized CBS-QB3 structures, *viz.* B3LYP/6-311G(2d,d,p) level. Contributions from internal rotors using Rotator,[12] are substituted for contributions from the corresponding internal rotor torsion frequencies. The rotator is a program for the calculation of thermodynamic functions from hindered rotations with arbitrary potentials based on the method developed by Krasnoperov, Lay and Shokhirev.[12] This technique employs expansion of the hindrance potential in the Fourier series, calculation of the Hamiltonian matrix in the basis of the wave functions of free internal rotation, and subsequent calculation of energy levels by direct diagonalization of the Hamiltonian matrix. Entropy and heat capacity calculation were performed using CBS -QB3 determined geometries and harmonic frequencies are summarized in Table 6.4.

Table 6.4 Ideal Gas-Phase Thermodynamic Property *vs.* Temperature

Species	$S^o(298)$ cal mol^{-1} K^{-1}	Cp (cal mol^{-1} K^{-1})						
		300 K	400 K	500 K	600 K	800 K	1000 K	1500 K
Isooctane Peroxide and its radicals								
C3CCCQC2	112.44	54.00	67.67	79.37	89.01	103.74	114.59	131.61
C3CCCQ•C2	109.43	52.29	65.60	76.99	86.35	100.66	111.18	127.63
C3•CCCQC2	107.61	52.93	66.45	77.76	86.93	100.78	110.91	126.85
C3CC•CQC2	117.63	54.53	67.34	78.21	87.13	100.83	110.96	126.96
C3CCCQC2•	117.39	54.26	67.06	77.96	86.89	100.58	110.70	126.73

6.4.5 Transition State Structures

Transition states are characterized as having only one negative eigenvalue of Hessian (force constant) matrices. The absence of imaginary frequencies verifies that structures are true minima at the respective levels of theory. Intrinsic reaction coordinate (IRC) calculations were performed at the B3LYP/6-31G(d,p) level to ensure connectivity of

stationary points. The final point geometries at both sides of TS were re-optimized to proper minima. The energy of each transition state structure is calculated from the corresponding reactant plus the energy difference between the TS structure and the reactant (adduct). If the TS is closer in structure to the product, then the energy of the transition state species is calculated from the corresponding product plus the energy difference between TS and product. The energy of the transition state are shown in Table 6.5.

Intramolecular isomerization in peroxy radicals is often the most important step in oxidation of hydrocarbons at lower temperatures. Geometry of lowest energy conformer transition state structures for intramolecular H transfer from ROO• (peroxy radical) to •ROOH (alkyl radical) are determined. These isomerization processes involving peroxy radical abstraction of a hydrogen atom from the secondary carbon C_3-position. TS1 is a 5-member ring transition state structure with H abstraction from C_3. TS2 is also 5-member ring transition state with an abstraction either from the two isopropyl carbons C_5 or C_6. H abstraction from either C_1, C_7 or C_8 is in TS3 with a 7-member ring transition state structure. The lowest energy conformers of transition states for H-Transfer are shown in Figure 6.3.
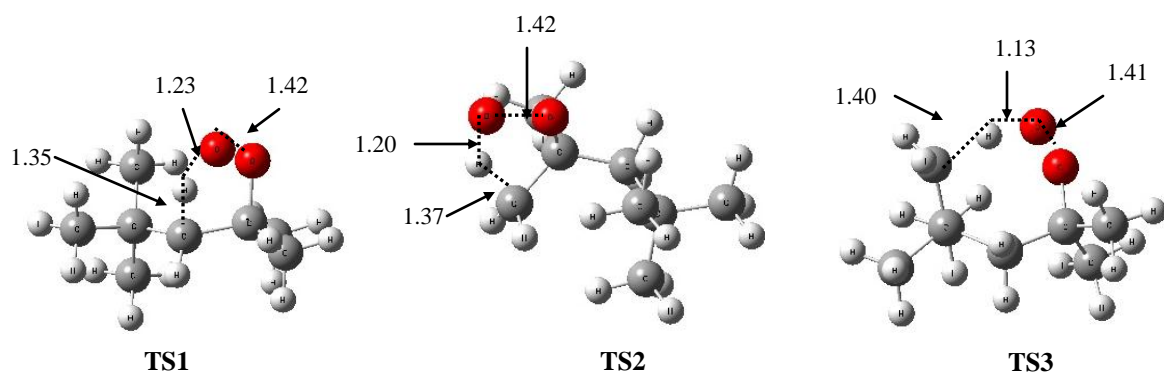
Figure 6.3 Geometry of lowest energy conformer of the transition state for H-transfer (isomerization).

Table 6.5 Evaluated Enthalpies of Formation at 298 K for Transition state in *tert*-Isooctane Radical + O$_2$ Reaction System
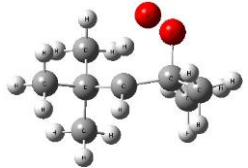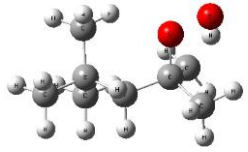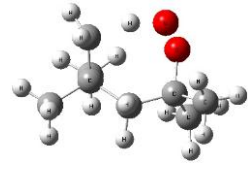
Species		Reaction	Energies (kcal mol^{-1})			
			B3LYP/6-31g(d,p)	CBS-QB3	G3MP2B3	Average CBS-QB3 and G3MP2B3
Isomerization						
	TS1	C3CCCQ•C2 --> C3CC•CQC2	-16.91	-16.52	-14.70	**-15.61**
	TS2	C3CCCQ•C2 --> C3CCCQC2•	-12.19	-10.90	-9.08	**-9.99**
	TS3	C3CCCQ•C2 --> C3•CCCQC2	-26.74	-25.06	-23.96	**-24.51**

Table 6.5 Evaluated Enthalpies of Formation at 298 K for Transition state in *tert*-Isooctane Radical + O$_2$ Reaction System (Continued)
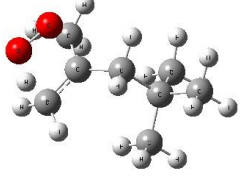
Species		Reaction	Energies (kcal mol^{-1})			
			B3LYP/6-31g(d,p)	CBS-QB3	G3MP2B3	Average CBS-QB3 and G3MP2B3
Molecular elimination						
	TS4	C3CCCQ•C2 --> C3CC=CC2 + HO$_2$	-22.94	-19.31	-18.56	**-18.93**
	TS5	C3CCCQ•C2 --> C3CCC(C)=C + HO$_2$	-24.58	-19.96	-19.21	**-19.59**

Table 6.5 Evaluated Enthalpies of Formation at 298 K for Transition state in *tert*-Isooctane Radical + O_2 Reaction System (Continued)
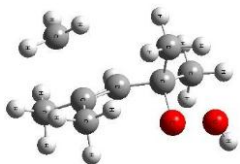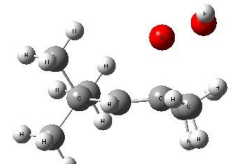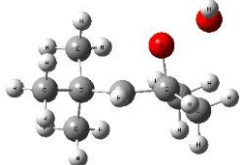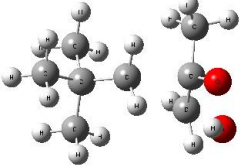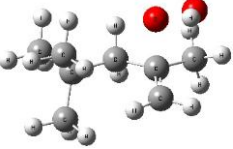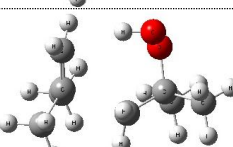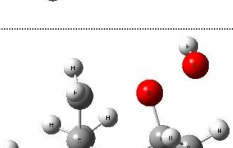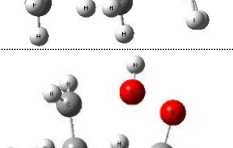
Species		Reaction	Energies (kcal mol^{-1})			
			B3LYP/6-31g(d,p)	CBS-QB3	G3MP2B3	Average CBS-QB3 and G3MP2B3
Dissociation						
	TS6	C3CC•CQC2 --> C2C=CC(OOH)C2 + CH$_3$	-3.09	-4.68	-3.17	**-3.92**
	TS7	C3CC•CQC2 --> C3CC=CC2 + HO$_2$	-16.82	-16.07	-13.84	**-14.96**
	TS8	C3CC•CQC2 --> C3COXRC2	-24.71	-22.82	-19.91	**-21.37**
	TS9	C3CCCQC2• --> C3CCj + CC(OOH)=C	1.84	0.22	1.92	**1.07**

Table 6.5 Evaluated Enthalpies of Formation at 298 K for Transition state in *tert*-Isooctane Radical + O₂ Reaction System (Continued)

Species		Reaction	Energies (kcal mol⁻¹)			
			B3LYP/6-31g(d,p)	CBS-QB3	G3MP2B3	Average CBS-QB3 and G3MP2B3
	TS10	C3CCCQC2• --> C3CCC(C)=C + HO₂	-16.09	-15.25	-13.51	**-14.38**
	TS11	C3CCCQC2• --> C3CCYC2OC	-19.99	-18.52	-15.76	**-17.14**
	TS12	C3•CCCQC2 --> C2C=C + C3jCOOH	-2.36	-4.36	-2.61	**-3.48**
	TS13	C3•CCCQC2 --> C2YC4OC2	-19.65	-17.4	-14.25	**-15.82**
	TS14	C3•CCCQC2 --> C2C(COH)CC(Oj)C2	-11.17	-10.89	-9.27	**-10.08**

6.4.6 Variational Transition State Theory Analysis

Potential energy surfaces for RC—O_2 bond dissociation in *tert*-isooctane hydroperoxide shown in Figure 6.4. The R• + O_2 → R-O_2 association reaction proceeds without any barrier, and determination of the kinetics of this reaction utilized via variational transition state theory (VTST). The simple dissociation reaction of the oxygen atom, R-OO → RO + O is also found to dissociate without a barrier, and this transition state is also treated variationally.

Potential energy scans were performed along the barrierless dissociations R–O_2 → R• + O_2 and RO–O → RO• + O bond cleavage reactions at 0.1A˚ intervals, and variational transition state kinetics calculated from thermochemical data at the unrestricted B3LYP/6-31G(d,p) level,. For each point on the UB3LYP reaction potential energy scans, the complex and reactant energies were multiplied by a scaling factor, that accounted for the ratio of the CBS-QB3 reaction enthalpy to the B3LYP reaction energy in order to obtain more correct dissociation limit energy. Frequency and thermodynamic calculations were performed at the discrete points along the potential energy surface.

Thermochemical properties and rate constants as a function of temperature were evaluated at each point along the potential energy surface. The minimum rate constant was located as a function of temperature and position for each reaction, providing the variational rate constant. Rate constants were fit to the three parameter form of the Arrhenius equation to yield the rate parameters A', n and E_a
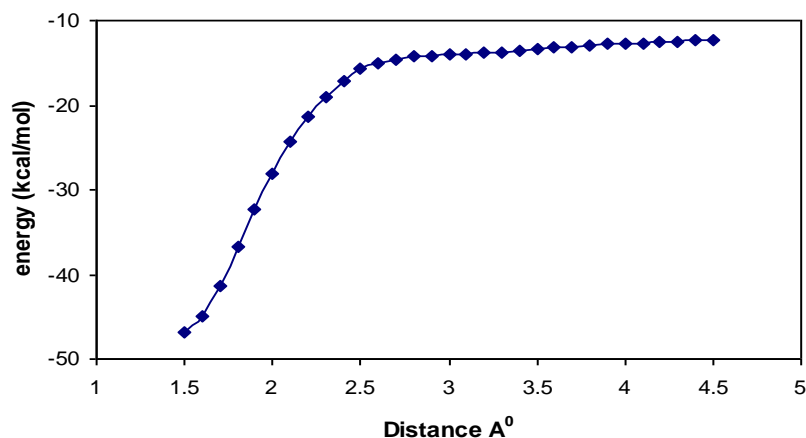
Figure 6.4 Potential energy surface for dissociation of the *tert*-isooctane hydroperoxide $((CH_3)_3CCH_2C(\text{--}OO\bullet)(CH_3)_2)$ the $R\text{—}O_2 \rightarrow R\bullet + O_2$.

For the *tert*-isooctane radical $+ O_2$ association, the transition state occurs at a $R\text{—}O_2$ bond length of 3.0 A° at 300 K, and decreases to 2.5 A° at 2000 K. Fitting the minimum rate constant as a function of temperature to the three parameter Arrhenius equation are calculated for the association reaction, $A' = 6.88E+22$, $n = -3.3$, $E_a = 1.9$ kcal mol^{-1} and $A' = 6.85E+22$, $n = -2.5$, $E_a = 34.7$ kcal mol^{-1} for dissociation reaction.

$$(CH_3)_3CCH_2C\bullet(CH_3)_2 + O_2 \rightarrow (CH_3)_3CCH_2C(OO\bullet)(CH_3)_2$$

$$k_{association} = 6.88 \times 10^{22}\, T^{-3.3} \exp(1005/T) \text{ cm}^3 \text{ mol}^{-1} \text{ s}^{-1}$$

$$k_{dissociation} = 6.85 \times 10^{22}\, T^{-2.5} \exp(-17456/T) \text{ s}^{-1}$$

There are several studies on rate constants for the association reaction of $R + O_2$. Lenhardt et al.[150] investigated reaction of *tert*-butyl radical with O_2 using tubular flow reactor and reported rate constant as 1.41×10^{13} cm^3 mol^{-1} s^{-1} at room-temperature. This same reaction was also studied using muon spin relaxation at a pressure of 1.5 bar by Dilger et al. [151]. They reported rate constant at room-temperature as 1.07×10^{13} cm^3 mol^{-1} s^{-1}. Rate constants for the association reaction of *tert*-$R\bullet + O_2$ at 298 is investigated using computational study by Villano et al.[152] and Miyoshi [153] reported as 1.41×10^{13} cm^3 mol^{-1}

s^{-1} and 1.26 x 10^{13} cm^3 mol^{-1} s^{-1}, respectively. Rate constant of *tert*-isooctane radical + O$_2$ at 298 in this study is 1.54 x 10^{13} cm^3 mol^{-1} s^{-1} which is slightly higher than that of *tert*-R• + O$_2$

Similar analysis was performed for the C3CCC(OO•)C2 → C3CCC(O•)C2 + O (R—O$_2$ → RO• + O) dissociation reaction. The location of the variational transition state is at a RO—O bond length of 2.8 A˚ at 300 K, tightening to the 2.3 A˚ at 2000 K. Fitting the variational rate constants to a three-parameter rate law are k (s^{-1}) = 1.01 x 10^{13} $T^{0.30}$ exp(-30011/T) (A' = 1.01E+13 n = 0.30 E_a = 59.6 kcal mol^{-1}) for dissociation reaction.

6.4.7 Kinetics

The potential energy surface and thermochemical properties are calculated with forward and reverse rate constants (high-pressure limit) for each elementary reaction step determined. Multifrequency quantum Rice Ramsperger- Kassel (QRRK) analysis is used for $k(E)$ with master equation analysis is used for falloff. The QRRK analysis is described by Chang et al. It is shown to yield reasonable results and provides a framework by which the effects of temperature and pressure can be evaluated in complex reaction systems. The QRRK code utilizes a reduced set of three vibration frequencies for densities of states which accurately reproduce the molecules'(adduct) heat capacity and include one external rotation in calculation in the density states. Comparisons of ratios of these $\rho(E)$/Q (partition function Q) with direct count $\rho(E)$/Q are shown to be in good agreement[53]. Nonlinear Arrhenius effects resulting from changes in the thermochemical properties of the respective transition state relative to the adduct with temperature are incorporated using a two parameter *Arrhenius* pre-exponential factor (A, n) in AT^n.

The master equation analysis uses an exponential-down model for the energy transfer function with (ΔE°_{down}) 900 cal mol^{-1} for N$_2$ as the third body. Rate constants, $k(E)$, were evaluated using energy 1.0 kcal mol^{-1} increments up to 70 kcal mol^{-1} above the highest barrier. Lennard-Jones parameters, σ (Å), and ε/κ (K) are obtained from tabulations and from an estimation method based on molar volumes and compressibility, $\sigma = 6.3$ Å and $\varepsilon/k_b = 584$ K. Table 6.6 presents high-pressure-limit elementary rate parameters used as input data to the QRRK calculations and the results versus pressure and temperature are presented in appendix D.

Table 6.6 High-Pressure-Limit Elementary Rate Parameter for Reactions in the *tert*-Isooctane Radical + O$_2$

Reaction			$k = A(T/K)^n \exp(-E_a/RT)$		
			A	n	E_a (kcal mol^{-1})
C3CCCJC2 + O$_2$	=>	C3CCCQJC2	6.88E+22	-3.3	2
C3CCCQJC2	=>	C3CCCJC2 + O$_2$	6.85E+22	-2.48	34.66
C3CCCQJC2	=>	C3CCJCQC2	7.79E+10	0.65	30.4
C3CCCQJC2	=>	C3CCCQC2J	6.45E+10	0.66	35.93
C3CCCQJC2	=>	C3JCCCQC2	2.76E+09	0.83	21.2
C3CCCQJC2	=>	C3CCDCC2 + HO$_2$	3.99E+11	0.75	27.02
C3CCCQJC2	=>	C3CCC2DC + HO$_2$	1.34E+12	0.48	26.47
C3CCCQJC2	=>	C3CCCOJC2 + O	1.01E+13	0.3	59.57
C3CCJCQC2	=>	C3CCCQJC2	2.95E+09	0.47	16.34
C3CCJCQC2	=>	C3CCDCC2 + HO$_2$	7.14E+12	-0.13	17.44
C3CCJCQC2	=>	C2CDCCQC2 + CH$_3$	4.63E+10	0.59	28.05
C3CCJCQC2	=>	C3COXRC2 + OH	3.16E+11	0.16	10.92
C3CCCQC2J	=>	C3CCCQJC2	1.19E+09	0.61	18.47
C3CCCQC2J	=>	C3CCC2DC + HO$_2$	4.02E+06	1.55	13.19
C3CCCQC2J	=>	C3CCJ + CCQDC	5.07E+05	2.1	28.39
C3CCCQC2J	=>	C3CCYC2OC + OH	2.82E+05	1.87	10.26
C3JCCCQC2	=>	C3CCCQJC2	9.06E+09	0.76	5.05
C3JCCCQC2	=>	C2CDC + C3JCQ	3.98E+14	-0.4	27.67
C3JCCCQC2	=>	C2YC4OC2 + OH	7.39E+11	0.18	14.39
C3JCCCQC2	=>	C2C(COH)CC(OJ)C2	2.58E+15	-0.98	21.17

6.4.8 Tertiary Isooctane Radical + O$_2$ Reaction System

Figure 6.5 shows the potential energy diagram for the C3CCC•C2 + O$_2$, the enthalpy values for reactants, intermediates and products are from the calculations at the CBS-QB3 level. Energies of TS structures are from the average between CBS-QB3 and G3B3MP2 calculation.

Bond dissociation energies, well depths, for *tert*-RO$_2$ → R + O$_2$ have been reported using computational study by Villano et al.[152] as 38.7 kcal mol^{-1}, by Simmie et al.[147] as 37.8 kcal mol^{-1}, by Zhu et al.[154] as 37.5 kcal mol^{-1} and by Miyoshi[153] as 40.0 kcal mol^{-1}. Reported experimental data for well depth of *tert*-butyl RO$_2$ → R + O$_2$ by Knyzev et al.[155] is 36.5 kcal mol^{-1}, by Blanksby et al.[149] is 37.5 kcal mol^{-1}, and Shuman et al.[156] is 35.8 kcal mol^{-1}. The well depth of C3CCC•C2 + O$_2$ reported by this study is 34.5 kcal mol^{-1} which is low compared to the literature data. The more shallow well is a result of the 93.1 kcal mol^{-1} tertiary C—H bond energy on this isooctane relative to the model compounds of the above studies, where the bond energies are ~ 96.5 kcal mol^{-1}

Addition of oxygen to the tertiary isooctane radical forms a chemically activated tertiary isooctane peroxy radical with a well depth of 34.5 kcal mol^{-1}. Seven possible reactions for this activated adduct at or below the entrance channel are shown, these include:

- Reverse reaction back to *tert*-isooctane radical + O$_2$ (non reaction)
- RO—O bond cleavage (Unimolecular dissociation), which is a chain branching channel.

- The intramolecular hydrogen transfer from the two different primary and the secondary carbon sites to the peroxy radical forming secondary and primary hydroperoxide isooctyl radicals (TS1, TS2 and TS3).

- HO_2 molecular elimination (TS4 and TS5) from tertiary isooctane radical to form 3 isooctene (+ HO_2)

- Beta scission, elimination reactions. TS7 and TS10 to form isooctene (+ HO_2), TS6, TS9 and TS12 to form an alkyl radical

- Three cyclic ether ring formations plus OH radical (TS8, TS11 and TS13)

- OH-transfer from the hydroperoxide to each of the alkyl radicals reaction (TS14)

Oxygen Atom Dissociation from the *tert*-Isooctane Hydroperoxide

Dissociation of the *tert*-isooctane peroxy radical adduct to C3CCC(O•)C2 + O is endothermic by 61.3 kcal mol^{-1} relative to the stabilized C3CCC(OO•)C2 radical; this is 26.6 kcal mol^{-1} above the entrance chanel. At low temperature, this reaction channel is not significant compare to the other channels; but it has a loose transition state structure and is important under higher temperature thermal and combustion conditions.

Isomerization of Peroxy Radicals

There are general notations for isomerization reaction of alkyl peroxy radicals. In this notation, the first number refers to the peroxy radical site, while the second number refers to the location of the radical site in the product relative to that in the reactant. The "p", "s" and "t" refer to reacting primary, secondary and tertiary sites. For example, CH_3CH_2OO• → $C•H_2CH_2OOH$ is called 1,4p and $CH_3CH_2CH_2OO$• → $CH_3C•HCH_2OOH$ is called 1,4s

Intramolecular H-transfer in smaller peroxy hydrocarbon radicals has been studied and general trends are established [154,157-160] Chan et al.[148] studied the H-migration reactions involving a primary and radical adjacent secondary abstraction site in the ethylperoxy through pentylperoxy radicals. Pfaendtner et al.[161] looked at 1,5 and 1,6 reactions involving a primary, terminal adjacent secondary, and tertiary abstraction site in methylated and unmethylated alkyl-2-peroxy radicals. Sharma et al.[157] reported on a series of 1,3 through 1,7 H-migrations involving primary, terminal adjacent secondary, and tertiary abstraction sites in alkylperoxy and hydroperoxyalkyl radicals. Alexander et al.[158] investigated all possible hydrogen migration pathways for the 1-ethyl, 1-propyl, 1-butyl, 1-pentyl, and 1-hexylperoxy radicals.

The 1,4-hydrogen migration barrier heights have been calculated for ethylperoxyl by Sheng et al.[43] as 36.3 kcal mol^{-1}, by Carstensen et al.[162] as 35.9 kcal mol^{-1}, by Miller et al.[163] as 36.0 kcal mol^{-1}, and by Sharma et al.[157] as 35.9 kcal mol^{-1}. Huynh et al.[160] reports 35.8 kcal mol^{-1} for $CH_3CH(OO\bullet)CH_3 \rightarrow C\bullet H_2CH(OOH)CH_3$. These data agree within 1.0 kcal mol^{-1} with the value of 36.3 kcal mol^{-1} calculated here for TS2, C3CCC(OO$\bullet$)C2 $\rightarrow$ C3CCC(OOH)C2$\bullet$ The higher barrier is due to increase strain in this higher substitute hydrogen carbon. The primary bond energies on the methyl sites are similar to methyl bond energies on smaller hydrocarbon.

The 1,4-hydrogen migration barrier heights calculated for TS1, C3CCC(OO$\bullet$)C2 $\rightarrow$ C3CC$\bullet$C(OOH)C2, is 30.7 kcal mol^{-1}. This data is in agreement with 1,4-hydrogen shift in *n*-propyl peroxy from Huynh et al.[149] at 31.2 kcal mol^{-1} The slightly lower barrier calculated for this secondary isooctane system results from the lower bond energy for the

secondary hydrocarbon in this system, 96.4 kcal mol^{-1} versus a normal secondary C—H bond of 97.8 kcal mol^{-1}

At room temperature, Villano et al.[152] evaluated rate constant from rate rule for 1,6p hydrogen shift from four 1,6p hydrogen shift reactions as 2.32×10^{-6} s^{-1} while Sharma et al.[157] reported 4.38×10^{-6} s^{-1} from $CH_3CH_2CH_2CH_2OO\bullet$ → $C\bullet H_2CH_2CH_2CH_2OOH$. Miyoshi[153] investigated rate constant for 1,6 tp as 1.15×10^{-6} s^{-1} at 298 K. Here, "tp" refer to alkyl substitution corresponding to the tertiary alkylperoxy radical abstract the primary hydrogen. This work reports $k = 8.52 \times 10^{-5}$ s^{-1} for C3CCC(OO•)C2 → C3•CCC(OOH)C2, 1,6p H-shift.

Abstraction of the hydrogen atom from one of the three primary, methyl carbons of the *tert*-butyl group (C_1, C_7 and C_8) by peroxy radical (TS3) involves a 7-membered ring TS and has a degeneracy of 9. This has the lowest energy barrier of the H-transfer reactions involving any *tert*-isooctane peroxy radical. The Ea is 21.8 kcal mol^{-1}, which is 10-15 kcal mol^{-1} lower than the two five member ring H-transfer paths (see below) but the pre-exponential factor is also lower, 2.75×10^{8} per hydrogen atom at 298 K. The low exponential is due to the extra internal rotor(s) lost in the TS structure relative to smaller ring TS structures.

This tertiary isooctane peroxy system has two different hydrogen transfer reactions that involve 5-membered ring TS structures. One is an abstraction of the hydrogen atom from secondary carbon (C_3); it has an activation barrier of 30.7 kcal mol^{-1} and a pre-exponential factor of 2.01×10^{11} per hydrogen atom at 298 K. A second 5 member ring path is transfer of a hydrogen atom from either of the primary carbons on the isopropyl group C_5 or C_6, where the barrier is 36.3 kcal mol^{-1} (and the pre-exponential

factor is 1.07×10^9/H at 298 K) The difference in barriers is mostly due to the weaker C—H bond on the secondary carbon, 96.4 versus 98.6 kcal mol^{-1}

For 1,4p H-shift, Sharma et al. Reported $k = 1.19 \times 10^{-13}$ s^{-1} for $(CH_3)_3COO\bullet \rightarrow$ $(CH_3)_2(C\bullet H_2)COOH$ at 298 K while Miyoshi (1,4tp) and Villano et al. (1,4p) reported 5.71×10^{-13} s^{-1} and 1.33×10^{-13} s^{-1}, respectively. These 1,4p reaction class above can compare to C3CCC(OO•)C2 $\rightarrow$ C3CCC(OOH)C2• reaction in this study for which reported a rate constant at room temperature as 1.15×10^{-14} s^{-1}

Rate constant for C3CCC(OO•)C2 $\rightarrow$ C3CCC(OOH)C2• , 1,4s H-shift, is calculated in this study as 1.47×10^{-10} s^{-1}. Miyoshi, Sharma et al. and Villano et al. reported rate constant as 1.03×10^{-9} s^{-1} for 1,4ts, 1.40×10^{-11} s^{-1} for $CH_3CH_2C(CH_3)_2OO\bullet$ $\rightarrow CH_3C\bullet HC(CH_3)_2OOH$ and 1.11×10^{-10} s^{-1} for 1,4s, respectively. Table 6.7 presents a comparison of the different classes of rate constants. Comparison of rate constant at each H-shift reaction as a function of temperature is reported in appendix D.

Table 6.7 Comparison of High-Pressure-Limit Rate Constants at Room-Temperature for Isomerization of Peroxy Radicals (Hydrogen shift) Reactions in the *tert*-Isooctane Radical + O_2 (s^{-1})

Reaction	Sumathi et al.[147]	Miyoshi.[153]	Villano et al.[152]	This work
C3CCQjC2 --> C2CCjCQC2	1.40×10^{-11}	1.03×10^{-9}	1.11×10^{-10}	1.47×10^{-10}
	1,4s H-shift	1,4ts H-shift	1,4s rate rule	
C3CCQjC2 --> C3CCCQC2j	1.19×10^{-13}	5.71×10^{-13}	1.33×10^{-13}	1.15×10^{-14}
	1,4p H-shift	1,4tp H-shift	1,4p rate rule	
C3CCQjC2 --> C3jCCCQC2	4.38×10^{-6}	1.15×10^{-6}	2.32×10^{-6}	8.52×10^{-5}
	1,6p H-shift	1,6tp H-shift	1,6p rate rule	

HO$_2$ Molecular Elimination and Beta Scission Reaction

The HO$_2$ direct molecular elimination reaction to form isooctene (C3CC=CC2, C3CCC(C)=C) + HO$_2$ from the peroxy radical can occur from both the chemically activated adduct and the stablilized peroxy radical. The barrier for this molecular elimination path is ~7.5 kcal mol^{-1} below the entrance channel for direct molecular elimination (TS4, TS5). The activation barrier to form the isooctenes + HO$_2$ is 26.5 kcal mol^{-1} respective to isooctane peroxy radical.

There are two additional paths which yields the same two isooctene + HO$_2$ product sets; these are β-scission (elimination) reactions from each of the two hydroperoxide alkyl radicals, where the radical sites are on the secondary and primary carbons adjacent to the tertiary peroxy carbon. Barriers and rate constants for the required first isomerization step are described above.

The activation energies for (TS7, TS10) elimination reaction from the hydroperoxide alkyl radicals are ~4 kcal mol^{-1} below the entrance channel higher than the above direct molecular elimination reaction. This β-scission - elimination of HO$_2$ requires a previous step, that is a 1,4H-transfer reaction to the peroxy oxygen atom forming the two radicals: C3CC•C(OOH)C2 and C3CCC(OOH)C2.

C3CC•C(OOH)C2 → C3CC=CC2 + HO$_2$ with 16.8 kcal mol^{-1} barrier respective to isooctane hydroperoxide alkyl radical; 2.7 kcal mol^{-1} below entrance channel. C3CCC(OOH)C2• → C3CCC(C)=C + HO$_2$ with a barrier of 8.9 kcal mol^{-1} from isooctane hydroperoxide alkyl radical, that is 7.3 kcal mol^{-1} below entrance channel.

Cyclic Ether Ring Formation

In an early n-hexane combustion study, Jones and Fenske[164] reported the formation of significant quantities of cyclic ethers in addition to olefins between 580 and 930 K. The results below show that one of the most important reaction channels in this tertiary isooctane radical plus O_2 system is the formation of a cyclic ether + OH. These reactions occur from the hydroperoxide alkyl radical isomers formed via the intramolecular H transfer reactions. Here the alkyl radical center attacks the oxygen on the carbon of the peroxide group; this results in a ring-closure (cyclic ether) and elimination of an OH-radical. The mechanism of this reaction step has been described by Chan *et al.* [165]. It is important to note that an H atom transfer from the alkyl carbon atom to the peroxy oxygen atom must occur prior to this cyclic ether + OH path.

The activation barrier to cyclic ether formation from secondary carbon (C_3), 3 member ring, is 10.4 kcal mol^{-1}. This is 9.0 kcal mol^{-1} below entrance channel. The cyclic formation activation barrier from primary carbon at *tert*-butyl group (C_1, C_6, C_7), 5 member ring, is 11.4 kcal mol^{-1}, 4.8 kcal mol^{-1} below entrance channel. And cyclic formation from primary carbon of i-propyl group (C_5, C_8); 3 member ring, to form C2YC4OC2 is 13.9 kcal mol^{-1}, 3.5 kcal mol^{-1} below entrance channel. Among cyclic ethers formed, the *2,2,4,4-tetramethyl-tetrahydrofurane* (C2YC4OC2) is the most abundant in combustion as shown in isooctane experiments [120-125]

OH-Transfer Reactions

An OH-transfer reaction also occurs after H transfer to the peroxy oxygen forming the hydroperoxide alkyl radicals. Here the alkyl carbon radical site attacks the oxygen of the OH of the hydroperoxide group. Wijaya *et al.*[166] have previously described these reactions for a series of different carbon number hydrocarbon. The alkyl carbon radical attacks the oxygen of the OH on the hydroperoxide. The OH transfers to the attacking carbon cleaves the week RO-OH bond. An alkoxy radical remains on the initial peroxide carbon (C2C(COH)CC(Oj)C2). Under combustion or thermal conditions, the alkoxy radical will rapidly form a carbonyl bond via a beta scission reaction. Here it rapidly decomposes to acetone and hydroxyl-neopentyl radical. Acetone is also an experimentally observed product [122, 123]. Cyclic ether and OH-transfer reactions are two lowest energy pathways in oxidation of isooctane in this study.
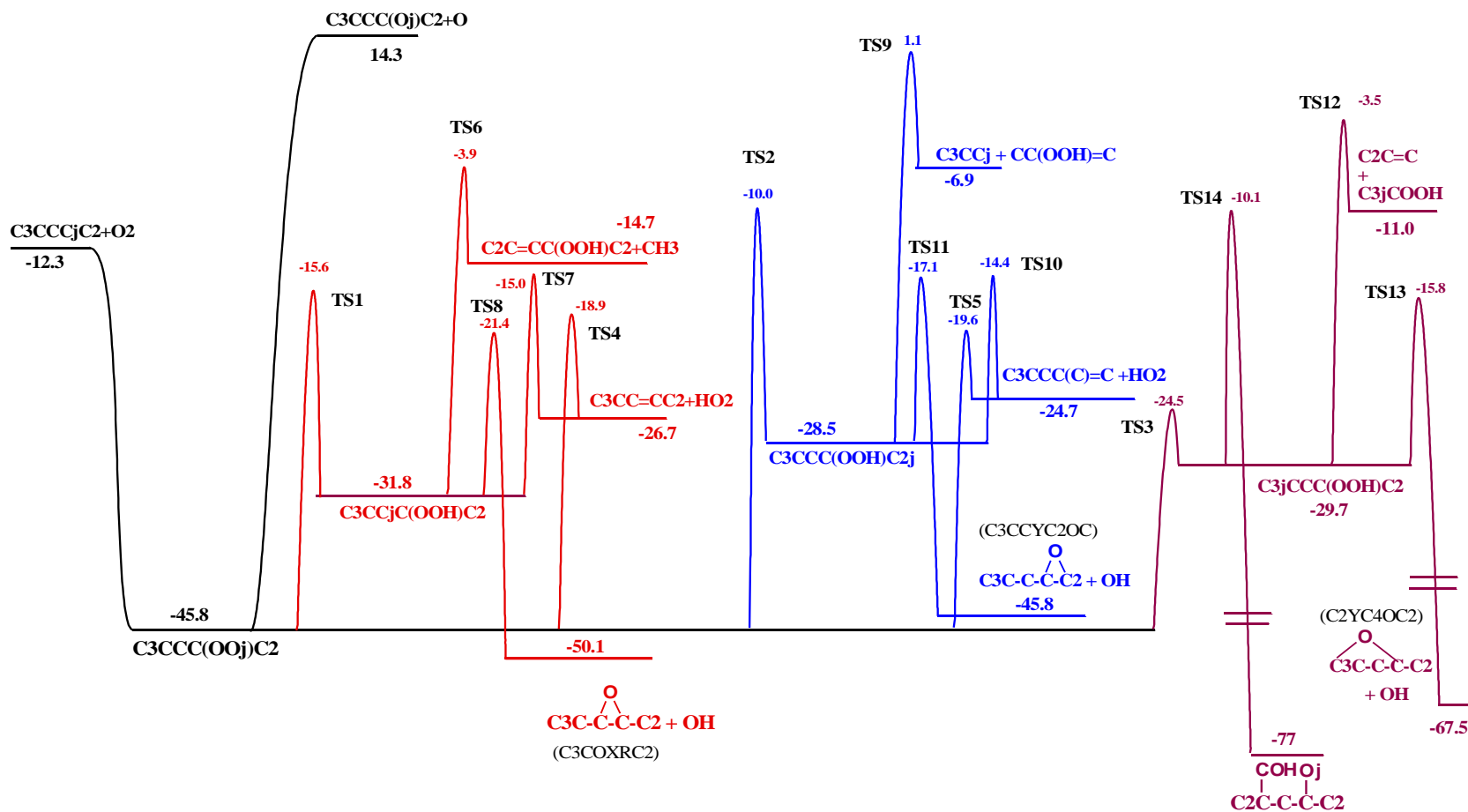
Figure 6.5 Potential energy diagram for C3CCC•C2 + O₂ reaction system.

Plots of calculated rate constants versus 1000/T (K) from chemical activation for C3CCC•C2 + O$_2$ → products at 1Atm and 60Atm are shown in Figure 6.6.A and Figure 6.6.B, respectively. Stabilization to adduct C3CCC(OO•)C2 channel is the most important reaction path in low to moderate temperature hydrocarbon oxidation. As temperature is increased, the rate through other channels begins to increase, while the stabilization rate decreases. At the higher temperatures, there is sufficient reaction of the energized adducts to overcome the barrier associated with the five-membered and seven-membered ring TS from both H-transfer reaction and HO$_2$ elimination. Forward reactions go to molecular elimination to form isooctene + HO$_2$ and to form cyclic ethers + OH. Dissociation to C3CCC(O•)C2 + O has an endothermicity of 26.6 kcal mol^{-1} above the reactant channel. And the rate constant at low temperature is not significant compared to the stabilization, HO$_2$ elimination, OH transfer and cyclic ether + OH channels. This channel does become important at high temperatures, above 1000 K.
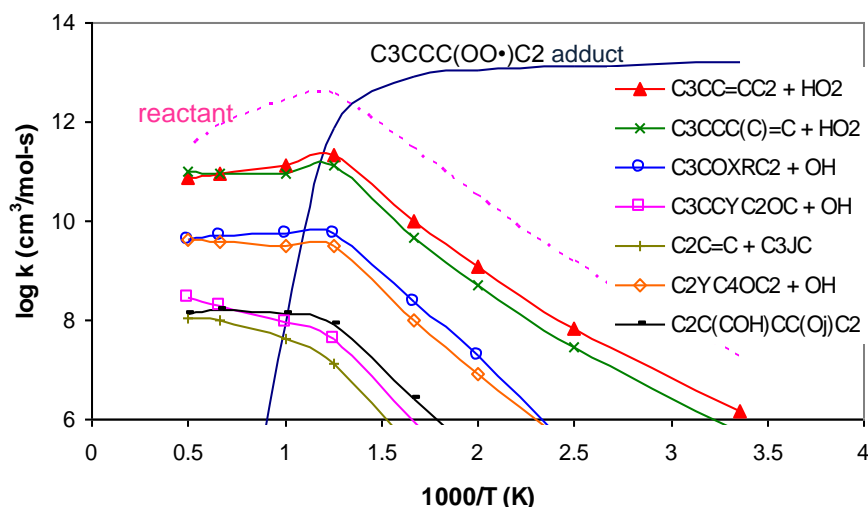
Figure 6.6.A Chemical activation plot of rate constants versus 1000/T (K) at 1atm for C3CCC•C2 + O$_2$ → products.
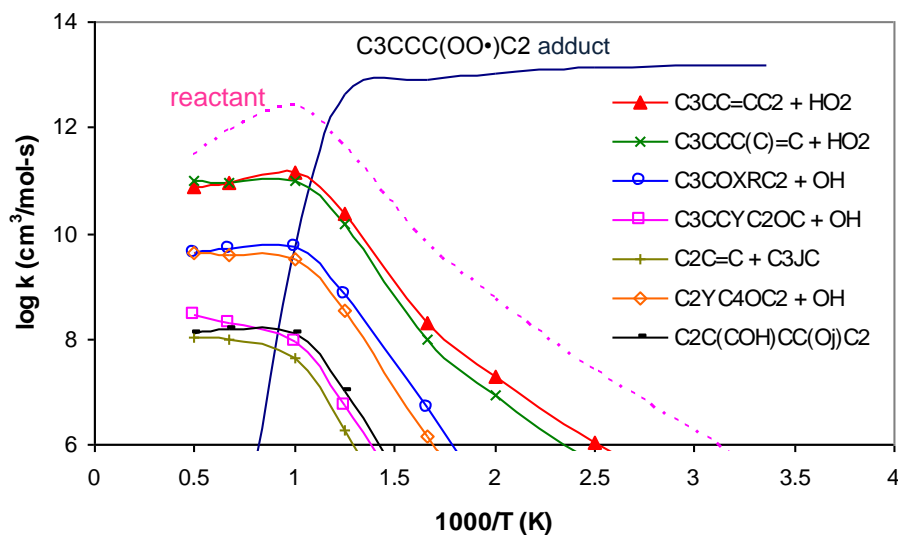
Figure 6.6.B Chemical activation plot of rate constants versus 1000/T (K) at 60 atm for C3CCC•C2 + O$_2$ → products.

At lower temperatures, stabilization of the peroxy adduct and the two reactions to isooctane plus HO$_2$ (molecular elimination) are important paths. At higher temperatures, the two isooctane + HO$_2$ products sets remain most important paths. At higher pressure, 60 atm, the stabilization and isooctane products are still most important. At lower pressure, 0.01 atm, the major reaction channels follow the same trend as the one at 1 atm and 60 atm.

Plots of calculated rate constants versus log P from chemical activation for C3CCC•C2 + O$_2$ → products at 298 K and 1000 K are shown in Figure 6.7.A and Figure 6.7.B, respectively. At room temperature tertiary isooctane peroxy radical adduct is the most important reaction path and is independent of the pressure. Other important product channels are molecular elimination reactions to form isooctene + HO$_2$ and cyclic ether + OH. At low pressures, some of the energized C3CCC(OO•)C2 adduct can isomerize to energize hydroperoxide alkyl radical prior to stabilization, but the subsequent rate of

stabilization of energized alkyl radical in the low-pressure environment is slower than the rate through concerted elimination to form isooctane + HO_2 and cyclic ether + OH, so the overall rate for stabilization remains low. At high temperatures, above 1000 K, all reactions are independent of pressure. Important forward reactions go molecular elimination to form isooctane + HO_2 and the cyclic ether + OH channels.
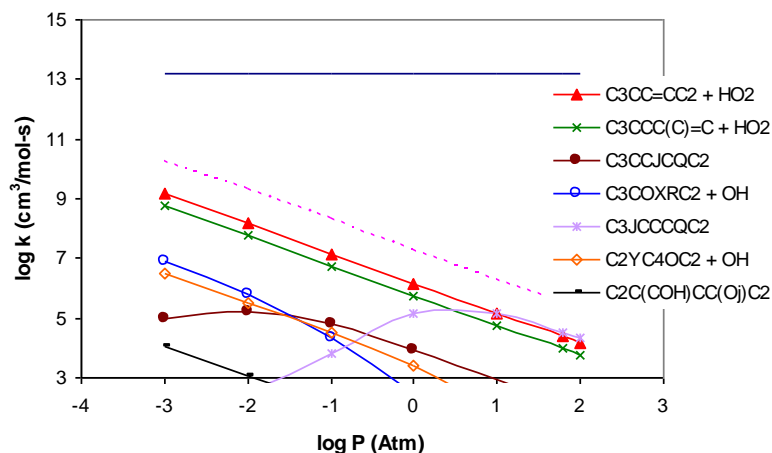
Figure 6.7.A Chemical activation plot of rate constants versus log pressure (atm) at 298 K for C3CCC•C2 + $O_2 \rightarrow$ products.
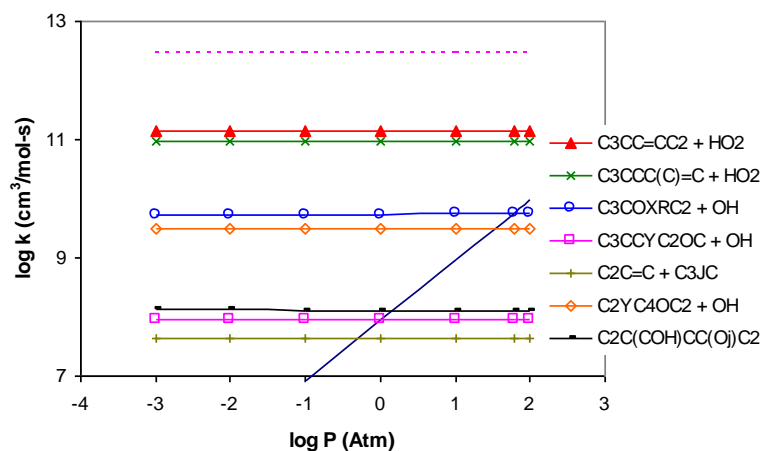
Figure 6.7.B Chemical activation plot of rate constants versus log pressure (atm) at 1000 K for C3CCC•C2 + $O_2 \rightarrow$ products.

Unimolecular Dissociation of *tert*-Isooctane Peroxide

Plots of rate constants versus 1000/T for stabilization to adduct C3CCC(OO•)C2 dissociation at 1 atm pressure are illustrated in Figures 6.8 and plots of rate constants versus log pressure at 298 K and 1000 K are illustrated in Figures 6.9.A and 6.9.B, respectively. Forward reactions are molecular elimination to isooctene + HO_2 and isomerization to C3•CCC(OOH)C2 are important at lower temperature with least activation energy, 21.8 kcal mol^{-1}, when compare to other dissociation reaction paths. At high temperature all dissociation reactions show some pressure dependence. The important reaction paths are formation of isooctene + HO_2 and isomerization to C3•CCC(OOH)C2.
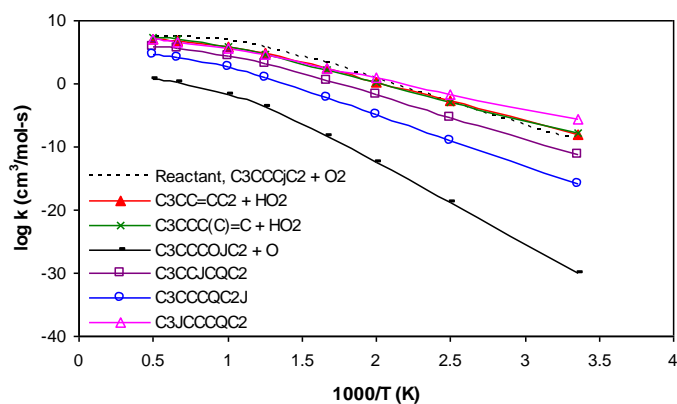
Figure 6.8 Plots of rate constants versus 1000/T (K) at 1atm for C3CCCQ•C2 dissociation.
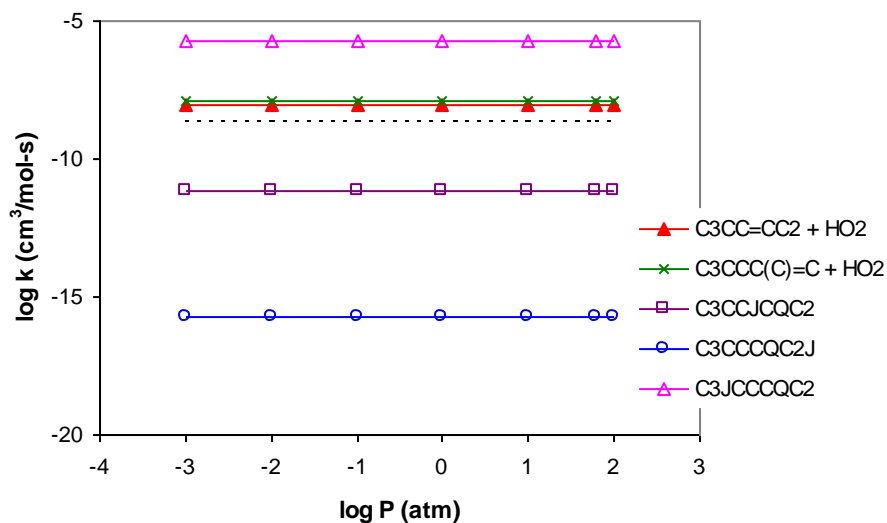
Figure 6.9.A Plots of rate constants versus log pressure (atm) at 298 K for C3CCCQ•C2 dissociation.
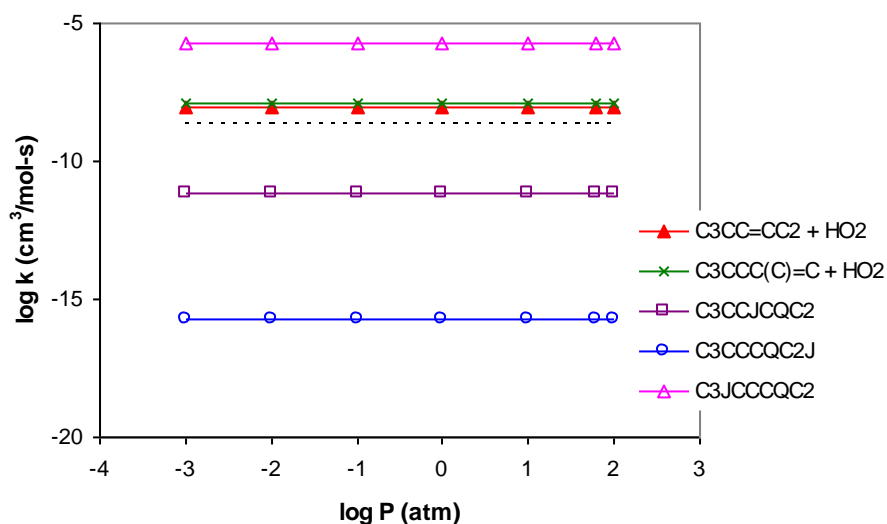
Figure 6.9.B Plots of rate constants versus log pressure (atm) at 2000 K for C3CCCQ•C2 dissociation.

Results from unimolecular dissociation of the stabilized peroxy adduct calculation show formation of the two isooctene + HO_2 and reaction back to isooctane radical are dominant. At higher pressure, 2000 K, molecular dissociation to isooctane radicals plus O_2 is dominant with important products isooctane isomer and HO_2 becoming equally

important to reaction back isooctane radical + O_2 at lower prerssure. The formations of the two hydroperoxy alkyl radical isomers are also important at high temperature.

6.5 Summary

The enthalpies of formation via isodesmic work reactions for *tert*-isooctane hydroperoxide -77.81 kcal mol^{-1} Bond energy values for the radicals are 100.2, 98.1, 101.4 and 84.1 kcal mol^{-1} for C3•CCCQC2, C3CC•CQC2, C3CCCQC2•and C3CCCQ•C2, respectively. The carbon-hydrogen bond energies were observed to be weaker than the conventional primary and secondary carbon-hydrogen bond by ~1 kcal mol^{-1}. Group additivity, *tert*-isooctane hydroperoxide has three gauche interactions and two of 1,5 interaction. The radicals have three gauche interactions with one 1,5 interaction.

The major reaction path at 1atm pressure is the stabilization of *tert*-isooctane peroxy radical adduct (C3CCCQ•C2) below 650 K. The major bimolecular product channels are isooctene + HO_2 from four channels; two channels from molecular elimination and other two channels from isomerization then beta scission. Other important reaction channel is cyclic ethers + OH. This study also observes OH-transfer reactions from the hydroperoxy radical to the alkyl-radical centers. The observed importance of this OH-transfer reaction is new with this reaction system, and a variety of significant chain propagation and acceleration product pathways.

CHAPTER 7

THERMOCHEMISTRY AND KINETIC MODELING FOR OH ADDITION TO PROPENE AND O_2 ASSOCIATION TO THE ACTIVATED $CH_2(OH)C \cdot HCH_3$ ADDUCT

7.1 Overview

Regeneration of OH radicals has recently been considered as an important process in atmospheric chemistry of unsaturated hydrocarbons, where current atmospheric modeling does not correctly predict levels during regeneration periods. The reaction of OH with propene and the subsequent reactions of the energized and stabilized hydroxypropyl radical adducts with O_2 are studied using density functional theory and CBS-QB3 ab initio theoretical methods. Enthalpies of formation ($\Delta_fH°_{298}$) are determined using isodesmic reaction analysis at the CBS QB3 composite and density functional levels. Entropies ($S°298$) and heat capacities ($C°p(T)$) are determined using geometric parameters and vibrational frequencies obtained at the B3LYP/6-311G(2d,d,p) level of theory. Internal rotor contributions are included in S and $Cp(T)$ values. Detailed potential energy surfaces for these reactions are presented with rate parameters calculated for each reaction step from transition state theory. The chemically activated hydroxypropyl radical + O_2 adducts are modeled using quantum Rice-Ramsperger-Kassel (QRRK) theory, with master equation analysis for falloff. The reaction system is modeled using the CHEMKIN modeling program (v3.1) under conditions of atmospheric chemistry for varied NO_x concentration using an elementary reaction mechanism with all reactions reversible.

Hydroxyl radical addition to propene forms an energized hydroxyl-propyl adduct with 29.2 kcal mol^{-1} of chemical activation energy from the new bond formation. The energized hydroxyl propyl radical is treated as having up to 60 energized adducts spaced

evenly between the ground state of the hydroxyl-propyl adduct, HO-C•CC-Add, and the entrance channel. {sixty energy bins at 0.5 kcal spacing, (HO-C•CC-Add*)i, i = 1 to 60, and * = energized}. Each of these adducts can be stabilized, or re-energized via collisions, or react further with O_2 (association) to form a second, new, energized adduct, which is a hydroxyl-propyl-peroxy adduct, (HO-CCOO•C-Add)i, with an additional 36.1 kcal mol^{-1} before stabilization.

The further chemical activation reactions of the distributed energized HO-CC•C-Add*)i, and the stabilized hydroxyl-propyl adduct, HO-CC•C-Add, with O_2 can lead to OH regeneration via two parallel paths: cyclic ether + OH and CH_2O and CH_3CHO + OH formation paths. Data is presented for different ΔE down step sizes and for presence of varied NO concentratons.

7.2 Previous Studies

Unsaturated hydrocarbon species are important reactive trace gases in the troposphere, originating from a number of natural and anthropogenic sources. The lighter alkenes, ethene and propene, are predominantly emitted from fossil fuel combustion, biomass burning, and the oceans.

Olefinic hydrocarbons, alkenes, can react with OH to form organic free radicals (R•), either by abstraction or addition pathways where addition occurs with no barrier and abstraction also has a low barrier[167-169]. Typically, in atmospheric chemistry addition is the dominant path. In the case of propene the OH addition generates a hydroxy propyl radical, will rapidly associate with $^3O_2$ to form the hydroxy-alkyl peroxy radical, HO-CCOO•C-Add)i. These peroxy radicals are often termed ROO•. The peroxy radicals can

undergo unimolecular isomerization or dissociation reactions or undergo bimolecular reactions with NO, HO$_2$, and with other RO$_2$ radicals. The reactions with NO$_x$, HO$_x$ and RO$_2$ ultimately form a range of oxygenated organics. The further isomerization reactions can result in OH radical re-generation. In propene oxidation, OH addition to an unsaturated carbon atom, can form two hydroxypropyl radicals. (i) initial OH attack at the 1-position forming HO-CC•C-Add (reaction a) and (ii) 2-position forming C•COHC-Add (reaction b).

$$OH + CH_2=CH-CH_3 \rightarrow (HO)CH_2-C•H-CH_3 \qquad (a)$$

$$OH + CH_2=CH-CH_3 \rightarrow C•H_2-CH(OH)-CH_3 \qquad (b)$$
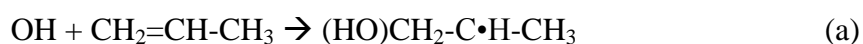
The subsequent addition of O$_2$ to the hydroxyl propyl radicals produces two β-hydroxyperoxy radicals, which can react with NO and other species to form oxidation products (HO-CCOO•C-Add*), and (COO•COHC-Add*),

This study focuses on the reaction of the β-hydroxyperoxy radicals formed from OH attack at the 1-position on propene, with subsequent association with O$_2$ that forms the hydroxyl-propyl-peroxy adduct (HO-CCOO•C-Add), and can result in the regeneration of OH. This study includes analysis of the reaction system modeled under conditions of atmospheric chemistry for varied NO$_x$ concentrations.

Thermochemical properties are estimated for reactants, intermediates, products, and transition states in the reaction paths using ab initio and density functional calculations. The thermochemical parameters are used to calculate high-pressure limit rate constants using canonical transition state theory (TST) and variational transition state theory (VTST). Rate constants as a function of temperature and pressure are estimated using a multifrequency quantum RRK analysis for k(E) and master equation analysis for

falloff. The data at relevant pressures and temperatures should be useful to both atmospheric and combustion models. As noted above, the reaction of the chemically activated adducts from the OH addition reaction to propene are studied by forming a distribution of sixty adducts in the chemical activation system and allowing each energy level adduct to further react with oxygen molecule to form the energized peroxy adducts. The reactions of the different level peroxy adducts to products, including the regeneration of OH are studied to determine if the chemical activation energy distribution amplifies the OH regeneration rate.

7.3 Computational Methods

7.3.1 Thermochemical Properties

The reactants, intermediates, products, and transition state structures are calculated at B3LYP hybrid density functional theory method, as well the complete basis set-QB3 composite method. CBS-QB3 is a multilevel model chemistry that combines the results of several *ab initio* and DFT individual methods and empirical correction terms to predict molecular energies with high accuracy and relatively low computational cost. All quantum chemical calculations have been performed within the Gaussian-03 suite of programs.

To evaluate the heats of formation of the molecule systems, a variety of homodesmic and isodesmic work reactions are used, where the bonding environments are similar in products and reagents. Several previous works[45, 46, 141-143] show that the computed enthalpies of formation via isodesmic work reactions for nitrogen species are in satisfactory agreement with the experimental data available. The energy of each

transition state structure is calculated from the corresponding reactant plus the energy difference between the TS structure and the reactant (adduct).

Entropy and heat capacity contributions as a function of temperature are determined from the calculated structures, moments of inertia, vibration frequencies, symmetry, electron degeneracy, number of optical isomers and the known mass of each molecule. The calculations use standard formulas from statistical mechanics for the contributions of translation, external rotation and vibrations using the "SMCPS" program.[11] This program utilizes the rigid-rotor-harmonic oscillator approximation from the frequencies along with moments of inertia from the optimized CBS-QB3 structures, *viz.* B3LYP/6-311G(2d,d,p) level. Contributions from internal rotors using Pitzer-Gwinn formalism are substituted for contributions from internal rotor torsion frequencies.

7.3.2 Kinetic Modeling

The thermochemical properties and potential energy surface are determined from the calculation of structures, energies, internal rotor potentials and vibration frequencies of stable parent molecules, products, intermediate radicals and transition state structures. High pressure limit kinetic parameters are determined from use of statistical mechanics and canonical transition state theory for reactions with saddle points. Variational transition state theory or literature data are used for association and dissociation reactions that have no barrier other than enthalpy of reactions. Quantum mechanical tunneling corrections have been applied using Erying Henry for intramolecular hydrogen transfer. Chemical activation and unimolecular dissociation reactions are analyzed using multifrequency quantum Rice Ramsperger- Kassel (QRRK) analysis for $k(E)$ with master equation analysis for falloff. The QRRK analysis is described by Chang et al. It is shown

to yield reasonable results and provides a framework by which the effects of temperature and pressure can be evaluated in complex reaction systems.

7.4 Results and Discussion

7.4.1 Thermochemical Properties

The optimized geometries at the CBS-QB3 composite level of theory (*viz.,* B3LYP/6-311(2d,d,p) calculations) for the target molecules and corresponding abbreviated nomenclatures are presented in Figure 7.1. Standard enthalpy of formation, $\Delta_f H^0_{298}$ were calculated for all species involved in the reaction of the hydroxypropyl radical + O_2. The enthalpies of formation of the target molecules obtained from the use of the reaction schemes are showed in Table 7.1.

$CH_2(OH)CH(OOH)CH_3$ (*cohcqc*) $CH_2(OH)CH(OO\bullet)CH_3$ (*cohcqjc*)

$C\bullet H(OH)CH(OOH)CH_3$ (*cjohcqc*) $CH_2(O\bullet)CH(OOH)CH_3$ (*cojcqc*)
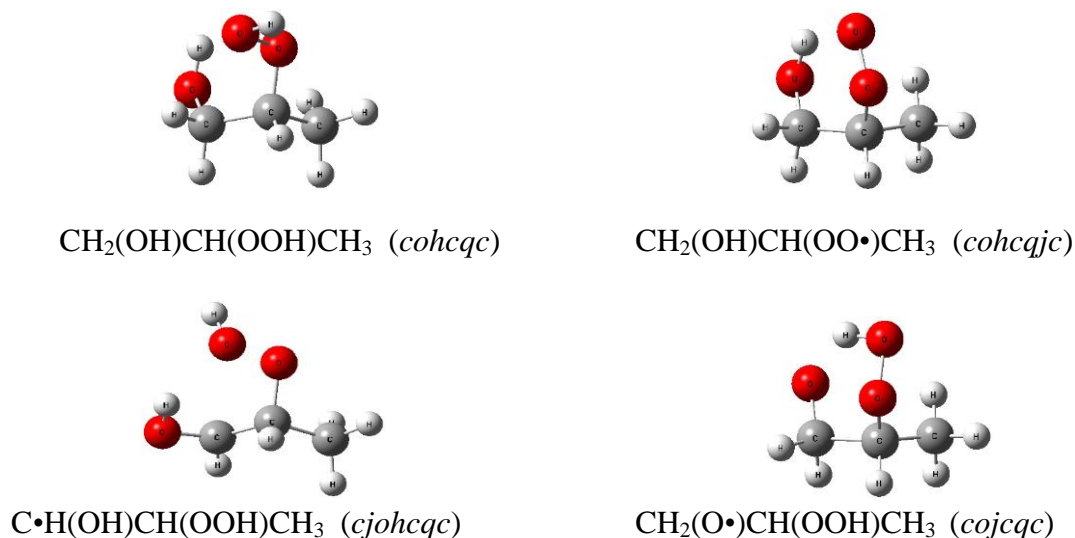
Figure 7.1 Geometry of the lowest energy conformer of the target molecules and abbreviated nomenclatures.

Table 7.1 Evaluated Enthalpies of Formation at 298 K of Target Molecules

Work Reactions							$\Delta H_f°298$ (kcal mol^{-1}) CBS-QB3
CH$_2$(OH)CH(OOH)CH$_3$ (*cohcqc*)							
cohcqc	+	C$_2$H$_6$	-->	CH$_2$(OH)CH$_2$(OOH)	+	C$_3$H$_8$	-85.53
cohcqc	+	C$_3$H$_8$	-->	CH$_2$(OH)CH$_2$(OOH)	+	C$_4$H$_{10}$	-85.44
cohcqc	+	CH$_3$OH	-->	CH$_2$(OH)CH$_2$(OOH)	+	C$_2$H$_5$OH	-85.61
			Average				**-85.52**
CH$_2$(OH)CH(OO)CH$_3$ (*cohcqjc*)							
cohcqjc	+	CH$_3$CH$_2$OOH	-->	*cohcqc*	+	CH$_3$CH$_2$OO•	-51.45
cohcqjc	+	CH$_3$C(=O)OOH	-->	*cohcqc*	+	CH$_3$C(=O)OO•	-49.98
cohcqjc	+	CH$_2$(OOH)C(=O)H	-->	*cohcqc*	+	CH$_2$(OO•)C(=O)H	-50.69
			Average				**-50.70**
CH$_2$(O)CH(OOH)CH$_3$ (*cojcqc*)							
cojcqc	+	CH$_3$OH	-->	*cohcqc*	+	CH$_3$O•	-29.85
cojcqc	+	CH$_3$CH$_2$OH	-->	*cohcqc*	+	CH$_3$CH$_2$O•	-29.80
cojcqc	+	CH$_3$CH$_2$CH$_2$OH	-->	*cohcqc*	+	CH$_3$CH$_2$CH$_2$O•	-30.46
			Average				**-30.04**
CH$_2$(OH)CH(OOH)CH$_2$ (*cohcqcj*)							
cohcqcj	+	CH$_3$CH$_2$OOH	-->	*cohcqc*	+	C•H$_2$CH$_2$OOH	-33.56
cohcqcj	+	C$_2$H$_6$	-->	*cohcqc*	+	C$_2$H$_5$	-34.70
cohcqcj	+	CH$_3$CH$_2$OH	-->	*cohcqc*	+	C•H$_2$CH$_2$OH	-33.41
			Average				**-33.89**

Hydroperoxy radical can be stabilized by intramolecular hydrogen bonding between the hydroxyl H and oxygen from of the peroxy group with a H--O distance of 2.12 A°. The H-bonded structure gives relative energies about 3.2 kcal mol^{-1} lower than the non-H-bonded structure. This is also occurs for alkoxy radical, hydrogen bonding between H from peroxy group and oxygen from oxy radical with a H--O distance of 1.88 A° provide stabilization of about 5.2 kcal mol^{-1}.

7.4.2 Variational Transition State Theory Analysis

Potential energy scans were performed along the dissociating R–OO (CH$_2$(OOH)CH(--OO)CH$_3$) and were calculated at the B3LYP/6-31G(d,p) level, at 0.1A° intervals. The B3LYP reaction energies between the points along the potential energy scans and the reactant were multiplied by a scaling factor, which is the ratio of the CBS-QB3 reaction enthalpy to the B3LYP reaction energy. This procedure effectively uses the CBS-QB3 energy to provide the enthalpy of reaction and results of the B3LYP/6-31G(d,p) scan to the correct dissociation limit energy. Frequency calculations were performed for transition-state structures along the minimum energy pathways start from R–OO and bond length of 1.48 A° to 3.86 A° with 0.1 A° intervals for the total of 25 points, yielding thermochemical properties as a function of temperature as described above.

Potential energy surfaces for R--OO (CH$_2$(OH)CH(--OO)CH$_3$) bond dissociations in hydroperoxy propyl radical are shown in Figure 7.2. Frequency calculations were performed at discrete points along the potential energy surface, for both reactions. Thermochemical properties and rate constants as a function of temperature were evaluated at each point along the potential energy surface. The minimum rate constant was located as a function of temperature and position for each reaction, providing the

variational rate constant. Rate constants were fit to the three parameter form of the Arrhenius equation to yield the rate parameters A', n and E_a
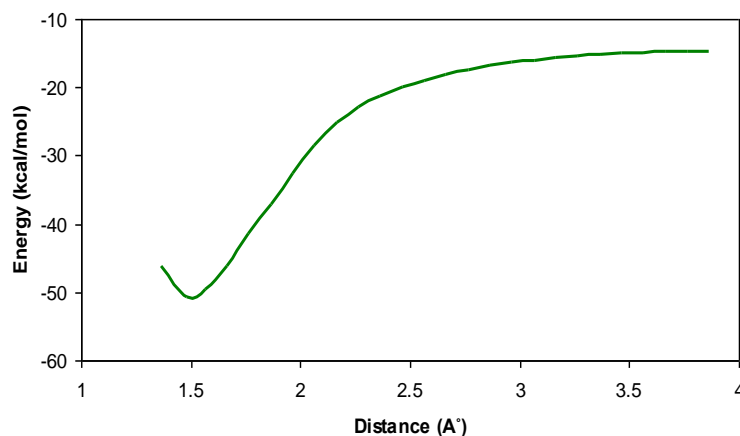
Figure 7.2 Potential energy surface for dissociation of the R--OO in the hydroperoxy propyl radical $CH_2(OH)CH(OO\bullet)CH_3$.

For the hydroxy propyl radical + O_2 association, the transition state occurs at a R—OO bond length of 3.06 A˚ at 300 K, decreasing to 2.26 A˚ at 2000 K. Fitting the minimum rate constant as a function of temperature to the three parameter Arrhenius equation calculated for the association reaction as $A = 4.28E+10$, $n = 0.46$, $E_a = -0.613$ kcal mol^{-1} and $A = 4.08E+24$, $n = -2.5$, $E_a = 37.14$ kcal mol^{-1} for dissociation reaction. Rate constants as a function of temperature for the hydroxy propyl radical + O_2 association are plotted in Figure 7.2 for the four contributing transition-state structures. A solid line in Figure 7.3 indicate an empirical three-parameter Arrhenius fit of $k(T)$.

$$CH_2(OH)CH\bullet CH_3 + O_2 \;\longleftrightarrow\; CH_2(OH)CH(OO\bullet)CH_3$$
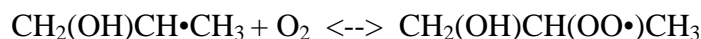
$$k_{association} \;=\; 4.28 \times 10^{10}\, T^{0.5}\, \exp(309/T)\;\; cm^3\, mol^{-1}\, s^{-1}$$

$$k_{dissociation} \;=\; 4.08 \times 10^{24}\, T^{-2.5}\, \exp(-18702/T)\;\; s^{-1}$$
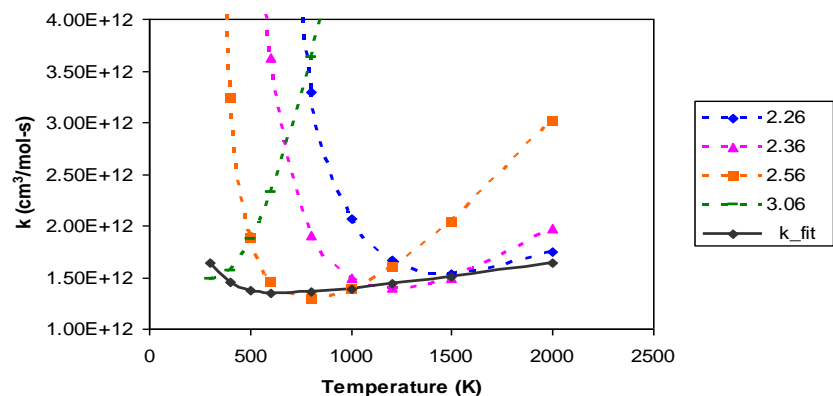
Figure 7.3 Rate constants as a function of temperature for contributing transition-state structures in the barrierless of the association hydroxypropyl radical with O_2 reaction. The solid line indicates a three-parameter Arrhenius fit of the variational rate constant.

7.4.3 Energy Diagram for Hydroxypropyl Radical + O_2 Reaction System

The potential energy diagrams for the chemical activation calculation of the hydroxypropyl radical + O_2 reactions are shown in Figure 7.4. This association reaction proceeds without barrier with a well depth of 36.1 kcal-mol^{-1}. This chemical activation energy can be use to further react by unimolecular reactions (intramolecular hydrogen shift, elimination, and dissociation reactions), reverse reaction back to the hydroxypropyl radical + O_2. The peroxy radical ($CH_2(OH)CH(OO\bullet)CH_3$) undergoes an intramolecular hydrogen shift through six-member ring transition state from the hydroxy group to the peroxy radical site results in an alkoxy radical ($CH_2(O\bullet)CH(OOH)CH_3$) after a barrier of 22.5 kcal mol^{-1}. Other reaction paths for this peroxy radical include intramolecular hydrogen transfer through 5-member ring to form hydroperoxide alkyl radical, $CH_2(OH)CH(OOH)C\bullet H_2$ and $C\bullet H(OH)CH(OOH)CH_3$, with 23.4 kcal mol^{-1} and 34.6 kcal mol^{-1} barrier, respectively.

The C•H(OH)CH(OOH)CH$_3$ formed via intramolecular H abstraction from the hydroxyl carbon radical can form a cyclic ether + OH. Here the alkyl radical center attacks the oxygen on the carbon of the peroxide group; this results in a ring-closure (cyclic ether) and elimination of an OH-radical.

The primary alkoxy radical can undergo dissociation to peroxyethyl radical + formaldehyde (Ea = 3.82 kcal-mol^{-1}) via CH$_2$(O•)---CH(OOH)CH$_3$ bond cleavage. Unimolecular dissociation of this adduct forms CH$_2$O + C•(OOH)CH$_3$, where the C•(OOH)CH$_3$ radical forms acetaldehyde plus OH radical (CH$_3$C=O + OH). This reaction channel is the dominant elimination pathway in the hydroxypropyl + O$_2$ reaction.

The primary alkoxy radical also undergo an intramolecular hydrogen transfer from the methyl carbon to the hydroxy group, yielding the hydroperoxyalkyl radical (CH$_2$(OH)CH(OOH)C•H$_2$) with 18.8 kcal mol^{-1} barrier. This radical can dissociate to vinyl alcohol (CH$_2$=CHCH$_2$OH) + HO$_2$ (15.1 kcal mol^{-1} barrier), vinyl peroxide (CH$_2$=CHOOH) + C•H$_2$OH (26.6 kcal mol^{-1} barrier) or undergo reverse reaction to the hydroperoxyalkyl radical (22.7 kcal mol^{-1} barrier).
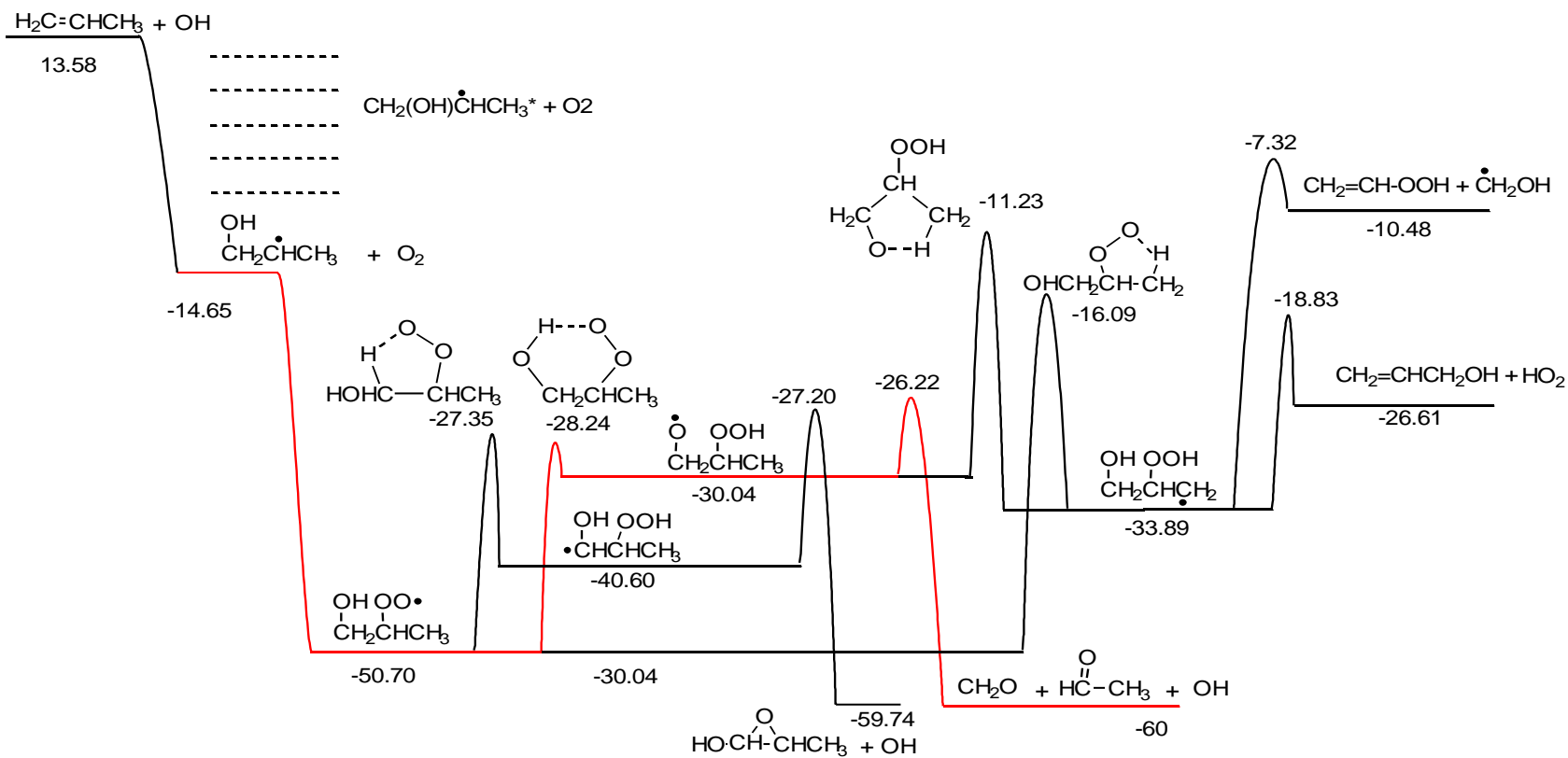
Figure 7.4 Potential energy diagrams for hydroxypropyl radical + O₂ reaction system.

7.4.4 Analysis of the Hydroxypropyl Radical + O$_2$ Chemical Activation Reaction

Multifrequency quantum Rice Ramsperger- Kassel (QRRK) calculations for $k(E)$ with master equation analysis are performed on hydroxypropyl radical + O$_2$ chemical activation reaction system to estimate rate constants and to determine important reaction paths as a function of temperature and pressure. This kinetic analysis is for the chemical activation and the dissociation reaction systems. The master equation analysis uses an exponential-down model for the energy transfer function with ($\Delta E^{\circ}_{\text{down}}$) 900 cal/mol for N$_2$ as the third body. Rate constants, $k(E)$, were evaluated at 0.1 kcal mol^{-1} increments, to 20 kcal mol^{-1} above the highest barrier. Lennard-Jones parameters, σ (Å), and ε/κ (K) are obtained from tabulations and from an estimation method based on molar volumes and compressibility; $\sigma = 5.3$ Å and $\varepsilon/k_{\text{b}} = 574$ K.

Rate constants at 1 atm pressure versus 1000/T (K) are illustrated in Figure 7.5. Regereration of OH radical from the two channels, (i) ring formation from alkyl radical and (ii) dissociation from alkoxy radical, are the most important reaction channels below 800 K. The reverse reaction to reactant, hydroxypropyl radical + O$_2$, becomes important and competes with the regeneration of OH channel above 800 K. The next important reaction channel is the dissociation to vinyl alcohol (C=CCOH + HO$_2$)

Plots of calculated rate constants for hydroxypropyl radical + O$_2$ at 300 K versus log pressure (atm) are shown in Figure 7.6. OH from cyclic formation is the dominant reaction path follow by OH from dissociation of alkoxy radical with 2 order of magnitude lower.

Rate constants versus pressure at 1200 K are shown in Figure 7.7. At this temperature, the reverse reaction to reactant dominates at both high and low pressures. All forword reactions go to the regenerated OH radical path. Peroxy radical stabilization falls off rapidly at high temperature.
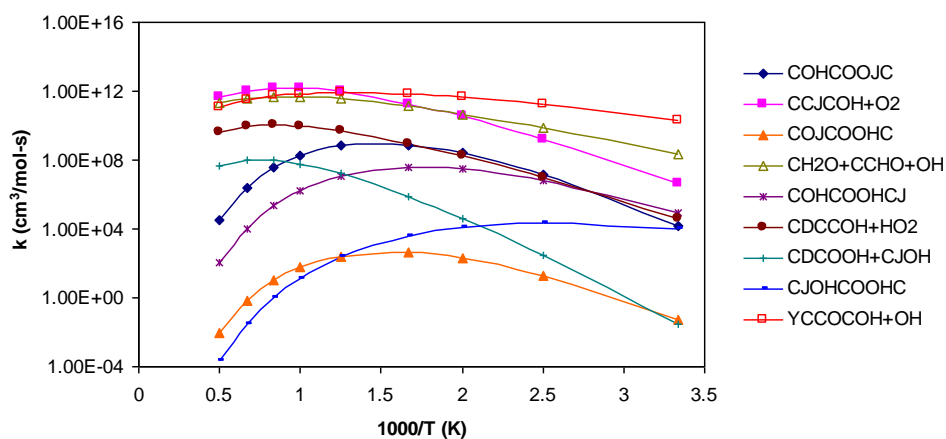
Figure 7.5 Plot of rate constants versus 1000/T (K) at 1atm pressure for hydroxypropyl radical + O_2
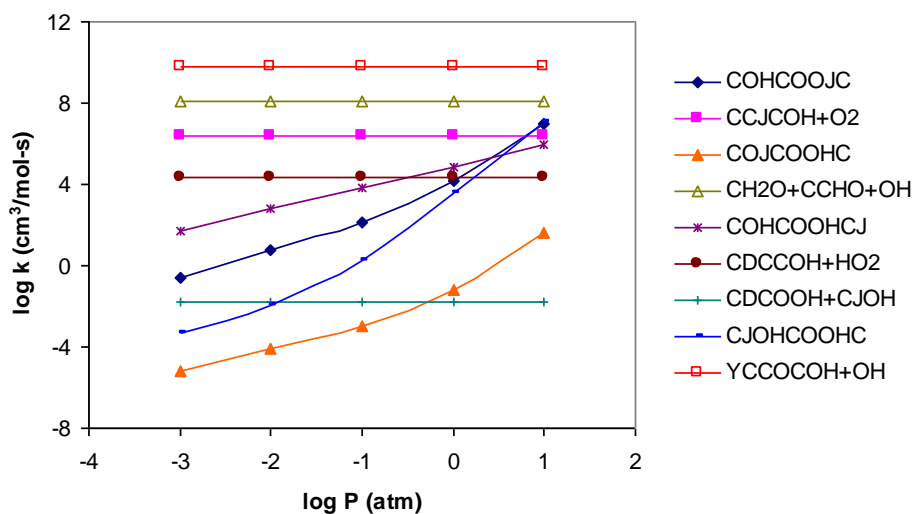
Figure 7.6 Plot of rate constants versus log pressure (atm) at 300 K for hydroxypropyl radical + O_2
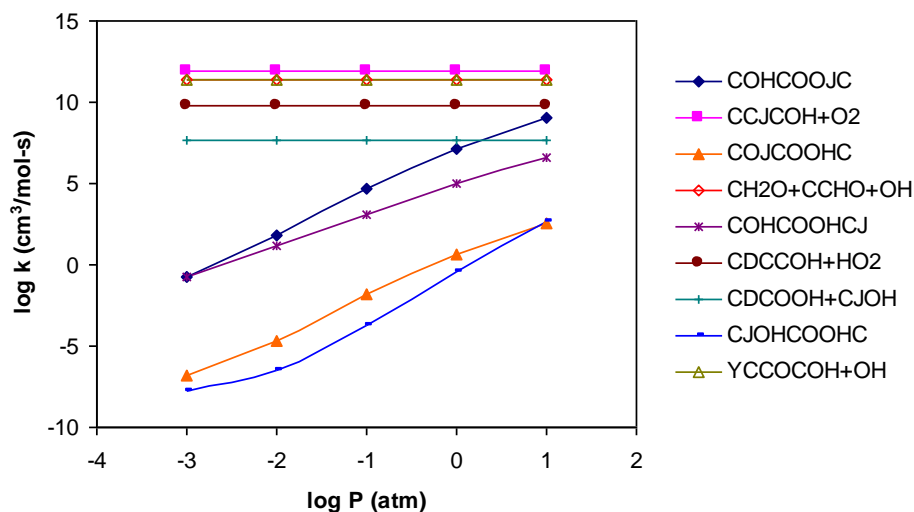
Figure 7.7 Plot of rate constants versus log pressure (atm) at 1300 K for hydroxypropyl radical + O_2

7.4.5 Detailed Mechanism of Hydroxypropyl Radical + O_2 Reactions

The reaction system is further modeled under conditions of atmospheric experiments under varied NO_x conditions using an elementary reaction mechanism with all reactions reversible. The peroxy radical decomposition reactions identified here are in direct competition with bimolecular reactions, particularly with NO and HO_2 radicals. The reaction of OH addition to propene and subsequent hydroxypropyl radical + O_2 reactions are analyzed to model tropospheric condition, 0-2.5 s, 300 K and 1atm at 20ppt and 50ppb of NO. Data on concentration versus time for reaction conditions identical to those above with are illustrated in Figure 7.7. Data on CHEMKIN kinetic calculation: comparison Single activation and double activation at vary E Down are shown on Table 7.2.

Recycling of OH from O_2 + OH-Olefin radical reaction is significant, up to 78% for single activation. Double activation, up to 60 well, does not show increase in OH

recycle. The OH regeneration is independent of concentration of NO present and effectively all regeneration is from the chemical activation path. Higher concentration of NO increase the importance reaction, peroxy radical (ROO•) + NO → alkoxy radical (RO•) + NO$_2$. All forward reaction of alkoxy radicals lead to OH regeneration at higher Temperature.
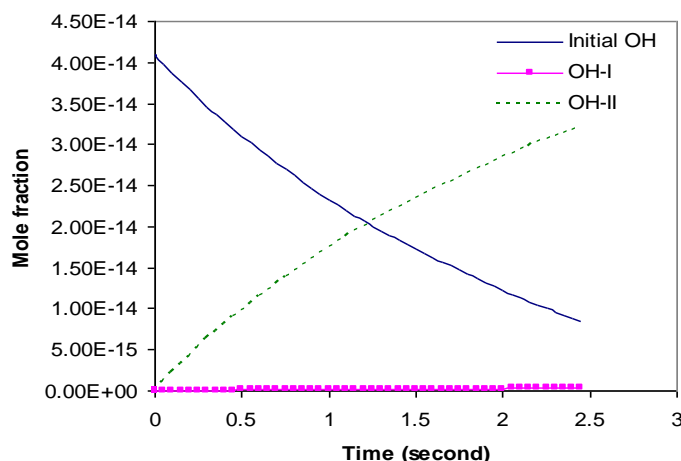
Figure 7.8 CHEMKIN kinetic calculation: concentration vs time. [NO] = 20 ppb, 300 K. (OH-I = OH regeneration from dissociation of alkoxy radical, OH-II = OH regeneration from cyclic ether formation).

Table 7.2 CHEMKIN Kinetic Calculation: Comparison of Single Activation and Double Activation

Reaction	Regenreated (At 2.4 s)		E Down
	OH I	OH II	(cal/mol)
CH$_2$(OH)C•HCH$_3$ + O$_2$ Single O$_2$ activation	2.97E-16	3.17E-14	-
60 wells	2.99E-16	3.17E-14	500
30 wells	2.98E-16	3.17E-14	1000
10 wells	2.97E-16	3.16E-14	3000

Figure 7.9 shows an effect the concentration of NO to the chemical activation system. The higher concentrations of NO, increase the reaction of peroxy radical (COHCOOjC)+ NO → alkoxyl radical (COHCOjC) + NO$_2$. And the 50 ppb concentration of NO does not effect OH regeneration in the chemical activation system.
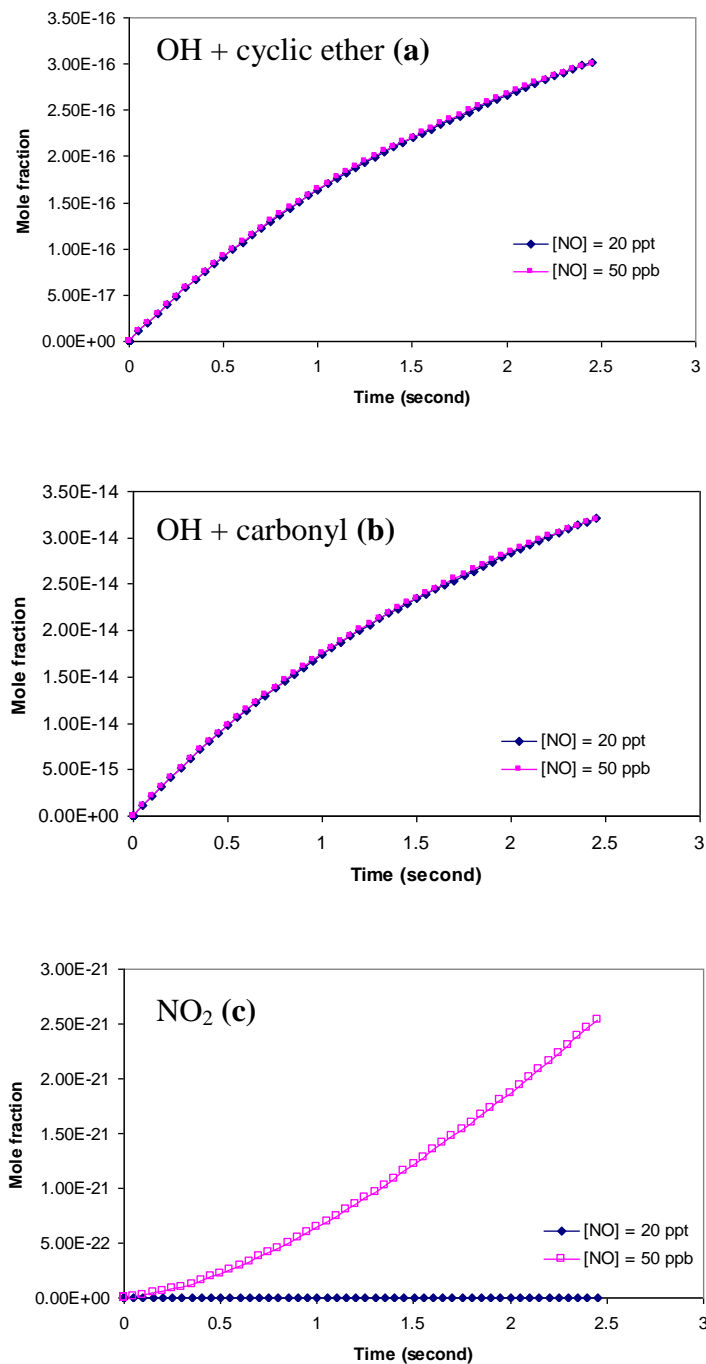
Figure 7.9 Kinetic calculations; concentration with time, comparison of the effect of concentration of NO. **(a)** OH; OH regeneration from cyclic ether formation, **(b)** OH; regeneration from dissociation of alkoxy radical, **(c)** concentration of NO$_2$

7.5 Summary

Thermochemical properties of the *β*-hydroxyperoxy radicals and related species in hydroxyl-propyl + O_2 reaction system are calculated using theoretical density functional theory and ab initio methods. OH add at 1° site and reaction with O_2 association 2nd radical sites further include. Detailed potential energy surfaces for the reaction of the beta radicals with molecular oxygen are developed showing the well depth (chemical activation energies) of 36.1 kcal mol^{-1}. This is sufficient energy so that a significant fraction of the beta radical reactions with O_2 result in new products from reaction of the energized peroxy radical before the peroxy radical is stabilized. The beta radical reacts mostly to OH radical plus ether ring formation and small quantities of the vinyl alcohol and vinyl peroxide are also formed at higher temperature. Elementary kinetic parameters are calculated for each reaction path. These elementary rate constants are used with QRRK analysis for $k(E)$ and master equation analysis for pressure fall-off to evaluate chemical activation and stabilization of the energy adducts. Reaction rate parameters are calculated for adduct and product-formation channels as a function of pressure and temperature. The calculations show that all forward reaction goes to regenerated OH radical channel for all range of temperature and pressure. And the recycling of OH from the decomposition of peroxyl radical is significant; up to 78%. Inclusion of activation energy resulting from OH addition to primary carbon (double activation) does not show increase in OH recycle. The introduction of the rate constants presented in this study into existing reaction mechanisms should lead to better kinetic models for olefin oxidation chemistry the atmospheric.

THERMOCHEMICAL PROPERTIES FOR A SERIES OF NITROCARBONYLS, NITROOLEFINS, CORRESPONDING NITRITES AND THEIR CARBON CENTERED RADICALS

Entropy and heat capacity calculation were performed using complete basis set -QB3

determined geometries and harmonic frequencies summarized in Table A.1.

Table A.1 Ideal Gas-phase Thermodynamic Property *vs* Temperature[a]

[a]Thermodynamic properties are referred to standard state of an ideal gas at 1 atm.
$S°(T)$ and $C°_p(T)$ in cal mol^{-1} K^{-1}
[b] Symmetry numbers used for calculation of $S°(T)$ are in parenthesis

T(K)	cc(=o)cno2		cjc(=o)cno2		cc(=o)cjno2		cc(=o)cono	
	Cp(T)	S°(T)(6)[b]	Cp(T)	S°(T)(2)	Cp(T)	S°(T)(6)	Cp(T)	S°(T)(3)
5	7.95	31.22	7.95	34.70	7.95	32.56	7.95	32.82
50	8.27	49.59	8.15	53.04	8.75	51.09	8.85	51.35
100	9.76	55.73	9.75	59.09	11.03	57.83	11.98	58.41
150	12.02	60.09	12.47	63.53	13.66	62.78	15.13	63.86
200	14.69	63.90	15.55	67.53	16.49	67.09	18.12	68.62
250	17.55	67.47	18.68	71.33	19.37	71.07	21.04	72.97
298	20.38	90.42	21.61	89.87	22.12	86.45	23.80	88.80
300	26.25	70.92	25.34	75.00	26.01	74.85	27.92	77.05
350	23.41	74.30	24.63	78.56	24.97	78.47	26.70	80.94
400	31.24	77.60	30.49	82.02	31.13	81.97	33.14	84.68
500	35.73	83.98	34.82	88.62	35.41	88.61	37.65	91.74
600	39.55	90.05	38.35	94.78	38.87	94.79	41.39	98.31
700	42.68	95.76	41.20	100.51	41.68	100.52	44.42	104.43
800	45.45	101.14	43.57	105.84	43.98	105.86	47.10	110.14
900	47.68	106.19	45.49	110.81	45.86	110.83	49.17	115.48
1000	49.70	110.95	47.18	115.45	47.52	115.47	51.19	120.48
1200	52.69	119.68	49.71	123.88	49.94	123.92	53.93	129.62
1300	53.92	123.68	50.74	127.73	50.93	127.77	55.09	133.81
1400	54.98	127.49	51.64	131.37	51.80	131.42	56.10	137.77
1500	56.05	131.10	52.50	134.82	52.71	134.87	57.33	141.53
2000	56.11	146.79	53.08	149.72	53.13	149.78	58.21	157.84
2500	57.89	159.51	54.55	161.73	54.59	161.80	59.95	171.03
3000	58.94	170.16	55.42	171.76	55.45	171.84	60.99	182.06
3500	59.61	179.30	55.97	180.34	56.00	180.43	61.64	191.51
4000	60.06	187.29	56.34	187.84	56.36	187.93	62.08	199.77
4500	60.37	194.38	56.61	194.49	56.62	194.58	62.38	207.10
5000	60.60	200.76	56.79	200.47	56.81	200.56	62.61	213.68

Table A.1 Ideal Gas-phase Thermodynamic Property *vs* Temperature[a] (Continued)

T(K)	cjc(=o)cono		c=cno2		cj=cno2	
	Cp(T)	S°(T)(1)	Cp(T)	S°(T)(1)	Cp(T)	S°(T)(1)
5	7.95	36.10	7.95	31.25	7.95	32.48
50	9.79	55.74	8.90	49.93	9.15	51.36
100	12.01	63.12	10.09	56.47	10.39	58.08
150	15.30	68.58	11.52	60.81	11.89	62.56
200	18.72	73.45	13.34	64.36	13.79	66.23
250	21.98	77.97	15.37	67.55	15.81	69.52
298	24.92	88.76	17.37	70.41	17.68	72.45
300	27.38	82.24	17.45	70.53	17.76	72.57
350	27.88	86.31	19.49	73.37	19.55	75.44
400	32.75	90.20	21.40	76.09	21.15	78.15
500	37.04	97.48	24.74	81.23	23.84	83.17
600	40.42	104.16	27.45	85.98	25.94	87.70
700	43.10	110.31	29.64	90.38	27.60	91.82
800	45.35	115.98	31.43	94.45	28.95	95.60
900	47.15	121.24	32.93	98.24	30.05	99.07
1000	48.77	126.13	34.19	101.77	30.98	102.28
1200	51.11	134.99	36.18	108.18	32.42	108.06
1300	52.08	139.02	36.97	111.11	32.99	110.68
1400	52.93	142.83	37.65	113.87	33.48	113.14
1500	53.81	146.43	38.25	116.49	33.90	115.46
2000	55.19	161.94	40.27	127.80	35.34	125.43
2500	56.62	174.42	41.38	136.91	36.12	133.41
3000	57.47	184.83	42.04	144.51	36.58	140.03
3500	58.01	193.73	42.46	151.03	36.88	145.70
4000	58.37	201.50	42.74	156.72	37.07	150.63
4500	58.62	208.38	42.94	161.76	37.21	155.01
5000	58.80	214.57	43.08	166.29	37.31	158.93

Table A.1 Ideal Gas-phase Thermodynamic Property *vs* Temperature[a] (Continued)

T(K)	c=cjno2		c=cono		cj=cono	
	Cp(T)	Sº(T)(2)	Cp(T)	Sº(T)(1)	Cp(T)	Sº(T)(1)
5	7.95	31.14	7.95	30.88	7.95	31.98
50	8.00	49.45	8.92	49.52	8.90	50.62
100	8.79	55.19	10.57	56.23	10.55	57.30
150	10.20	59.00	12.09	60.79	12.23	61.88
200	11.92	62.17	13.78	64.49	14.07	65.65
250	13.73	65.02	15.61	67.76	15.92	68.98
298	15.44	73.37	17.41	76.03	17.58	77.34
300	17.78	67.67	19.76	70.77	19.94	72.03
350	17.19	70.19	19.29	73.59	19.20	74.87
400	20.82	72.58	23.31	76.28	22.90	77.52
500	23.27	77.05	26.19	81.28	25.11	82.37
600	25.24	81.15	28.48	85.86	26.78	86.71
700	26.86	84.91	30.31	90.07	28.06	90.63
800	28.13	88.37	31.84	93.97	29.19	94.21
900	29.20	91.58	33.10	97.58	30.04	97.50
1000	30.12	94.57	34.20	100.94	30.86	100.54
1200	31.50	99.96	35.89	107.05	31.98	106.01
1300	32.07	102.40	36.58	109.84	32.45	108.48
1400	32.58	104.71	37.17	112.47	32.85	110.81
1500	32.99	106.89	37.77	114.97	33.35	113.01
2000	33.32	116.28	38.39	125.74	33.44	122.44
2500	34.12	123.81	39.46	134.43	34.19	129.99
3000	34.59	130.07	40.10	141.69	34.64	136.26
3500	34.89	135.43	40.51	147.90	34.92	141.62
4000	35.08	140.10	40.78	153.33	35.11	146.30
4500	35.22	144.24	40.98	158.14	35.24	150.44
5000	35.32	147.95	41.11	162.47	35.34	154.16

Table A.1 Ideal Gas-phase Thermodynamic Property *vs* Temperature[a] (Continued)

T(K)	cc(=o)no2		cjc(=o)no2		cc(=o)ono		cjc(=o)ono	
	Cp(T)	S°(T)(6)	Cp(T)	S°(T)(2)	Cp(T)	S°(T)(3)	Cp(T)	S°(T)(1)
5	7.95	29.61	7.95	33.01	7.95	31.17	7.97	34.56
50	8.00	47.92	7.99	51.32	9.87	50.93	10.04	55.15
100	9.17	53.73	9.27	57.13	11.51	58.26	11.92	62.62
150	11.34	57.84	11.86	61.35	13.34	63.26	14.27	67.89
200	13.64	61.41	14.56	65.13	15.32	67.36	16.67	72.32
250	15.86	64.69	17.05	68.65	17.32	70.98	18.93	76.28
298	17.91	79.82	19.21	77.82	19.21	85.19	20.91	85.75
300	21.68	67.77	21.60	71.95	22.68	74.31	23.23	79.91
350	20.03	70.69	21.30	75.08	21.17	77.42	22.83	83.28
400	25.18	73.48	25.42	78.04	26.37	80.36	26.79	86.43
500	28.25	78.75	28.34	83.52	29.51	85.83	29.50	92.19
600	30.86	83.62	30.58	88.50	32.08	90.83	31.56	97.34
700	32.97	88.14	32.28	93.04	34.13	95.43	33.15	101.99
800	34.91	92.34	33.73	97.20	35.91	99.69	34.43	106.22
900	36.21	96.26	34.83	101.03	37.34	103.65	35.50	110.11
1000	37.80	99.92	35.83	104.59	38.59	107.35	36.34	113.70
1200	39.39	106.60	37.21	110.98	40.49	114.06	37.74	120.14
1300	40.17	109.65	37.77	113.88	41.25	117.13	38.27	123.06
1400	40.84	112.53	38.27	116.60	41.90	120.02	38.72	125.80
1500	42.07	115.27	38.82	119.17	42.52	122.77	39.09	128.38
2000	42.11	127.08	39.10	130.20	42.18	134.61	39.19	139.44
2500	43.28	136.61	39.96	139.03	43.33	144.16	40.01	148.28
3000	43.97	144.57	40.46	146.36	44.00	152.12	40.50	155.62
3500	44.41	151.38	40.78	152.62	44.43	158.94	40.81	161.89
4000	44.70	157.33	40.99	158.08	44.72	164.89	41.01	167.35
4500	44.90	162.61	41.14	162.92	44.92	170.17	41.16	172.19
5000	45.05	167.35	41.25	167.26	45.06	174.91	41.27	176.53

THERMOCHEMISTRY AND KINETICS OF THE ACETONYL RADICAL AND ACETYL RADICAL + NO₂ REACTION SYSTEM: A THEORETICAL STUDY

Frequencies calculation for the transition states are presented in Table B.1. Results QRRK calculation; rate constant versus pressure and temperature are in Table B.2A - B.2D. Rate constants as a function of temperature for the $CH_3C(=O)CH_2ONO$ <--> $CH_3C(=O)CH_2O\bullet$ + NO dissociation is shown in Figure B.1. Figure B.2 shows the potential energy surfaces for R-NO₂ dissociation in nitroacetate.

Table B.1 Calculated Frequencies by CBS-QB3 for Transition State

System	Frequencies, cm⁻¹									
TS 1	-299.3	80.1	107.9	148.3	237.0	318.8	377.6	396.2	523.9	587.8
	720.5	791.8	839.3	949.7	970.9	1040.9	1072.3	1187.8	1332.8	1398.7
	1464.1	1481.4	1506.5	1553.6	1635.1	3024.6	3092.3	3130.7	3158.0	3273.1
TS 2	-649.1	4.5	31.7	114.5	177.9	193.5	300.1	372.7	504.1	537.9
	750.8	769.4	777.9	970.4	994.5	1106.7	1116.2	1214.7	1260.4	1396.0
	1432.6	1461.7	1469.9	1624.6	1775.2	3049.7	3113.1	3141.9	3145.8	3258.9
TS 3	-1054.8	66.9	105.5	127.4	191.1	220.7	294.1	422.5	462.9	516.7
	565.9	716.6	777.7	955.0	1002.9	1097.3	1219.6	1259.7	1302.6	1387.0
	1412.1	1458.5	1462.6	1504.8	1792.9	1926.6	2913.7	3038.6	3096.8	3150.0
TS 4	-441.4	88.8	141.7	282.3	317.2	426.3	461.5	525.8	772.0	957.7
	1014.5	1084.5	1257	1402.5	1462.2	1469.7	1632.1	2031.2	3051.4	3117.4
	3191.4									
TS 5	-1244.3	81.7	148.6	276.3	345.5	410.0	474.6	522.9	645.0	820.7
	915.4	1034.7	1060.7	1228.9	1383.8	1412.3	1606.4	1773.8	2188.6	3081.4
	3156.8									
TS 6	-1292.1	109.7	190.5	257.0	332.5	423.2	516.1	586.9	6 10.0	830.8
	928.0	1049.4	1069.2	1282.2	1371.2	1379.5	1431.1	1652.4	2198.8	3079.7
	3173.9									

Table B.2A Results QRRK Calculation, Rate Constant Versus Pressure and Temperature for $C \cdot H_2C(=O)CH_3 + NO_2 \Rightarrow CH_3C(=O)CH_2ONO^* \Rightarrow$ Products

Calculated Reaction Parameters at P = 0.01 atm, $k = A(T/K)^n \exp(-E_a/RT)$ (300 ≤ T/K ≤ 2000)

Reaction			A	n	E_a (cal/mol)
$C \cdot H_2C(=O)CH_3 + NO_2$	<=>	$CH_3C(=O)CH_2ONO$	1.63E+53	-16.4	23467
$C \cdot H_2C(=O)CH_3 + NO_2$	<=>	$CH_3C(=O)CH_2O \cdot + NO$	4.91E+00	3.2	8505
$C \cdot H_2C(=O)CH_3 + NO_2$	<=>	$CH_3C(=O)HC(=O)+HNO$	7.58E-09	5.5	8987
$C \cdot H_2C(=O)CH_3 + NO_2$	<=>	$CH_3C(=O)CH_2NO_2$	4.45E+46	-13.6	31442
$CH_3C(=O)CH_2ONO$	<=>	$CH_3C(=O)CH_2O \cdot + NO$	1.65E+63	-15.8	51522
$CH_3C(=O)CH_2ONO$	<=>	$CH_3C(=O)HC(=O)+HNO$	6.82E+43	-10.1	44772
$CH_3C(=O)CH_2ONO$	<=>	$CH_3C(=O)CH_2NO_2$	1.44E+40	-11.9	74252

Calculated Reaction Parameters at P = 0.1 atm, $k = A(T/K)^n \exp(-E_a/RT)$ (300 ≤ T/K ≤ 2000)

Reaction			A	n	E_a (cal/mol)
$C \cdot H_2C(=O)CH_3 + NO_2$	<=>	$CH_3C(=O)CH_2ONO$	3.47E+55	-16.1	23300
$C \cdot H_2C(=O)CH_3 + NO_2$	<=>	$CH_3C(=O)CH_2O \cdot + NO$	4.91E+00	3.2	8505
$C \cdot H_2C(=O)CH_3 + NO_2$	<=>	$CH_3C(=O)HC(=O)+HNO$	7.43E-09	5.5	8977
$C \cdot H_2C(=O)CH_3 + NO_2$	<=>	$CH_3C(=O)CH_2NO_2$	2.17E+37	-10.0	30810
$CH_3C(=O)CH_2ONO$	<=>	$CH_3C(=O)CH_2O \cdot + NO$	1.38E+58	-14.0	50907
$CH_3C(=O)CH_2ONO$	<=>	$CH_3C(=O)HC(=O)+HNO$	9.83E+37	-8.1	43538
$CH_3C(=O)CH_2ONO$	<=>	$CH_3C(=O)CH_2NO_2$	3.44E+42	-11.4	74394

Calculated Reaction Parameters at P = 1 atm, $k = A(T/K)^n \exp(-E_a/RT)$ (300 ≤ T/K ≤ 2000)

Reaction			A	n	E_a (cal/mol)
$C \cdot H_2C(=O)CH_3 + NO_2$	<=>	$CH_3C(=O)CH_2ONO$	1.84E+54	-15.0	22159
$C \cdot H_2C(=O)CH_3 + NO_2$	<=>	$CH_3C(=O)CH_2O \cdot + NO$	6.80E+00	3.1	8604
$C \cdot H_2C(=O)CH_3 + NO_2$	<=>	$CH_3C(=O)HC(=O)+HNO$	8.69E-09	5.5	8996
$C \cdot H_2C(=O)CH_3 + NO_2$	<=>	$CH_3C(=O)CH_2NO_2$	7.82E+21	-4.8	27609
$CH_3C(=O)CH_2ONO$	<=>	$CH_3C(=O)CH_2O \cdot + NO$	3.99E+53	-12.3	50337
$CH_3C(=O)CH_2ONO$	<=>	$CH_3C(=O)HC(=O)+HNO$	1.96E+33	-6.5	42572
$CH_3C(=O)CH_2ONO$	<=>	$CH_3C(=O)CH_2NO_2$	2.37E+48	-12.3	74815

Calculated Reaction Parameters at P = 10 atm, $k = A(T/K)^n \exp(-E_a/RT)$ (300 ≤ T/K ≤ 2000)

Reaction			A	n	E_a (cal/mol)
$C \cdot H_2C(=O)CH_3 + NO_2$	<=>	$CH_3C(=O)CH_2ONO$	3.17E+48	-12.6	21116
$C \cdot H_2C(=O)CH_3 + NO_2$	<=>	$CH_3C(=O)CH_2O \cdot + NO$	1.17E+02	2.8	9647
$C \cdot H_2C(=O)CH_3 + NO_2$	<=>	$CH_3C(=O)HC(=O)+HNO$	1.24E-07	5.2	9983
$C \cdot H_2C(=O)CH_3 + NO_2$	<=>	$CH_3C(=O)CH_2NO_2$	3.08E+04	1.0	23328
$CH_3C(=O)CH_2ONO$	<=>	$CH_3C(=O)CH_2O \cdot + NO$	3.71E+46	-9.9	48752
$CH_3C(=O)CH_2ONO$	<=>	$CH_3C(=O)HC(=O)+HNO$	1.22E+27	-4.5	40986
$CH_3C(=O)CH_2ONO$	<=>	$CH_3C(=O)CH_2NO_2$	2.75E+46	-11.0	73760

Table B.2B Results QRRK Calculation, Rate Constant Versus Pressure and Temperature for C•H$_2$C(=O)CH$_3$+ NO$_2$ => CH$_3$C(=O)CH$_2$NO$_2$* => Products

Calculated Reaction Parameters at P = 0.01 atm, $k = A(T/\mathrm{K})^n \exp(-E_a/RT)$ (300 ≤ T/K≤ 2000)

Reaction			A	n	E$_a$ (cal/mol)
C•H$_2$C(=O)CH$_3$ + NO$_2$	<=>	CH$_3$C(=O)CH$_2$NO$_2$	2.75E+38	-15.4	3702
C•H$_2$C(=O)CH$_3$ + NO$_2$	<=>	CH$_3$C(=O)CH$_2$ONO	1.01E+45	-18.1	-4273
C•H$_2$C(=O)CH$_3$ + NO$_2$	<=>	CH$_3$C(=O)CH$_2$O• + NO	3.03E-08	1.4	-19235
C•H$_2$C(=O)CH$_3$ + NO$_2$	<=>	CH$_3$C(=O)HC(=O)+HNO	4.68E-17	3.7	-18753
CH$_3$C(=O)CH$_2$NO$_2$	<=>	CH$_3$C(=O)CH$_2$ONO	5.15E+57	-14.4	77672
CH$_3$C(=O)CH$_2$ONO	<=>	CH$_3$C(=O)CH$_2$O• + NO	1.65E+63	-15.8	51522
CH$_3$C(=O)CH$_2$ONO	<=>	CH$_3$C(=O)HC(=O)+HNO	6.82E+43	-10.1	44772

Calculated Reaction Parameters at P = 0.1 atm, $k = A(T/\mathrm{K})^n \exp(-E_a/RT)$ (300 ≤ T/K≤ 2000)

Reaction			A	n	E$_a$ (cal/mol)
C•H$_2$C(=O)CH$_3$ + NO$_2$	<=>	CH$_3$C(=O)CH$_2$NO$_2$	1.34E+29	-11.8	3070
C•H$_2$C(=O)CH$_3$ + NO$_2$	<=>	CH$_3$C(=O)CH$_2$ONO	2.14E+47	-17.9	-4440
C•H$_2$C(=O)CH$_3$ + NO$_2$	<=>	CH$_3$C(=O)CH$_2$O• + NO	3.03E-08	1.4	-19235
C•H$_2$C(=O)CH$_3$ + NO$_2$	<=>	CH$_3$C(=O)HC(=O)+HNO	4.59E-17	3.8	-18763
CH$_3$C(=O)CH$_2$NO$_2$	<=>	CH$_3$C(=O)CH$_2$ONO	1.49E+49	-11.3	76457
CH$_3$C(=O)CH$_2$ONO	<=>	CH$_3$C(=O)CH$_2$O• + NO	1.38E+58	-14.0	50907
CH$_3$C(=O)CH$_2$ONO	<=>	CH$_3$C(=O)HC(=O)+HNO	9.83E+37	-8.1	43538

Calculated Reaction Parameters at P = 1 atm, $k = A(T/\mathrm{K})^n \exp(-E_a/RT)$ (300 ≤ T/K≤ 2000)

Reaction			A	n	E$_a$ (cal/mol)
C•H$_2$C(=O)CH$_3$ + NO$_2$	<=>	CH$_3$C(=O)CH$_2$NO$_2$	4.83E+13	-6.5	-131
C•H$_2$C(=O)CH$_3$ + NO$_2$	<=>	CH$_3$C(=O)CH$_2$ONO	1.14E+46	-16.7	-5581
C•H$_2$C(=O)CH$_3$ + NO$_2$	<=>	CH$_3$C(=O)CH$_2$O• + NO	4.20E-08	1.4	-19136
C•H$_2$C(=O)CH$_3$ + NO$_2$	<=>	CH$_3$C(=O)HC(=O)+HNO	5.37E-17	3.7	-18744
CH$_3$C(=O)CH$_2$NO$_2$	<=>	CH$_3$C(=O)CH$_2$ONO	2.56E+37	-7.4	73675
CH$_3$C(=O)CH$_2$ONO	<=>	CH$_3$C(=O)CH$_2$O• + NO	3.99E+53	-12.3	50337
CH$_3$C(=O)CH$_2$ONO	<=>	CH$_3$C(=O)HC(=O)+HNO	1.96E+33	-6.5	42572

Calculated Reaction Parameters at P = 10 atm, $k = A(T/\mathrm{K})^n \exp(-E_a/RT)$ (300 ≤ T/K≤ 2000)

Reaction			A	n	E$_a$ (cal/mol)
C•H$_2$C(=O)CH$_3$ + NO$_2$	<=>	CH$_3$C(=O)CH$_2$NO$_2$	1.90E-04	-0.8	-4412
C•H$_2$C(=O)CH$_3$ + NO$_2$	<=>	CH$_3$C(=O)CH$_2$ONO	1.96E+40	-14.3	-6624
C•H$_2$C(=O)CH$_3$ + NO$_2$	<=>	CH$_3$C(=O)CH$_2$O• + NO	7.23E-07	1.1	-18093
C•H$_2$C(=O)CH$_3$ + NO$_2$	<=>	CH$_3$C(=O)HC(=O)+HNO	7.66E-16	3.4	-17757
CH$_3$C(=O)CH$_2$NO$_2$	<=>	CH$_3$C(=O)CH$_2$ONO	1.58E+25	-3.5	70285
CH$_3$C(=O)CH$_2$ONO	<=>	CH$_3$C(=O)CH$_2$O• + NO	3.71E+46	-9.9	48752
CH$_3$C(=O)CH$_2$ONO	<=>	CH$_3$C(=O)HC(=O)+HNO	1.22E+27	-4.5	40986

Table B.2C Results QRRK Calculation, Rate Constant Versus Pressure and Temperature for $CH_3C\bullet(=O) + NO_2 => CH_3C(=O)NO_2^* =>$ Products

Calculated Reaction Parameters at P = 0.01 atm, $k = A(T/K)^n \exp(-E_a/RT)$ ($300 \leq$ T/K ≤ 2000)

Reaction			A	n	E_a (kcal/mol)
$CH_3C\bullet(=O) + NO_2$	<=>	$CH_3C(=O)NO_2$	9.77E+70	-22.6	6081
$CH_3C\bullet(=O) + NO_2$	<=>	$CH_2=C=O + HONO$	3.57E+08	1.1	-888
$CH_3C\bullet(=O) + NO_2$	<=>	$CH_3C(=O)ONO$	1.33E+54	-17.2	4255
$CH_3C\bullet(=O) + NO_2$	<=>	$CH_3C(=O)O\bullet + NO$	5.45E+14	-0.7	-97
$CH_3C(=O)NO_2$	<=>	$CH_2=C=O + HONO$	1.80E+53	-13.7	45198
$CH_3C(=O)NO_2$	<=>	$CH_3C(=O)ONO$	4.16E+50	-12.1	42126
$CH_3C(=O)ONO$	<=>	$CH_2=C=O + HONO$	4.66E+30	-7.5	50540
$CH_3C(=O)ONO$	<=>	$CH_3C(=O)O\bullet + NO$	9.12E+49	-11.9	47235

Calculated Reaction Parameters at P = 0.1 atm, $k = A(T/K)^n \exp(-E_a/RT)$ ($300 \leq$ T/K ≤ 2000)

Reaction			A	n	E_a (kcal/mol)
$CH_3C\bullet(=O) + NO_2$	<=>	$CH_3C(=O)NO_2$	4.01E+94	-28.3	16318
$CH_3C\bullet(=O) + NO_2$	<=>	$CH_2=C=O + HONO$	1.21E+10	0.7	-8
$CH_3C\bullet(=O) + NO_2$	<=>	$CH_3C(=O)ONO$	2.27E+77	-22.8	14539
$CH_3C\bullet(=O) + NO_2$	<=>	$CH_3C(=O)O\bullet + NO$	7.05E+15	-1.0	496
$CH_3C(=O)NO_2$	<=>	$CH_2=C=O + HONO$	1.62E+52	-12.9	46549
$CH_3C(=O)NO_2$	<=>	$CH_3C(=O)ONO$	3.24E+48	-11.2	42288
$CH_3C(=O)ONO$	<=>	$CH_2=C=O + HONO$	4.50E+32	-7.7	51083
$CH_3C(=O)ONO$	<=>	$CH_3C(=O)O\bullet + NO$	1.81E+50	-11.7	48053

Calculated Reaction Parameters at P = 1 atm, $k = A(T/K)^n \exp(-E_a/RT)$ ($300 \leq$ T/K ≤ 2000)

Reaction			A	n	E_a (kcal/mol)
$CH_3C\bullet(=O) + NO_2$	<=>	$CH_3C(=O)NO_2$	7.60E+89	-25.3	19403
$CH_3C\bullet(=O) + NO_2$	<=>	$CH_2=C=O + HONO$	6.36E+13	-0.4	2504
$CH_3C\bullet(=O) + NO_2$	<=>	$CH_3C(=O)ONO$	2.09E+73	-20.2	17980
$CH_3C\bullet(=O) + NO_2$	<=>	$CH_3C(=O)O\bullet + NO$	1.17E+20	-2.2	3145
$CH_3C(=O)NO_2$	<=>	$CH_2=C=O + HONO$	6.19E+44	-10.2	45563
$CH_3C(=O)NO_2$	<=>	$CH_3C(=O)ONO$	2.58E+43	-9.4	41326
$CH_3C(=O)ONO$	<=>	$CH_2=C=O + HONO$	1.98E+32	-7.2	51571
$CH_3C(=O)ONO$	<=>	$CH_3C(=O)O\bullet + NO$	3.09E+48	-10.8	48342

Calculated Reaction Parameters at P = 10 atm, $k = A(T/K)^n \exp(-E_a/RT)$ ($300 \leq$ T/K ≤ 2000)

Reaction			A	n	E_a (kcal/mol)
$CH_3C\bullet(=O) + NO_2$	<=>	$CH_3C(=O)NO_2$	1.02E+68	-17.7	15309
$CH_3C\bullet(=O) + NO_2$	<=>	$CH_2=C=O + HONO$	3.53E+13	-0.2	4068
$CH_3C\bullet(=O) + NO_2$	<=>	$CH_3C(=O)ONO$	3.75E+51	-12.7	14011
$CH_3C\bullet(=O) + NO_2$	<=>	$CH_3C(=O)O\bullet + NO$	5.59E+19	-2.0	4743
$CH_3C(=O)NO_2$	<=>	$CH_2=C=O + HONO$	1.06E+31	-5.7	42082
$CH_3C(=O)NO_2$	<=>	$CH_3C(=O)ONO$	1.55E+34	-6.4	38831
$CH_3C(=O)ONO$	<=>	$CH_2=C=O + HONO$	1.94E+29	-6.0	51481
$CH_3C(=O)ONO$	<=>	$CH_3C(=O)O\bullet + NO$	3.60E+44	-9.4	47857

Table B.2D Results QRRK Calculation, Rate Constant Versus Pressure and Temperature for $CH_3C\bullet(=O) + NO_2 => CH_3C(=O)ONO^* =>$ Products

Calculated Reaction Parameters at P = 0.01 atm, $k = A(T/K)^n \exp(-E_a/RT)$ ($300 \le T/K \le 2000$)

Reaction			A	n	E_a (kcal/mol)
$CH_3C\bullet(=O) + NO_2$	<=>	$CH_3C(=O)ONO$	3.63E+08	-4.8	1216
$CH_3C\bullet(=O) + NO_2$	<=>	$CH_2=C=O + HONO$	2.45E-17	7.4	2184
$CH_3C\bullet(=O) + NO_2$	<=>	$CH_3C(=O)O\bullet + NO$	8.54E+02	2.6	2478
$CH_3C\bullet(=O) + NO_2$	<=>	$CH_3C(=O)NO_2$	4.43E+43	-16.4	7325
$CH_3C(=O)ONO$	<=>	$CH_2=C=O + HONO$	4.66E+30	-7.5	50540
$CH_3C(=O)ONO$	<=>	$CH_3C(=O)O\bullet + NO$	9.12E+49	-11.9	47235
$CH_3C(=O)ONO$	<=>	$CH_3C(=O)NO_2$	1.03E+35	-8.2	44358
$CH_3C(=O)NO_2$	<=>	$CH_2=C=O + HONO$	1.80E+53	-13.7	45198

Calculated Reaction Parameters at P = 0.1 atm, $k = A(T/K)^n \exp(-E_a/RT)$ ($300 \le T/K \le 2000$)

Reaction			A	n	E_a (kcal/mol)
$CH_3C\bullet(=O) + NO_2$	<=>	$CH_3C(=O)ONO$	6.67E+35	-12.0	10632
$CH_3C\bullet(=O) + NO_2$	<=>	$CH_2=C=O + HONO$	2.45E-17	7.4	2184
$CH_3C\bullet(=O) + NO_2$	<=>	$CH_3C(=O)O\bullet + NO$	8.54E+02	2.6	2478
$CH_3C\bullet(=O) + NO_2$	<=>	$CH_3C(=O)NO_2$	3.87E+73	-24.0	18560
$CH_3C(=O)ONO$	<=>	$CH_2=C=O + HONO$	4.50E+32	-7.7	51083
$CH_3C(=O)ONO$	<=>	$CH_3C(=O)O\bullet + NO$	1.81E+50	-11.7	48053
$CH_3C(=O)ONO$	<=>	$CH_3C(=O)NO_2$	6.10E+33	-7.6	44693
$CH_3C(=O)NO_2$	<=>	$CH_2=C=O + HONO$	1.62E+52	-12.9	46549

Calculated Reaction Parameters at P = 1 atm, $k = A(T/K)^n \exp(-E_a/RT)$ ($300 \le T/K \le 2000$)

Reaction			A	n	E_a (kcal/mol)
$CH_3C\bullet(=O) + NO_2$	<=>	$CH_3C(=O)ONO$	4.86E+41	-12.2	17190
$CH_3C\bullet(=O) + NO_2$	<=>	$CH_2=C=O + HONO$	2.45E-17	7.4	2184
$CH_3C\bullet(=O) + NO_2$	<=>	$CH_3C(=O)O\bullet + NO$	8.54E+02	2.6	2478
$CH_3C\bullet(=O) + NO_2$	<=>	$CH_3C(=O)NO_2$	3.67E+74	-22.5	23781
$CH_3C(=O)ONO$	<=>	$CH_2=C=O + HONO$	1.98E+32	-7.2	51571
$CH_3C(=O)ONO$	<=>	$CH_3C(=O)O\bullet + NO$	3.09E+48	-10.8	48342
$CH_3C(=O)ONO$	<=>	$CH_3C(=O)NO_2$	4.81E+30	-6.4	44415
$CH_3C(=O)NO_2$	<=>	$CH_2=C=O + HONO$	6.19E+44	-10.2	45563

Calculated Reaction Parameters at P = 10 atm, $k = A(T/K)^n \exp(-E_a/RT)$ ($300 \le T/K \le 2000$)

Reaction			A	n	E_a (kcal/mol)
$CH_3C\bullet(=O) + NO_2$	<=>	$CH_3C(=O)ONO$	3.49E+29	-7.4	12363
$CH_3C\bullet(=O) + NO_2$	<=>	$CH_2=C=O + HONO$	2.42E-17	7.4	2184
$CH_3C\bullet(=O) + NO_2$	<=>	$CH_3C(=O)O\bullet + NO$	8.54E+02	2.6	2478
$CH_3C\bullet(=O) + NO_2$	<=>	$CH_3C(=O)NO_2$	1.57E+52	-14.6	20013
$CH_3C(=O)ONO$	<=>	$CH_2=C=O + HONO$	1.94E+29	-6.0	51481
$CH_3C(=O)ONO$	<=>	$CH_3C(=O)O\bullet + NO$	3.60E+44	-9.4	47857
$CH_3C(=O)ONO$	<=>	$CH_3C(=O)NO_2$	1.89E+26	-4.9	43601
$CH_3C(=O)NO_2$	<=>	$CH_2=C=O + HONO$	1.06E+31	-5.7	42082
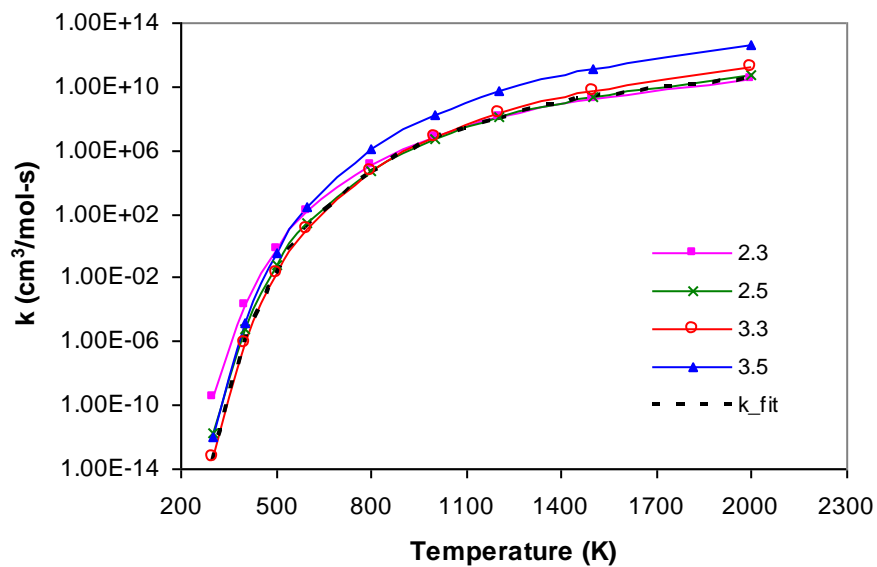
Figure B.1 Rate constants as a function of temperature for the $CH_3C(=O)CH_2ONO$ <--> $CH_3C(=O)CH_2O\bullet$ + NO dissociation.
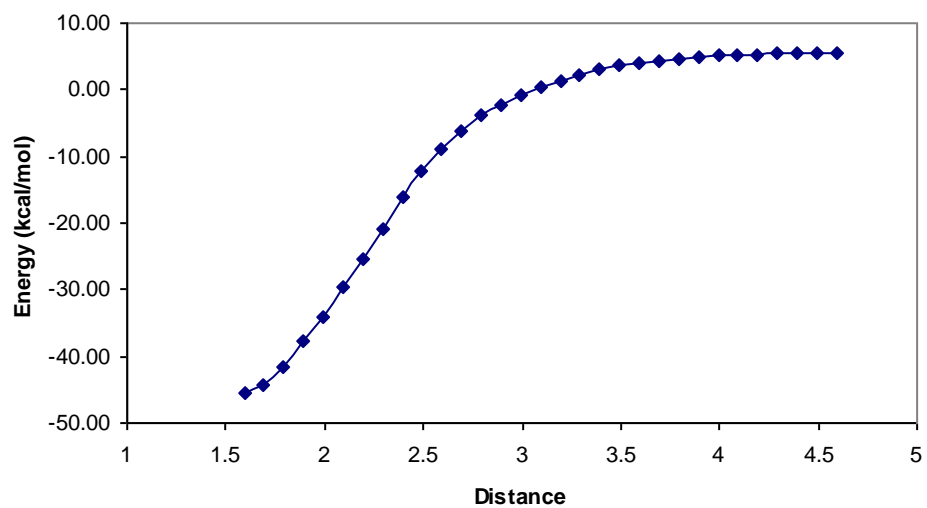
Figure B.2 Potential energy surfaces for R-NO_2 dissociation in nitroacetate.

THERMOCHEMICAL PROPERTIES FOR ISSOCTANE AND CARBON RADICALS: A COMPUTATIONAL STUDY

Vibration frequencies, and moments of inertia for target structures are available in Table C.1 and Table C.2, respectively. Work reactions, enthalpies of formation and bond dissociation energies for tertiary radicals, 2-methylbut-2-yl, 2-methylpent-2-yl and the secondary radical, 2-methylbut-3-yl are listed in Table C.3. And the harmonic potential vs. bend angle for the frequency describing the symmetric bending of the isopropyl group in isooctane is illustrated in Figure C.1.

Table C.1 Calculated at CBS-QB3 Composite, *viz.* B3LYP/6-311G(2d,d,p) Level Vibration Frequencies (cm^{-1}) **.** Number in bold are vibration frequencies which were replaced by internal rotors.

C3CCCC2			C3CCCC2•			C3CCC•C2		
56.2	**98.8**	187.9	**38.0**	122.6	**154.1**	58.7	**83.9**	**91.2**
223.3	**231.3**	**259.6**	184.5	**228.2**	**249.6**	**124.5**	176.3	**228.4**
265.6	**287.6**	291.4	**260.4**	**280.0**	288.8	**271.7**	**274.9**	294.5
308.6	354.0	385.7	307.2	339.2	373.1	296.2	311.2	374.8
410.0	416.1	455.8	397.9	420.7	450.7	389.4	421.5	427.5
504.4	740.6	832.7	498.3	567.4	743.6	498.5	721.7	791.1
872.2	901.8	929.2	843.4	865.6	908.3	885.2	889.2	933.2
931.4	940.0	959.3	928.3	935.0	939.4	938.4	941.7	959.7
963.2	984.7	1032.4	961.8	987.0	1016.2	978.1	1004.4	1030.1
1040.1	1116.3	1134.0	1028.4	1053.5	1117.2	1044.4	1054.2	1142.5
1188.9	1222.2	1230.3	1145.0	1221.7	1226.5	1217.2	1243.1	1273.3
1267.4	1309.4	1330.6	1267.3	1304.0	1315.1	1285.7	1338.9	1344.9
1368.4	1385.4	1399.9	1366.5	1381.2	1397.6	1396.5	1399.7	1400.3
1401.4	1402.6	1421.6	1399.1	1401.9	1430.2	1413.2	1429.2	1471.9
1432.0	1482.9	1484.6	1459.4	1481.2	1483.0	1475.4	1477.1	1483.3
1488.5	1491.3	1493.0	1488.8	1490.1	1495.0	1487.0	1489.4	1491.5
1498.4	1506.8	1509.3	1500.4	1507.8	1512.2	1496.7	1509.8	1510.6
1512.4	1514.6	1521.5	1519.3	2993.3	3010.6	1520.5	2921.2	2926.0
2998.6	3011.2	3012.1	3012.1	3015.0	3016.4	2976.5	3012.3	3014.2
3013.4	3016.0	3020.7	3022.1	3033.2	3072.6	3015.9	3021.9	3022.3
3024.3	3033.4	3069.8	3074.5	3078.5	3081.2	3025.6	3073.1	3074.4
3074.1	3074.6	3078.0	3081.6	3086.3	3091.2	3078.0	3081.1	3086.2
3079.8	3082.3	3083.3	3093.0	3124.6	3225.8	3088.6	3088.8	3091.9
3086.2	3091.7	3103.1						

Table C.1 Calculated at CBS-QB3 Composite, *viz.* B3LYP/6-311G(2d,d,p) Level Vibration Frequencies (cm^{-1}) **.** Number in bold are vibration frequencies which were replaced by internal rotors. (Continued)

C3CC•CC2			C3•CCCC2		
25.5	**45.8**	165.3	49.8	122.9	**151.5**
219.3	**227.7**	**246.0**	182.0	**232.5**	**244.3**
261.1	**272.5**	**277.7**	**255.8**	**278.2**	288.4
287.3	288.6	349.1	306.0	325.8	379.1
381.3	399.6	443.8	403.3	415.9	450.5
511.2	545.1	745.5	485.5	575.0	757.6
838.9	899.2	913.7	816.6	875.3	895.9
929.1	931.7	952.7	926.0	933.9	943.1
957.0	1020.6	1026.6	961.7	973.1	991.6
1039.2	1086.4	1145.6	1024.3	1089.5	1118.6
1183.4	1200.3	1229.6	1169.2	1190.7	1231.0
1262.4	1313.6	1337.2	1253.5	1313.2	1330.2
1390.3	1392.6	1393.7	1374.9	1380.5	1391.3
1403.1	1418.9	1430.7	1401.4	1410.0	1421.2
1480.8	1486.7	1486.8	1458.3	1477.7	1486.6
1489.8	1491.1	1501.1	1488.6	1490.5	1497.1
1503.9	1504.3	1508.8	1501.1	1505.5	1510.0
1520.7	3012.2	3012.8	1515.4	2990.0	3006.6
3012.9	3015.6	3016.9	3010.8	3011.4	3017.2
3022.1	3071.1	3074.2	3022.0	3029.6	3068.8
3077.8	3078.8	3083.5	3076.7	3077.3	3082.1
3085.5	3088.8	3090.8	3083.0	3090.3	3093.0
3090.9	3093.0	3124.6	3095.8	3123.9	3225.8

Table C.2 Moments of Inertia (amu units)

Species	Moments of Inertia (amu)		
C3CCCC2	620.60	1500.79	1668.95
C3CCCC2•	600.29	1474.00	1620.31
C3CCC•C2	625.20	1416.46	1599.14
C3CC•CC2	618.48	1498.55	1668.67
C3•CCCC2	597.27	1474.64	1618.38

Table C.3 Evaluated Enthalpies of Formation and Bond Energy at 298 K for $(CH_3)_2C\bullet CH_2CH_3$, $(CH_3)_2C\bullet CH_2CH_2CH_3$ and $(CH_3)_2CHC\bullet HCH_3$.

[a] Uncertainty is square root of the sum of squares the uncertainty in the reference species and the uncertainties; 95% confidence limit, of each method: $\pm$ 1.56 kcal mol^{-1} for CBS-QB3 and $\pm$ 2.84 kcal mol^{-1} for B3 B3LYP/6-31g(d,p) as shown in Table 3.1.

Work Reactions						$\Delta_fH^o(298)$ kcal mol^{-1}	
						B3LYP/6-31g(d,p)	CBS-QB3
$(CH_3)_2C\bullet CH_2CH_3$							
$(CH_3)_2C\bullet CH_2CH_3$	+	C_3H_8	-->	$CH_3C\bullet HCH_3$	+ $(CH_3)_2CHCH_2CH_3$	5.99 ± 2.89	7.35 ± 1.65
$(CH_3)_2C\bullet CH_2CH_3$	+	$CH_3CH_2CH_2CH_3$	-->	$CH_3CH_2C\bullet HCH_3$	+ $(CH_3)_2CHCH_2CH_3$	6.07 ± 2.90	7.43 ± 1.66
$(CH_3)_2C\bullet CH_2CH_3$	+	$(CH_3)_3CH$	-->	$(CH_3)_3C\bullet$	+ $(CH_3)_2CHCH_2CH_3$	6.44 ± 2.94	6.44 ± 1.73
$(CH_3)_2C\bullet CH_2CH_3$	+	C_3H_8	-->	$CH_3CH_2C\bullet H_2$	+ $(CH_3)_2CHCH_2CH_3$	4.61 ± 2.90	7.07 ± 1.66
$(CH_3)_2C\bullet CH_2CH_3$	+	C_2H_6	-->	C_2H_5	+ $(CH_3)_2CHCH_2CH_3$	4.79 ± 2.90	7.28 ± 1.66
					Average	5.58 ± 2.90	**7.11 ± 1.67**
		Bond dissociation energy	**$(CH_3)_2(C----H)CH_2CH_3$**				95.95 ± 1.69
$(CH_3)_2C\bullet CH_2CH_2CH_3$							
$(CH_3)_2C\bullet CH_2CH_2CH_3$	+	C_3H_8	-->	$CH_3C\bullet HCH_3$	+ $(CH_3)_2CHCH_2CH_2CH_3$	0.69 ± 2.89	2.04 ± 1.65
$(CH_3)_2C\bullet CH_2CH_2CH_3$	+	$CH_3CH_2CH_2CH_3$	-->	$CH_3CH_2C\bullet HCH_3$	+ $(CH_3)_2CHCH_2CH_2CH_3$	0.76 ± 2.90	2.11 ± 1.66
$(CH_3)_2C\bullet CH_2CH_2CH_3$	+	$(CH_3)_3CH$	-->	$(CH_3)_3C\bullet$	+ $(CH_3)_2CHCH_2CH_2CH_3$	1.14 ± 2.94	1.12 ± 1.73
$(CH_3)_2C\bullet CH_2CH_2CH_3$	+	C_3H_8	-->	$CH_3CH_2C\bullet H_2$	+ $(CH_3)_2CHCH_2CH_2CH_3$	-0.70 ± 2.90	1.76 ± 1.66
$(CH_3)_2C\bullet CH_2CH_2CH_3$	+	C_2H_6	-->	C_2H_5	+ $(CH_3)_2CHCH_2CH_2CH_3$	-0.51 ± 2.90	1.97 ± 1.66
					Average	0.27 ± 2.90	**1.80 ± 1.67**
		Bond dissociation energy	**$(CH_3)_2(C----H)CH_2CH_2CH_3$**				95.68 ± 1.69

Table C.3 Evaluated Enthalpies of Formation and Bond Energy at 298 K for $(CH_3)_2C \cdot CH_2CH_3$, $(CH_3)_2C \cdot CH_2CH_2CH_3$ and $(CH_3)_2CHC \cdot HCH_3$. (Continued)

Work Reactions						$\Delta_f H^o(298)$ kcal mol^{-1}	
						B3LYP/6-31g(d,p)	CBS-QB3
$(CH_3)_2CHC \cdot HCH_3$							
$(CH_3)_2CHC \cdot HCH_3$	+	C_3H_8	-->	$CH_3C \cdot HCH_3$	+ $(CH_3)_2CHCH_2CH_3$	9.06 ± 2.89	9.26 ± 1.65
$(CH_3)_2CHC \cdot HCH_3$	+	$CH_3CH_2CH_2CH_3$	-->	$CH_3CH_2C \cdot HCH_3$	+ $(CH_3)_2CHCH_2CH_3$	9.14 ± 2.90	9.34 ± 1.66
$(CH_3)_2CHC \cdot HCH_3$	+	$(CH_3)_3CH$	-->	$(CH_3)_3C \cdot$	+ $(CH_3)_2CHCH_2CH_3$	9.51 ± 2.94	8.35 ± 1.73
$(CH_3)_2CHC \cdot HCH_3$	+	C_3H_8	-->	$CH_3CH_2C \cdot H_2$	+ $(CH_3)_2CHCH_2CH_3$	7.68 ± 2.90	8.98 ± 1.66
$(CH_3)_2CHC \cdot HCH_3$	+	C_2H_6	-->	C_2H_5	+ $(CH_3)_2CHCH_2CH_3$	7.86 ± 2.90	9.19 ± 1.66
					Average	8.65 ± 2.90	$\mathbf{9.02 \pm 1.67}$
		Bond dissociation energy		**$(CH_3)_2CH(CH\text{----}H)CH_3$**		**97.86 ± 1.69**	
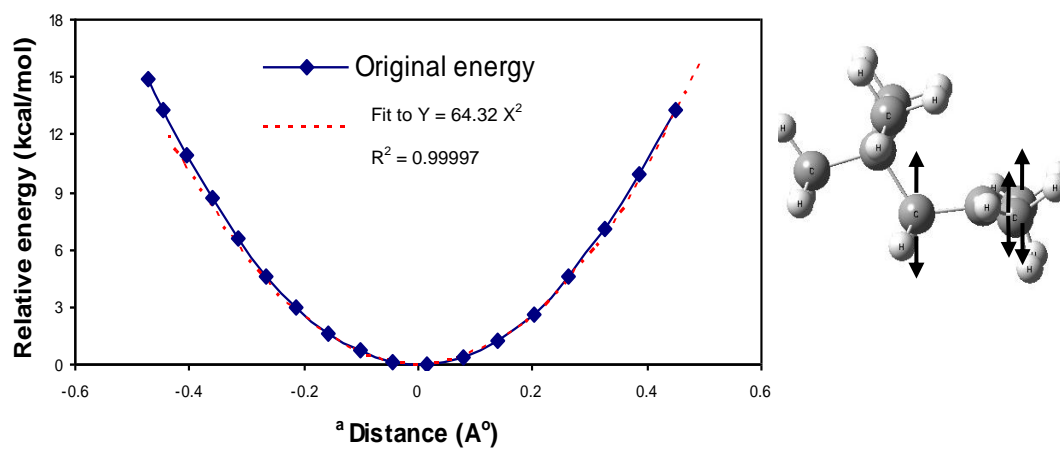
Figure C.1 Inversion potential energy profile of C3CCC•C2 on isopropyl group.

[a] Distance is the height of the pyramid formed by the inverting atom and its three neighbors.

THERMOCHEMISTRY, REACTION PATHS AND KINETICS ON THE
***tert*-ISOOCTANE PEROXIDE, REACTION WITH O$_2$**

QRRK calculations and the results versus pressure and temperature are presented in Figure D.1. Comparison of rate constant at each H-shift reaction as a function of temperature is reported in Figure D.2A – D.2D. Vibration frequencies, and moments of inertia for target structures are presentes in the Table D.1 and Table D.2, respectively.
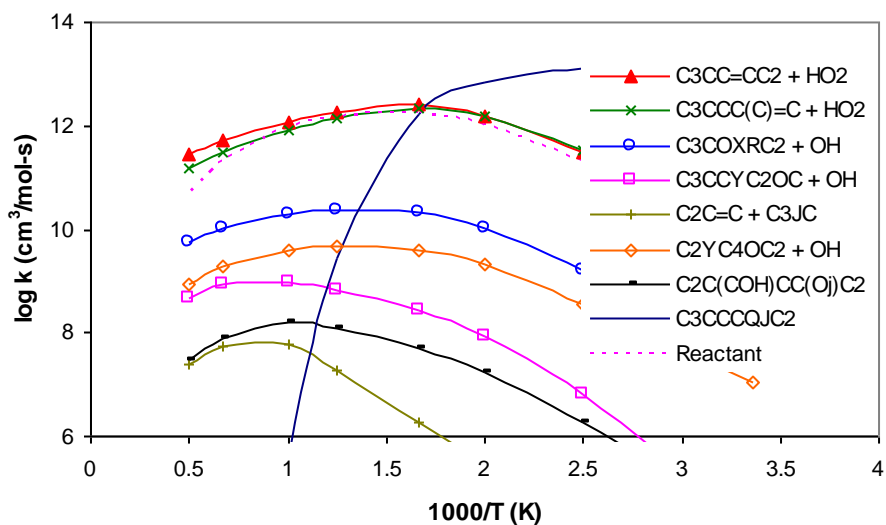
Figure D.1 Chemical activation plot of rate constants versus 1000/T (K) at 0.01atm for C3CCC•C2 + O$_2$ → Products.
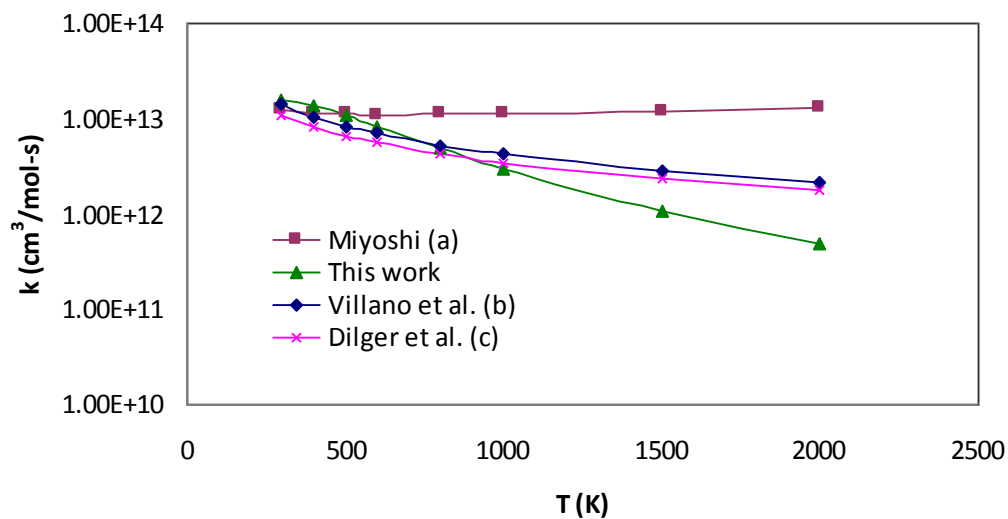
Figure D.2A Comparison rate constant as a function of temperature for association reaction, C3CCC•C2 + O$_2$. (a) Miyoshi[153] (b) Villano et al.[152] (c) Dilger et al.[151]
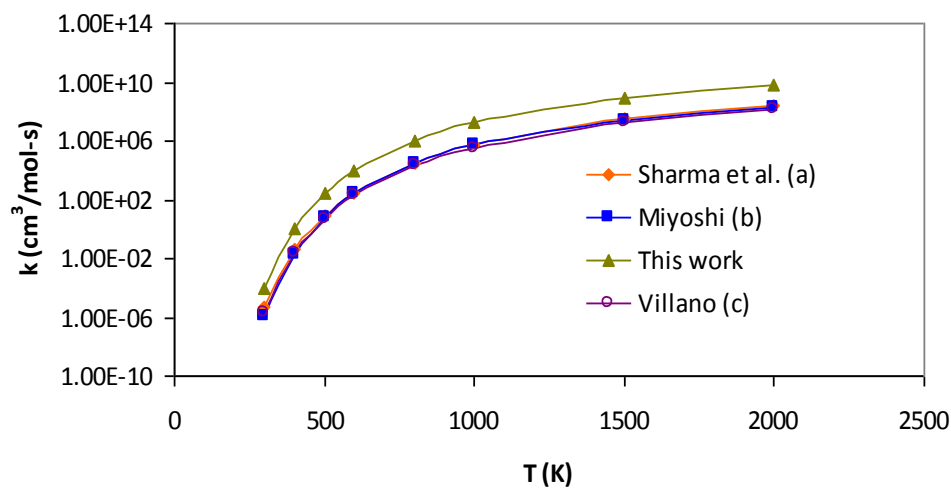
Figure D.2B Comparison rate constant as a function of temperature for 1,6 H-Shift reaction, C3CCC(OO•)C2 → C3•CCC(OOH)C2. (a) Sharma et al.[157] (b) Miyoshi[153] (c) Villano et al.[152]
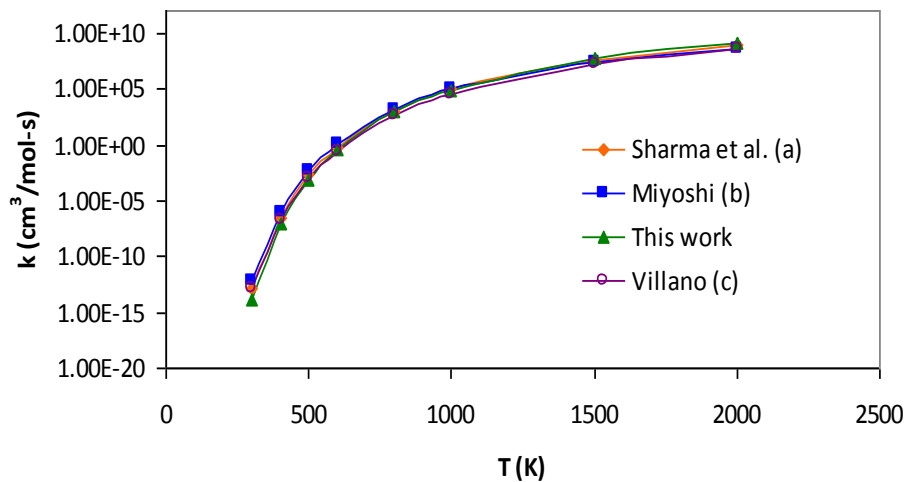
Figure D.2C Comparison rate constant as a function of temperature for 1,4p H-Shift reaction, C3CCC(OO•)C2 → C3CCC(OOH)C2•. (a) Sharma et al.[157] (b) Miyoshi[153] (c) Villano et al.[152]
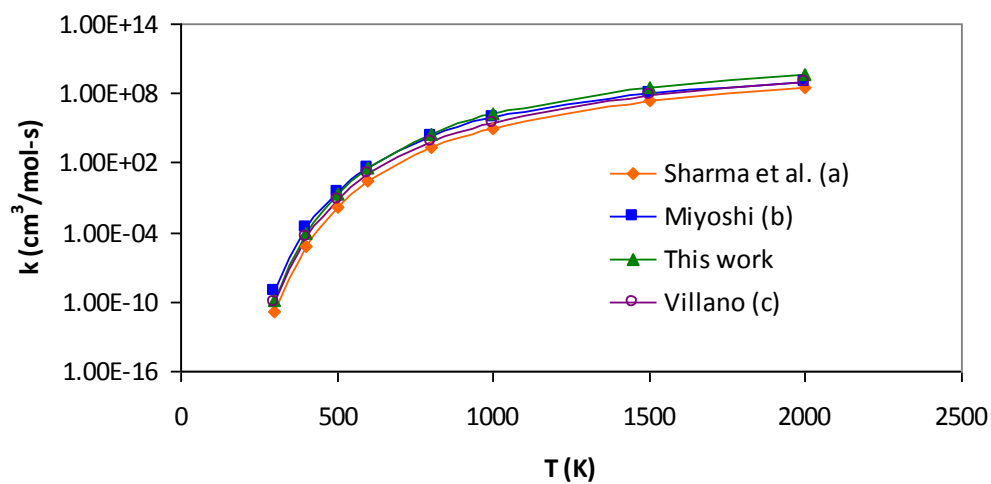
Figure D.2D Comparison rate constant as a function of temperature for 1,4s H-Shift reaction, C3CCC(OO•)C2 → C3CC•C(OOH)C2. (a) Sharma et al.[157] (b) Miyoshi[153] (c) Villano et al.[152]

Table D.1 Calculated at CBS-QB3 Composite, *viz.* B3LYP/6-311G(2d,d,p) Level Vibration Frequencies (cm^{-1}) **.** Number in bold are vibration frequencies which were replaced by internal rotors.

c3cccqc2			c3cccqc2j		
31.1	111.2	166.8	**61.0**	104.1	126.8
188.0	**206.9**	**224.5**	**152.9**	195.9	**221.6**
237.0	241.6	**257.2**	**228.5**	242.7	**250.1**
268.6	**276.3**	307.9	**267.7**	282.1	**293.6**
319.8	334.9	374.5	307.5	312.8	360.4
378.9	404.9	415.2	394.7	416.1	418.6
468.4	526.8	572.2	440.0	499.3	508.8
738.4	778.4	840.9	637.2	742.3	776.6
869.6	909.4	922.9	829.6	881.5	905.8
932.3	939.2	944.2	923.4	925.8	939.8
961.6	983.8	1019.5	957.2	963.2	991.2
1047.0	1053.7	1144.4	1045.4	1052.3	1129.3
1175.5	1233.2	1235.6	1149.3	1177.0	1231.8
1264.3	1273.2	1346.6	1249.3	1271.2	1339.0
1363.3	1385.5	1395.7	1362.8	1370.9	1397.1
1398.9	1403.2	1419.8	1398.9	1405.1	1433.3
1431.9	1468.8	1476.2	1450.2	1462.7	1483.3
1482.8	1490.1	1493.5	1485.8	1487.8	1490.0
1495.0	1500.2	1506.9	1504.5	1507.0	1511.4
1511.7	1524.3	1527.9	1519.3	3015.4	3016.8
3009.5	3013.6	3017.9	3020.9	3029.9	3040.0
3027.4	3038.7	3049.2	3059.6	3074.7	3082.2
3057.6	3064.6	3074.6	3084.4	3090.9	3098.5
3080.5	3083.4	3104.3	3106.7	3109.4	3132.5
3110.9	3113.6	3117.1	3146.2	3251.7	3771.9
3124.4	3134.8	3770.7			

Table D.1 Calculated at CBS-QB3 Composite, *viz.* B3LYP/6-311G(2d,d,p) Level Vibration Frequencies (cm^{-1}) **.** Number in bold are vibration frequencies which were replaced by internal rotors. (Continued)

c3cccqjc2			c3ccjcqc2			c3jcccqc2		
61.6	95.2	155.2	**61.5**	75.4	124.1	**57.4**	133.1	**155.0**
188.1	**216.5**	**232.8**	167.4	**216.0**	**234.6**	**172.5**	175.2	**218.6**
249.7	262.9	275.7	244.5	**251.3**	262.7	**240.0**	**264.9**	**273.2**
281.7	**300.7**	314.6	**279.8**	**286.7**	290.2	284.2	300.1	329.6
333.9	364.9	379.7	300.0	**304.5**	333.0	345.8	363.0	377.6
402.3	421.6	466.4	379.2	389.1	405.1	399.9	411.1	458.8
540.9	558.8	726.4	437.2	502.1	575.2	479.2	529.2	567.5
751.6	805.3	871.7	604.4	733.0	765.8	676.9	754.6	783.7
911.6	933.1	941.2	867.1	893.0	916.2	854.7	874.3	908.1
946.2	963.0	988.7	920.7	936.0	939.5	928.4	933.7	943.7
1021.8	1050.8	1056.3	965.1	1005.9	1030.6	947.8	978.8	986.2
1129.8	1173.8	1194.9	1036.6	1052.1	1157.3	1026.7	1040.0	1130.3
1232.3	1234.3	1267.9	1163.9	1198.3	1232.4	1150.3	1197.3	1235.2
1280.0	1347.1	1388.3	1260.3	1282.1	1350.3	1249.3	1271.7	1335.9
1400.4	1402.8	1409.1	1382.7	1389.2	1392.2	1371.6	1392.5	1398.7
1427.0	1438.0	1468.9	1397.6	1410.0	1430.1	1408.0	1413.5	1418.9
1480.6	1486.3	1490.1	1478.1	1480.7	1490.0	1456.3	1473.4	1482.2
1492.6	1493.1	1499.3	1491.3	1497.2	1500.3	1490.8	1493.0	1495.0
1509.8	1514.0	1522.0	1505.2	1508.4	1514.8	1496.2	1506.2	1519.1
1524.3	3015.7	3021.4	1527.4	3013.8	3017.8	1525.0	3014.7	3021.1
3024.0	3031.6	3040.9	3028.0	3035.3	3047.5	3028.2	3037.1	3049.1
3048.9	3067.2	3075.6	3075.1	3080.3	3083.2	3055.9	3081.4	3085.8
3082.0	3086.0	3091.7	3087.5	3103.0	3111.7	3094.2	3100.6	3106.9
3104.6	3106.0	3111.3	3117.0	3118.0	3124.1	3111.2	3118.4	3129.4
3115.7	3126.3	3135.9	3140.2	3141.3	3779.1	3146.7	3211.0	3531.1

Table D.3 Calculated at CBS-QB3 Composite, *viz.* B3LYP/6-311G(2d,d,p) Level Vibration Frequencies (cm^{-1}) **.** Number in bold are vibration frequencies which were replaced by internal rotors. (Continued)

TS2 (TSqj-c2j)			TS1 (TSqj-c3ccj)			TS3 (TSqj-c3j)		
-2201.2	**63.1**	98.0	-2080.9	**80.4**	114.8	-1475.7	88.7	143.5
162.5	**202.1**	233.3	176.9	**211.4**	**215.8**	211.6	**204.7**	246.0
244.8	249.3	**262.1**	231.4	**236.2**	**266.9**	**265.9**	**273.1**	280.5
283.0	300.0	301.2	**269.5**	280.3	300.5	299.8	**320.6**	346.3
342.9	383.2	405.2	307.5	355.8	364.2	349.1	370.5	380.2
414.7	416.0	482.2	408.5	418.4	461.2	414.7	453.8	480.7
561.3	593.0	682.9	547.4	606.6	630.0	533.6	588.0	619.3
748.5	786.0	818.1	752.8	821.3	843.9	761.0	783.2	869.0
887.5	907.4	921.5	877.9	912.7	929.1	881.7	913.2	934.5
940.7	944.7	954.6	933.6	944.6	957.0	940.2	944.5	980.1
964.7	999.2	1007.7	968.1	994.9	1022.1	985.3	999.5	1025.1
1050.2	1060.9	1119.7	1047.4	1057.2	1131.3	1032.8	1050.3	1131.5
1125.3	1168.7	1221.3	1177.2	1187.3	1223.7	1156.0	1190.2	1225.2
1244.1	1260.9	1279.5	1238.2	1268.9	1287.5	1244.6	1262.8	1281.6
1348.1	1388.7	1413.1	1376.7	1405.5	1408.3	1340.8	1376.3	1405.7
1416.7	1419.6	1449.0	1415.9	1425.6	1447.2	1408.1	1426.0	1426.6
1464.9	1474.8	1494.1	1485.9	1494.3	1497.8	1465.4	1486.8	1495.7
1496.6	1500.2	1504.1	1499.5	1502.0	1507.9	1497.2	1502.4	1505.7
1514.9	1521.2	1523.3	1516.2	1520.3	1526.9	1506.7	1508.3	1518.0
1529.7	1721.0	3026.6	1532.4	1709.1	3035.3	1528.5	1536.7	3029.5
3032.5	3040.1	3048.3	3040.5	3052.5	3053.8	3034.9	3042.8	3051.8
3055.7	3069.8	3100.0	3061.8	3100.3	3103.3	3062.7	3074.2	3087.8
3105.7	3108.1	3116.2	3110.3	3113.9	3124.3	3100.8	3105.3	3113.4
3125.5	3128.4	3133.5	3124.6	3130.6	3138.3	3122.5	3133.1	3148.1
3138.8	3149.1	3225.7	3143.9	3148.2	3163.1	3149.6	3156.1	3178.1

Table D.4 Moments of Inertia (amu units)

Species	Moments of Inertia (amu)		
c3cccqc2	1018.92	1947.58	2204.80
c3cccqc2j	876.89	2199.63	2325.62
c3cccqjc2	989.89	1929.09	2162.89
c3ccjcqc2	912.54	2151.57	2273.52
c3jcccqc2	1003.30	1850.77	2090.98
TS qj-c2j	862.44	2173.20	2286.93
TS qj-c3ccj	993.60	1847.73	2090.36
TS qj-c3j	984.70	1791.71	2015.31

REFERENCES

1. Hehre, W.; Random, L.; Schleyer, P. R.; Pople, J. A. *Ab Initio Molecular Orbital Theory*; John Wiley & Son; New York, NY, 1986.

2. Foresman, J. B.; Frisch, A. *Exploring Chemistry with Electronic Structure Methods*, 2nd ed.; Gaussian, Inc.: Pittsburgh, PA, 1996.

3. Levine, I. N. *Quantum Chemistry*, 5th ed.: Prentice Hall: Upper Saddle River, NJ 07485, 2000.

4. Becke, A. D. *Physical Review A: Atomic, Molecular and Optical Physics* **1988**, *38*, 3098.

5. Pople, J. A.; Head-Gordon, M.; Raghavachari. K. *J. Chem. Phys.* **1987**, *87*, 5968.

6. Ochterski, J. W.; Petersson, G. A.; Montgomery, J. A.. *J. Chem. Phys.* **1996**, *104*, 2598.

7. Hehre, W. J. *A Guide to Molecular Mechanics and Quantum Chemical Calculations*; Wavefunction, Inc.: Irvine, CA 92612, 2003.

8. Asatryan, R.; Bozzelli, J.W.; Simmie, J. M. *J. Phys. Chem. A* **2008**, *112*, 3172.

9. Scott, A. P.; Radom, L. *J. Phys. Chem*. **1996,** *100*, 16502.

10. Minkin,V. I. *Pure Appl Chem* **1999**, *71*, 1919.

11. Sheng, C. Ph.D. dissertation, Department of Chemical Engineering, New Jersey Institute of Technology, 2002.

12. Lay, T. H.; Krasnoperov, L. N.; Venanzi, C.A.; Bozzelli, J. W.; Shokhirev, N. V. *J. Phys. Chem*. **1996**, *100*, 8240.

13. Benson, S. W. *Thermochemical Kinetics,* 2nd ed.; Wiley-Interscience: New York, 1976.

14. Metz, C. R. *Theory and Problems of Physical Chemistry;* McGraw-Hill Book Company: New York, NY, **1976**.

15. Pitzer, K. S. *J. Chem. Phys.* **1937**, *5*, 469.

16. Pitzer, K. S. *J. Chem. Phys.* **1946**, *14*, 239.

17. Pitzer, K. S.; Gwinn, W. D. *J. Chem. Phys.* **1942**, *10*, 428.

18. Kilpatrick, J. E.; Pitzer, K. S. *J. Chem. Phys.* **1949**, *17*, 1064.

19. Lay, T. H.; Bozzelli, J. W.; Dean, A. M.; Ritter, E. 1 R. *J. Phys. Chem.* **1995**, *99,* 14514.

20. Dean, A. M., Westmoreland, P. W. Longwell, J., Howard, J. and Sarofim, A. *AICHE Journal* **1986,** *32,* 1971.

21. Kee, R.J., Miller, J.A. and Jefferson, T.H., CHEMKIN: *Fortran Chemical Kinetics Code Package,* Sandia Report, SAND80-8003. UC-4 (1980)

22. Lutz, A.E., Kee, **R.J.** and Miller, J.A., SENKIN: *A Fortran Program for Predicting Homogeneous Gas Phase Chemical Kinetics with Sensitivity Analysis,* Sandia Report, SAND87-8248.UC-4 (1988)

23. Golden, D. M., *J. Chem. Education* **1971,** *48,* 235.

24. Lindemann, F. A. *Trans. Faraday Soc.* **1922,** *17,* 598.

25. Hinshelwood, C. N. *Proc. Roy. Soc. A* **1927,** *113,* 230.

26. Slater, N. B. *Proc. Comb. Phil. Soc.* **1939,** *56,* 35.

27. Rice, 0. K.; Ramsperger, H. C. *J. Am. Chem. Soc.* **1927,** *49,* 1617.

28. Kassel, L. S. *J. Phys. Chem.* **1928,** *32,* 225.

29. Kassel, L. S. *J. Phys. Chem.* **1928,** *32,* 1065.

30. Kassel, L. S. *Kinetics of Homogenous Gas Reaction;* Chemical Catalog Co.: New York, NY, 1932.

31. Steinfeld, J. I.; Franciso, J. S.; Hase, W. L. *Chemical Kinetics and Dynamics;* Prentice Hall: Upper Saddle River, NJ, 1989.

32. Robinson, P. J.; Holbrook, K. A. Unimolecular Reactions; John Wiley and Sons: New York, NY, 1971.

33. Chang, A. Y.; Bozzelli, J. W.; Dean, A. M. *Into. J. Res. Phys. Chem. Chem. Phys. (Zeit. Phys. Chem)* **2000,** *214,* 1533.

34. Dean, A. M. *J. Phys. Chem.* **1985,** *89,* 4600.

35. Dean, A. M.; Ritter, A. R.; Bozzelli, J. W. *Combust. Sci. Technol.* **1991,** *80,* 63.

36. Gilbert, R. G.; Smith, S. C. *Theory of Unimolecular and Recombination Reactions;* Oxford Press: New York, NY, 1990.

37. Gilbert, R. G.; Smith, S. C.; Jordan, M. J. T. *UNIMALL Program Suite (Calulation of Fall-off Curve for Unimolecular and Recombination Reactions),* Sidney, Australia, 1993.

38. Gilbert, R. G.; Luther, K.; Troe, J. *Ber. Bunsen-Ges. Phys. Chem.* **1983,** *87,* 169.

39. Ritter, A. R. *J. Chem. Info. Comp. Sc.* **1991,** *31,* 400.

40. Bozzelli, J. W.; Chang, A. Y.; Dean, A. M. *Into. I Chem. Kinet.* **1997,** *29,* 161.

41. Hirschfelder, J. O.; Curtiss, C. F.; Bird, R. B. *Molecular Theory of Gases and Liquids;* Wiley: London, 1963.

42. Reid, R. C.; Prausnitz, J. M.; Polling, B. E. *Properties of Gases and Liquids;* McGraw-Hill: New York, 1989.

43. Sheng, C. Y.; Bozzelli, J. W.; Dean, A. M.; Chang, A. *Y. I Phys. Chem. A* **2002,** *106,* 7276.

44. Luo, Y. R. *Handbook of Bond Dissociation Energies in Organic Compounds*; CRC Press: Boca Raton, FL, 2003.

45. Asatryan, R.; Bozzelli, J.W.; Simmie, J.M. *Int. J. Chem. Kinet.* **2007**, *39*, 378.

46. Asatryan, R.; Bozzelli, J.W.; Simmie, J.M. *J. Phys. Chem. A* **2008,** *112,* 3172.

47. Dean, A. M.; Bozzelli, J.W. Combustion Chemistry of Nitrogen. In *Gas-Phase Combustion Chemistry*; Gardiner, W. C., Jr.; Springer: New York, NY, 1999; pp 125.

48. Alexander, M. H.; Dagdigian, P. J.; Jacox, M. E.; Kolb, C. E.; Melius, C. F. *Prog. Energy Combust. Sci.* **1991**, *17*, 263.

49. Brill, T. B. In *Chemistry and Physics of Energetic Materials*; Bulusu, S., Ed.; Kluwer Academic Publ.: Dordrecht, The Netherlands, 1990; p 277.

50. Kuo, K. K.; Summerfield, M. *Fundamentals of Solid Propellant Combustion, Progress in Astronautics and Aeronautics*; AIAA, Inc.: New York, NY, 1984, p 90.

51. Manelis, G. B.; Nazin, G. M.; Rubtsov, Yu. I.; Strunin, V. A. *Thermal decomposition and combustion of explosives and propellants*; Nauka: Moscow, Russia, 1996 (in Russian).

52. Dechaux, J. C; Perche, A. *Oxidat. Commun.* **1983**, *3*, 77.

53. Guirguis, R.; Hsu D. S. Y.; Bogan, D.; Oran, E. *Combust. Flame* **1985**, *61*, 51.

54. Tricot, J. C; Perche, A.; Lucquin, M. *Combust. Flame* **1981**, *40*, 269.

55. Cotrell, T.; Graham, T.; Reid, T. *Trans. Farad. Soc.* **1951**, *47*, 584.

56. Separate reviews of Dagdigian et al. (Dagdigian, P. J.; Bernstein, E. R.; Thompson, D. L.) as well as the overview of Anderson et al. (Anderson, W. R.; Fontijn, A.) In *Advanced Series in Physical Chemistry 16. Overview of Recent Research on*

Energetic Materials; Shaw, R. W., Brill, T. B., Thompson, D. L., Eds.; World Sci. Publ.: Singapore, 2005.

57. Dewar, M. J. S.; Ritchie, J. P.; Alster, J. *J. Org. Chem.* **1985**, *50*, 1031.

58. Brower, K. R. *J. Org. Chem.* **1988**, *53*, 3776.

59. Rasmussen C. L.; Wassard K. H.; Dam-Johansen K.; Glarborg P. *Int J Chem Kinet.* **2008**, *7*, 423.

60. Bromly, J. H.; Barnes, F. J.; Nelson, P. F.; Haynes, B. S. *Int. J.Chem.Kinet.* **1995**, *27*, 1165.

61. Dagaut P.; Dayma G. *J. Phys. Chem. A*. **2006**; *110,* 6608-6616.

62. Gutowski, K. E.; Rogers, R. D.; Dixon, D. A. *J. Phys. Chem. A* **2006**, *110*, 11890.

63. McKee, M. L. *J. Am. Chem. Soc.* **1986**, *108*, 5784.

64. McKee, M. L. *J. Phys. Chem.* **1989**, *93*, 7365.

65. Manaa, M. R.; Fried, L. E. *J. Phys. Chem. A* **1998**, *102*, 9884.

66. Denis, PA.; Ventura, O. N.; Le, H. T.; Nguyen, M. T. *Phys. Chem. Chem. Phys.* **2003**, *5*, 1730.

67. Gutsev, G. L.; Jena, P.; Bartlett, R. J. *J. Chem. Phys.* **1999**, *110*, 403.

68. Jursic, B. S. *Int. J. Quantum Chem.* **1997**, *64*, 263.

69. Farnell, L.; Ogilvie, J. F. *Proc. R. Soc. London. Ser. A* **1982**, *381*, 443.\

70. Lammertsma, K.; Prasad, B. V. *J. Am. Chem. Soc.* **1993**, *115*, 2348.

71. Khrapkovskii, G. M.; Shamov, A. G.; Shamov, G. A.; Shlyapochnikov, V. A. *Russ. Chem. Bull. (Iz*V. *AN, Ser. Khim.)* **2001**, *50*, 952-957. (b) Khrapkovski, G. M.; Shamsutdinov, T. F.; Chachkov, D. V.; Shamov, A. G. *J. Mol. Struct. (THEOCHEM)* **2004**, *6*, 1.

72. Turner, P. H.; Corkill, M. J.; Cox A. P. *J. Phys. Chem.* **1979**, *83*, 1473.

73. Wodtke, A. M.; Hintsa, E. J.; Lee, Y. T. *J. Phys. Chem.* **1986**, *90*, 3549.

74. Khrapkovski, G. M.; Shamov, A. G.; Shamov, G. A.; Nikolaeva, E. G.; Chachkov, D. V. *Chem. Comput. Simul. Butlerov. Commun.* **2002**, *686*, 185.

75. Taylor, H. A.; Vesselovsky, V. V. *J. Phys. Chem.* **1935**, *39*, 1095.

76. Spokes, G. N.; Benson, S. W. *J. Am. Chem. Soc.* **1967**, *89*, 6030.

77. Sutter, H. U.; Nonella, M. *J. Phys. Chem. A* **1997**, *101*, 5580.

78. Hu, W.-F.; He, T.-J.; Chen, D.-M.; Liu, F.-C. *J. Phys. Chem. A* **2002**, *106*, 7294.

79. Rebbert, R. E.; Laidler, K. J. *J. Chem. Phys.* **1952**, *20*, 574.

80. Conboy, C. B.; Chauvel, J. P.; Moreno, P. O.; True, N. S.; Ott C. M. *J. Phys. Chem.* **1986**, *90*, 4353.

81. Shao, J.; Cheng, X.; Yang, X. *Struct. Chem.* **2005**, *16*, 457.

82. Shao, J.-X.; Cheng, X.-L.; Yang, X.-D.; He, B. *Chin. Phys.* **2006**,*15*, 329.

83. Shao, J.-X.; Cheng, X.-L.; Yang, X.-D.; Xiang, S.-K.*Chin. Phys. Lett.* **2006**, *23*, 819.

84. Arens, F.; Amman, M.; Gutzwiller, L.; Baltensperger, U.; Ga¨ggeler, H. W. *J. Aerosol Sci.* **2000**, *31*, S1035.

85. Curtiss, L. A.; Raghavachari, K.; Redfern, P. C.; Rassolov, V.; Pople, J. A. *J. Chem. Phys.* **1997**, *106*, 1063.

86. Rice, B. M.; Pai, S. V.; Hare, J. *Combust Flame* **1999**, *118*, 445.

87. Osmont, A.; Catoire, G¨okulp, I.; Yang, V. *Combust Flame* **2007**, *151*, 262.

88. Li, X.-H.; Zhang, R.-Z.; Yang, X.-D.; H. Z. *JMol Struct: THEOCHEM* **2007**, *815*, 151.

89. Gaussian 03, Revision D.01. Frisch, M. J.; Trucks, G. W.; Schlegel, H. B.; Scuseria, G. E.; Robb, M. A.; Cheeseman, J. R.; Montgomery, J. A., Jr.; Vreven, T.; Kudin, K. N.; Burant, J. C.; Millam, J. M.; Iyengar, S. S.; Tomasi, J.; Barone, V.; Mennucci, B.; Cossi, M.; Scalmani, G.; Rega, N.; Petersson, G. A.; Nakatsuji, H.; Hada, M.; Ehara, M.; Toyota, K.; Fukuda, R.; Hasegawa, J.; Ishida, M.; Nakajima, T.; Honda, Y.; Kitao, O.; Nakai, H.; Klene, M.; Li, X.; Knox, J. E.; Hratchian, H. P.; Cross, J. B.; Adamo, C.; Jaramillo, J.; Gomperts, R.; Stratmann, R. E.; Yazyev, O.; Austin, A. J.; Cammi, R.; Pomelli, C.; Ochterski, J.W.;Ayala, P.Y.; Morokuma, K.; Voth, G. A.; Salvador, P.; Dannenberg, J. J.; Zakrzewski, V. G.; Dapprich, S.; Daniels, A. D.; Strain, M. C.; Farkas, O.; Malick, D. K.; Rabuck, A. D.; Raghavachari, K.; Foresman, J. B.; Ortiz, J. V.; Cui, Q.; Baboul, A. G.; Clifford, S.; Cioslowski, J.; Stefanov, B. B.; Liu, G.; Liashenko, A.; Piskorz, P.; Komaromi, I.; Martin, R. L.; Fox, D. J.; Keith, T.; Al-Laham, M. A.; Peng, C. Y.; Nanayakkara, A.; Challacombe, M.; Gill, P. M. W.; Johnson, B.; Chen, W.; Wong, M. W.; Gonzalez, C.; Pople, J. A. Gaussian, Inc.: Pittsburgh, PA, 2003.

90. Ashcraft, R. W.; Green, W. H. *J Phys Chem A* **2008**, *112*, 9144.

91. NIST Chemistry Webbook; available at http://webbook.nist.gov/chemistry/

92. Sebbar, N.; Bockhorn, H.; Bozzelli, J. W. *Phys. Chem. Chem.Phys*. **2002**, *4*, 3691.

93. El-Nahas, A. M.; Bozzelli, J. W.; Simmie, J. M.; Navarro, M. V.; Black, G.; Curran, H. J. *J. Phys. Chem. A* **2006**, *110*, 13618.

94. Stevens, R. W.; Ruscic, B.; Baer, T. *J. Phys. Chem. A* **2010**, *114*, 13134.

95. Kemnitz, C. R.; Loewen, M. J. *J Am Chem Soc* **2007**,*129*, 2521.

96. Benson, S. W. Thermochemical Kinetics; Wiley-Interscience: New York, NY, 1976.

97. Holmes, J. L.; Lossing, F. P. *J. Am. Chem. Soc*. **1982**, *104*, 2648.

98. Wang, Y. H.; Jacob, D. J.; Logan, J. A. *J. Geophys. Res*., [Atmos.] **1998**, *103*, 10713.

99. Jacob, D. J.; Field, B. D.; Jin, E. M.; Bey, I.; Li, Q.; Logan, J. A.; Yantosca, R. M. *J. Geophys. Res.* **2002**, *107*

100. Singh, H. B.; OHara, D.; Herlth, D.; Sachse, W.; Blake, D. R.; Bradshaw, J. D.; Kanakidou, M.; Crutzen, P. J. *J. Geophys. Res*., [Atmos.] **1994**, *99*, 1805.

101. Singh, H.; Chen, Y.; Staudt, A.; Jacob, D.; Blake, D.; Heikes, B.; Snow, *J. Nature* **2001**, *410*, 1078.

102. McKeen, S. A.; Gierczak, T.; Burkholder, J. B.; Wennberg, P. O.; Hanisco, T. F.; Keim, E. R.; Gao, R. S.; Liu, S. C.; Ravishankara, A. R.; Fahey, D. W. *Geophys. Res. Lett*. **1997**, *24*, 3177.

103. Blanksby, S. J.; Ellison, G. B. *Acc. Chem. Res*. **2003**, *36*, 255.

104. Berkowitz, J.; Ellison, G. B.; Gutman, D. *J. Phys. Chem.* **1994**, *98*, 2744.

105. Sehested, J.; Christensen, L.K.; Nielsen, O.J.; Bilde, M.; Wallington, T.J.; Schneider, W.F.; Orlando, J.J.; Tyndall, G.S. *Int. J. Chem. Kinet.* **1998,** *30*, 475.

106. Ochterski, J. W.; Pererson, G. A.; Wiberg, K. B. *J. Am. Chem. Soc*. **1995**, *117*, 11299.

107. Ochterski, J. W.; Pererson, G. A.; Montgomery, J. A., Jr. *J. Chem.Phys*. **1996**, *104*, 2598.

108. Curtiss, L. A.; Raghavachari, K.; Trucks, G. W.; Pople, J. A. *J. Chem. Phys*. **1991**, *94*, 7221.

109. Curtiss, L. A.; Redfern, P. C.; Raghavachari, K. *J. Chem. Phys*. **2007**, *126*, 84108.

110. Tsang, W., Heats of Formation of Organic Free Radicals by Kinetic Methods in Energetics of Organic Free Radicals, Martinho Simoes, J.A.; Greenberg, A.; Liebman, J.F., eds., Blackie Academic and Professional, London, UK, 1996, 22-58

111. Benson, S. W. Thermochemical Kinetics; Wiley-Interscience: New York, NY, 1976.

112. Lay, T. H.; Bozzelli J. W.; Dean, A. M.; Ritter, E. R. *J. Phys. Chem.*, **1995**, *99*, 14514.

113. Ritter, E. R.; Bozzelli, J. W. *Int J. Chem. Kinet*. **1991** *23*, 767

114. Moulds, L.V.; Riley, H.L. *J. Chem. Soc.*, **1938**, 621.

115. Chase, M.W., Jr., NIST-JANAF, *J. Phys. Chem. Ref. Data, Monograph 9*, **1998**, 1.

116. Anderson, W. R. *Combust. Flame* **1999**, *117*, 394.

117. Orlov, V.M.; Krivoruchko, A.A.; Misharev, A.D.; Takhistov, V.V. *Bull. Acad. Sci. USSR, Div. Chem. Sci.*, **1986**, 2404.

118. Shen, H.-P. S.; Vanderover, J.; Oehlschlaeger, M. A. *Combust. Flame.* **2008,** *155*, 739.

119. He, X.; Walton, S. M.; Zigler, B. T.; Wooldridge, M. S.; Atreya A. *Int. J. Chem. Kinet.* **2007,** *39*, 498.

120. Ciajolo, A.; D'Anna, A. *Combust. Flame.* **1998,** *112*, 617.

121. Minetti, R.; Carlier, M.; Ribaucour, M.; Therssen, E.; Sochet, L. R. *Proc. Combust. Inst.* **1996,** *26*, 747

122. Chen, J. -S.; Litzinger, T. A.; Curran, H. J. *Comb. Sci. and Tech*. **2001,** *172*, 71.

123. Chen, J. -S.; Litzinger, T. A.; Curran, H. J. *Comb. Sci. and Tech*. **2000,** *156*, 49.

124. Buda F.; Bounaceur R.; Warth V.; Glaude P. A.; Fournet R.; Battin-Leclerc F. *Combust. Flame* **2005** *142,* 170.

125. Curran, H. J.; Gaffuri, P.; Pitz, W. J.; Westbrook, C. K. *Combust. Flame.* **2002,** *129*, 253.

126. Prosen, E. J.; Rossini, F. D. Heats of combustion and formation of the paraffin hydrocarbons at 25° C, *J. Res. NBS* **1945**, 263.

127. Stull, D. R.; Westrum, E. F. Jr.; Sink,e G. C.; The Chemical Thermodynamics of Organic Compounds, Robert E. Krieger Publishing Company Malabar, FL, 1987

128. Rossini, F. D.; Pitzer, K. S.; Arnett, R. L.; Braun, R. M.; Pimentel, G. C. Selected Values of Physical and Thermodynamic Properties of Hydrocarbons and Related Compounds, Carnegie Press, Pittsburgh, PA, 1953

129. Scott D. W., Chemical Thermodynamic Properties of Hydrocarbons and Related Substances. Properties of the Alkane Hydrocarbons, C1 through C10 in the Ideal Gas State from 0 to 1500 K. U.S. Bureau of Mines, Bulletin 666, Bartlesville, OK, 1974

130. Pedley, J. B.; Naylor, R. D.; Kirby, S. P. Thermochemical Data of Organic Compounds, 2nd, Chapman and Hall, London, UK, 1986

131. Ruscic, B. J.; Litorja, M.; Asher, R. L. *J. Phys. Chem. A* **1999**, *103*, 8625.

132. Seetula, A. J.; Slagle, R. I. *J. Chem. Soc., Faraday T rans.* **1997**, 93, 1709.

133. Wallington, T. J.; Kaiser, E.W.; Farrell, J.T. *Chem. Soc. Rev*. **2006**, *35*, 335.

134. Farrell, J.T.; Cernansky, N.P.; Dryer, F.L.; Friend, D.G.; Hergart, C.A.; Law, C.K.; McDavid, R.; Mueller, C.J.; Pitsch, H. *SAE Paper* 2007-01-0201, **2007**.

135. Simmie, J.M. *Progress in Energy and Combust. Sci.* **2003**, *29*, 599.

136. He X.; Walton S.M.; Zigler B.T.; Wooldridge M.S.; Atreya A. *Int. J. Chem. Kinet.* **2007**, *39*, 498.

137. Snitsiriwat, S.; Bozzelli, J. W *J. Phys. Chem. A*, **2013**, *117*, 421.

138. Redfern, P. C.; Zapol, P.; Curtiss, L. A.; Raghavachari, K. *J. Phys. Chem. A* **2000**, *104*, 5850.

139. Baboul, A. G.; Curtiss, L. A.; Redfern, P. C.; Raghavachari, K. *J. Chem. Phys.* **1999**, *110*, 7650.

140. Montgomery, J. A., Jr.; Frisch, M. J.; Ochterski, J. W.; Petersson, G. A. *J. Chem. Phys.* **1999**, *110*, 2822.

141. Hudzik, J. M.; Asatryan, R.; Bozzelli, J. W. *J. Phys. Chem. A* **2010,** *114,* 9545.

142. Snitsiriwat, S.; Asatryan, R.; Bozzelli, J. W. *Int. J. Chem. Kinet.* **2010,** *42,* 181.

143. Snitsiriwat, S.; Asatryan, R.; Bozzelli, J. W. *J. Phys. Chem. A*, **2011**, *115*, 13921.

144. Curtiss, L. A.; Redfern, P. C.; Raghavachari, K.; Rassolov, V.; Pople, J. A. *J. Chem. Phys.* **1999**, *110*, 4703.

145. Pittam, D.A.; Pilcher, G. *J. Chem. Soc. Faraday Trans. 1* **1972** 68, 2224.

146. Seakins, P. W.; Pilling, M. J.; Niiranen, J. T.; Gutman, D.; Krasnoperov, L. N. *J. Phys. Chem.* **1992**, *96*, 9847.

147. Simmie, J.M.; Black, G.; Curran, H.J.; Hinde, J.P. *J. Phys. Chem. A* **2008**, *112,* 5010.

148. Chan, W.; Hamilton, I. P.; Pritchard, H. O. J. *Chem. Soc., Faraday Trans*. **1998**, *94*, 2303.

149. Blanksby, J. S.; Ramond, M. T.; Davico, E. G.; Nimlos, R. M.; Kato, S.; Bierbaum, M. V.; Lineberger, W. C.; Ellison,G. B.; Okumura, M. *J. Am. Chem. Soc.* **2001**, *123*, 9585.

150. Lenhardt, T. M.; McDade, C. E.; Bayes, K. D. *J. Chem. Phys*. **1980**, *72*, 304.

151. Dilger, H.; Stolmar, M.; Tregenna-Piggott, P. L. W.; Roduner, E.; Reid, I. D. *Ber. Bunsen-Ges. Phys. Chem*. **1997**, *101*, 956.

152. Villano, S.M.; Huynh, L.K.; Carstensen, H.H.; Dean, A.M. *J. Phys. Chem. A* **2011**, *115*, 13425.

153. Miyoshi, A. *J. Phys. Chem. A* **2011**, *115*, 3301.

154. Zhu, L.; Bozzelli, J.W.; Kardos, L.M. *J. Phys. Chem.* **2007**, *111*, 6361.

155. Knyazev, V. D.; Slagle, I. R. *J. Phys. Chem. A* **1998**, *102*, 1770.

156. Shuman, N. S.; Bodi, A.; Baer, T. *J. Phys. Chem. A* **2010**, *114*, 232.

157. Sharma, S.; Raman, S.; Green, W.H. *J. Phys. Chem. A,* **2010**, *114*, 5689.

158. Davis, A.C.; Francisco, J.S. *J. Phys. Chem. A,* **2010**, *114*, 11492.

159. Zheng, J.; Truhlar, D.G. *Phys. Chem. Chem. Phys.,* **2010**, 12, 7782.

160. Huynh, L.K.; Carstensen H.-H.; Dean, A.M. *J. Phys. Chem. A,* **2010,** *114*, 6594.

161. Pfaendtner, J.; Yu, X.; Broadbelt, L. J. J. *Phys. Chem. A* **2006**, *110*, 10863.

162. Carstensen, H.-H.; Naik, C. V.; Dean, A. M. *J. Phys. Chem. A* **2005**, *109*, 2264.

163. Miller, J. A.; Klippenstein, S. J.; Robertson, S. H. *Proc. Combust. Inst.* **2000**, *28*, 1479.

164. Jones, J.; Fenske, M. *Ind. Eng. Chem. Res.* **1959**, *51*, 262.

165. Chan, W.-T.; Pritchard, H.O.; Hamilton, I.P. *Phys. Chem. Chem. Phys.,* **1999**, *1*, 3715.

166. Wijaya, C.D.; Raman, S.; Green, W.H. Jr. *J. Phys. Chem.,* **2003**, *107*, 4908.

167. Dasilva, G.; Graham, C.; Wang, Z.F. *Environ. Sci. Technol.,* **2010**, *44,* 250.

168. Dasilva, G.; Bozzelli, J. W.; Liang, L.; Farrell, J.T. *J. Phys. Chem. A.,* **2009,** *113,* 8923.

169. Atkinson, R. *Atmos. Environ.,***2000,** *34*, 2063.